PENNSTATE

1855

AN IN-SEAM SEISMIC (ISS) METHOD BASED MINE VOID DETECTION TECHNIQUE

FINAL REPORT FOR PHASE I

Prepared for

U. S. Department of Labor
Mine Safety and Health Administration
1100 Wilson Boulevard
Suite 2132
Arlington, Virginia 22209 – 3939

RFP# MSHA J53R1011
(Geo-physical Void Detection Demonstrations)

October 29, 2006

By
Maochen Ge

The Pennsylvania State University
Department of Energy and Geo-Environmental Engineering
201 Hosler Building, University Park, PA 16802

Executive summary

On October 8, 2004, MSHA awarded The Pennsylvania State University ("Penn State") a three-year contract for demonstration of the ISS based void detection technique based on the *Revised working plan* submitted to MSHA by Penn State on August 25, 2005. This *Revised working plan* was revised from the original Penn State proposal entitled *An In-seam seismic (ISS) method based mine void detection technique* submitted to MSHA on November 17, 2003. Revisions were made in accordance with guidelines given by MSHA during contract negotiations held on July 28 and August 24, 2004.

There were two main objectives for Phase I of the project, namely 1) to demonstrate the ISS based void detection technique developed by Penn State in two types of mines: a trona mine and an anthracite mine, and 2) to develop a preliminary version of a Users Manual for the ISS based void detection technique. Note that this Manual is the final product of this three-year contract.

1. Project scope and challenges

Field tests are a core part of the project. A total of seven tests, including two demonstrations, were carried out for three types of minerals: trona, anthracite coal and bituminous coal. Two demonstrations were given at FMC and the Harmony Mine on August 23 and November 15, 2005, respectively. The results of these seven field tests are discussed in Chapters 3 through 9.

Demonstration of the ISS method for void detection is not a simple application of the original ISS technique. In order to adopt the ISS technique to void detection, certain aspects of the technique need to be carefully addressed. The success of the ISS based void detection technique largely depends on how well these problems have been handled.

There are three major challenges for the ISS based void detection project carried out by Penn State. First, Penn State was dealing with two versions of the ISS based void detection technique: the conventional ISS technique and the unconventional ISS technique. In the conventional technique, the seam under study is weaker than the country rocks and channel waves are used for void detection. For the unconventional technique, the seam is stronger than the country rocks and, instead of channels waves, body waves (e.g. P- and S-waves) are used for void detection. In addition to the completely different relative physical condition, the types of waves used for void detection are also completely different. In addition to these differences, it is understood that the unconventional ISS technique does not possess the technical advantage associated with in-seam seismic technique, which is the use of more defined wave types for void location. Consequently, the unconventional ISS technique presents a more difficult analytical problem to solve.

The second challenge is the underground environment associated with ISS based void detection. For the ISS survey, the test site is surrounded by mine openings and both sources and receivers are located in the same seam under study. This environment creates many unique problems and, from a practical point of view, the success of ISS based void detection largely depends on how well these problems have been addressed.

The third challenge is that although geophysical methods, including ISS, are convenient, efficient and relatively inexpensive, these methods can also be very ambiguous in regards to data retrieval and interpretation. If a geophysical method is to be reliable for void detection, the problem of ambiguity must be addressed.

2. Technical development for the ISS based void detection

Demonstration of the ISS based void detection is not a simple application of the existing technique. In order to address challenges confronted, certain techniques were developed, including sensor installation, experimental design, data analysis and void mapping. The development of these techniques not only allowed Penn State to initiate field tests and to acquire quality data needed for the project, but also provided the basic means for experimental design and data analysis. Although, many initiatives are still in developmental stages, we believe efforts put forth in this study have laid a solid foundation for the further development of the ISS based void detection. The details of these techniques are discussed in the companion document *Users Manual for the ISS based void detection*.

Retrievable sensor installation technique

Proper sensor installation is a critical component of the ISS based void detection technique. This requires grouting of the sensor in the borehole to achieve a suitable coupling effect. However, to be economically feasible, the sensors must be retrievable so that they can be used repeatedly at the same or another location. Because of these concerns, a retrievable sensor installation technique was developed. This technique enables the sensor to effectively detect high frequency signals yet is simple and convenient for both installation and retrieval operations. The technique has been used for all seven field tests. Sensors installed in the prescribed manner have exhibited predictable, consistent, and repeatable performance.

The use of this sensor installation is the basic reason that we are able to acquire broadband signals, including high frequency signals, on a predictable and repeatable basis. High quality, high frequency signal data are critical for the project. For non-conventional applications of the ISS technique, such as in the trona mine, high frequency signals are a necessary condition for void detection. For the conventional applications, such as coal mines, high frequency signals provide a much better waveform for detailed data analysis.

Experimental design

One of the main issues discussed in the Penn State void detection proposal is how to avoid the problem of ambiguity that is commonly encountered with geophysical methods. A fundamental approach to deal with the problem of ambiguity is a sound experimental design. Based on both the theoretical research and field test experience, a systematical approach was developed to address this problem. From a theoretical point of view, the experimental design should be considered from four aspects: adequate coverage of the target area, sufficient survey resolution, stability of the associated mathematical system, and facilitation for data analysis. The sensitivity analysis carried out by Penn State and the use of angled sensor hole pairs enhanced our understanding of these issues and provided additional validation of analytical solutions.

On the practical side, based on both the theoretical considerations and the problems particular to the ISS survey environment, Penn State outlined five special design issues as well as

corresponding solutions. These five issues are: 1) choosing a suitable site for sensor installation, 2) reducing the impact of direct arrivals, 3) reducing the impact of (air) shock waves, 4) reducing unwanted reflected signals, and 5) improving signal strength.

Signal detection

Signal detection is another critical aspect of the ISS based void detection technique. This coupled with the underground environment adds another dimension to ISS based void detection that does not exist in conventional seismic exploration. The efficiency of data analysis largely depends whether these special issues can be addressed. Similar to the experimental design, a systematical approach was developed to signal detection and is discussed in detail in the Users Manual.

The approach includes five general steps, which are 1) data collection, 2) reviewing original waveforms, 3) assessing typical wave trends associated with the ISS based void survey, 4) performing signal frequency analysis for void detection, and 5) identifying P- and S-waves. In addition to this, Penn State also enhanced data analysis with the use of angled sensor pairs and signal separation by wavelet analysis.

Void mapping

In this project, the elliptical method was utilized for mapping mine voids. The method provides a simple and convenient means for void detection. It can utilize all signals reflected from given locations to delineate the void boundary in the area regardless of the locations of sources and receivers, the type of signals, and the survey sequence. As the method represents the reflection data directly, it avoids many mathematical manipulations which would be necessary otherwise if other methods are used. This characteristic makes the method much more stable than any other methods. The method also provides an intuitive means to analyze the cause of missing data so that missing data becomes part of the process of void location.

3 Field tests and demonstration of the ISS based void detection

A total of seven tests, including two demonstrations, were carried out for three types of mining conditions: trona, anthracite coal and bituminous coal. Two demonstrations were given at FMC and the Harmony Mine on August 23 and November 15, 2005, respectively.

Demonstration and field tests at the trona Mines

Penn State held the trona mine demonstration at FMC on August 23, 2005. The void was water-filled and the void distance was about 270 ft. Based on the result of the demonstration as well as two previous tests carried out at the trona mines, the following conclusions can be made:

1) The P- and S-wave velocities at the mine sites appear extremely consistent with velocity errors in the range of 1%, which provides a very favorable situation for reliable void detection.
2) The reflected signals observed at the trona mine sites are associated with very high frequencies, typically in the range of 3000 – 5000 Hz. This characteristic is a precondition for high resolution surveys and also greatly facilitates identification of reflected signals.
3) Three types of reflected signals were observed under both water filled and dry conditions, which are P-wave, S-wave and S-wave due to mode conversion. Using three types of reflected signals significantly increases the data which can be used for void detection.

4) The elliptical mapping method provides an efficient means to use all available data simultaneously, including 1) data from different surveys, 2) data from different source locations, and 3) the three different types of reflected signals. The method is also simple, convenient, and reliable.
5) The mapping error for void detection in trona is about ± 10 ft for pillars up to 340 ft wide based on the actual survey results from FMC and General Chemical.

Based on the above observations, the ISS based void detection technique developed by Penn State appears to be a promising tool for the trona industry to study the pillar dissolution problem. The void detection experience at the trona mines should be useful for many other mines where the seam is stronger than the country rocks.

Demonstration and field tests at the Harmony Mine

Penn State carried out the demonstration of the ISS based void detection at the Harmony Mine, an anthracite mine, on November 15, 2005, and two field tests on February 7-8, and April 29, 2005, respectively. The site for the demonstration was a 150 ft wide pillar.

The significance of the tests at the Harmony Mine is threefold. First, these tests demonstrated the critical importance of the retrievable sensor installation technique for the ISS based void detection. At the Harmony site, the signal frequency ranges from 500 Hz for channel waves to over 3000 Hz for P- and S-waves from the roof and floor. In order to differentiate channel waves from the other wave types as well as to obtain a complete signal profile for the site in terms of the signal frequency, velocity and attenuation, the ability to acquire broadband signals is essential. The retrievable sensor installation provides a reliable means to fulfill this requirement.

The second aspect was the demonstration of the existence of channel waves and the reliability of using these channel waves for void detection under the anthracite mine condition. The presence of the channel waves were demonstrated from three different types of the tests, which are transmission survey, reflection survey, and a uniquely designed “roof and floor” survey.

Finally, the ISS technique was demonstrated for the void detection distance up to 150 ft under the anthracite mine conditions, a distance that was large enough to validate the applicability of the technique. Since the same site was used for the second test as that used for demonstration purposes with very similar results being achieved, the reliability of the technique was also demonstrated in terms of repeatable performance.

Field test at the Agustus Mine

On December 8, 2005, the Penn State project team carried out a field test of the in-seam seismic (ISS) based void detection technique at the Agustus Mine. The Agustus Mine is a small bituminous mine located in Shade Township, Somerset County, PA.

Both direct arrival and reflected channel waves were observed during the transmission test. The direct arrival channel waves were also observed from the reflection surveys. The dominant frequency for the channel waves is about 200 Hz. The velocity of the channel wave is about 3300 ft/s.

We could not positively identify reflected channel waves because they were overshadowed by strong (air) shock waves. The shock waves encountered at the Agustus Mine were much stronger than the ones from any previous tests where the equivalent explosives were used. Other than the layout of the mine at the site, it is unknown whether there were any other contributing factors.

Blast induced shock waves cause a special problem with the ISS based void detection as ISS testing is conducted in confined environments. Penn State has paid a special attention to the problem since the beginning of the project and has taken several measures to deal with it. In particular, three measures have been taken, which are 1) sealing sensor holes with the commercial insulation material, 2) reducing shock wave strength by arranging the blasting holes in other entries emote from the sensor locations, and 3) reducing the amount of explosives, if possible.

Penn State researchers believe that the problem encountered at the Agustus Mine is solvable. The basic solution is to develop an air-tight sensor hole sealing technique, which should be simple and easy to do while not posing any potential problem for using the retrievable sensor installation technique. The second measure is systematical testing on the amount of explosives needed for each site.

4. Conclusions and future work

Although we believe the work in Phase I has laid a solid foundation for the further development of the ISS based void detection technique and has demonstrated for feasibility of the ISS based void detection technique for the trona and the anthracite coal conditions, the first year of work was limited to the most critical issues involving field testing and data analysis. There are a number of problems that remain to be studied. If the ISS based void detection technique is to be a reliable industrial tool, these problems have to be adequately addressed. In this sense, the ISS based void detection technique is still in early stages of evaluation and has to be further developed, refined and enhanced.

Future industrial testing and applications

The future studies discussed here are two potential applications of the ISS based void detection technique. They are not part of the proposed work for Phase II and Phase III, but, we believe, are significant for MSHA's void detection program.

Pilot study on the pillar dissolution problem in trona mines

One of the major concerns with the trona industry is whether barrier pillars, which are used to separate the mined out and active mining areas, will be gradually dissolved by water, and if so, the rate of this process. As the dissolution rate is a function of saturation, which in turn depends on the local conditions (mining, geology and hydrogeology), data from field monitoring would be essential for making a reliable assessment.

The horizontal drilling, the method which is considered the most reliable means for detecting abandoned mines in the coal industry, is not suitable for trona mining conditions, as the drill holes would induce water into the pillars. Non-destructive methods would be ideal for solving this problem.

Based on the result of three successful tests at FMC and General Chemical, the ISS based void detection technique seems to be a promising solution for the problem. The idea is that permanent monitoring stations (sensor holes with sensor attachment assembly) are established at locations of concern and reflection surveys are carried out at these stations periodically (say, every one or two years) to determine the pillar width. All reflection survey results will be preserved as "X-ray" records for the pillars under study.

With the ISS based void detection technique developed at Penn State, the cost for using this technique is minimal. As sensors can be installed at the time when a survey is needed and only one set of the monitoring equipment would be needed for all existing trona mines in Wyoming.

Further study at another mine with a strong ore seam

A hypothesis based on testing result from trona mines is that the ISS based void detection technique is not only effective for trona mines, but also a viable means for mines with stronger ore seams in general. If this is the case, a large array of non-coal mines, such as limestone and various salt mines, would also benefit from the MSHA's void detection program. In order to test this hypothesis, two field tests are recommended with one at a limestone mine and other at a salt mine. If the test results are encouraging for both sites, additional confidence in the hypothesis will be obtained.

Acknowledgement

The Penn State ISS void detection project team gratefully thanks all individuals and organizations that supported the project:

To the mining companies which graciously offered their mines to Penn State as the testing sites: Westpoint Mining: Harmony Mine, FMC, General Chemical, Agustus Mine, Quecreek Mine, Amfire Mining Co., Red River Coal, and Seldom Seen Valley Mine.

To Mr. E. Smock, President of Westpoint, Mr. R. Steenberg, Mine Manager of FMC, Mr. S. Britton, Mine Manager of General Chemical, and Mr. D. Rebuck, President of Quecreek Mine. The vision and the enthusiastic support provided by these industrial leaders are invaluable for the project.

To numerous individuals from the mining industry, who helped Penn State for site identification and field tests. Without their help, the project would be impossible. In particular, we would like to thank: *Harmony Mine*: E. Smock, President, T. McMahon, President UAE CoalCorp Associates, A. Flick, Mine Superintendent, Ivan Swinehart, Mine Foreman, George Manhart, Assistant Mine Foreman, and R. Flick, Business Manager; *FMC Trona Mine:* R. Steenberg, Mine Manager, G. Shelton, Mine Technology Business Leader, C. Pritchard, Sr. Mine Engineer, and J. Norgord, Sr. Engineering Associate; *General Chemical Trona Mine:* S. Britton, Manager Mining Operations, D. Graham, Manager Occupational Safety and Health, T. L. Mink, Mining Engineer, K. Mullins, Mine Safety Supervisor, and M. Richardson, Supervisor Mine Engineering; *Agustus Mine:* J. Hickman, Mine chief engineer, and J. Folton, Mine Superintendent; *Quecreek Mine:* D. Rebuck, President, and J. Gallo, Vice President; *Amfire Mining Co.:* R. Bottegal, Manager of Engineering, L. Pianetti, Jr., Mine Manager, and Jim Pablic, Director of safety; *Seldom Seen Valley Mine:* State Rep. G. Haluska; *Red River Coal:* H. Ross; *Appalachian Mining & Engr.:* D. A. Newman, President.

To Dr. W. Khair and West Virginia University for lending the velocity measurement equipment, which was one of the key equipments used for the project..

To Webb Manufacturing of Midkiff WV and Minova USA of Georgetown KY for their donation of stem clay and resin, respectively, the materials used for the field tests.

To Pennsylvania Bureau of Deep Mine Safety for its ongoing support of the ISS project: Mr. J. A. Sbaffoni, Director, Mr. M. McCaffrey; D. Williams, T. A. Wolfgang, and J. L. Kerch.

We would like to thank the Mine Safety and Health Administration for providing funding for the ISS Demonstration Project. We thank Mr. D. Cooper, Director, Acquisition Management Division, Dr. K. Wu, Chief, Mine Waste and Geotechnical Engineering Division, and Mr. G. Gardner, Manager, MSHA's void detection program for their leadership and guidance. We thank Dr. D. Choi, the Contracting Officer's Technical Representative, for ongoing excellent stewardship and administration for the Penn State team. We also thank many other MSHA personals, who provided various technical supports for the project: J. Kuzar, Manager, District 1;

W. Sparvieri, Assistant Manager, District 1; G. Mehalchick, Mining Engineer, District 1; L. P. Sargent, Mining Engineer, District 1; D. Swentosky, District 2; E. Lewetag, District 2; D. Silvers, Electrical Inspector, District 1; and S. Pilling, Field Office Supervisor, Rocky Mountain District, Metal & Nonmetal.

Finally, we would like to thank Dr. R. L. Nigbor from University of California at Los Angeles, Dr. Dai S. Choi and Dr. Janet Simms from U.S. Army Engineer Research and Development Center for their constructive comments and suggestions in revising the report.

Table of Content

1. Introduction

1.1 MSHA's void detection program

Inundation is one of the major safety problems faced by the mining industry, worldwide. For the coal mining industry in the United States alone, more than 100 such incidences have been reported since1995 (Gardner and Wu, 2005). The urgency of this problem was highlighted by a severe inundation incident that occurred at the Quecreek Mine on July 24, 2002 and the dramatic rescue operations that followed.

In response to the Quecreek incidence, the U.S. Congress appropriated $10 million for mine mapping and void-detection research, and MSHA promptly established the geophysical void detection program, aimed to advance the current state of practice for detecting underground mine voids. On September 16, 2003, MSHA announced the Request for Proposals (RFP) and subsequently received 58 different proposals from eight universities, two state geological survey organizations and 13 private companies. Eight teams of engineers, scientists and university professors formally evaluated each proposal. Ultimately, MSHA selected eight organizations for contract awards to demonstrate several types of technologies for detecting underground mine voids.

1.2 Penn State proposal on the ISS based void detection technique

A proposal entitled *An In-seam seismic (ISS) method based mine void detection technique* was submitted to MSHA on November 17, 2003 by the Penn State project team headed by the author. The goal of this proposal was to demonstrate a reliable, accurate, and cost-efficient ISS based mine void detection technique.

After the initial evaluation of the submitted proposals, Penn State was invited by MSHA to make an oral presentation of the proposed technique. During the presentation meeting on July 28, 2004, Penn State also discussed a potential coal mine testing site: Harmony Mine, which was identified after the submission of the original proposal. Harmony Mine is an anthracite mine, which would approach an abandoned mine in several years. The owner of the mine, Mr. Smock expressed his strong interest to participate in the project and offered his mine as a testing site after he learned of the Penn State proposal.

During the meeting, MSHA discussed with Penn State on how to modify the proposal to make it consistent with MSHA's mandate and priority. Regarding the overall planning of the project, MSHA had two major suggestions. First, Penn State had to "condense" the three-year work plan in the original proposal to a one-year work plan in which Penn State would demonstrate the framework for the proposed technique by the end of the first year. Second, Penn State might reduce the demonstrations from two to one due to time constraints. However, the demonstration sites must include a trona mine. This request was due to MSHA's geographical consideration of its void detection program as well as demands by the trona industry.

On August 24, 2004, MSHA and Penn State further discussed how to modify the proposal. During the meeting, Penn State expressed to MSHA that it was willing to have two field demonstrations during the first year: one at a trona mine and one at a coal mine. Even though

Penn State knew that the plan might be somewhat too ambitious, which would stretch Penn State to its limit, the benefit of the plan was too significant to be ignored. With this plan, MSHA would have some preliminary data on how the ISS technique would work for both trona and coal mines at the end of the first year and valuable information for MSHA to assess the ISS based void detection techniques for its void detection program.

The use of Harmony Mine as a testing and demonstration site at the initial stage has several advantages. First, the mine, as many others, faces the problem of void detection as it approaches an abandoned mine in several years. The identification of a reliable and economic void detection technique has become a real issue for the mine. Second, the site is suitable for testing the ISS based void detection technique as it is a coal mine (technically, void detection under the trona mine condition is not ISS based). Although the mine is not a bituminous mine, they are similar from the ISS technical point of view in that the seam is much weaker than the country rocks.

In addition to these technical considerations, the operational advantages of the site can not be underestimated. Because of its short distance from the Penn State campus, about two-hour drive, it is much easier for Penn State to carry out the testing at this site and address any problems encountered. If a mine is remote, such as the trona mines in Wyoming, logistics present an additional problem. A particular advantage to use anthracite coal Harmony Mine is the enthusiastic support by the mine owner and mine management, which, as shown by our experience, was invaluable for the smooth start and progress of this project.

Based on the guidance given by MSHA and the discussion between MSHA and Penn State on July 28 and August 24, 2004, Penn State modified its proposal and submitted MSHA a *Revised working plan* on August 25, 2004. With the *Revised working plan*, the project is divided into three phases. The focus of the *Revised working plan* is Phase I (first year). According to the plan, Penn State would give two demonstrations: one at a trona mine and one at Harmony Mine. Seven field tests were planned for this phase: three at trona mines (including the demonstration), three at anthracite coal Harmony Mine (including the demonstration) and one at a bituminous mine.

The proposed final product for phase I is a preliminary version of the guidelines for the ISS based mine void detection technique which includes experimental design, the associated data analysis procedure, and the database for key ISS parameters.

The *Revised working plan* provided a balanced approach for the project. It emphasized void detection for the trona mine condition which was consistent with MSHA's priority. Meanwhile, it provided Penn State an opportunity to work in coal mines. The void detection in coal mines is the central issue that MSHA would like to address. On October 8, 2004, MSHA approved the *Revised working plan* and awarded Penn State a three-year contract for demonstration of the proposed technique.

1.3 Technical scope of the project

In order to understand the technical scope of the project, we need to discuss two important issues: the technical meaning of the ISS based void detection technique as used for this project and the development of the techniques required for the ISS based void detection technique.

1.3.1 Technical meaning of the ISS based void detection technique as used for this project

The term of *in-seam seismics* conventionally refers to the methods which utilize channel waves. Channel waves are commonly known as the waves which are "trapped" in weak seams. The advantage to use "trapped" waves is that their energy is better preserved and therefore these waves can be detected over much larger distances in comparison with those radiating three-dimensionally.

A necessary condition for developing channel waves is that the wave propagation velocity in the seam under study must be much lower than in the country rocks. This implies that the seam must be much weaker than the country rocks. It is for this reason that the ISS technique has been often used in coal mines as coal, in general, is much weaker than roof and floor. When the ISS based void detection technique is used in coal mines, the idea is that one may have the better chance to detect voids as "trapped" waves can travel the longer distance.

When the seam under study is stronger than the country rocks, as the trona mine condition, there will be no "trapped" waves which could be developed and utilized for void detection. The void detection under this condition, technically, is no longer ISS based as the waves used for void detection are conventional P- and S-waves, not "trapped" ones.

The impact of using non-channel (trapped) waves for in-seam void detection can be viewed from two aspects. First, it no longer possesses the basic advantage of the ISS method by using the better preserved signals. Signal detection in this case, in general, is much more difficult because waves propagate three-dimensionally. Second, the signals used for void detection as well as the associated data analysis methods are significantly different. The reflected waves are a special type of Love waves for the conventional ISS based method while they can be several body waves, such as P-waves, S-waves and converted S-waves, but not channel waves, for the non-ISS condition, such as trona mines. Because of these basic differences, the ISS based and non-ISS based void detections are technically two different approaches.

Because of these differences, it is understood that the ISS based void detection technique as used for this project should not be conventionally interpreted as in-seam seismic based, or ISS based. Rather, it should be broadly understood as the void detection method which may use either channel waves or body waves (P- and S-waves) traveling within the seam, depending on the relative condition of the seam and its country rocks.

Although the void detection with in-seam body waves is a non-conventional approach and presents an additional challenge to the project, the study of the technique is important as it is needed for a frequently encountered mining condition: seams are stronger than the country rocks. For trona mines, the need for a reliable geophysical method for void detection is even more urgent as mechanical drilling, a primary method used by coal mines, is not practical for the trona

condition (mechanical drilling may induce water into the pillar under concern, causing pillar degradation).

1.3.2 Development of techniques for ISS based void detection technique

It has been fifty years since Evison's in-seam experiment (Evison, 1955). The experiment, which led to the discovery of "guided waves may find useful applications in mining", marked the beginning of the ISS technique.

During the past fifty years, the in-seam seismics has grown into a recognized science and engineering discipline. The basic theory and method of the ISS technique were well summarized and elucidated by Dresen and Ruter in their book: *Seismic Coal Exploration, Part B: In-seam Seismics* (Dresen and Ruter, 1994). Among researchers who contributed the development of the ISS technique, Evison (1955), Krey (1962, 1963, 1976a, 1976b), and Brentrup (1970, 1971, 1979a, 1979b) are considered the representatives of the early developers. The ISS research in US stared in 1960s. The early work included Leitinger (1969), Darken (1975), Guu (1975), Su (1976), Young (1976), etc. Among the recent studies, the work by Rodriguez is most notable (Rodriguez, *et al*., 1994; Rodriguez and Naumann, 1995; Rodriguez, 1996).

The past work has laid a solid foundation for the current project. However, like the past work, a new application, such as the demonstration of the ISS based void detection technique, will not be a simple application of the existing technique. In order to adopt the ISS technique for the purpose of void detection, a range of the technical and practical problems have to be addressed. Four of them are of particular importance, namely retrievable sensor installation technique, experimental design, signal analysis, and void mapping.

Retrievable sensor installation technique

Among many challenges faced by the project, the first and probably the most critical one is the retrievable sensor installation technique. To be a technique which is capable of void detection, it has to be able to acquire high frequency signals over large distances. This usually requires grouting entire sensors in boreholes in order to achieve the better coupling effect. However, to be economically feasible, sensors must be retrievable, that is, they can be repeatedly used at same or different locations. The development of a reliable retrievable sensor installation technique is therefore pivotal for the project.

Experimental design

One of the main issues discussed in Penn State void detection proposal is how to avoid the problem of ambiguity that is commonly encountered with geophysical methods. The geophysical methods are convenient and relatively inexpensive, and can be very efficient if used properly. The methods, however, can be very vulnerable because of two reasons: 1) the data is often unrepeatable, inconsistent, and inconclusive, and 2) the result and conclusion depend heavily on how the data is interpreted. If a geophysical method is to prove reliable for void detection, the problem of ambiguity must be adequately addressed.

A fundamental approach to deal with the problem of ambiguity is a sound experimental design. Experimental design has a basic effect on accuracy and reliability as it determines the stability of the associated mathematical system and the degree to which the data can be resolved.

Unfortunately, the focus on geophysical methods has been mostly on data analysis and little attention has been given to experimental design. This unbalanced approach has resulted in many severe and even catastrophic results, as two high profile cases given in our original proposal: the microseismic monitoring of rockbursts and a major geotomography program in Canada (Ge and Laverdure, 1995). Emphasizing experimental design is a major strategy for improving the accuracy and reliability of the ISS based void detection technique.

Signal analysis

Signal analysis is a difficult problem which involves a large array of issues. One of the basic problems for the ISS based void detection technique is separation and identification of the reflected signals. For instance, the reflected signals in trona mines may include P-wave, S-waves and S-waves due to conversion. To be able to use these waves for void detection, one has to 1) separate them from the background noise, 2) identify the wave type for each signal, and 3) determine the incident direction. In order to do so, some specialized techniques have to be developed.

Void mapping method

The principal imaging approaches used by the ISS method are signal stacking and seismic tomography. Both approaches, however, present some serious problems for void mapping.

Signal stacking is a basic data analysis method for mapping geological structures. In order to use a stacking method, receivers and sources have to be on a straight line and to be equally spaced. These requirements create a problem for the ISS based void detection. The locations of receivers and sources for void detection in underground have to be arranged with the consideration of the local conditions. It is in general very difficult to make these locations fit a rigid pattern as required for signal stacking procedures. Although the corrections may be made, they are limited to small deviations. For large deviations, the corrections may not possess any physical meaning even they could be done mathematically.

Seismic tomography is a technique which is widely used to image geological structures, from global earth structures to local mine anomalies. An important application condition for the technique is that the area under study has to be well surrounded by survey stations (receivers and sources). The ISS based void detection is characterized by the survey line on one side of voids and, therefore, is not appropriate for the method.

In addition to these restrictions, an efficient void mapping method has to be able to accommodate several special requirements, which are: 1) simultaneously using different types of reflected signals, 2) simultaneously using reflected signals from different surveys, 3) no limitations on the locations of seismic sources and receivers, and 4) suitable for delineating irregular void boundaries. It is clear given these considerations that a different approach is needed.

1.4 Report structure

The main body of this report is the presentation of seven field tests, including two demonstrations. These tests will be discussed in chapter 3 – 9 with each chapter covering a field test.

Chapter 2 will be used to outline the techniques and methods which were developed and/or used for the ISS based void detection. For the detailed discussion, readers may refer to the User's Manual since most of these techniques and methods are essential for the ISS based void detection, the approached used by Penn State.

Our assessment of the status of the project as well as recommendation for future work is given in Chapter 10, the last chapter of this report.

There are two appendices, Appendix I and Appendix II. Appendix I lists all of the equipment and software used in the project, and Appendix II lists the main directories of the recorded data which are contained in a CD included with the report.

1.5 Penn State project team

Members of Penn State project team for Phase I:

Dr. Maochen Ge,	PI, Associate Professor of Mining Engineering,
Dr. Andrew Schissler	Co-PI, Assistant Professor of Mining Engineering,
Dr. Mark Radomsky	Director of Field Services, Miner Training Program
Dr. H. Reginald Hardy	Professor Emeritus,
Dr. Raja Ramani	Professor Emeritus
Mr. Hongliang Wang	Graduate Research Assistant, PhD Candidate,
Mr. Jin Wang	Graduate Research Assistant, Master of Science Candidate

2. Technical development for ISS based void detection

2.1 General

The successful application of the ISS method for void detection in underground environment is not simply an application of the original ISS technique as this environment presents unique issues that have to be addressed.

To make the ISS based void detection technique in such situations a reliable and practical industrial tool, a number of technical issues have to be resolved. Development work in Phase I prioritized the issues which were deemed critical to field testing and data analysis. As this development work was substantial and highly relevant for the techniques demonstrated in this study, it is an important part of this research project. This chapter provides a general summary of these techniques. The discussion given in this chapter will also facilitate the reader's ability to review subsequent chapters.

2.1.1 An overview of the techniques developed

Most of the techniques developed during Phase I were used to support either field operations or data analysis needs. These techniques are:

- retrievable sensor installation technique,
- experimental (source-receiver configuration) design,
- signal analysis, and
- elliptical void mapping.

As these techniques are also major components of the ISS based void detection technique demonstrated by Penn State, they are discussed in detail in the *User's manual: ISS based void detection*, which is attached to this report. To avoid repetition, discussions in this chapter provide only a brief introduction to these techniques.

During Phase I, Penn State engaged in three studies that went beyond the techniques routinely utilized in the ISS method including non-explosive seismic sources, simple mechanical impact systems (SMIS), and retrievable three-dimensional sensor installation techniques. These studies are exploratory and preliminary, but they have potentially important applications for the ISS based void detection. The status of work on these techniques will be given in this chapter.

Another important technique to be discussed in this chapter is laboratory velocity measurement. This work is not apparent for the ISS method, but is essential for ISS based void detection.

2.2 Retrievable sensor installation technique

Sensor installation is a critical component of the ISS based void detection technique. To be a technique capable of void detection, it has to be able to detect high frequency signals over large distances. This usually requires grouting entire sensors in boreholes to achieve better coupling effects. However, to be economically feasible, sensors must be retrievable, that is, they can be repeatedly used at the same or different locations. The retrievable sensor installation technique was developed to address these concerns.

2.2.1 Retrievable sensors

A retrievable uniaxial sensor consists of two parts, a sensor body and a screw assembly (Figure 2.1). The screw assembly is the anchor of the sensor, grouted at the bottom of the sensor hole. Figure 2.2 is a schematic illustration of a retrievable sensor installed at the bottom a borehole.

Figure 2.1 A retrievable uniaxial sensor consists of a sensor body and a sensor anchor made of a screw assembly.

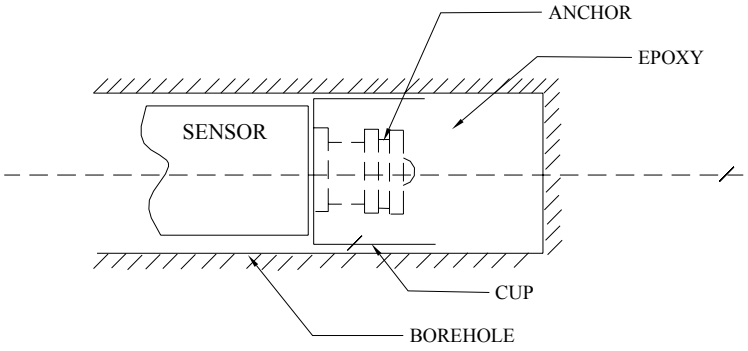

Figure 2.2 Schematic illustration of a retrievable sensor installed at the borehole bottom.

2.2.2 Components of retrievable sensor installation technique

For the ISS based void detection technique, the basic requirement on sensor installation is that the installed sensors must be able to acquire broadband signals over large distances, including high frequency signals. This implies that the installation technique has to be able to deliver superior coupling effects between sensors and surrounding rocks. The retrievable sensor installation was developed as a convenient and efficient tool for this purpose.

The retrievable sensor installation technique has five basic components: epoxy, installation devices, simulation facility, field work procedures, and pull-out test. Epoxy is used to grout sensor anchors at the borehole bottom. Installation devices are the hardware used for sensor installation, which include an epoxy mixing device, installation assembly and installation tool kit. . The simulation facility is used for two purposes: sensor installation training and evaluation of in-situ anchorage strength. The field work procedure deals with the work involving sensor-hole preparation and sensor installation. The pull test is a quantitative means to assess various parameters related to sensor installation, which is the basic technique used for developing the retrievable sensor installation technique and will be discussed first. The detailed discussion of the technique is given in Chapter 4 of *User's manual*.

2.2.3 Field applications

The retrievable sensor installation technique was used for all seven field tests carried out by Penn State. It is simple and convenient for both installation and retrieval operations. Figure 2.3 shows sensor installation by the Penn State crew at the Harmony Mine. Most importantly, the technique is reliable for acquiring broadband signals, including high frequency signals. The signals shown in Figure 2.4 are the reflected S-wave signals recorded at General Chemical trona mine. The dominant frequency for these signals is 2500 Hz. The amazing fact about these high frequency signals is that they had traveled 700 ft. Without a superb coupling effect, this would be impossible. All our field tests have demonstrated that the performance of the technique is predictable, consistent, and repeatable.

Figure 2.3 Installation of a retrievable sensor at the Harmony Mine.

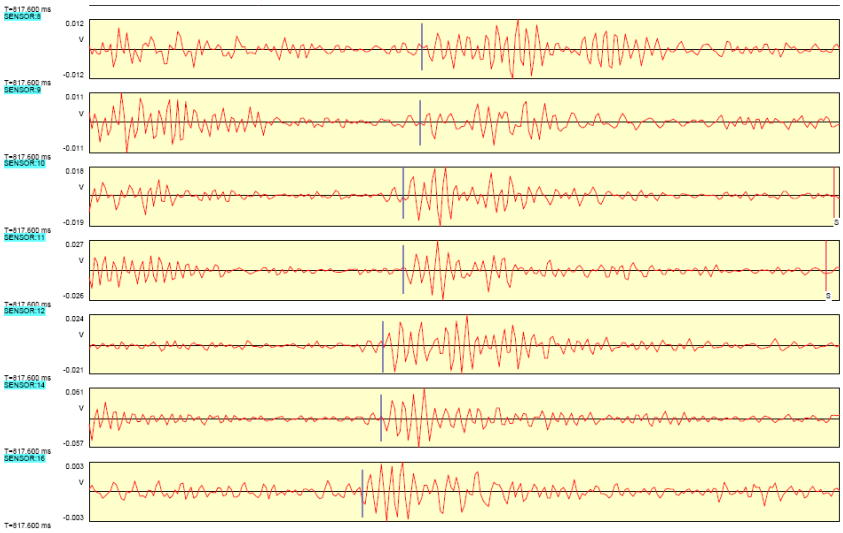

Figure 2.4 The reflected signals detected at the General Chemical Trona Mine, which have the dominant frequency of 2500 Hz with a travel distance of 700 ft.

2.3 Experimental design

One of the main issues discussed in the Penn State void detection proposal is how to avoid the problem of ambiguity that is commonly encountered with geophysical methods. A fundamental approach to deal with the problem of ambiguity is a sound experimental design. Based on both theoretical research and field test experience, a systematical approach was developed to address this problem. From a theoretical point of view, experimental design should be considered from four aspects: adequate coverage of the target area, sufficient survey resolution, stability of the associated mathematical system, and facilitation for data analysis.

On the practical side, based on both the theoretical considerations and the problems pertaining particularly to the ISS survey environment, Penn State outlined five special design issues as well as corresponding solutions. These five issues are: 1) choosing a suitable site for sensor installation, 2) reducing the impact of direct arrivals, 3) reducing the impact of (air) shock waves, 4) reducing unwanted reflected signals, and 5) improving signal strength.

In an effort to optimize the experimental design, Penn State conducted two specific theoretical studies: sensitivity analysis and angled sensor pairs.

2.3.1 Sensitivity analysis

Errors in input data, such as signal arrival time and signal travel velocity, are inevitable. The effect of these errors on the void detection accuracy largely depends on the experimental setup. Because of the fundamental importance of this, a theoretical study was initiated to assess the effect of the test setup on the accuracy and reliability of void detection.

The study shows that the survey error on the void distance is governed by the relative dimension of the void distance and the distance between the receiver and the source, which is shown by Figure 2.5. It can be seen from the figure that the sensitivity of the void mapping error, Δh, is governed by θ approximately. If this angle is small, a minor initial error could cause a large survey error. Therefore, the distance between the source and the receiver, theoretically, should be as small as possible.

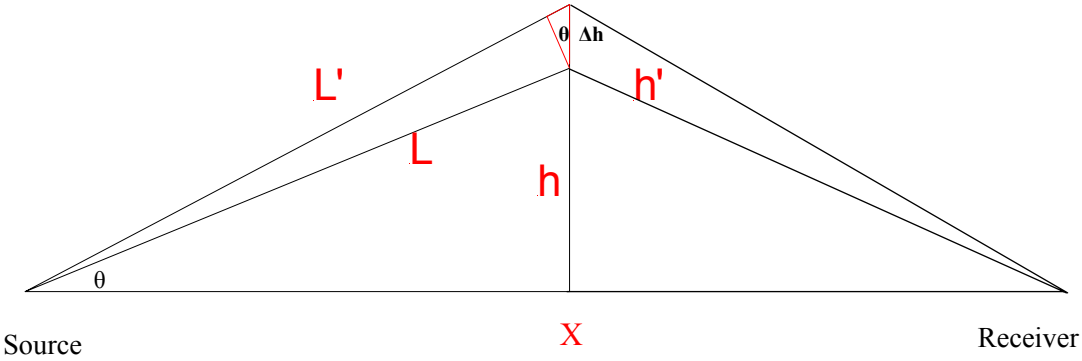

$$\Delta h = \frac{\Delta L}{Sin\theta}$$

Figure 2.5 Sensitivity analysis: the impact of the initial error on the result of reflection surveys.

2.3.2 Angled sensor holes

The ISS technique relies on positive identification of incoming signals, including wave types/ wave groups and their incident directions. With a single trace information (waves from one component sensor), this identification work is generally difficult, and often impossible. A basic means to solve this problem is to use three-dimensional (3D) sensors. A major difficulty with the use of 3D sensors for void detection is the problem of suitable field installation. Conventionally, 3D sensors have to be installed in cement filled boreholes. This technique provides intimate sensor-to-rock coupling. However, it also prevents removal of the sensor for use at other locations. The relatively high cost of 3D sensors, $1000 – 2500 each, makes it impossible to use 3D sensors for the ISS based void detection at present.

A simple and efficient solution for this problem is to use a pseudo-2D sensor arrangement. With this arrangement, sensor holes are drilled in pairs. These pairs are oriented orthogonally, with the tips of the borehole located very close to one another. The operational principle of the pseudo-2D sensor is shown in Figure 2.6. With the given arrangement, the sensor on the left of each pair is more sensitive to the P-waves while the one on the right is more sensitive to S-waves.

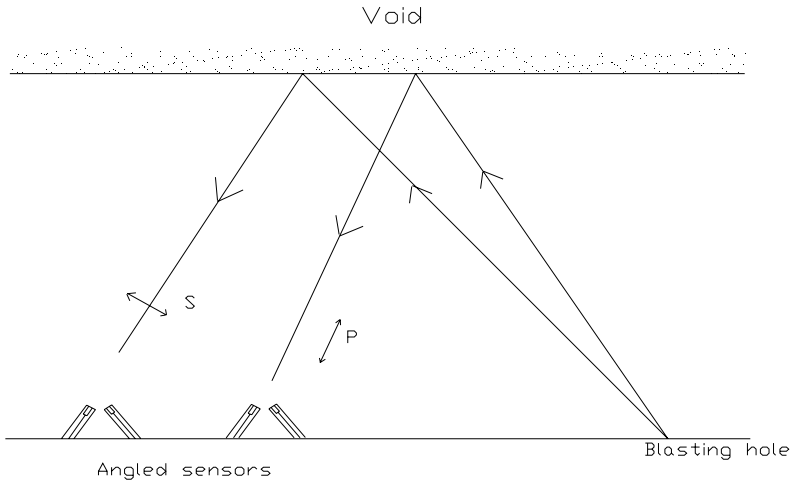

Figure 2.6 Using angled sensor pairs for polarization analysis.

The technique of angled sensor pairs provides a simple and efficient means to study signal polarizations which is shown in the following example.

Figure 2.7 shows the experimental setup and the acquired signals from a transmission survey carried out at a trona mine, where the concept of angled sensor pairs was used. The pillar was about 290 ft wide. The sensor section and the blasting section were offset about 150 ft horizontally. The incident angle corresponding to this arrangement was about 30 degrees. The orientations for the seven sensor holes are clearly shown in the figure.

From the direction of the transmission signals and the orientation of the sensor holes, it is known that sensors S7 and S5 should be most sensitive to P-waves, but less sensitive to S-waves. This is because they are oriented in almost the same direction from which the transmission signals propagate. On the other hand, S1 and S3 should have the opposite sensitivity because of their orientation. They should be more sensitive to S-waves instead of P-waves. The acquired signal waveforms for these sensors are shown in Figure 2.7b, which are almost a perfect confirmation of the design expectation.

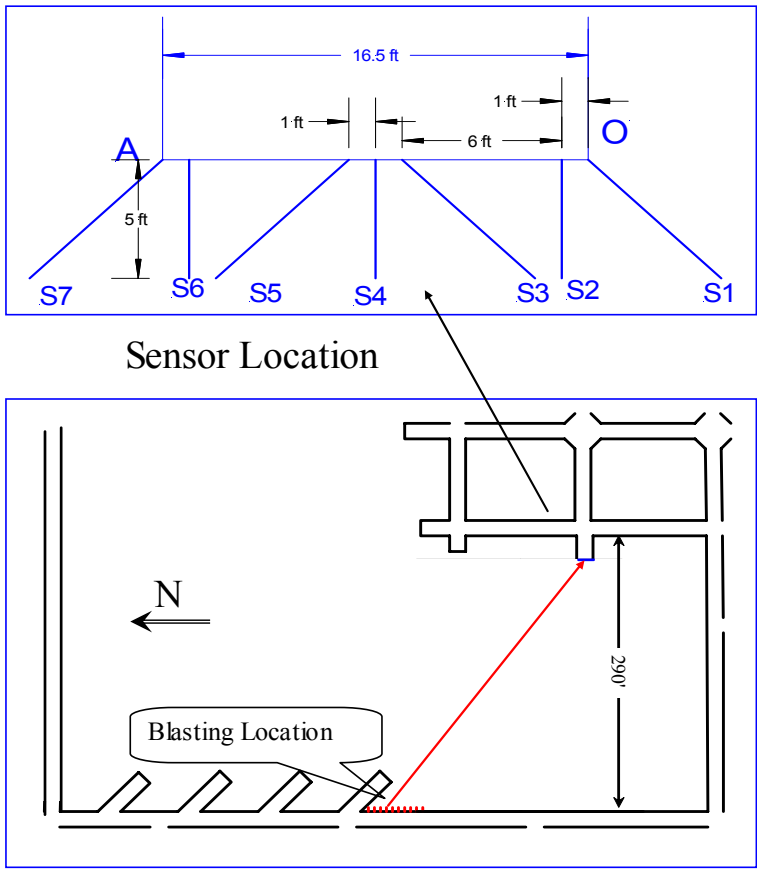

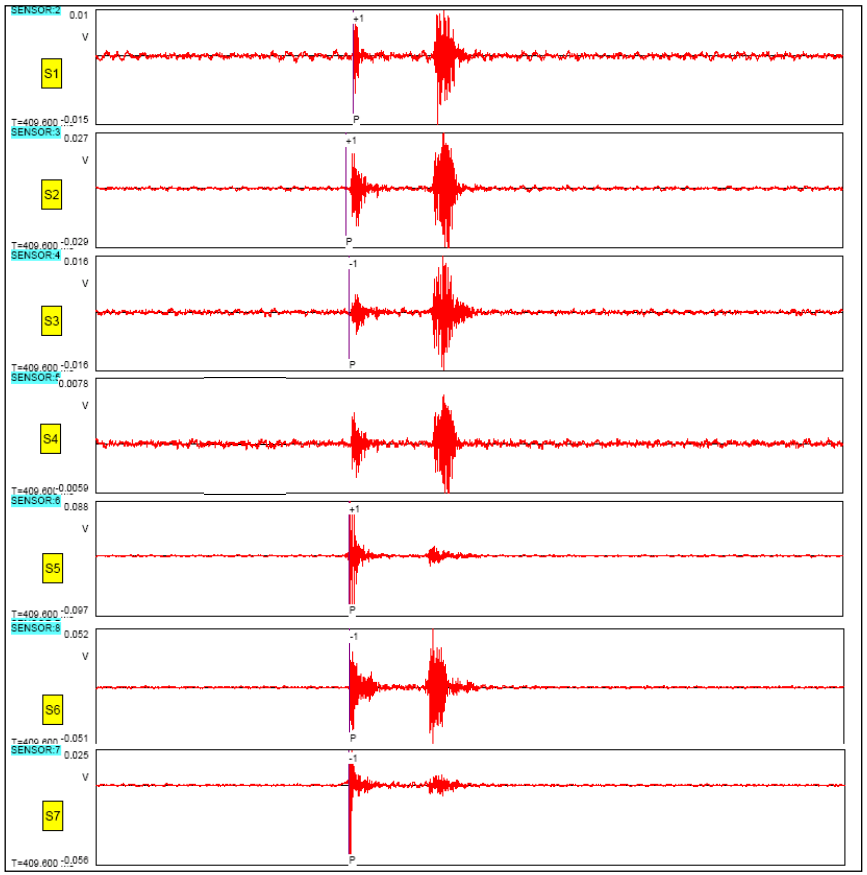

a. Experimental layout.

b. Transmission signals.

Figure 2.7 Transmission survey carried out at a trona mine, where the concept of angled sensor pairs was used.

2.4 Signal analysis

Signal detection is another critical aspect of the ISS based void detection. In comparison with conventional exploration seismology, there is another aspect of the ISS based void detection: the underground environment. The efficiency of data analysis largely depends on whether the related issues can be addressed. Similar to the experimental design, a systematic approach was developed to signal detection, which was discussed in detail in Users Manual.

The approach includes five general steps, which are 1) data collection, 2) reading original waveforms, 3) typical wave trends associated with the ISS based void survey, 4) signal frequency analysis for void detection, and 5) identification of P- and S-waves.

2.4.1 Signal arrival trends

In comparison with conventional exploration seismology, a major difference for the ISS based reflection survey is the existence of multiple arrival trends for each reflection survey, which include direct arrivals, reflected wave arrivals, and (air) shock wave arrivals. The trend for the reflected waves can be either positive or negative, depending on the relative position of the void and the survey line. In addition, some reflected signals may be caused by nearby underground workings, not the void. Understanding these arrivals and knowing the characteristics associated with these trends are important for identifying the signals reflected from voids.

Trend of direct arrivals

Direct arrivals are the first wave arrivals which reach to the sensors directly from the seismic source. The impact of the direct arrivals on signal detection is two-fold. First, they may interfere with the arrivals of reflected signals because of their long duration. Second, direct arrivals often have the much higher amplitude and tend to dominate the signal record. Figure 2.8 shows two such examples.

Trend of reflected arrivals

The other major difference between the ISS based survey and the conventional exploration seismology is the trend of reflected arrivals. During the ISS survey, one may observe both positive and negative trends, while, for a great majority of applications, especially for the conventional exploration seismology, positive trend is the only case to be considered. A positive trend means that the receiver which is closer to the source gets the reflected signal earlier. Negative trend refers to the opposite situation. A negative trend can be caused by either an actual void or mine openings at the survey site. Such an example is shown in Figure 2.9.

The example is a reflection survey carried out at a trona mine. It is seen from the figure that there are two trends, a positive one and a negative one. The corresponding ray paths for these reflected signals are shown in Figure 2.10. The positive one is due to the signals reflected from the void and the negative one is caused by a mine opening in the survey area.

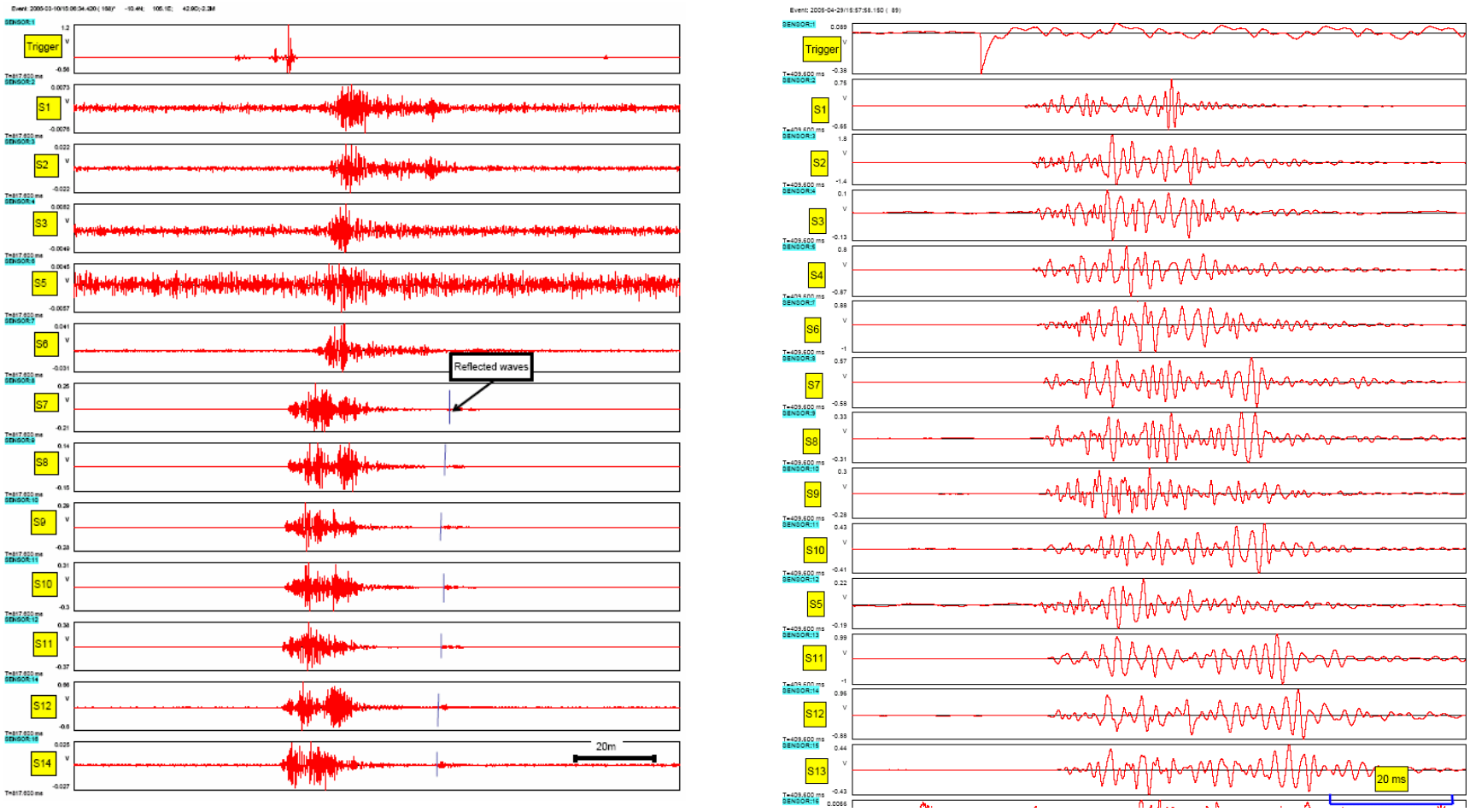

a. Event 168, reflection survey at General Chemical trona mine. b. Event 89, reflection survey at Site II, Harmony anthracite mine.

Figure 2.8 Waveforms showing direct arrivals from reflection surveys, which are strong and exhibit long duration signal signatures.

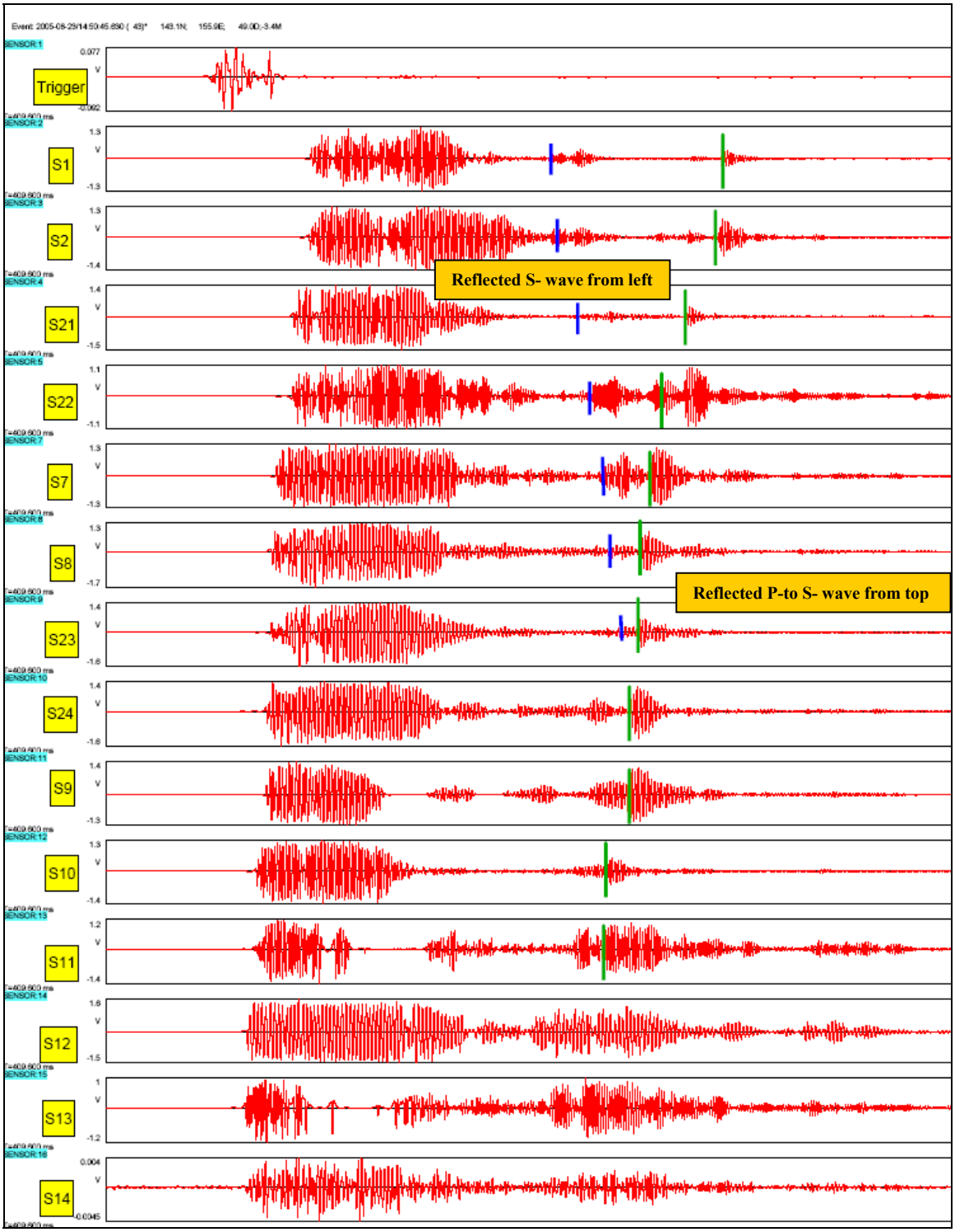

Figure 2.9 Signals associated with an ISS survey at a trona mine (display window: 65 - 86 ms for event 118).

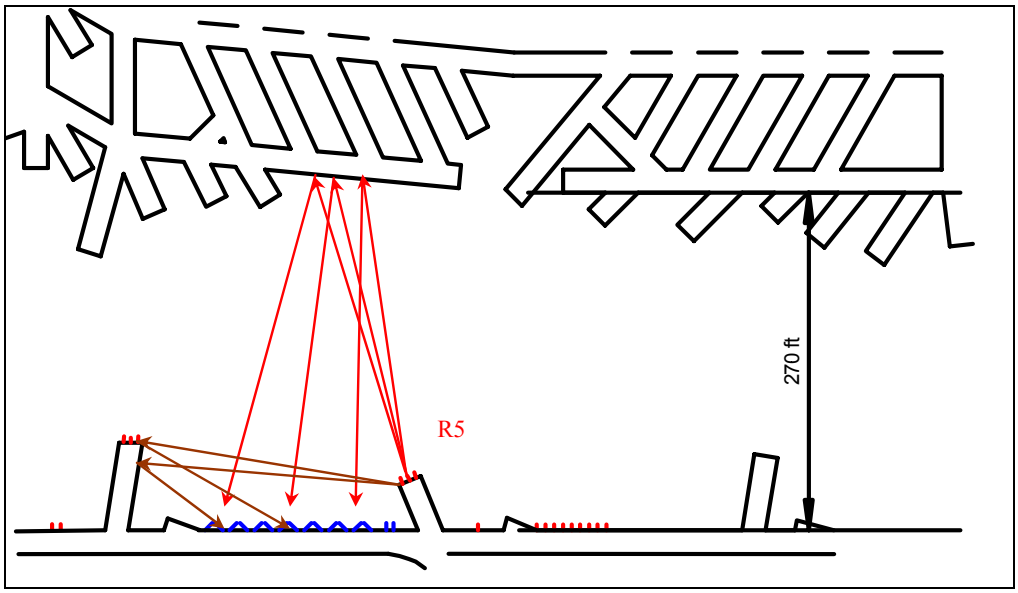

Figure 2.10 Test setup for event 118 and ray paths from top and left reflectors.

Trend of air waves due to blasting

Because the ISS based void detection is carried out in underground workings, the blasting caused air shock waves may severely affect survey results. Similar to direct arrivals, strong shock waves can significantly reduce system sensitivity. The worst situation is that the shock waves are strong and they arrive earlier than the reflected waves. When this happens, the reflected signals, which are usually weak, are most likely buried by the shock waves and can not be identified. Figure 2.11 shows such an example.

Because of their severe effect, measures have to be taken to reduce the magnitude and impact of shock waves. There are three possible measures. The first one is to seal sensor holes with insulation materials, which should be a standard operational procedure. The second one is to reduce the amount of explosives to be used if possible. The third one is to place blasting holes in different entries if it is feasible. The third measure is a very effective means based on our experience.

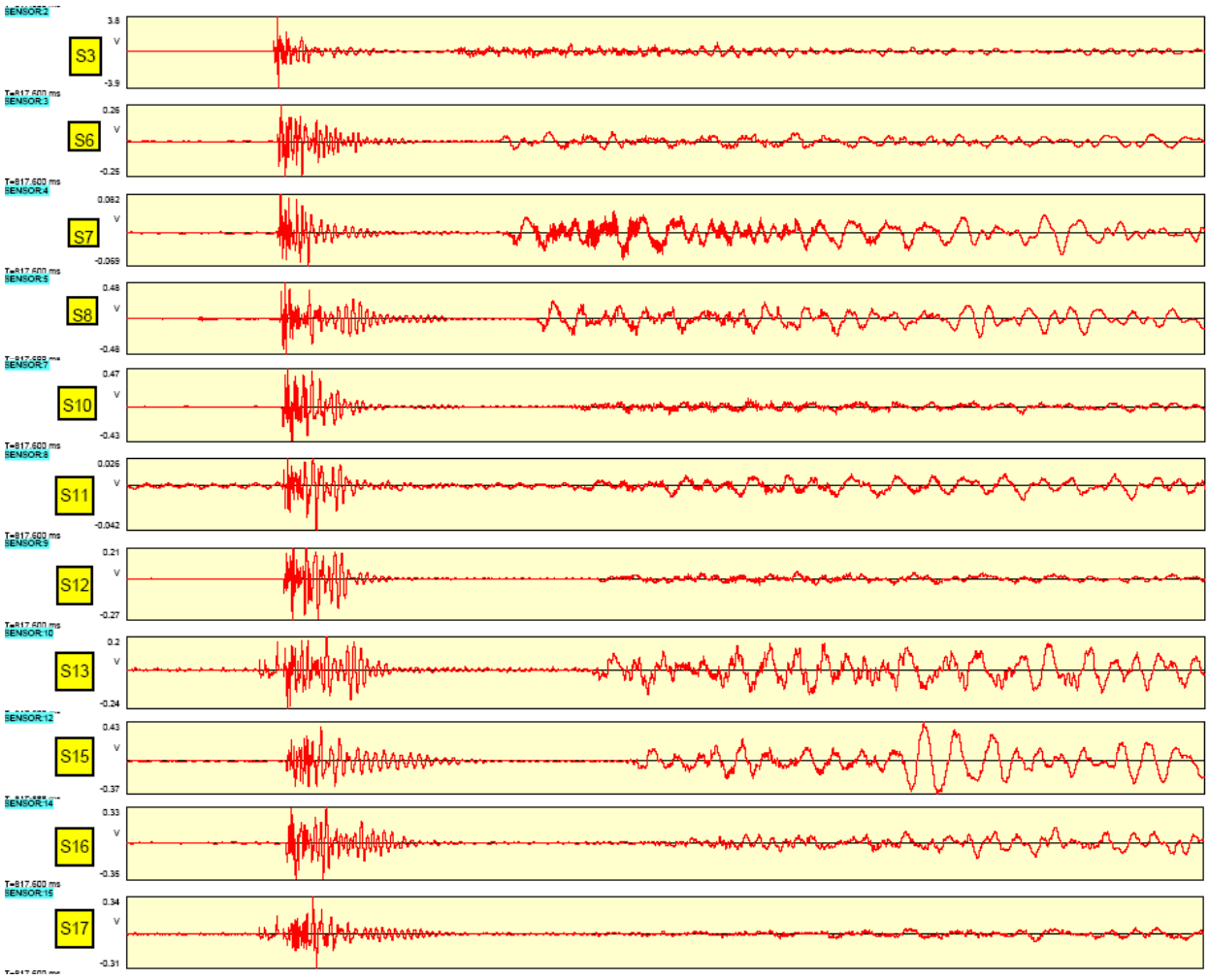

Figure 2.11 Air shock waves recorded during a reflection survey at a bituminous mine.

2.4.2 Wavelet analysis

One of the basic problems for the ISS based void detection technique is separation and identification of the reflected signals from others. Wavelet analysis, a mathematical tool for studying non-stationary frequency characters, provides an ideal means for detecting newly merged signals. With the help of a 3D display of wavelet transform, many reflected signals, which are difficult to see in the original waveforms, can be identified.

Case study of wavelet analysis: delineating direct and reflected channel waves

The example given in Figure 2.12 is to show how to use the wavelet technique to separate channels waves. The figure consists of three parts. The top one is the original signal, which contains two groups of channel waves. The first was a direct arrival and the second one is a reflected arrival. It is seen from the figure that the arrival of the direct channel wave is mixed with S-wave arrivals earlier through the roof. The middle waveform is the wavelet transform coefficient (or amplitude) at the frequency (500 Hz). Gabor wavelet was used for the transform. The bottom one is the wavelet transform. The arrivals of two channel waves are indicated by two sharp onsets shown by part *(b)*.

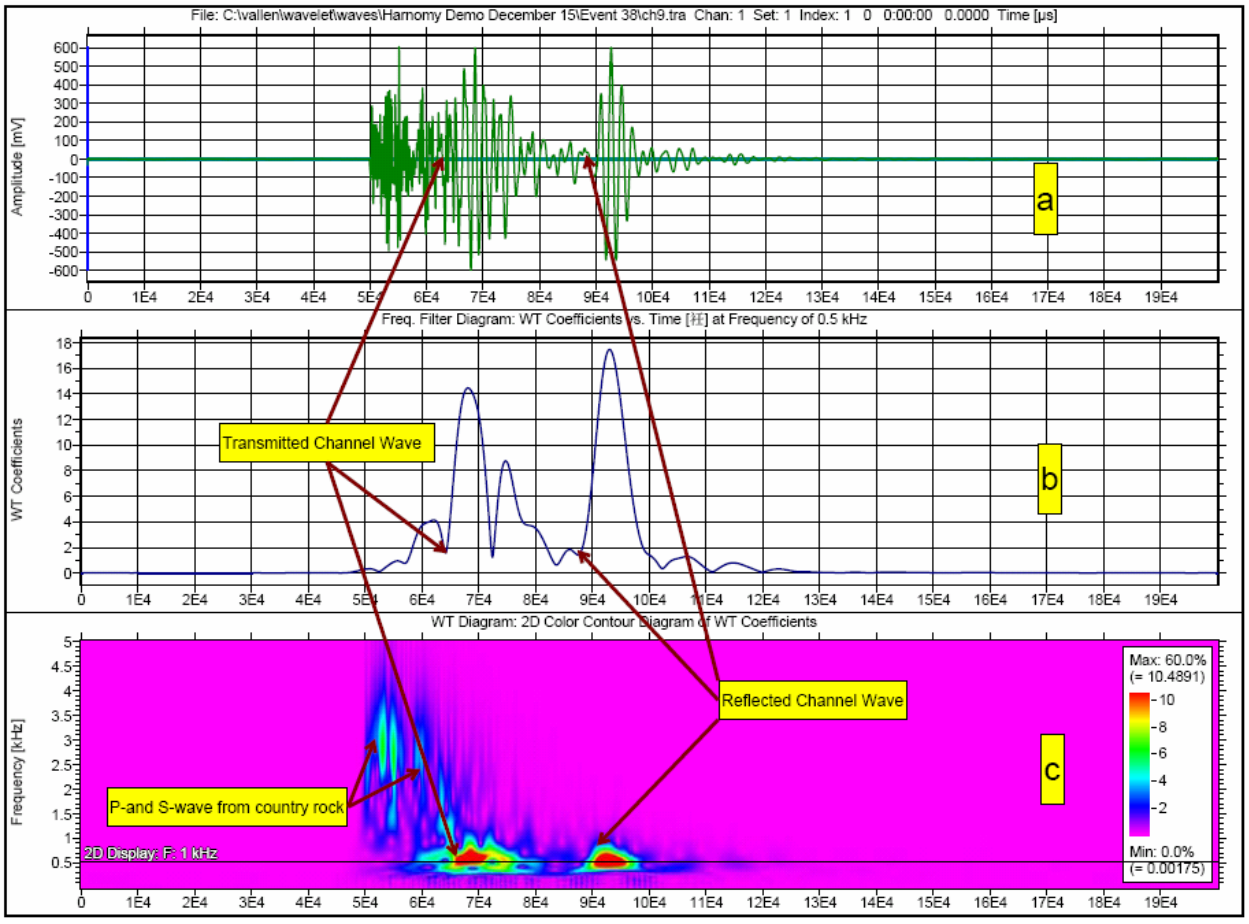

Figure 2.12 Application of wavelet transform for the ISS based void detection: timing the arrivals of direct and reflected channel waves (plot *(a)*: original waveform of channel S8 of event 38; plot *(b)*: filtered wavelet transform coefficient at frequency indicated in plot *(c);* plot *(c)*: 2D color contour of wavelet coefficient).

2.5 Elliptical void mapping method

Imaging the void location with the reflected data is the final step of the ISS based void detection method. An important decision for this project is to use the elliptical method as the principal imaging tool for void detection.

2.5.1 Method concept

An ellipse is a trace such that the sum of the distances from any point of the trace to the two points is a constant. These two points, which are represented by F1 and F2 in figure 2.13, are called foci of the ellipse.

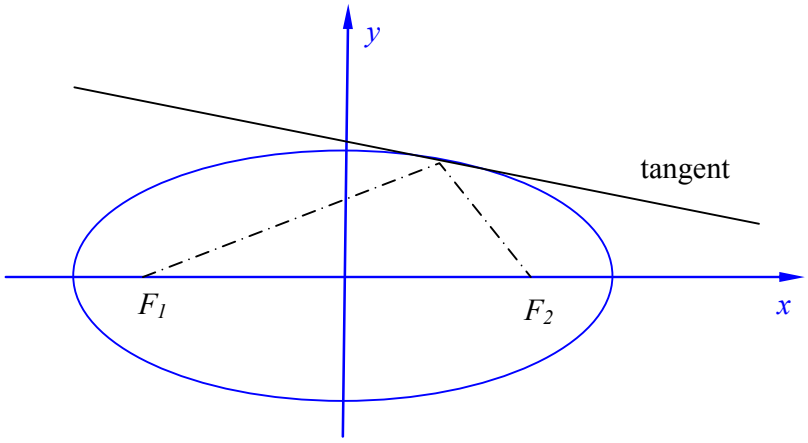

Figure 2.13 An ellipse, its foci and reflecting property.

It is known that reflection survey relies on two pieces of information: locations of seismic sources and receivers, and signal travel distances between sources and receivers. If we consider a source and a receiver as the foci and use the signal travel distance as the sum of the distances, it is immediately known that an ellipse is uniquely defined and that the reflection point must be on the ellipse.

Furthermore, according to the analytical geometry, the ellipse not only defines the trace of the potential reflection point, but also the direction of the reflector, which is the tangent line of that point. This reflecting property is of critical importance for void mapping. Based on this property, the void can be delineated by a common tangent line and the idea is illustrated in Figure 2.14.

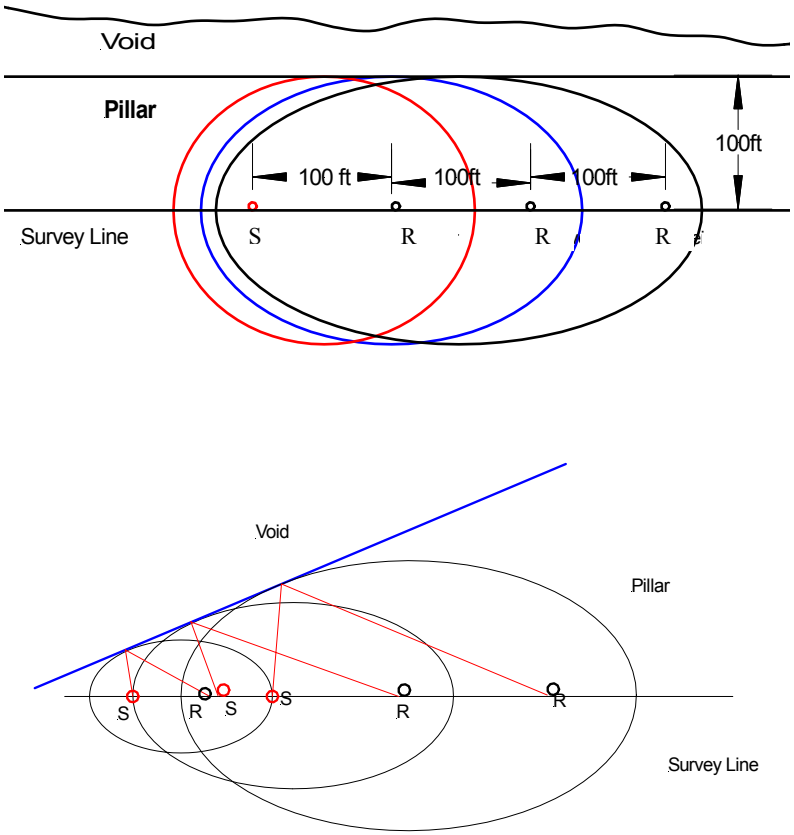

Figure 2.14 Delineating the void by the common tangent line of ellipses.

2.5.2 Advantages of the elliptical method for void mapping

The use of the elliptical method as the principal imaging tool for void detection is due to a number of considerations. The first and the most important one is the compatibility of the imaging method and the void detection condition.

The basic character of the experimental setup for the ISS based void detection is that the survey line is located on one side of the void. With this in mind, it is immediately known that seismic tomography is not a choice. An important application condition for the technique is that the area under study has to be well surrounded by survey stations (receivers and sources).

The testing setup for the ISS based void detection also makes it difficult to use the approach of signal stacking. In order to use a stacking method, receivers and sources have to be on a straight line and be equally spaced. These requirements create a problem for ISS based void detection. Although the corrections may be made, they are limited for small deviations. For large deviations, the corrections may not possess any physical meaning even they could be done mathematically.

In addition to this problem, the other major concern is the vulnerability of the geometry. With reflection surveys, the shape of the structure is viewed from one side, which makes the method

more sensitive to survey errors than other surveys which map the structure from multiple directions, such as seismic tomography. In other words, the approach is mathematically suspect. An important approach to deal with systems which are sensitive to initial errors is to avoid those mathematical manipulations which may potentially introduce new errors. Unfortunately, signal stacking is a process involving heavy mathematical manipulations and errors could be introduced at many "correction" stages. A simple example is the error which may be introduced at its first correction stage: moving all the seismic time traces to a reference line.

The elliptical method, however, does not have the potential pitfalls associated with the conventional methods. As the method represents the reflection data directly, it avoids many mathematical manipulations which might be requested otherwise. This character makes the method much more stable than any other methods. The method also provides an intuitive means to analyze the cause of missing data so that using the missing data becomes part of the process of void location.

In addition to its flexibility to accommodate testing conditions typically encountered in ISS based void detection, the method is also robust for data processing and offers a number of unique advantages, which include simultaneously using different types of reflected signals, simultaneously using reflected signals from different surveys, and suitability for dealing with irregular void boundaries. Finally, the method is simple and easy to use.

2.5.3 Application of the elliptical mapping method

The elliptical mapping method has been used as the principal imaging technique for the project. The main operational advantage of the technique is its data handling capability, which, as an example, is shown in Figure 2.15. From three distinctive groups of ellipses, it is known that the reflection data utilized are associated with three very different source locations. It is also known that they are the result of multiple seismic survey (blasting) operations. Furthermore, these ellipses represent not just one type of reflected signal; they represent three types of reflected signals observed at the site, including reflected P-wave, reflected S-waves, and reflected S-waves due to mode conversion. The importance of the unified expression of the reflection data is that it significantly enhanced the database for an optimized solution.

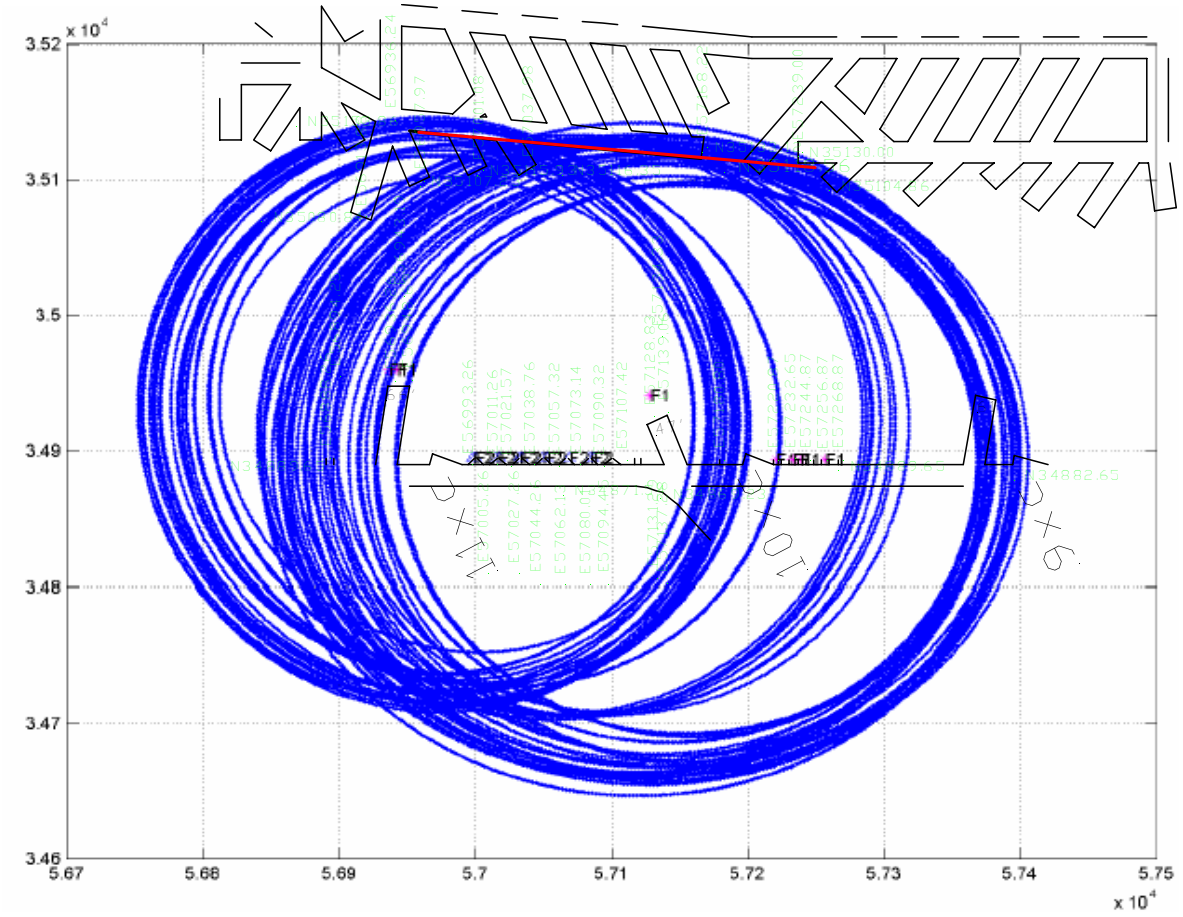

Figure 2.15 Elliptical void mapping at a testing site, where the void was delineated by the common tangent line represented by a red line segment.

2.6 Non-explosive seismic sources

The study of non-explosive seismic sources was carried out for two purposes: 1) identifying suitable methods for laboratory and field calibration studies, and 2) assessing the possibility of using non-explosive sources for reflection survey. This study was aimed for the long-term potential of the technique and was exploratory and preliminary at this stage.

2.6.1 Types of mechanical sources tested

The mechanical sources which were tested include:

- metal hammers (0.75 lbs) (Figure 2.16a),
- metal hammers (3.25 lbs) (Figure 2.16a),
- rubber-headed hammer(1.28 lbs) (Figure 2.16a),
- special non-rebound hammer (1.72 lbs) (Figure 2.16a),
- pneumatic source (Figure 2.16b), and
- Schmidt Hammer (Figure 2.16c).

a. Four different hammers.

b. Pneumatic source ("paint gun").

c. Schmidt hammer.

Figure 2.16 Types of the mechanical sources tested.

2.6.2 Laboratory testing facility and arrangement

The basic testing facility for non-explosive seismic sources includes a 2 x 2 x 12 ft^3 concrete block and an attached testing frame specially designed and constructed for this project (Figure 2.17a). Sensors may be installed at three general locations, depending on the testing need. One is at the top of the block where sensors can be installed in several existing sensor holes which were prepared during the construction of the block. The other two locations are the rear end and front end of the block (Figure 2.17 b & c). Special concrete panels were designed and attached to the block at these locations for sensor installation.

a. 2 ft x 2 ft x 12 ft concrete block and attached testing frame.

b. Sensors and sensor panel attached at the rear end of the block.

c. Sensor and testing panel installed at the front of the concrete block.

d. Using SMIS for a hammer impact test.

Figure 2.17 Testing facility and arrangement for non-explosive seismic sources.

2.6.3 Some observations from testing

The typical signals for the non-rebound hammer, Schmidt hammer and "paint" gun are given in Figure 2.18.

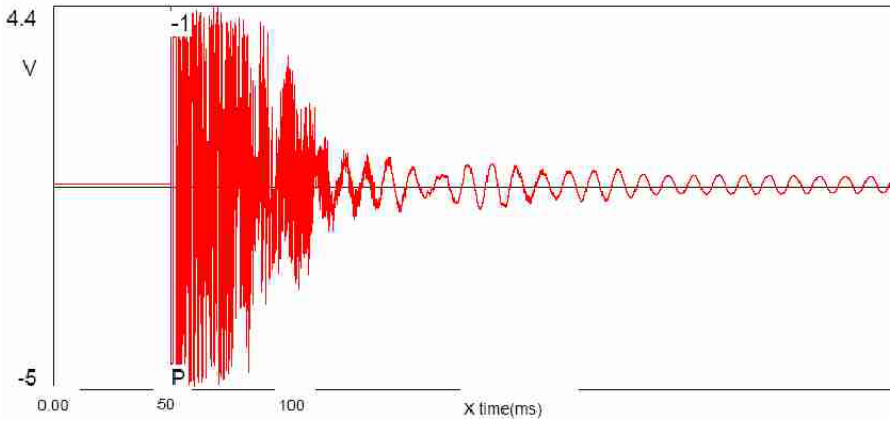

a. Signal from non-rebound hammer.

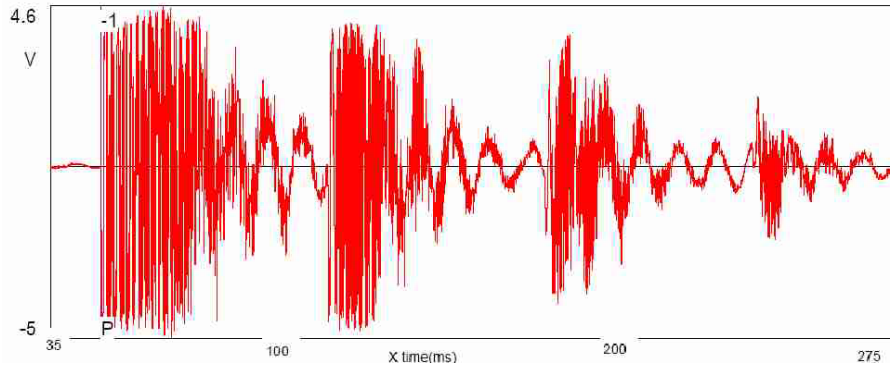

b. Signal from Schmidt hammer.

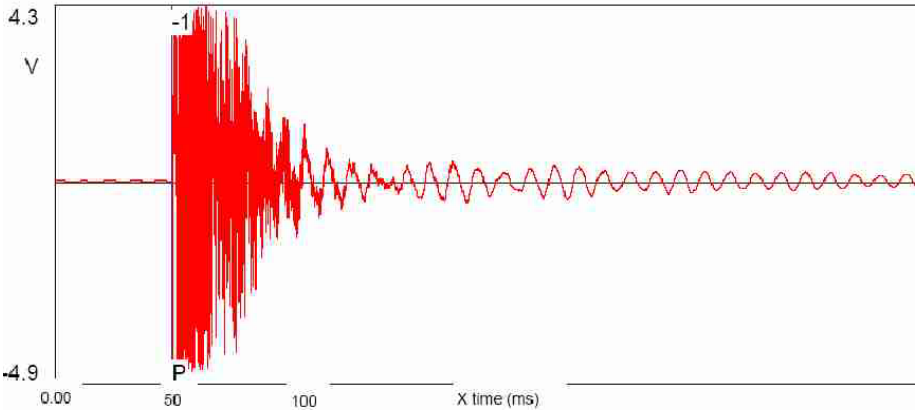

c. Signal from "paint" gun.

Figure 2.18 Typical signals for various non-explosive seismic sources.

Hammers

Four different hammers were tested as impact sources, which included two metal hammers with different weights of (3.25 & 0.75 lbs), a rubber-headed hammer (1.28 lbs), a special non-rebound hammer (1.72 lbs), and a "Schmidt Hammer", commonly used in geomechanics for evaluation of rock properties.

The large metal hammer, the rubber-headed hammer and the non-rebound hammer were found to provide relatively similar seismic signals. A typical example is given in Figure 2.18a. However each type of hammer exhibited a variety of unique frequency components. The frequency spectra of these types of hammers indicated significant energy up to at least 5 kHz.

Frequency spectra for all the above hammers showed a considerable amount of strong energy in the range of 100 – 1000 Hz. All hammers, except the non-rebound hammer, exhibited a strong peak in the range 500 – 600 Hz. The spectra of the non-rebound hammer was relatively low in the range 100 – 300 Hz.

Visual examination of the data from a number of consecutive impacts by a "trained operator", using the same type of hammer, indicated generally consistent results. However, variations in certain features were clearly evident.

All hammers were tested in the field at the Harmony Mine and significant impact signals (see Figure 2.25 in the next section as an example) were received.

Schmidt Hammer

Data obtained using the "Schmidt Hammer" was somewhat unique as the device appeared to generate a series of four or more separate seismic events for each activation (Figure 2.18b). Similar data was observed using the Schmidt hammer during the February 2005 field study at the Harmony Coal Mine site. This effect is considered to be a result of a rebound process within the mechanism of the Schmidt hammer itself.

"Paint gun"

A series of preliminary tests were carried out using a pneumatic source ("paint gun") to fire liquid-filled projectiles at the end of source boreholes as a means of generating seismic signals (Figure 2.18c). Here a block of concrete containing a 2 in. diameter closed-end borehole was mounted to the end of the borehole test frame developed earlier in the project. As in the earlier hammer tests, the sensor was located at the far end of the 12 foot long concrete block. PVC tubing which is 5 ft long and 2 in. O.D. was connected between the borehole in the concrete block and the end of the test frame. A series of test shots were fired along the PVC tubing in order to impact the bottom of the borehole in the concrete block (Figure 2.19). The muzzle velocity of the gun was approximately 300 ft/sec.

The time series plot for the paint gun test was found to be somewhat unique with a preliminary low level component appearing prior to the larger main body of seismic signal. This is assumed to be a result of the associated sound wave traveling at approximately 1086 ft/sec, reaching the bottom of the borehole ahead of the paint filled projectile which travels at the muzzle velocity, approximately 300 ft/sec. Examination of the frequency spectra associated with one of the tests

indicated considerable energy in the range 100 – 5000 Hz. Pronounced peaks were noted in the range 400 – 600 Hz and strong peaks were noted at 1.4 kHz and 3 kHz. The paint gun was also tested underground at General Chemical (Figure 2.20).

Figure 2.19 Laboratory test of paint gun.

Figure 2.20 Paint gun test at General Chemical.

2.7 Simple mechanical impact system (SMIS)

For a non-explosive seismic source to be a practical tool, there are two problems to be addressed: strength and repeatability. When a seismic source is generated by the mechanical impact at the pillar surface, such as the rib of a coal pillar, both the strength and repeatability will be difficult to achieve. The simple mechanical impact system (SMIS) was developed to address this problem.

2.7.1 Structure of SMIS

The SMIS consists of an impact head, a steel rod with extensions, and an anchoring system (Figure 2.21). Figure 2.22 shows the detail of the anchoring system. Note the wooden pin laying by the steel anchor and the small holes on the steel anchor and the white pipe. Before installation, the wooden pin is used to hold the steel anchor to the white pipe and the steel rod is then connected to the anchor. The other end of the white pipe is used to hold the resin. After the SMIS reaches to the bottom of the borehole, an impact by hammer at the impact head will break the wooden pin and force the anchor sliding down along the white pipe, squeezing the resin out of the pipe. The anchor is then firmly grouted by the squeezed resin at the bottom of the borehole. Since the connection between the steel rod and the anchor is a screw connection, the steel rod and impact head can be retrieved or reinstalled.

Figure 2.21 Simple mechanical impact system (SMIS).

Figure 2.22 SMIS anchor structure.

2.7.2 Mechanics of SMIS

It is known from the structure of SMIS and the installation process of SMIS that the system is in effect an energy delivery system. It enhances impact sources by three mechanisms. First, the attenuation effect of the fractured surface is significantly reduced by anchoring the system at a suitable depth. Second, the system can deliver much larger impact energy because of its anchoring structure at the borehole bottom. Third, it is a repeatable energy delivery system in that the source has a fixed location and the energy that will be transferred to the rockmass is a constant function of impact sources, which makes it possible to produce a similar seismic source by using a similar impact. This will be difficult if the impact is made on the pillar surface as the energy which will be transferred to the rockmass will depend largely on local conditions.

2.7.3 Laboratory and field test of SMIS

SMIS was tested both in the laboratory (Figure 2.23) and field. Figure 2.24 shows the field installation of SMIS at Harmony mine. The signals generated by a hammer impact at this SMIS and received by the sensors located on the other side of the pillar, which is approximately 50 feet away, are shown in Figure 2.25. Both P- and S-wave arrivals can be clearly seen. Their frequencies are approximately 3,000 Hz and 1,100 Hz, respectively.

Figure 2.23 Laboratory testing of non-explosive sources with the help of SMIS.

Figure 2.24 A Simple Mechanical Impact System (SMIS) installed in a coal pillar.

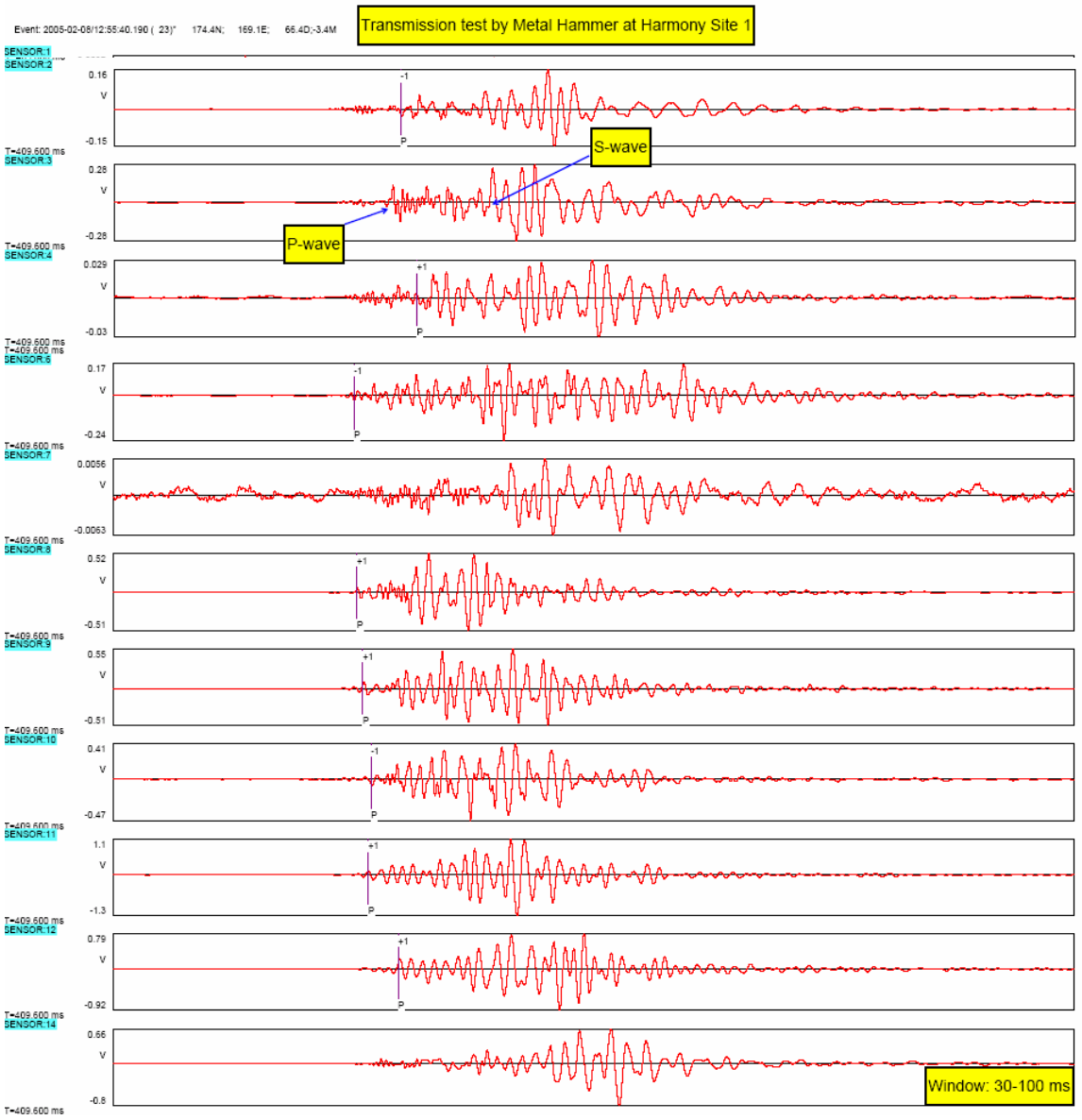

Figure 2.25 Signals generated by the hammer impact at the SMIS shown in Figure 2.24 and received by the sensors located on the other side of the pillar, which is approximately 50 feet away.

2.8 Three-dimensional sensor installation technique

In order to determine whether an incoming signal is a reflected signal, the type (P- or S-wave) and direction of this signal must be known. A reliable means of acquiring this information is to compare how signals are polarized and three-dimensional sensors are ideal for this purpose. A three-dimensional accelerometer is shown in Figure 2.26. Figure 2.27 is an illustration of the 3D sensor configuration and the signals detected by a 3D sensor.

Figure 2.26 A three-dimensional accelerometer.

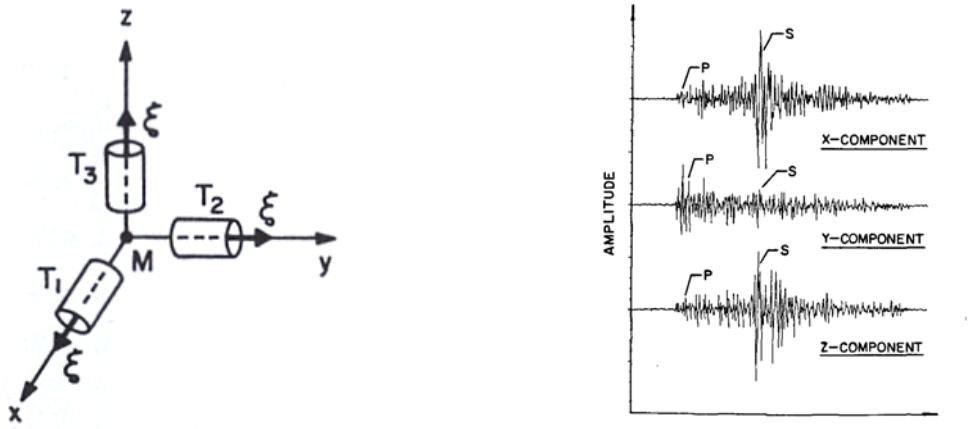

a. 3D sensor configuration. b. Waveforms from a 3D sensor.

Figure 2.27 3D sensor configuration and signals detected by a 3D sensor.

A major difficulty with the use of 3D sensors for void detection is the problem of suitable field installation. Conventionally, 3D sensors have to be installed in cement filled boreholes. This technique provides an intimate sensor-to-rock coupling. However, it also prevents removal of the sensor for use at other locations. The relatively high cost of 3D sensors, $1000 – 2500 each, necessitates the development of an installation technique in which the sensor can be easily retrieved.

2.8.1 Testing facilities

In preparation for testing of future 3-D installation tools, a number of testing facilities were developed, including 1) a large concrete block and a borehole support frame (Figure 2.28), 2) two large specially prepared limestone blocks with drill holes for 3D and 1D sensor installation (Figure 2.29), 3) a hydraulic platform for supporting limestone blocks (Figure 2.30a), and 4) a specially designed borehole system (Figure 2.30b).

Figure 2.28 Concrete block and borehole support frame for 3D sensor testing.

a. 7” x 10” x 18” in limestone block.

b. 5” x 7” x 10“ in limestone block.

Figure 2.29 Limestone blocks with boreholes for 3D sensor installation.

a. Hydraulic supporting platform.

b. Specially designed borehole system.

Figure 2.30 3D sensor testing support systems.

2.8.2 Development of prototype of retrievable 3D sensor installation device

A review of the literature associated with the field installation of geotechnical monitoring devices indicated that some type of "wedging system" would be most suitable. Such systems have proven successful in the past for the installation of a variety of stressmeters. In these cases the body of the stressmeter and an associated installation shell were each machined with a 1 degree taper. When the combined unit was set at the required position in a borehole the stressmeter was thrust into the installation shell pushing it into intimate contact with the top and bottom of the borehole.

Before proceeding with the final design of a 3D sensor installation system, the testing facilities discussed in the previous section were utilized to study the behavior of the sensor in response to various simple installation techniques. These studies indicated that the quality of the installation of the 3D sensor is extremely important. Widely different results were observed for even small variations in installation procedure.

The 3D sensor installation device developed at Penn State is based on the "expandable mandrel" concept used in holding odd sized hollow cylindrical work pieces in a lathe (Figure 2.31). In this case, the inside of the mandrel and an associated center rod are each machined with a 1 degree taper. When the horizontal center rod is thrust into the mandrel it expands radially and uniformly in all directions in the vertical plane insuring that the 3-D sensor is in intimate contact with the borehole wall.

a. Outer sleeve.

b. Inner sleeve.

c. Assembled unit.

Figure 2.31 Retrievable 3D sensor installation device.

2.9 Laboratory velocity measurement

Laboratory velocity measurement is rarely mentioned in ISS literature, but is an essential part of the ISS based void detection technique. This section discusses the basic purpose of laboratory velocity measurement and the associated laboratory measuring technique.

2.9.1 Why laboratory measurement of velocities?

The transmission survey, which is considered the basic means for determining velocities required for the reflection survey, is only efficient for determining the velocities associated with the high velocity layer. It is quite difficult to use this method alone to determine the velocities associated with low velocity layers, such as coal seams, as the first received signal is in general from media with the higher velocities. This phenomenon is shown in Figure 2.32.

The waveforms shown in the figure are the transmission signals recorded at Harmony mine, an anthracite mine. Even though both the seismic source and receivers were located in the middle of the coal seam, the first signal arrivals were not from the coal seam, but from the sandstone roof. The P- and S-waves from the coal seam itself arrived much later. As these signals are often mixed with others, timing of these arrivals is often not easy. However, if one has prior knowledge of propagation velocities, timing the incoming signals can be estimated. There are many different ways to acquire reference velocity data, such as from literature. The most reliable means, however, is laboratory measurement of the field study medium(s) as the velocities are highly site dependent.

It is important to note that there is always some discrepancy between the values measured in the field and those measured in the laboratory. Therefore, the velocities determined from small samples in the laboratory can only be considered as a reference of the velocities in the field. For most cases, these discrepancies are small in terms of the order of error so that they can be utilized as reference velocities. There are also situations in which the velocities measured in the laboratory and in the field are very close, such as for trona. The discrepancies can provide some useful information on the rockmass property, which may be used to study the variation of the velocities.

2.9.2 Instrument, and measuring principle and procedure

The instrument used for the laboratory velocity measurement is the New Sonicviewer Rock Sample Velocitymeter (Model – 5217A) manufactured by OYO Corporation, Japan. As implied by name, the instrument was specially designed for measuring velocities in rock samples (Figure 2.33).

The setup of the measurement is shown in Figure 2.34. The velocity values of the rock specimens are calculated by the equation:

$$V_{p/s} = \frac{L}{t_{p/s}} \tag{2.90}$$

Where $V_{p/s}$ is P or S wave velocity to be measured, L is the length of the specimen, and $t_{p/s}$ is the traveling time of the P- or S-wave between two ends.

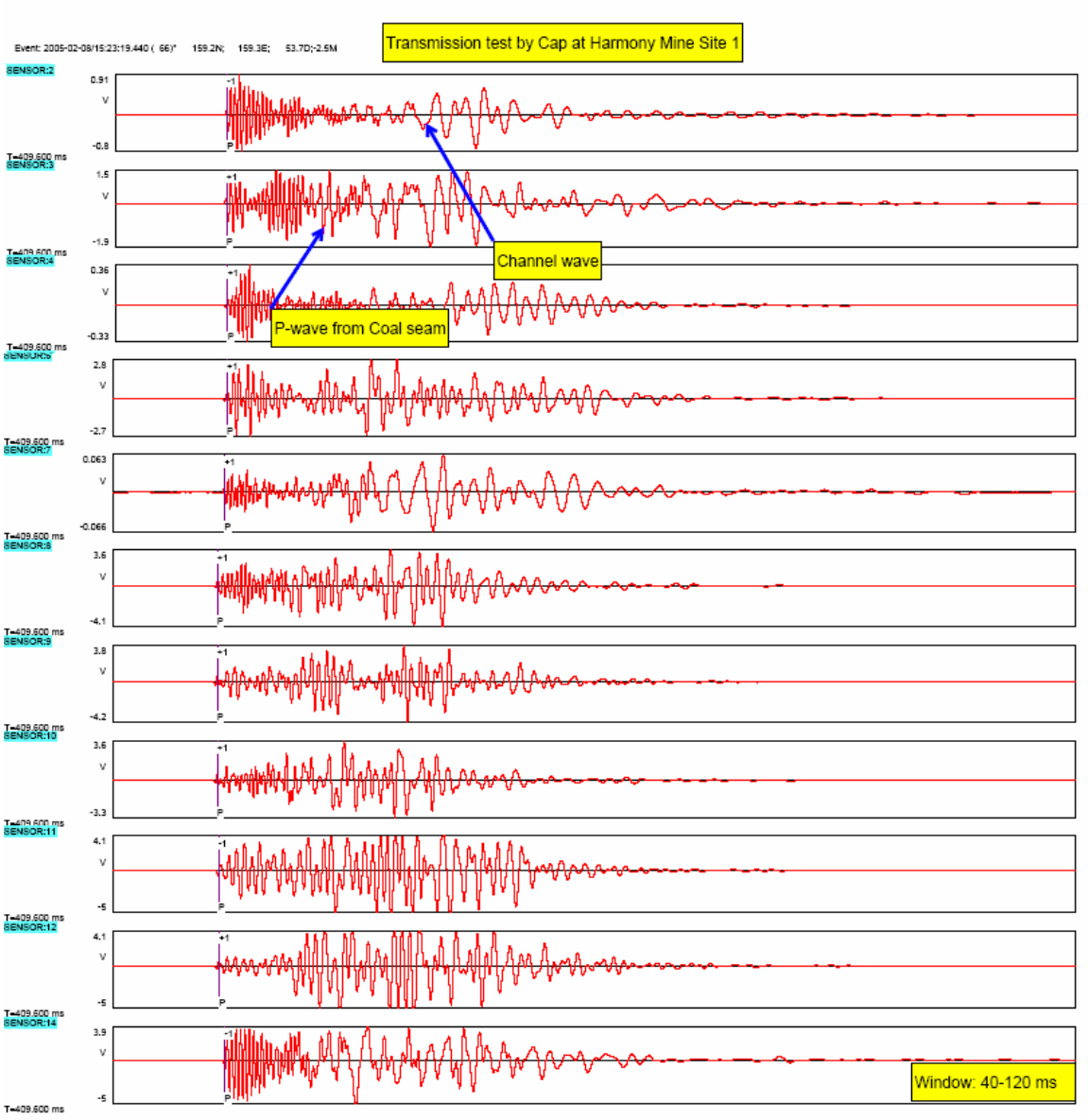

Figure 2.32 Transmission signals recorded at Harmony mine.

Figure 2.33 New Sonicviewer Rock Sample Velocitymeter (Model – 5217A).

a. Specimens ready for the test.

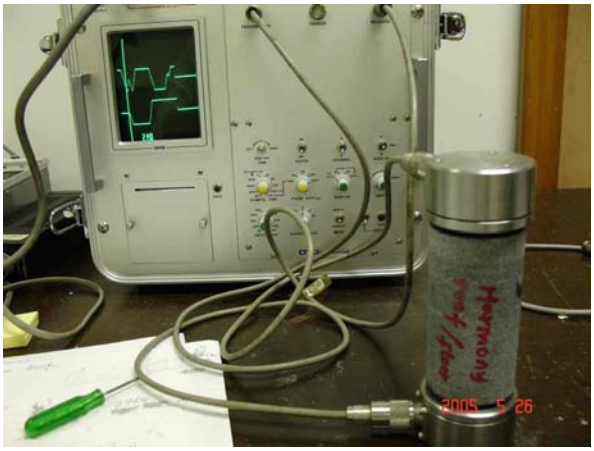

b. Testing setup.

Figure 2.34 Laboratory velocity measurement.

The measurement procedure consists of seven simple steps, which are

1. zeroing adjustment,
2. spreading vaseline on the contact surfaces of the transducers to insure good contact with the specimen (only used for P wave),
3. adjusting the instrument for clear display,
4. setting mode switch ENHANCE until the first arrival is clearly distinguished,
5. using SHIFT adjustor to match first arrival with the vertical index line (Figure 2.35a),
6. recording the time of transmission (Figure 2.35b), and
7. Computing P- or S-wave velocity.

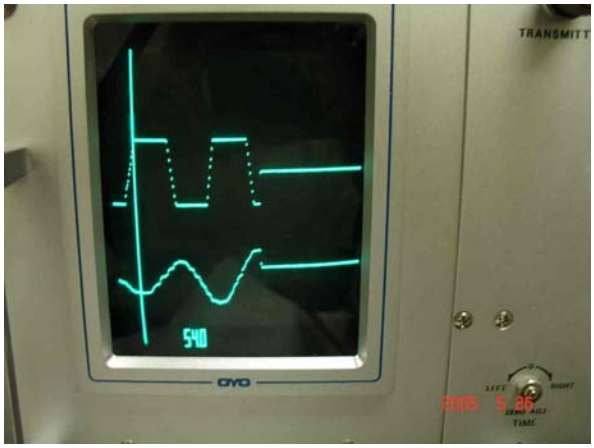

a. Matching the first arrival.

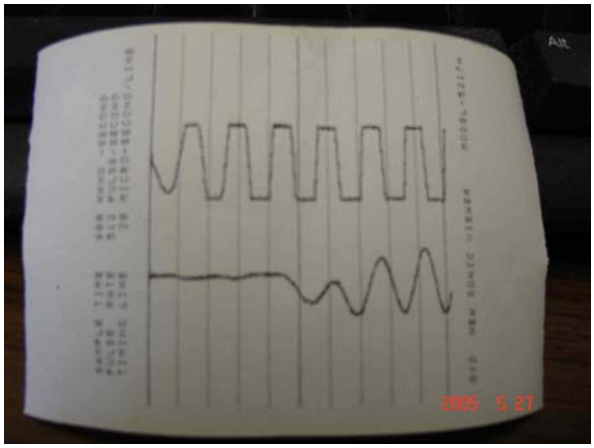

b. A recorded signal.

Figure 2.35 Signal displaying and recording.

2.9.3 Velocity measurement for three field sites

During Phase I, Penn State carried out seven field tests with three different mine site conditions: FMC and General Chemical trona mines in Wyoming; Harmony Mine, an anthracite coal mine, and Agustus Mine, a bituminous mine. The samples of the seam, roof and floor were collected from each site and their laboratory velocities were measured (Table 2.1).

Table 2.1 Laboratory measurement of P-wave velocities for three mine sites

Mine Name	Mine Type	Rock/ore Type	Vp (ft/s)
Agustus Mine	Bituminous	Bituminous coal	3,300
		Shale (floor)	11,477
		Shale (roof)	13,478
Harmony Mine	Anthracite	Anthracite coal	7,639
		Sandstone (roof)	15,810
General Chemical	Trona	Trona	16,710
		Shale (floor)	5,619
		Weak shale (roof)	2,897

The laboratory velocity measurement has serves two important purposes. First, it provides data to evaluate site conditions before field testing. For instance, a difficulty associated with working in bituminous mines is the unknown effect of the shale because of its widely varying velocity. However, it is no longer a problem if laboratory velocity measurements are available. The second important usage, as discussed earlier, is to assist with timing of the incoming signals.

2.10 Summary on technical development

In order to use the ISS technique for void detection, development work was carried out to resolve several critical issues for field testing and data analysis, which are 1) retrievable sensor installation technique, 2) experimental (source-receiver configuration) design, 3) signal analysis, and 4) elliptical void mapping method.

The retrievable sensor installation technique is needed to obtain a superior coupling effect while controlling the cost by making expensive sensors reusable. The field tests have shown that the technique provides a reliable means for capturing broadband signals, including high frequency components up to 5000 Hz. This capability is basic and essential for the ISS based void detection.

A suitable experimental design is the fundamental approach for reducing the ambiguity associated with geophysical data. A relatively detailed discussion on the subject for the ISS based void detection was given in users' manual (Chapter 2). Penn State's contribution was the sensitivity analysis and using angled sensor pairs. The sensitivity analysis reveals that the stability of the mapping system is a function of the source-receiver layout. Therefore, a suitable sensor-source layout is a basic necessity to reduce the mapping error. Using angled sensor pairs is a simple and efficient means for acquiring the signal data in orthogonal directions, which are essential for polarization analysis.

Signal analysis is a subject involving a wide range of issues. An important aspect for the ISS based void detection, which often plays a central role, is the effect of the underground environment. A systematical approach was developed by Penn State to deal with this problem, which was discussed in users' manual (Chapter 4). Another contribution by Penn State in the area of data analysis is the application of the wavelet analysis for identifying incoming signals.

The elliptical method was used as the principal means for void mapping. The basic reason for this decision is the irregular survey lines, which make it very difficult to use the staking method, the method that is conventionally used for reflection surveys. In addition to its compatibility with the physical condition of void detection, the elliptical method possesses two other important advantages. First, the method is much more stable than any other methods as it avoids many mathematical manipulations which would be otherwise required. Second, it is very flexible for simultaneous data processing.

During Phase I, Penn State also engaged in three other development tasks: non-explosive sources, simple mechanical impact system, and three-dimensional sensor installation technique. These areas are considered important for the future application of the ISS based void detection technique and were carried out for this purpose.

3. First field Test at Harmony Mine

3.1 Introduction

On February 7 – 8, 2005, the Penn State project team carried out its first field test on the ISS based void detection technique at the Harmony Mine.

There were two main objectives for the test. The first one was to test the techniques which were specially "assembled" for the ISS based void detection by the project team over a very short time period, which include 1) the suitability of the data acquisition system and sensors, 2) the effectiveness of the retrievable sensor installation technique, 3) the reliability of blasting and associated triggering system, and 4) the efficiency of techniques used to execute experimental design and data analysis.

The second objective was to acquire first hand information on ISS testing, including channel wave detection, physical environment surrounding the channel waves, and issues specially related to void detection.

The use of the Harmony Mine as the first test site was threefold. First, void detection is a real issue for the mine as it will approach an abandoned mine in several years. Second, it gave the Penn State team a logistical advantage because of the short distance between the mine and Penn State campus. Third, and most importantly, was the enthusiastic support by the mine owner and mine management, which, as shown by our experience, was invaluable to the smooth start and progress of this project.

3.1.1 Harmony mine

Harmony is a modern efficient underground coal mine, located near Mt. Carmel in east central Pennsylvania (Figure 3.1). The mine began operations in 1988. Its annual production ranges between 160,000 and 195,000 tons for the past 10 years, making it the largest underground anthracite mine in North America.

The anthracite seam at the mine site varies from less than 1 ft thick to over 13 ft thick, averaging 54 inches. The seam is overlain by 255 ft to 400 ft of overburden. The immediate roof and floor is a very light gray to yellowish brown conglomerate interbedded sandstone with uniaxial compressive strength greater than 12,000 psi. The immediate roof conglomerate is 30 to 65 ft thick and 10 ft in the floor.

The mine presently is level in pitch operating on the apex of an anticline. The room-and-pillar mining system is utilized to extract the coal (Figure 3.2).

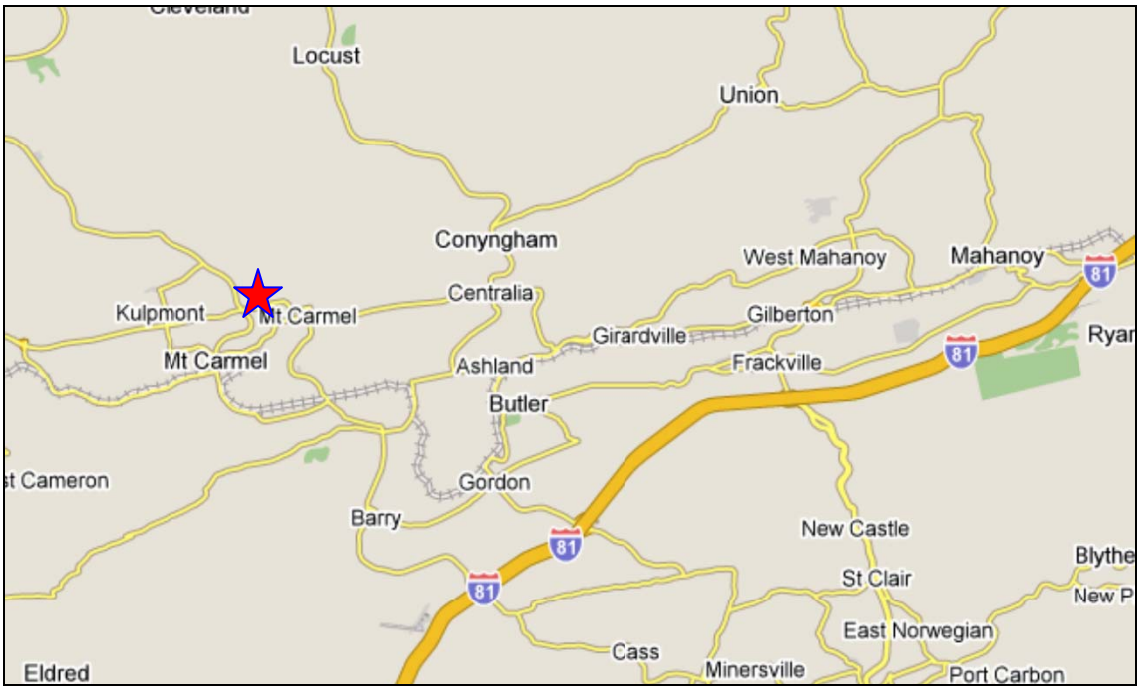

Figure 3.1 Geographic location of Harmony Mine.

Figure 3.2 Low Seam scoop at Harmony Mine.

3.2. Testing site and experimental design

Penn State carried out three tests on the ISS based void detection technique at two different sites of the mine. The site used for the first test was named Site I. Site I is a long pillar, approximately 60 – 70 ft wide. The section of the pillar which was used for the first test is shown in Figure 3.3.

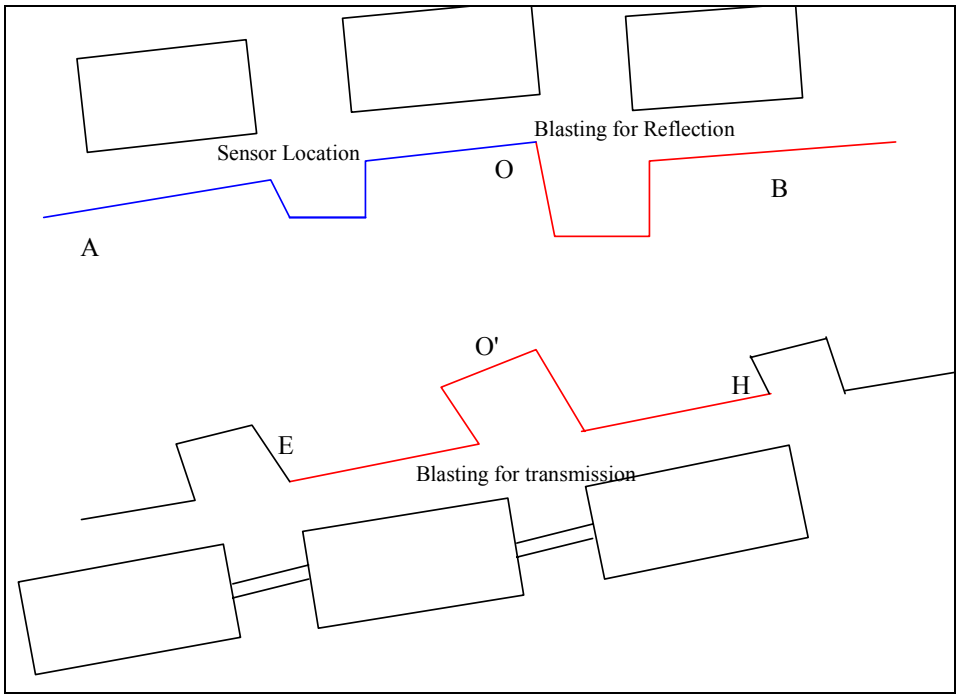

Figure 3.3 Site I: testing site used for the first ISS test at the Harmony Mine.

The site was utilized for both transmission and reflection surveys. The testing setup included three general areas: sensor section, blasting sections for transmission survey, and blasting sections for reflection survey. The locations of these sections are as marked on the map.

The specifications on the sensors, the data acquisition system, and the major operational parameters used for the test are given in Appendix I. The sampling rate and the recording window used for the test are 50,000 samples/second and 0.4 second, respectively.

3.2.1 Sensor section

There were 17 sensor holes prepared for the regular transmission and reflection test, which were numbered from S1 to S9 and N1 to N8. The locations and orientation of these sensor holes are shown in Figure 3.4. The diameter of the sensor holes is 1.75". The length of the sensor holes vary. In general, the straight ones are 5 ft long and the angled ones are 7 ft long. Among these 17 sensor holes, 12 were used for the test. The related information for these sensor holes is given in Table 3.1.

In addition to those sensor holes prepared for the regular transmission and reflection test, two roof sensor holes and two floor sensor holes were prepared. All these four holes are 7 ft long, drilled with a 45° angle into roof and floor. The two roof holes and two floor holes have same horizontal coordinates. Their collar locations are shown in the figure (behind S4 and S5). These sensor holes were prepared for a special comparison study to be discussed in section 3.3.3.

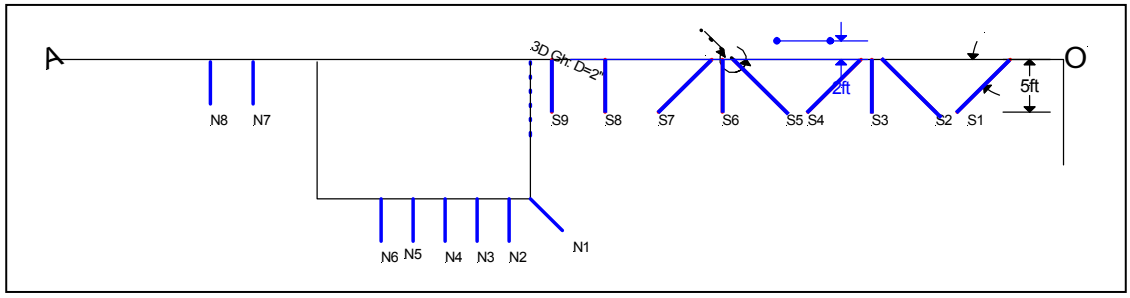

a. Plan view of sensor section.

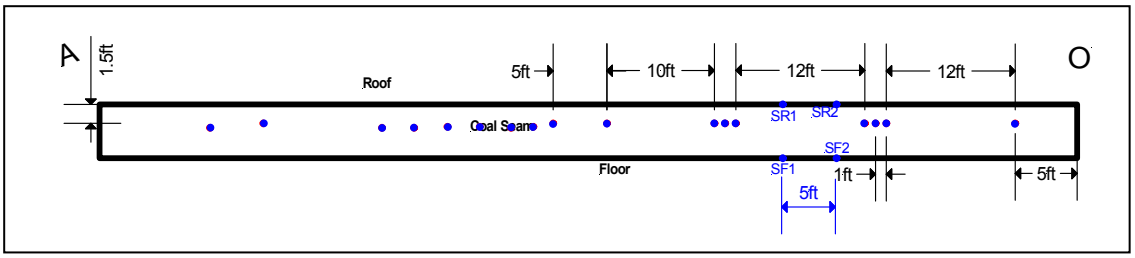

b. Longitudinal view of sensor section.

Figure 3.4 Layout of sensor section at Site I, Harmony Mine.

Table 3.1 Sensor hole information for Site I, Harmony Mine.

Hole #	Channel #	Length (ft)	Sensor coordinate (ft)	
			East (x)	North (y)
S3	2	5	5615.01	13134.39
S4	3	7	5615.11	13128.66
S6	4	7	5614.03	13120.34
S7	6	5	5614.02	13114.4
S8	7	7	5612.49	13109.73
N1	8	7	5598.84	13109.45
N2	9	5	5598.17	13102.55
N3	10	5	5597.54	13100.63
N5	11	5	5596.06	13095.69
N6	12	5	5596.32	13092.69
N7	14	5	5600.51	13075.13
N8	15	5	5597.42	13066.34
SR1	2	7	5620.50	13124.12
SR2	3	7	5620.59	13124.10
SF1	7	7	5621.04	13128.96
SF2	4	7	5620.96	13129.03

3.2.2 Blasting section for transmission survey

There were 21 blasting holes prepared for the transmission survey, which were numbered from B1 to B21. Among these 21 prepared drillholes, 5 were actually used for the survey. The coordinates for these drillholes are given in Table 3.2. All blasting holes were 4 feet long and 1.5 inches in diameter, drilled in the middle of the seam.

In addition to the blasting holes for the regular transmission test, six additional blasting holes were prepared, three in the roof and three in the floor. All these blasting holes were 4 ft deep, drilled vertically. Horizontally, they located in the short entry marked by F and G. These blasting holes were prepared for a special comparison study to be discussed in section 3.3.3.

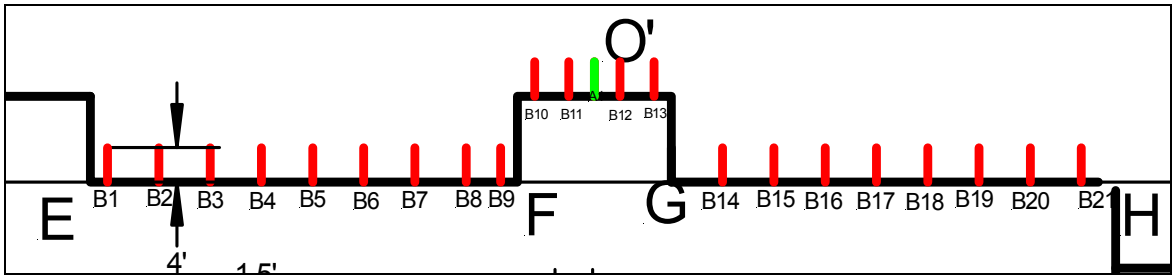

(a) plan view of blasting section for transmission test.

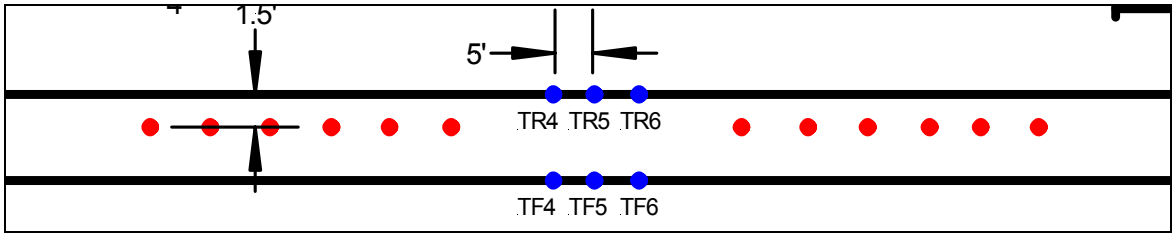

(b) longitudinal view of blasting section for transmission test.

Figure 3.5 Blasting boreholes prepared for transmission survey and a special study.

Table 3.2 Coordinates of blasting holes for transmission survey at Site I, Harmony Mine.

Hole #	Source coordinate (ft)	
	East (x)	North (y)
B4	5533.809	13104.26
B7	5536.618	13118.93
B18	5552.877	13183.73
B20	5555.875	13189.89
B21	5557.052	13192.05
TF6	5564.894	13135.037
TR6	5564.894	13135.037
TF4	5559.352	13128.216
TR4	5559.352	13128.216

3.2.3 Blasting section for reflection survey

A total of 13 blasting holes were prepared for the reflection survey, which were number from RN1 to RN6 and R5 to R9, as shown in Figure 3.6. All blasting holes are 4 feet long and 1.5 inches in diameter. The coordinates of the drill holes which were used for the survey are given in Table 3.3.

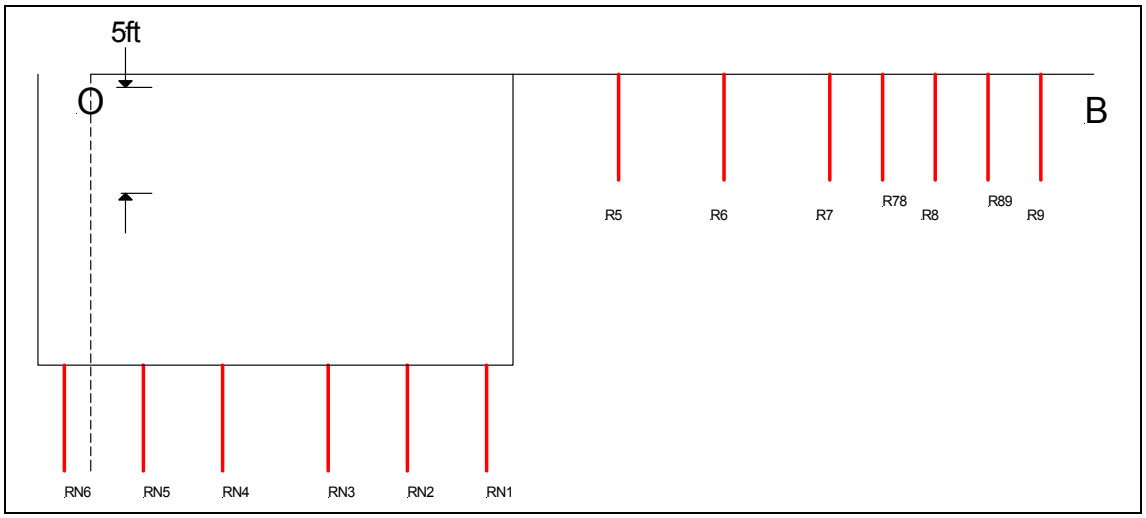

Figure 3.6 Blasting section for reflection survey at Site I, Harmony Mine.

Table 3.3 Coordinates of blasting holes for reflection survey at Site I, Harmony Mine

Hole #	Source coordinate (ft)	
	East (x)	North (y)
NR1	5591.579	13168.77
NR2	5591.53	13167.08
NR3	5591.574	13164.75
NR4	5591.679	13162.43
NR5	5590.846	13160.52
NR6	5591.091	13158.01
R7	5612.005	13186.73
R78	5611.818	13188.9
R8	5611.646	13191.42
R89	5611.478	13193.96
R9	5611.223	13196.55

3.3 Transmission survey

Five individual transmission surveys were carried out at Site I. The ray paths associated with these surveys are illustrated by Figure 3.7, where B4 and B21 are the boundary locations for these blasting holes. Because of the short distance, caps were used most surveys. Only one survey used 125 gram (1 inch) explosives. The detailed information is summarized in Table 3.4.

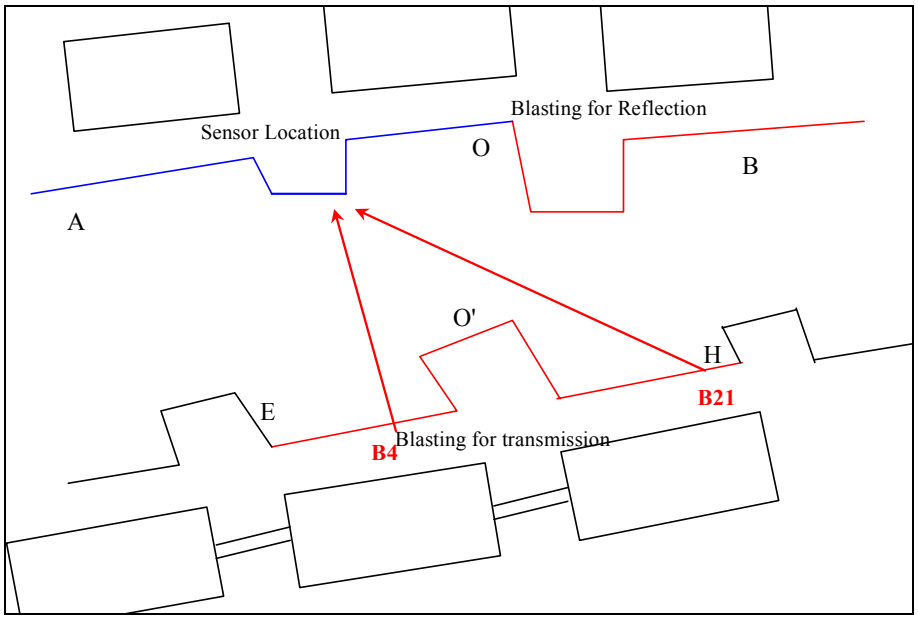

Figure 3.7 Illustration of ray paths associated with the transmission survey.

Table 3.4 A summary of the transmission survey at Harmony Mine Site I

Hole #	Explosive (g)	Event #
B4	Cap	62
B7	Cap	66
B18	Cap	87
B20	Cap	50
B21	Explosive (1”)	91
TF6	Cap	158
TR6	Cap	162
TF4	Cap	166
TR4	Cap	171

3.3.1 Characteristics of transmission signals

The results from 5 transmission surveys are similar and, as an example, event 50, the survey associated with seismic source B20, is discussed here. The locations of B20 and the sensors as well as the corresponding ray paths for this event are illustrated in Figure 3.8. The original signals for the event are given in Figure 3.9.

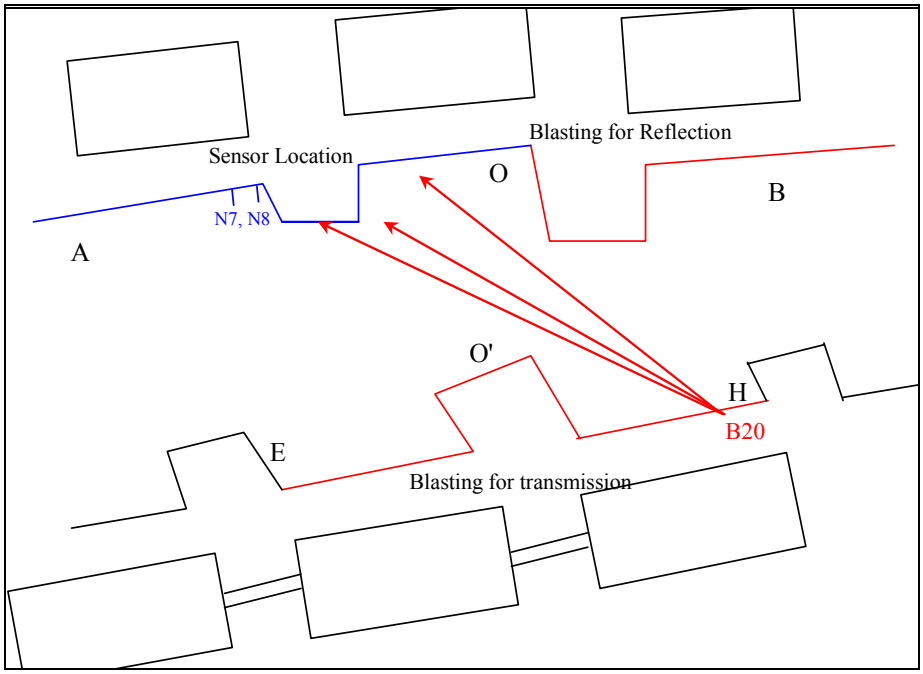

Figure 3.8 Testing setup for Event 50.

The first impression of the waveforms shown in figure 3.9 is the very high frequency associated with the signals within the first 20 ms for each channel. The frequencies for these signals vary from 2,000 to 3,000 Hz with a typical value of 3,000 Hz. These high frequency signals are the P- and S-waves from the roof and floor, not from the coal. It is also evident from the figure that this first wave of high frequency signals are composed by a number of subgroups: one can clearly see in sequence the emergence of newly arrived signal groups. The benefit of data with this precision for the ISS based void detection is huge. For the conventional applications, such as Harmony, it allows the precise assessment of the P- and S-wave velocities as well as detailed data analysis. For non-conventional applications of the ISS technique, such as the trona mine, high frequency signals are the necessary condition for void detection.

After the high frequency time period, signals with much lower frequencies begin to appear in the signature. The characteristics for these signals is that they are very resilient, having a long duration with a very slow attenuation. These are the channel waves. Their frequencies are about 400 -600 Hz.

To highlight the signals with the lower frequencies from the coal seam, a 100-1000 Hz bandpass filter was applied to the original signals. The result of this filtering process is shown in Figure 3.10. Three observations can be made from review of this figure. First, it demonstrates that the major frequency component for the P- and S-waves from the roof and floor are higher than 1000 Hz. Second, the channel waves are clearly delineated both in terms of the signal shape and the general trend. Third, the arrivals of the P-waves from the coal seam, which were originally overshadowed by strong P- and S-waves from the roof and floor, become apparent for most channels after eliminating these shadowing elements. The P-waves from the coal seam is not detectable for N7 and N8. The likely reason is that those "would be" signals were blocked by the short entry the sensors as shown by Figure 3.8 The arrival time readings for channel waves and P-waves from the coal are listed in the following table.

Table 3.5 P- and Channel wave arrival time reading

1. P-wave from coal arrival time reading for Event 50

		Channel #	2	3	4	6	7	8	9	10	11	12
trig.	Event #		S3	S4	S6	S7	S8	N1	N2	N3	N5	N6
44.25	50	B20	54.55		54.85	55.90	55.85	55.75	55.75	55.85	56.35	56.75

2. Channel wave from coal arrival time reading for Event 50

		Channel #	2	3	4	6	7	8	9	10	11	12
trig.	Event #		S3	S4	S6	S7	S8	N1	N2	N3	N5	N6
44.25	50	B20	61.05	61.25	61.95	62.10	63.40	65.95	66.95	67.60	69.70	70.25

3.3.2 Velocity calculations for Site I

Based on the data from the transmission survey, four velocities were calculated: P- and S- wave velocities associated with the sandstone roof and the P- and channel wave velocities associated with the coal seam. These calculated velocities are listed in Table 3.6. The raw data used for coal related velocity calculations are given in Tables 3.7 and 3.8.

Based on the data from the transmission survey, P- wave velocities associated with the sandstone roof and the coal and the channel wave velocity were calculated (Table 3.6). The raw data used for coal related velocity calculations are given in Tables 3.7 and 3.8.

Table 3.6 Velocities associated with Site I, Harmony Mine**.**

Strata	Velocity Type	Velocity (ft/s)
Roof (sandstone)	P-wave	15903
Coal (anthracite)	P-wave	7488
	Channel wave	4413

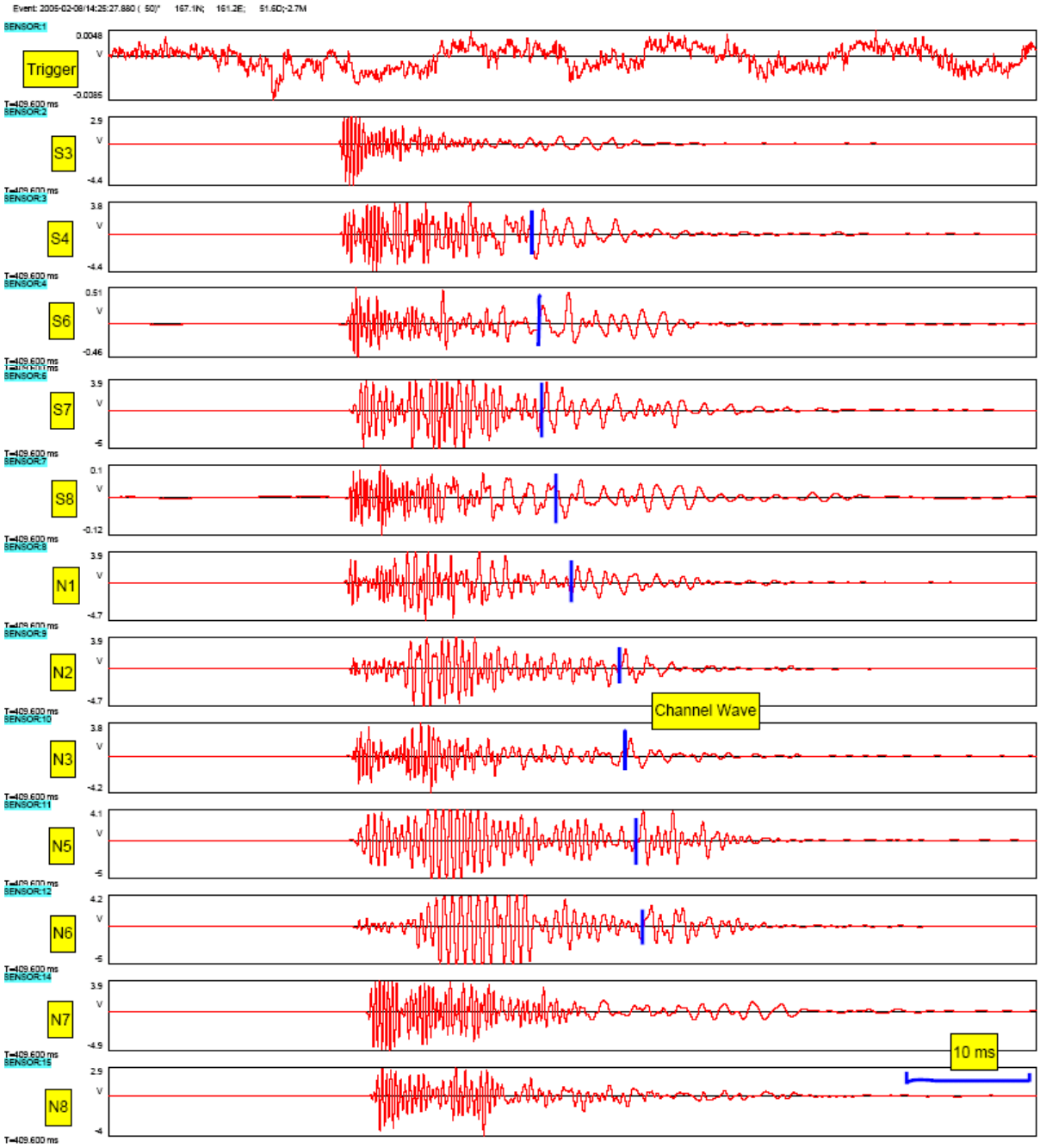

Figure 3.9. Original signal waveform for a transmission survey (Event 50) carried out at Site I, Harmony Mine (display window: 30-110 ms).

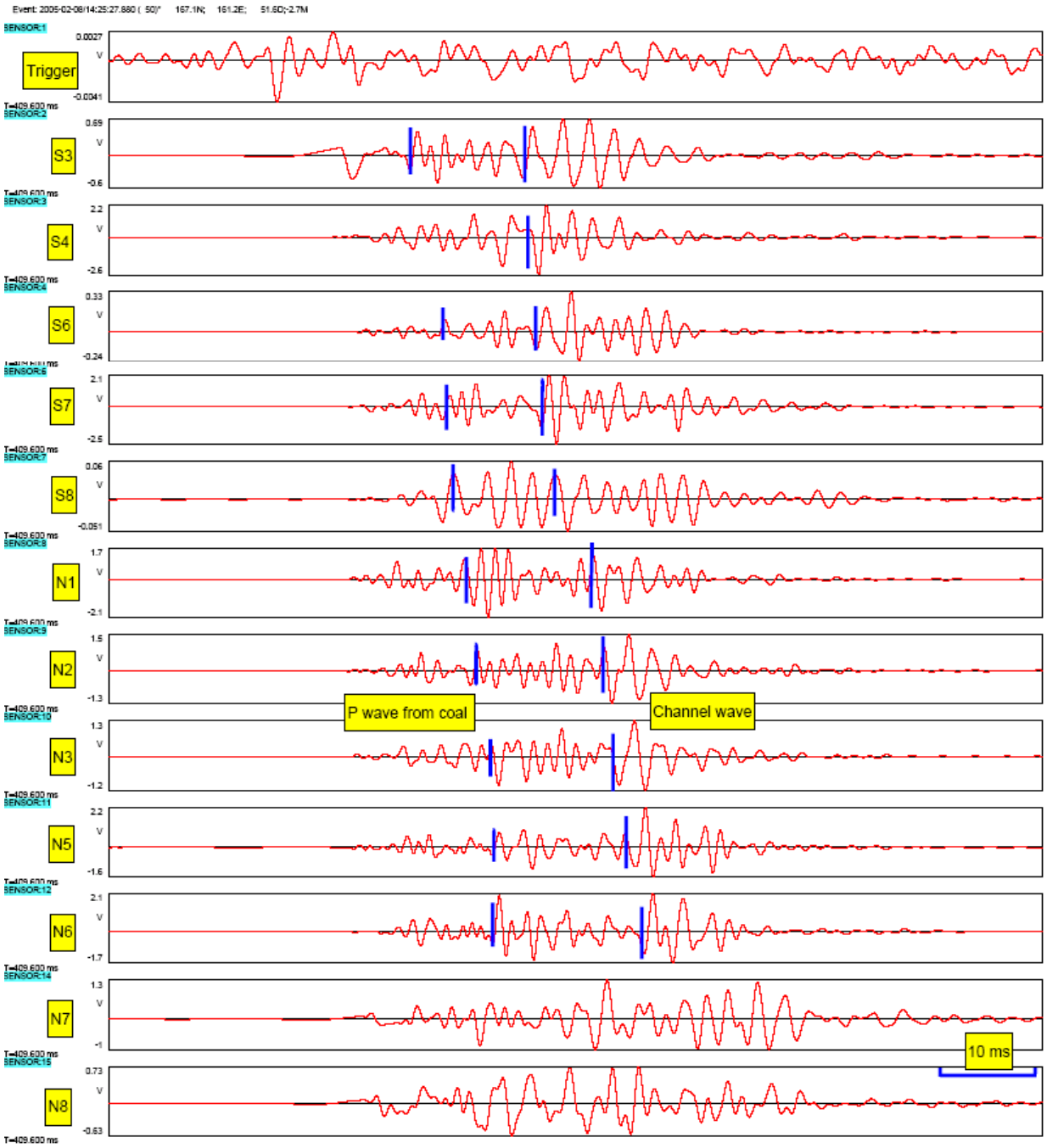

Figure 3.10 Signal waveform for Event 50 carried out at Site I, Harmony after 100-1000 Hz bandpass filtering (display window: 30-110 ms).

Table 3.7 Source – receiver distances (ft) at Harmony Mine Site I

	Channel #	2	3	4	6	7	8	9	10	11	12	14	15
Event #		S3	S4	S6	S7	S8	N1	N2	N3	N5	N6	N7	N8
62	B4	86.6	84.9	81.8	80.8	78.9	65.2	64.4	63.8	62.8	63.6	72.8	74.1
66	B7	79.9	79.1	77.4	77.5	76.4	62.9	63.7	63.6	63.8	65.2	77.5	80.4
87	B18	79.3	83.1	88.1	92.4	95.0	87.3	93.0	94.3	98.1	100.9	118.6	125.6
50	B20	81.1	85.2	90.7	95.3	98.1	91.2	97.0	98.5	102.4	105.3	123.1	130.3
91	B21	81.8	86.0	91.6	96.3	99.2	92.6	98.5	100.0	104.0	106.8	124.7	132.0
131	NR1	41.6	46.5	53.4	58.8	62.6	59.8	66.5	68.4	73.2	76.2	94.1	102.6
125	NR2	40.2	45.1	51.9	57.3	61.1	58.1	64.9	66.7	71.5	74.5	92.4	100.9
120	NR3	38.4	43.1	49.8	55.1	58.9	55.8	62.5	64.4	69.2	72.2	90.1	98.6
113	NR4	36.5	41.1	47.7	53.0	56.7	53.5	60.2	62.1	66.9	69.9	87.7	96.3
103	NR5	35.6	40.0	46.4	51.6	55.2	51.7	58.4	60.3	65.0	68.0	85.9	94.4
99	NR6	33.6	37.9	44.1	49.3	52.8	49.2	55.9	57.7	62.5	65.5	83.4	91.9
135	R7	52.4	58.2	66.4	72.4	77.0	78.4	85.3	87.3	92.4	95.3	112.2	121.3
139	R78	54.6	60.3	68.6	74.5	79.2	80.5	87.4	89.4	94.5	97.5	114.3	123.4
143	R8	57.1	62.9	71.1	77.1	81.7	83.0	89.9	91.9	97.0	99.9	116.8	125.9
147	R89	59.7	65.4	73.7	79.6	84.2	85.5	92.4	94.4	99.5	102.4	119.3	128.4
151	R9	62.3	68.0	76.3	82.2	86.8	88.0	94.9	96.9	102.0	104.9	121.9	130.9

Table 3.8 P-wave and Channel wave from coal seam velocities determined from transmission survey at Harmony mine site I

P-wave	Channel #	2	3	4	6	7	8	9	10	11	12	14	15	
Event #		S3	S4	S6	S7	S8	N1	N2	N3	N5	N6	N7	N8	
62	B4	7247.9	7073.7	6963.2	6765.7	7234.0	7091.1	6706.6	6790.8					**6984.1**
66	B7		7461.6	6912.9		6763.6	6801.0	6818.0	7425.0		6928.0			7015.7
87	B18	6990.2	7419.5	8007.0	7365.5	8227.0	7662.0	7290.8	7201.4	7513.9	8200.9	7879.3		**7614.3**
50	B20	7873.7		8552.7	8179.0	8460.0	7929.9	8438.3	8491.7	8463.8	8422.2			8312.3

Ch.-wave	Channel #	2	3	4	6	7	8	9	10	11	12	14	15	
Event #		S3	S4	S6	S7	S8	N1	N2	N3	N5	N6	N7	N8	
62	B4	4340.4	4254.7	4024.0	4374.1	4348.7	4244.2	4177.9	4059.4					4227.9
66	B7	4258.2	4080.6	4090.8	4455.0		4476.9	4147.8			4156.8			4238.2
87	B18	4936.2	4597.2	4374.5	4320.8	4194.1	4451.7	4804.2	4419.3	4413.4	4920.5	4727.6		4568.6
50	B20	4827.3	5011.3	5121.9	5338.1	5124.6	4202.5	4274.9	4218.6	4024.0	4049.1			4619.2

3.3.3 Transmission surveys through roof and floor: a comparison study

One of the main objectives set by Penn State for its first test was to demonstrate the presence of channel waves without any ambiguity. In order to provide further evidence of channel waves observed during the conventional transmission survey (that is, both the seismic sources and receivers were located in the coal seam), four nonconventional transmission surveys were carried out. These nonconventional transmission surveys consisted of seismic sources located in the roof and floor and sensors placed in roof, floor and coal seam.

The general layout of these four nonconventional tests is shown in Figure 3.11. There were two blasting holes in the roof and two in the floor. The blasting holes in the roof and floor had same horizontal locations. All these holes were 4 ft deep, drilled vertically. The similar arrangement was made for the sensor holes in the roof and floor: two in the roof and two in the floor. These drillholes were 7 ft, inclined 45° towards the pillar. During the survey, sensors, which were originally installed in the coal, were also used.

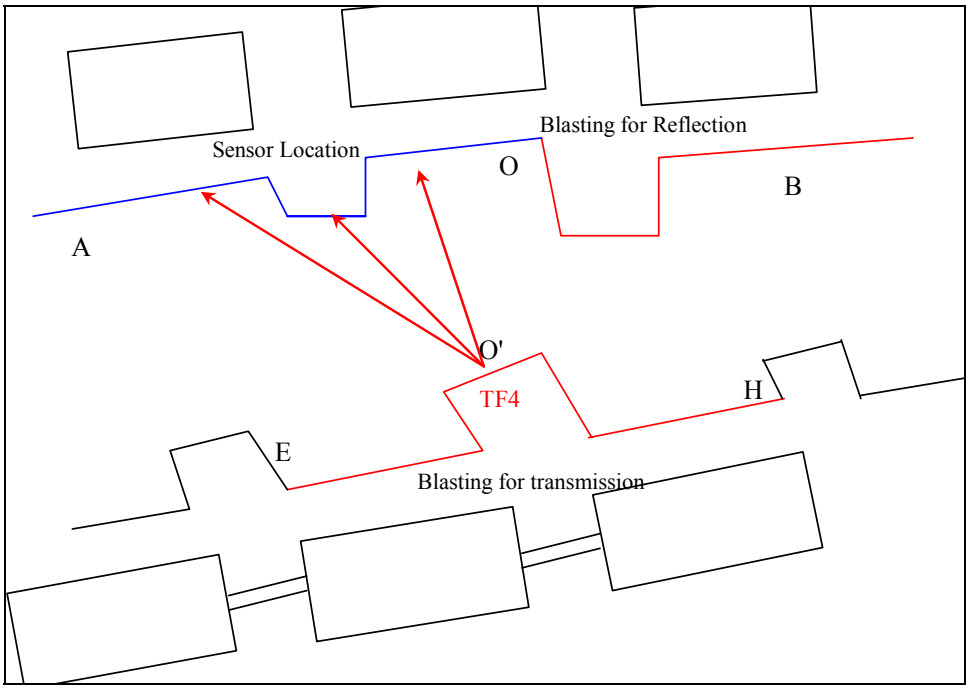

Figure 3.11 Testing setup and associated ray paths for a nonconventional transmission survey (event 166).

The results of these irregular surveys are similar and event 166 is discussed here as an example (Figure 3.12). The source associated with event 166 was initiated with a blasting cap in the floor. First, let us examine the signals from the sensors installed in the roof and floor (which are marked as “roof sensor” and “floor sensor”). These signals are very similar. Both are featured with high frequencies which taper off rapidly. For those sensors installed in the coal, however, their signals are very different. They resemble the ones from the regular transmission survey: very long duration with two distinctive parts. The high frequency signals associated with the first part were from the floor and roof. Channel waves were developed at a much later stage. In the

figure, they are visible for several channels without any "zoom-in" process. A very interesting observation is that the signal amplitude for the sensors installed in the coal is much higher than the ones in the roof and floor. The average amplitude for the coal channels is about 2.5 volts, while it is only 0.5 for the sensors installed in the roof and floor.

The other very interesting observation is the difference between two roof sensors (channels 2 & 3). These two roof sensors are only 5 ft apart. Their signals, however, are completely different. For channel 2, both the frequency and amplitude are very low. The amplitude (voltage) is only 0.0064, less than 1% of the amplitude associated with channel 3, which is 0.74. The poor signal quality for the channel is due to the sensor installation. For channel 2, the sensor was not tightly anchored at the borehole bottom. Its installation status is equivalent to "wedging" the sensor in place, a commonly used sensor installation method in geophysics. The strong contrast of the signal quality between channel 2 and other channels is convincing evidence of the importance of a reliable sensor installation technique. In other words, one may not be able to get the signals required for the ISS survey if one uses the conventional sensor installation technique.

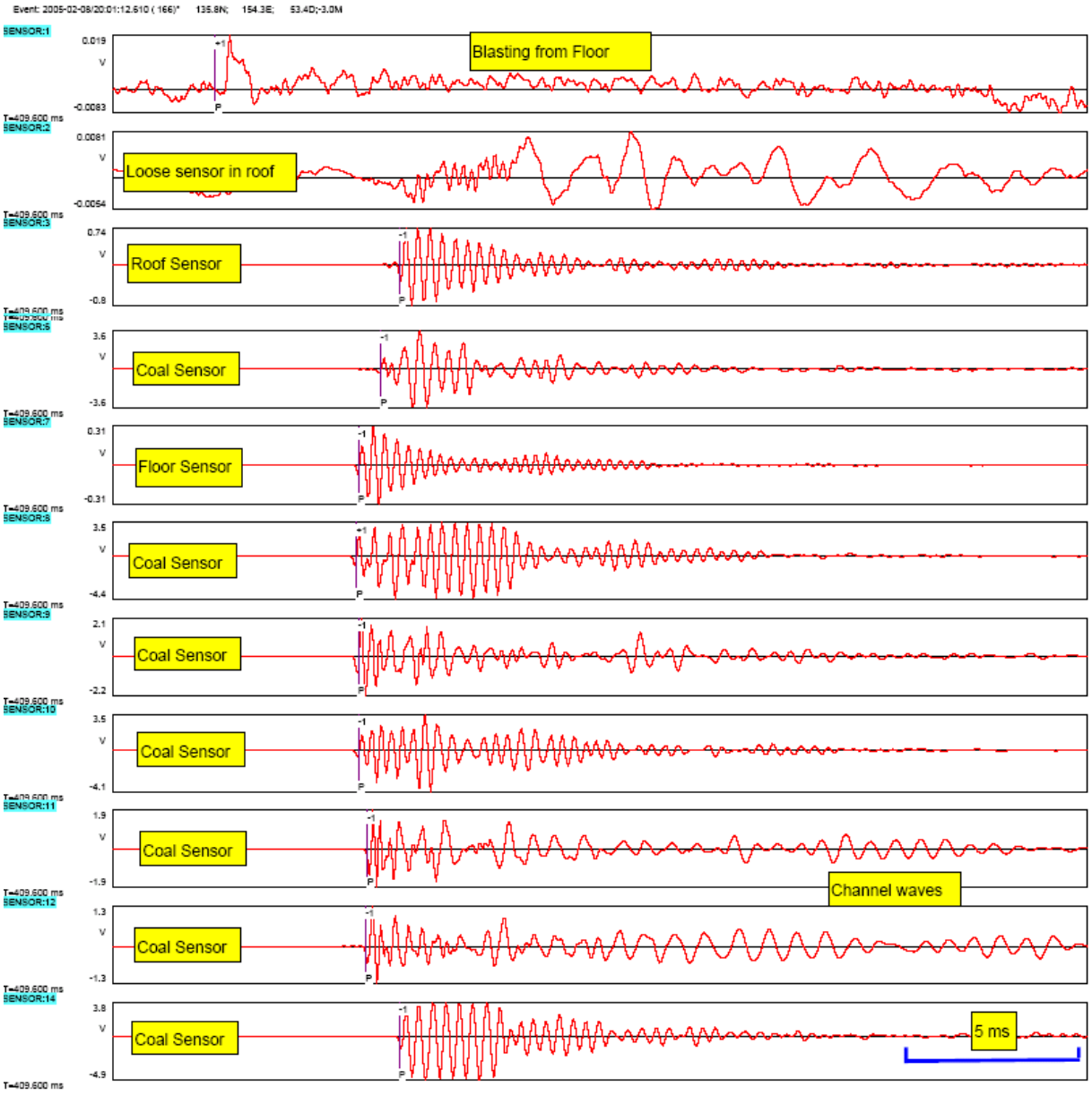

Figure 3.12 Event 166 showing signals associated with a specially designed transmission survey at an anthracite mine. Sensors were located on one side of the pillar, one in the floor, two in the roof and the rest in the coal, and the blasting hole was in the floor on the other side of the pillar. The pillar is approximately 60 ft wide. The roof and floor are strong sandstone (display window: 47-73 ms).

3.4 Reflection survey at Site I, Harmony Mine

The reflection survey at Site I included 11 individual surveys (blasting events). Caps were used for all these surveys. The event numbers for these surveys are listed in Table 3.9.

Table 3.9 A summary of the reflection surveys at Harmony Mine Site I

Hole #	Explosive (g)	Event #
NR6	Cap	99
NR 5	Cap	103
NR 4	Cap	113
NR 3	Cap	120
NR 2	Cap	125
NR 1	Cap	131
R7	Cap	135
R 78	Cap	139
R 8	Cap	143
R 89	Cap	147
R 9	Cap	151

The pattern of the reflected channel waves at Site I is relatively complex because of the pillar geometry. The original design of the testing setup was based on the layout shown by the general mine map (Figure 3.13). According to this design, most blasts should generate some reflected signals which were detectable by the sensors. However, the actual layout as shown in the chapter is somewhat different from the one used for design. Because of this difference, the number of detectable reflected signals was less than that expected by design.

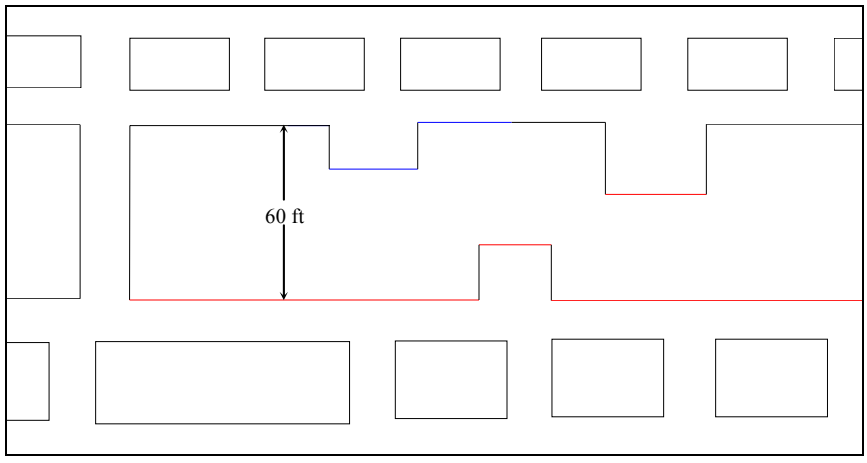

Figure3.13 Layout of the testing section given by the general mine map.

3.4.1 Case Study: Event 99

Event 99 refers the reflection survey related to seismic source NR6. The locations of NR6 and the sensors are shown in Figure 3.14. The recorded event is given in Figure 3.15. The direct channel waves are clearly shown in the figure. However, there are no signs of reflected channel waves for most sensors. The ray paths sketched in Figure 3.14 seem to be a good explanation. The arrival readings for the direct channel waves are given in the following table.

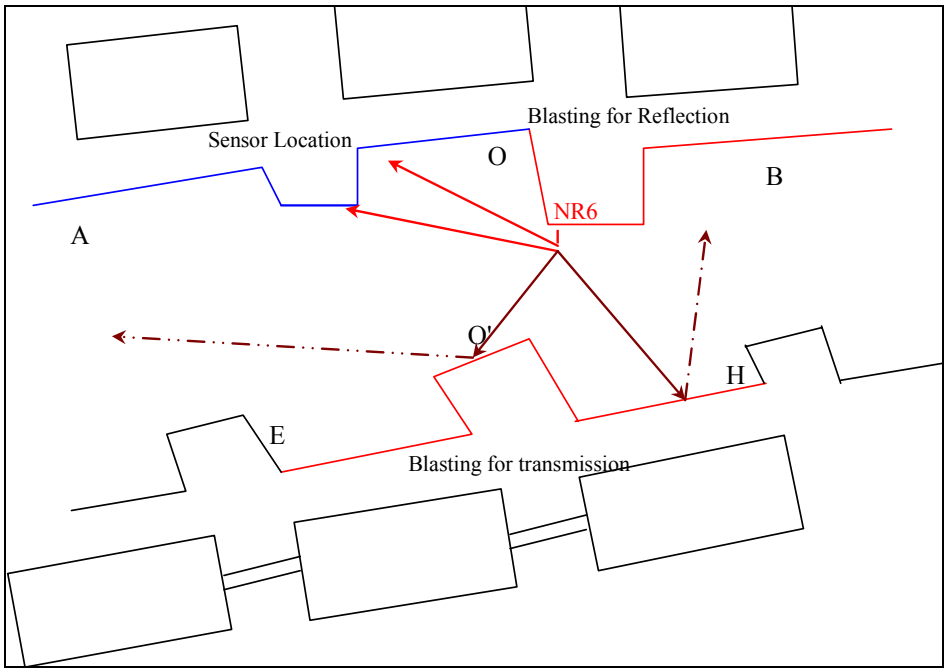

Figure 3.14 Testing setup for event 99.

Triggering time (ms)	Sensor #	S6	S7	S8	N1	N2	N3	N5	N6	N7	N8
50	Arrival time		63.85	63.35	67.1	68.9	69.25	72.7	73.25	75.75	76.5
	Velocity (ft/s)		3557.7	3956.1	2876.0	2958.5	2999.8	2754.3	2818.7	3239.5	3467.7

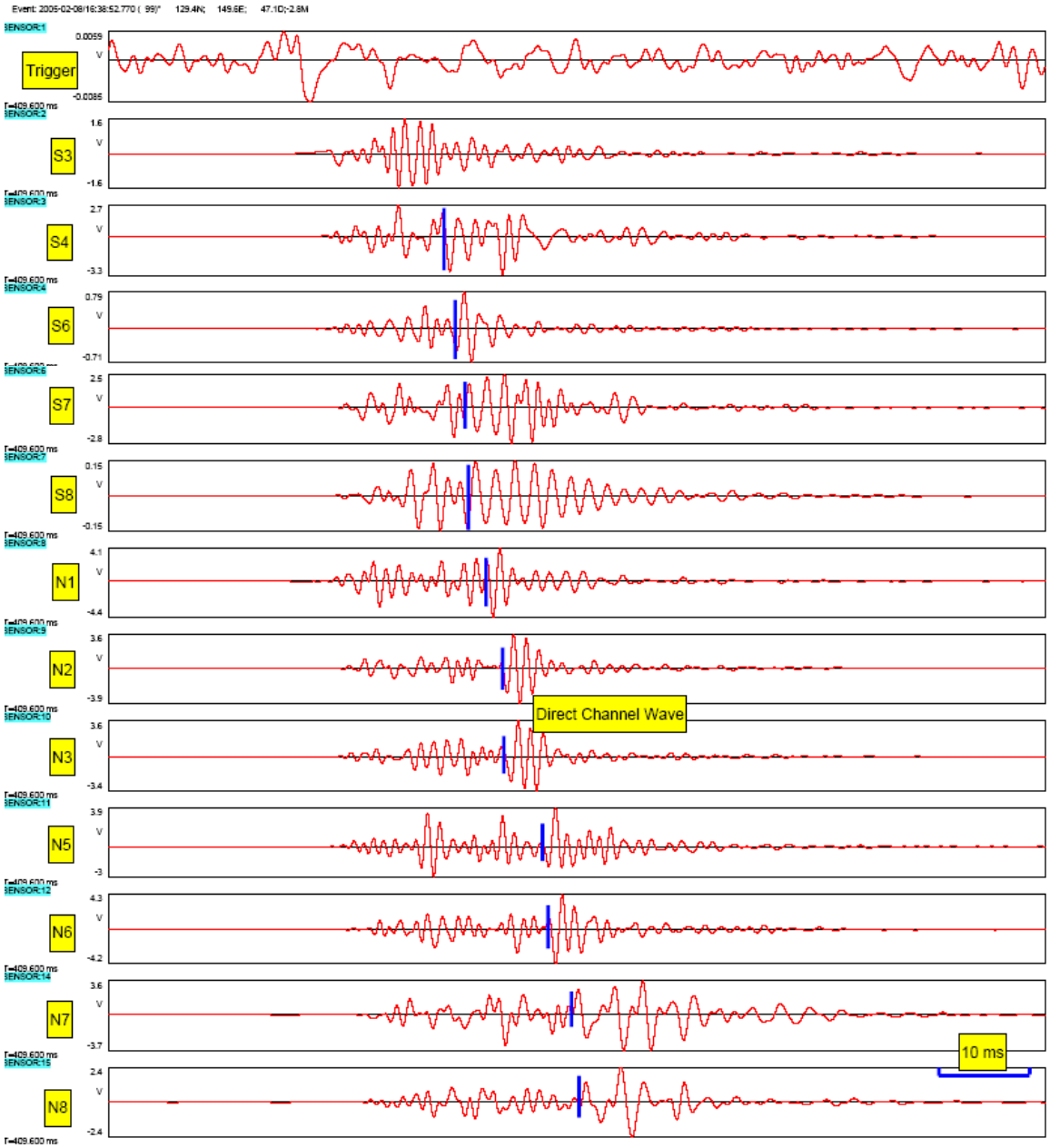

Figure 3.15 Signal waveform for event 99 (display window: 30-110 ms).

3.4.2 Case study: Event 147

Event 147 refers the reflection survey related to seismic source R89. The locations of R89 and the sensors are shown in Figure 3.16. The waveform for the event is given in Figure 3.17. Two trends can be observed from the figure: direct S- waves from roof and reflected channel waves. The arrival readings of reflected channel waves are given in the following table.

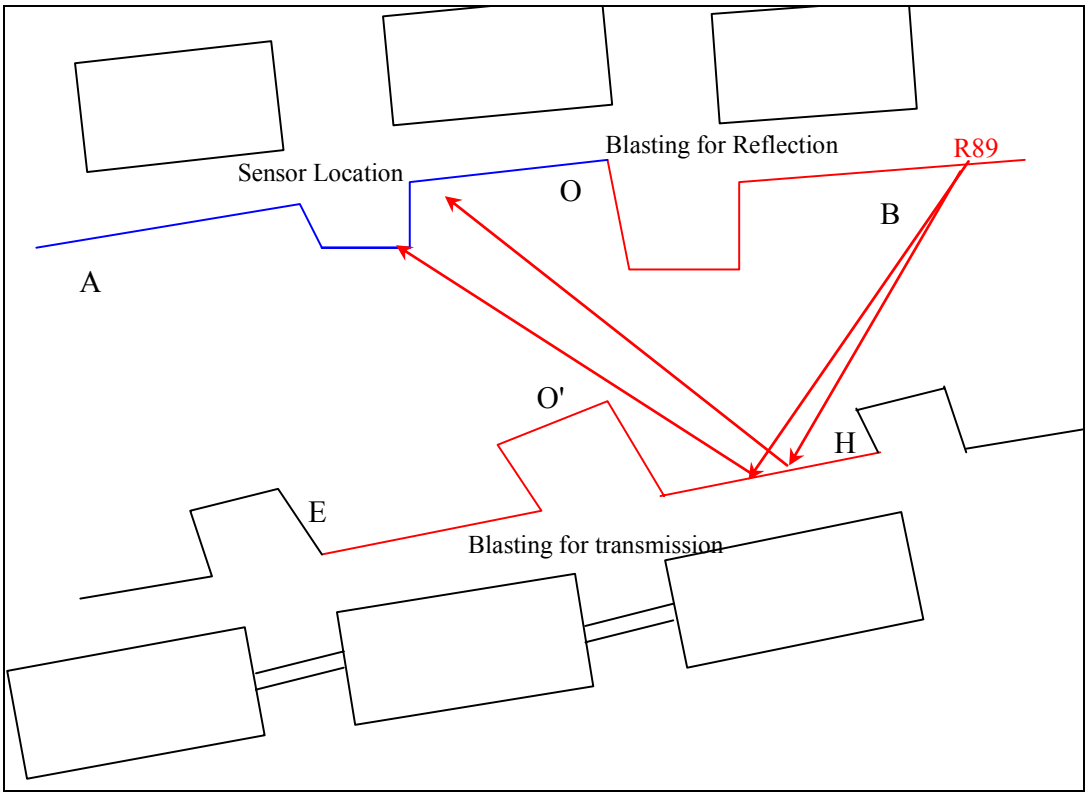

Figure 3.16 Testing setup for event 147.

Triggering time (ms)	Sensor #	S6	S7	S8	N1	N2	N3	N5	N6
50	Arrival time	77.8	78	79.81	76.8	76	76.5	77.5	78.7

Table 3. 10 Parameters of ellipses associated with event 147

Source*	Sensor**	Travel time (ms)	Travel distance (ft)	Half of foci distance (ft)	Half of major axis (ft)	Half of minor axis (ft)
R89	S6	27.8	122.9	36.8	61.5	49.2
R89	S7	28.0	123.7	39.8	61.9	47.3
R89	S8	29.8	131.3	42.1	65.7	50.4
R89	N1	26.8	118.2	42.7	59.1	40.8
R89	N2	26.0	114.6	46.2	57.3	33.9
R89	N3	26.5	116.8	47.2	58.4	34.4
R89	N5	27.5	121.3	49.7	60.7	34.7
R89	N6	28.7	126.7	51.2	63.4	37.3

* See Table 3.3 for source coordinates
** See Table 3.1 for sensor coordinates
*** Channel wave velocity: 4413 ft/s

The ellipses calculated based on the travel times given in the above table are plotted in Figure 3.18. It is evident from the figure that these ellipses delineated the void with a fair accuracy.

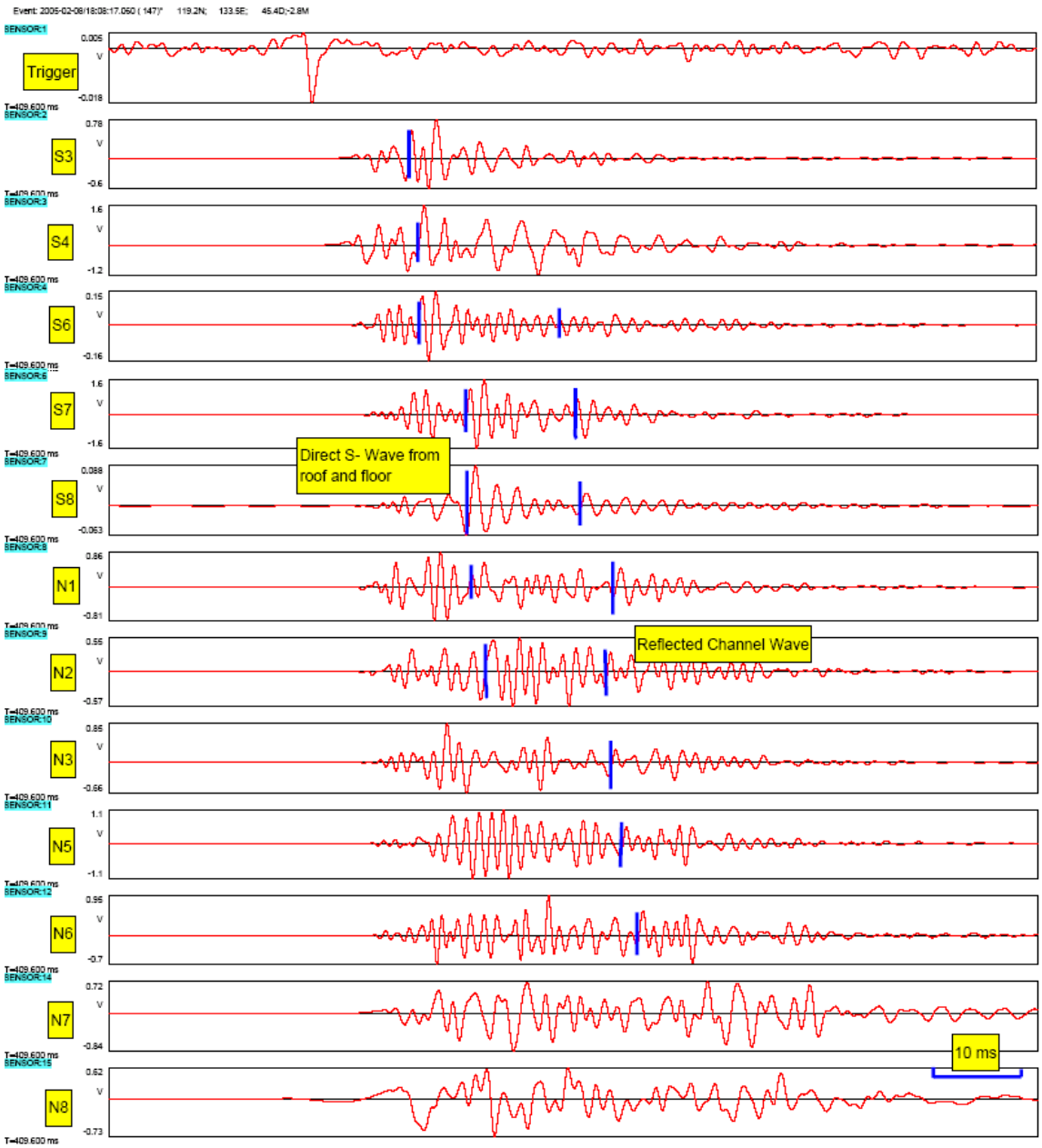

Figure 3.17 Signal waveform for a reflection survey carried out at Site I, Harmony Mine (display window: 30-120 ms for event 147).

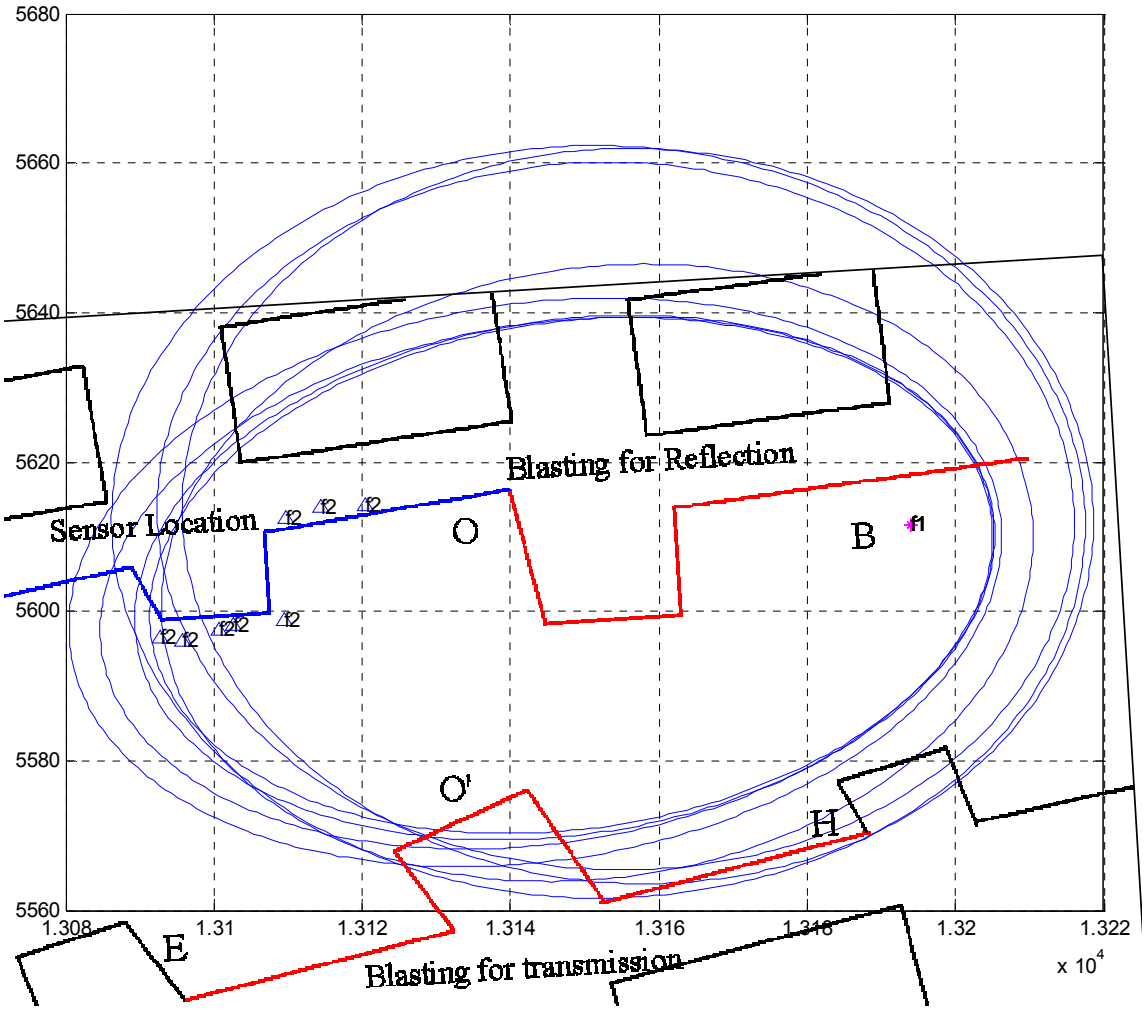

Figure 3.18 Void mapping with the ellipses associated with event 147 at Harmony Mine testing site. The void boundary is represented by a short red line. The locations of the sensors and the source as well as the associated ray paths are illustrated in Figure 3.16.

3.5 Void mapping

The elliptical method was used to map the void location and the result is given by two plots, Figure 3.19a and Figure 3.19b. The channel wave velocity used for void mapping is 4413 ft/s.

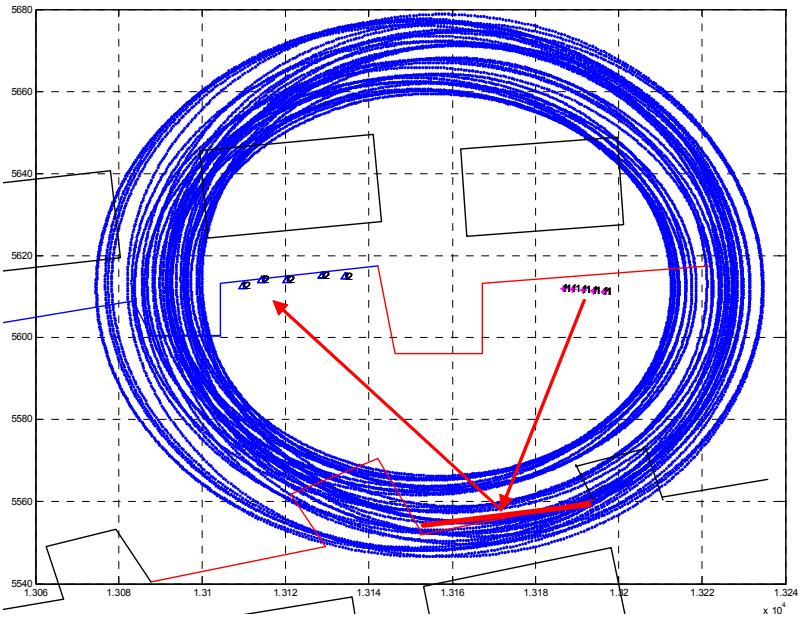

a. Ellipses associated with blasting locations of R7, R78, R8, R89, and R9.

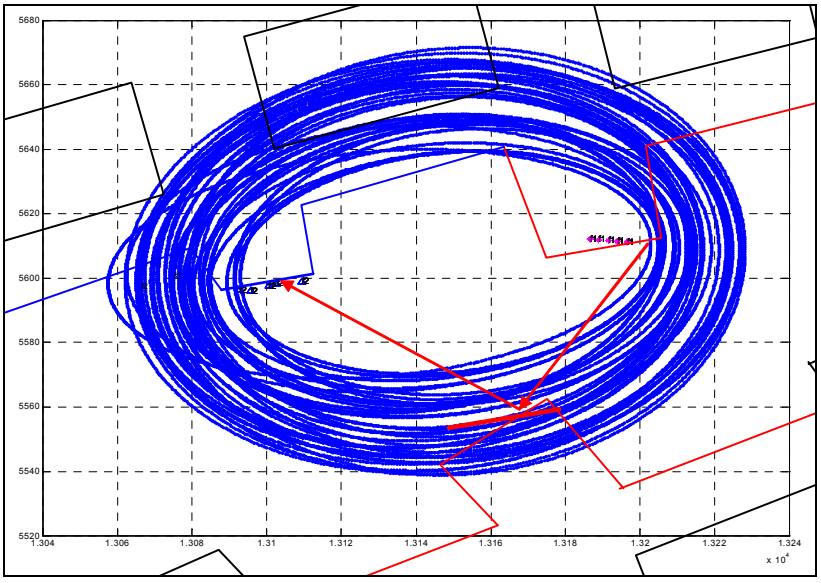

b. Ellipses associated with blasting locations of NR1, NR3, NR4, NR5, and NR6.

Figure 3.19 "Void" location determined by the elliptical location method at Site I, Harmony Mine).

The ellipses in these two plots were associated with the signals reflected from two locations. The first one, as shown by Figure 3.19a, is a section between two short entries. The second one is the back of the short entry shown by Figure 3.19b. Because of the site geometry and the testing setup, the ray paths which could access these two locations were limited. For the section between two entries, the ray paths were practically limited to those between blasting hole R7, R78, R8, R89 and R9 and sensor S3, S4, S6, S7 and S8. For the second location, the ray paths were primarily associated with Blasting hole NR1,NR2, NR3, NR4, NR5 and NR6 and sensor N1, N2, N3, N5 and N6.

The void location result shown in Figure 3.19 is a demonstration of the importance of the elliptical mapping method for void detection. Because of the site restrictions, sensors had to be installed at three different locations and blasting holes had to be drilled at two very different locations. Furthermore, the void in this case had two distinctive sections. With the elliptical method, none of these "special" issues became a problem. It, however, would be very difficult for any other method, such as stacking.

3.6 Summary of the first test at the Harmony Mine

The first test at the Harmony Mine was also the first opportunity for Penn State to test the ISS based void detection technique. The importance for this test might be viewed from two different aspects.

First, the test confirmed the suitability of the data acquisition technique assembled by Penn State, which includes the choice of the data acquisition system, the sensors used, the sensor installation technique, the blasting procedure and design, and the triggering technique. The most satisfactory aspect of this technique is its capability of acquiring high quality, broadband signals. At the site, it recorded the high frequency signals up to 3000 Hz on a very consistent basis. Broadband signals with high frequency components are important for the ISS based void detection in many ways, such as survey resolution, signal recognition and data processing. The broadband signals also insure that no desired signals will be missed if they are there.

Second, the test unequivocally demonstrated the existence of the channel waves at the site and the feasibility to use these waves for void detection. The channel waves at the site have a typical frequency range of 400 – 600 Hz, with the traveling velocity of 4400 ft/s. It should be noted that the Harmony mine is an anthracite mine with a seam thickness of 4 – 6 ft. Both the roof and floor are strong sandstone.

4. Second Field Test at Harmony Mine

4.1 Introduction

On April 29, 2005, the Penn State project team carried out its second field test at the Harmony Mine. The testing site, Site II, was near the portal of the mine. The main purpose of this test was to investigate the effectiveness of the ISS based void detection technique over longer distances. Site I was not chosen as the average pillar width at this site is about 60 ft, which is reasonable for the first test, but not large enough for demonstrating the practical effectiveness of the technique. To demonstrate a practical, useable void detection technique, a minimum width of 150 ft is considered necessary.

One of the main difficulties for testing the ISS based void detection technique was to find the pillar of suitable size. When Penn State conducted its first test at the Harmony Mine, the mine had no pillars with the dimension on the order of 150 – 200 ft. After the mine became aware that Penn State needed such a pillar, Mr. Edward Smock, the President and owner of the mine, decided to create one for Penn State. Hence, the pillar for Site II testing was developed by the mine for this study. The initiative and cooperation of Mr. Spock is deeply appreciated.

Figure 4.1 Mr. Edward Smock (middle), President and owner of the Harmony Mine, who's decision led to the development of Site II testing site for MSHA's void detection project.

4.2 Testing site and experimental design

Site II, the site for the second test at the Harmony Mine, is shown in Figure 4.2. The site is located within a room and pillar development area near the portal of the mine. The pillar width as shown is approximately 150 ft.

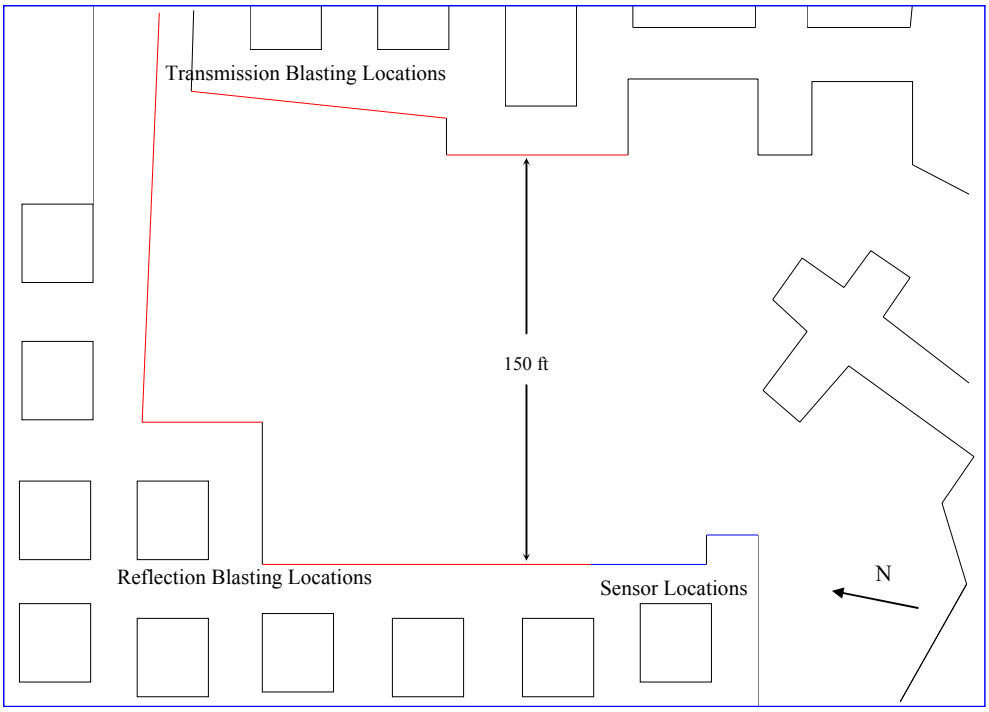

Figure 4.2 General layout and testing setup at Site II, Harmony Mine.

The site was utilized for both transmission and reflection surveys. The experimental setup consisted of three general sections: sensor section, blasting sections for transmission survey, and blasting sections for reflection survey.

The specifications on the sensors, the data acquisition system, and the major operational parameters used for the test are given in Appendix I. The sampling rate and the recording window used for the test are 50,000 samples/second and 0.4 second, respectively.

4.2.1 Sensor section

The sensor section included 15 sensor holes, which were numbered from S1 to S15. The locations and orientation of these sensor holes are shown in Figure 4.3. The diameter of the sensor holes is 1.75". The length of the sensor holes vary. In general, the straight holes are 5 ft long and the angled holes are 7 ft long. The actual length of the sensor holes and the sensor coordinates are given in Table 4.1.

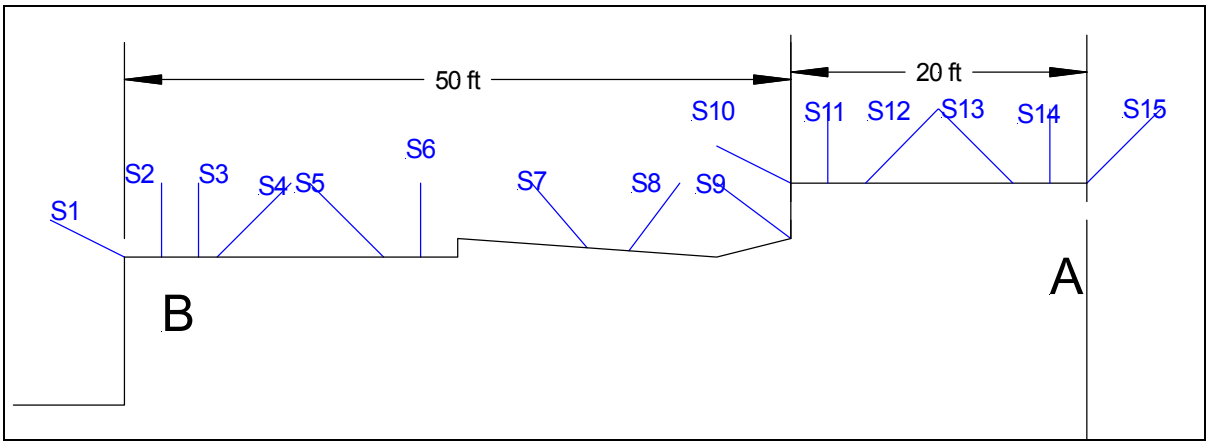

Figure 4.3 Sensor section at Site II, which was designed for both transmission and reflection surveys.

Table 4.1 Sensor hole information for Site II, Harmony Mine

Hole #	Channel #	Length (ft)	Sensor coordinate (ft)	
			East (x)	North (y)
S1	2	7	6184.0	14168.7
S2	3	5	6171.1	14170.6
S3	4	5	6168.6	14170.7
S4	5	7	6164.5	14170.7
S5	12*	7	6161.1	14171.2
S6	7	5	6156.8	14172.2
S7	8	7	6144.9	14173.3
S8	9	7	6142.3	14173.8
S9	10	7	6137.2	14173.6
S10	11	7	6137.2	14183.1
S12	6**	7	6128.7	14187.6
S13	13	7	6124.2	14188.5
S14	14	7	6120.6	14188.9
S15	15	7	6113.0	14190.1

*Geophone was used for the channel

** Channel # 6 was not working.

4.2.2 Blasting section for transmission survey

There were 12 blasting holes prepared for the transmission survey, which were numbered from T1 to T12. Among these 12 prepared drillholes, 8 were actually used for the survey. The coordinates for these drillholes are given in Table 4.2. All blasting holes were 4 ft long and 1.5" in diameter, drilled in the middle of the seam.

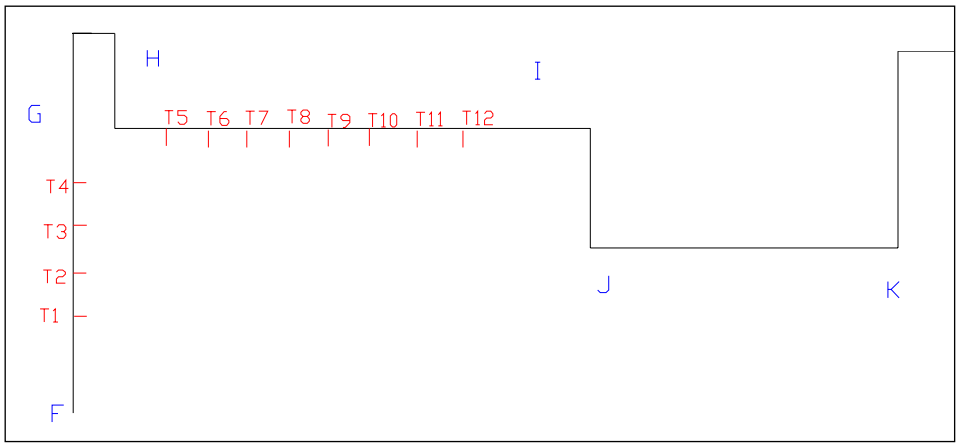

Figure 4.4 Blasting hole locations for transmission survey.

Table 4.2 Coordinates of blasting holes for transmission survey at Site II, Harmony Mine

Hole #	Source coordinate (ft)	
	East (x)	North (y)
T12	6269.2	14320.3
T11	6279.4	14319.6
T10	6289.1	14317.9
T9	6298.8	14316.0
T8	6308.2	14314.5
T7	6317.8	14312.3
T1	6379.4	14266.9
T2	6382.6	14276.9

4.2.3 Blasting section for reflection survey

A total of 17 blasting holes were prepared for the reflection survey, which were number from R1 to R17. Because of the site condition, these 17 holes were grouped at three locations as shown in Figure 4.5. All blasting holes are 4 feet long and 1.5 inches in diameter. The coordinates of the drill holes which were used for the survey are given in Table 4.3.

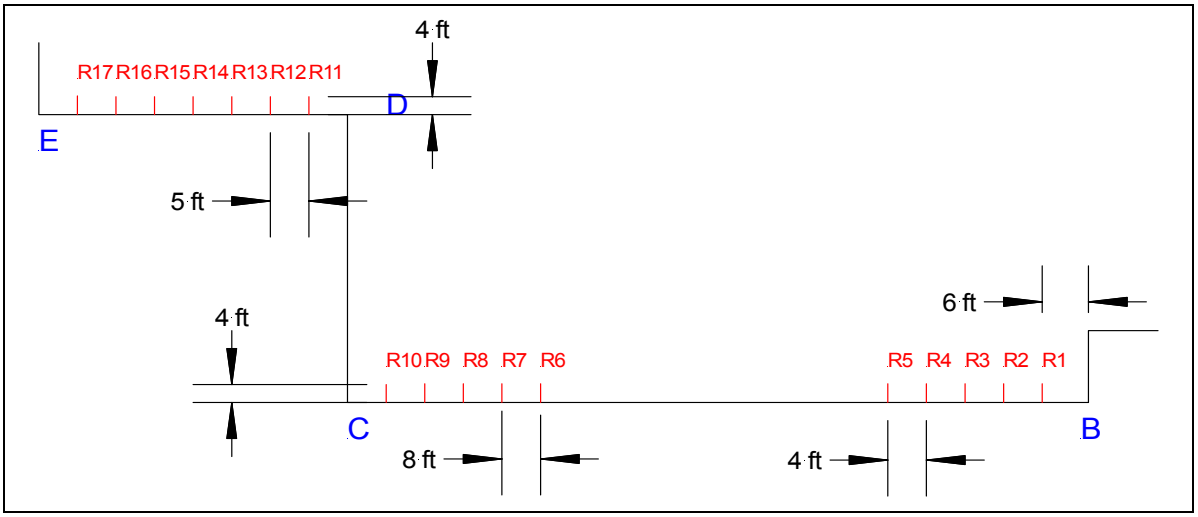

Figure 4.5 Blasting section for reflection survey at Site II, Harmony Mine.

Table 4.3 Coordinates of blasting holes for reflection survey at Site II, Harmony Mine

Hole #	Source coordinate (ft)	
	East (x)	North (y)
R16	6337.4	14168.8
R13	6325.5	14179.6
R11	6317.0	14183.4
R9	6278.0	14128.9
R8	6270.8	14130.6
R7	6263.6	14132.2
R5	6196.5	14141.2
R4	6193.4	14143.3
R2	6187.2	14148.1
R1	6185.1	14151.7

4.3 Transmission survey

The transmission survey at Harmony mine consisted of eight individual surveys (Figure 4.6). Caps or 125 gram (1 inch) explosives were used as the seismic source. The detailed information is summarized in Table 4.4.

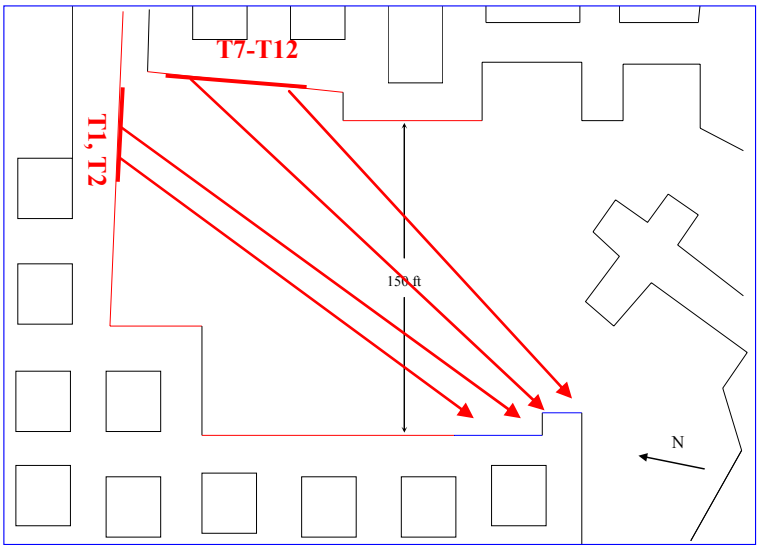

Figure 4.6 Illustration of ray paths associated with the transmission survey.

Table 4.4 A summary of the transmission survey at Harmony Mine Site II

Hole #	Explosive (g)	Event #
T12	Cap	7
T11	Cap	17
T10	125	22
T9	125	27
T8	Cap	31
T7	Cap	37
T1	Cap	43
T2	Cap	47

4.3.1 Characteristics of transmission signals

The transmission signals from these eight surveys are similar and, for illustration, the signals associated with event 17 are discussed herein. Event 17 refers the reflection survey related to seismic source T11. The location of T11 and the sensors as well as the corresponding ray path for this event are illustrated in Figure 4.7. The signals for the event are given in Figure 4.8.

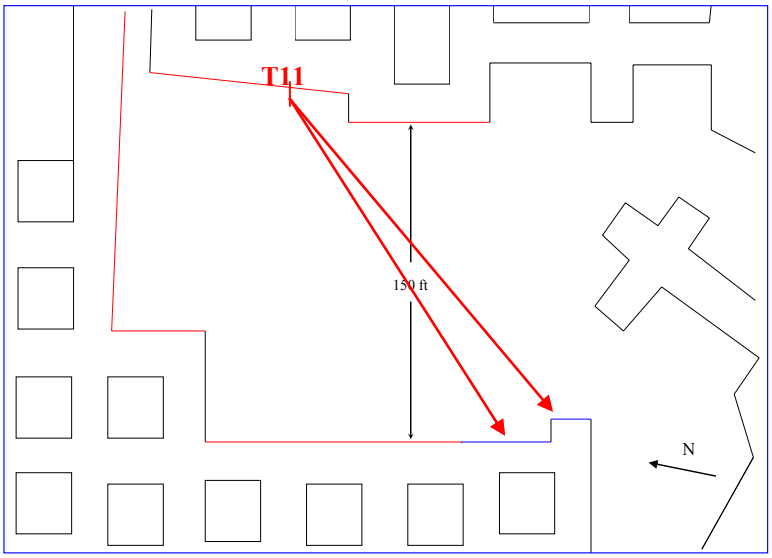

Figure 4.7 Testing setup for Event 17.

The first arrivals shown in Figure 4.8 are due to the P-waves from the sandstone roof. It is seen from the figure that all these arrivals are clearly defined. They have almost a constant frequency (about 3000 Hz) throughout the phase and sharp arrivals. The arrivals of the S-waves from the roof are also evident from the figure. During this time period, the P-waves from the coal also arrive. The arrivals of the channel waves are clear seen in the figure. They have large amplitude with a well defined low frequency which is in the range of 400 -600 Hz. The arrival time readings for channel waves as well as for P-waves from roof and coal are listed in the following table.

Table 4.5 Arrival time reading for Event 17

PC CH. #	2	3	4	5	12	7	8	9	10	11	13	14	15	16
Sensor #	S1	S2	S3	S4	S5	S6	S7	S8	S9	S10	S12	S13	S14	S15
P- from roof	60.2	60.8	60.85	61.05	61.3	61.15	61.4	61.45	61.6	61.35	61.55	61.7	62	60.2
P-from coal	71.15	71.4	71.75	72.95	71.55	72.85	74	74.3	73.9	73.35	72.8	72.95	73.85	71.15
Channel wave	83.36	83.5	84.05	84.1			84.25					85.25	85.6	

* trigger time 50 ms.

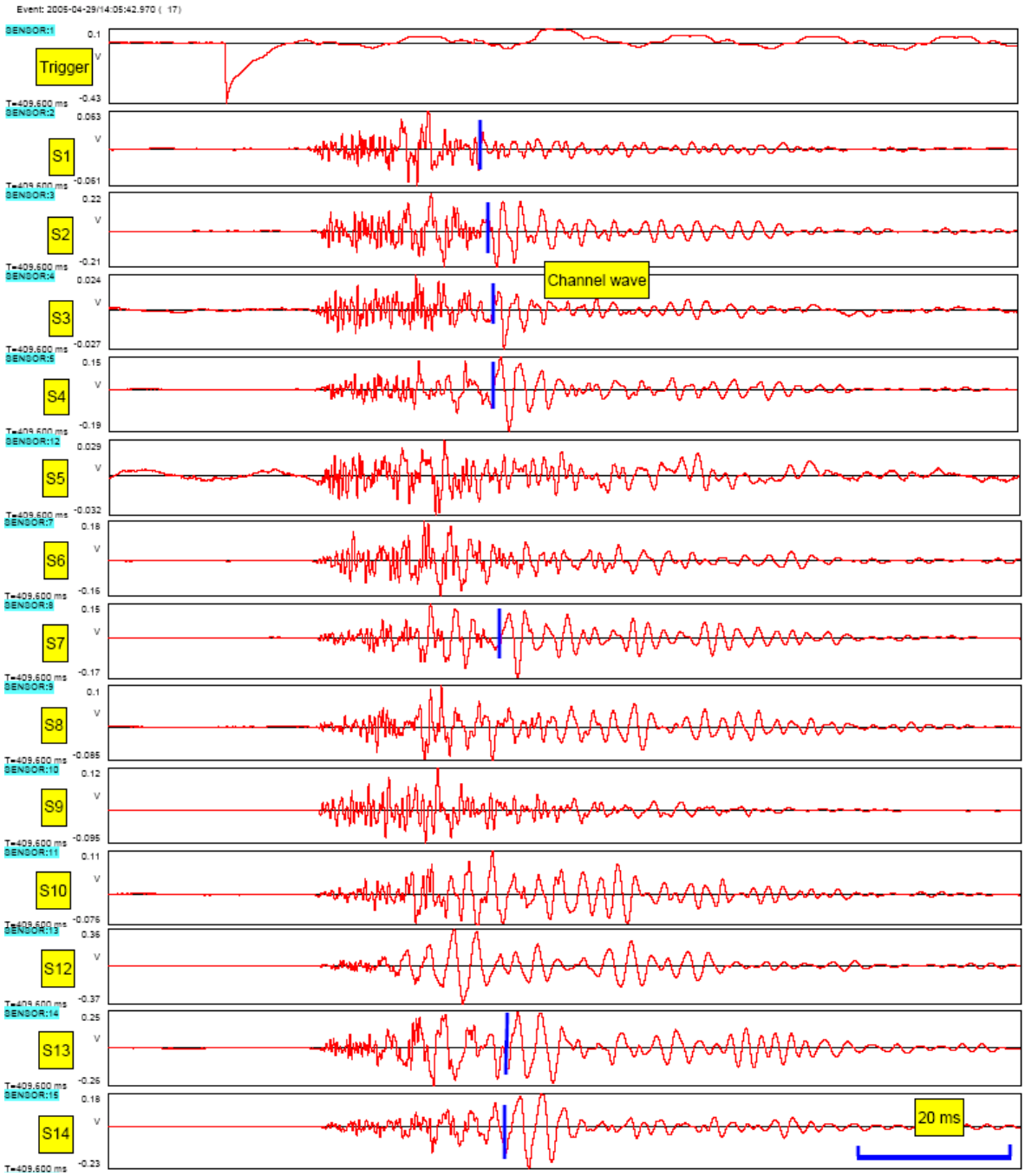

Figure 4.8 Signal waveform for a transmission survey carried out at Site II, Harmony Mine (display window: 35 - 160 ms for event 17).

The signal amplitude of the channel waves for 8 surveys are well correlated with the source strength. The related data are given in Table 4.6.

Table 4.6 Source strength and signal amplitude

Hole #	Event #	Explosives (g)	Average amplitude (Peak voltage)	Gain
T12	7	Cap	0.236	0
T11	17	Cap	0.15	0
T10	22	125	0.21	0
T9	27	125	0.46	10
T8	31	Cap	0.19	10
T7	37	Cap	0.15	10
T1	43	Cap	0.16	10
T2	47	Cap	0.14	10

4.3.2 Velocity calculations for Site II

The channel wave velocity as well as the P- and S-wave velocities associated with coal and roof was calculated. The average velocity for the channel wave at Site II is 5160 ft/s. The raw data used for the calculation of the channel wave velocity are given in Tables 4.7 and 4.8.

Table 4.7 Source – receiver distances (ft) at Harmony Mine Site II

				Direct Travel Distance										
CH. #	2	3	4	5	12	7	8	9	10	11	13	14	15	16
	S1	**S2**	**S3**	**S4**	**S5**	**S6**	**S7**	**S8**	**S9**	**S10**	**S12**	**S13**	**S14**	**S15**
T12	173.9	179.0	180.3	182.6	184.2	186.0	192.6	193.9	197.5	190.5	193.3	196.0	198.5	203.5
T11	178.6	184.3	185.7	188.1	189.8	191.8	198.8	200.2	204.0	197.2	200.4	203.3	205.9	211.0
T10	182.5	188.7	190.2	192.9	194.7	196.8	204.3	205.8	209.6	203.2	206.7	209.7	212.4	217.7
T9	186.8	193.6	195.2	197.9	199.9	202.2	210.0	211.6	215.6	209.4	213.2	216.3	219.2	224.7
T8	191.6	198.9	200.6	203.4	205.5	208.0	216.1	217.8	221.9	216.0	220.0	223.3	226.2	231.8
T7	196.4	204.2	206.0	208.9	211.1	213.7	222.2	223.9	228.2	222.5	226.8	230.2	233.2	239.0
T1	219.5	230.5	232.8	236.5	239.3	243.0	253.7	255.9	260.9	257.6	264.0	268.2	271.8	278.6
T2	226.9	237.7	239.9	243.6	246.4	249.9	260.5	262.6	267.6	264.0	270.1	274.3	277.8	284.5

Table 4.8 Channel wave from coal seam velocities determined from transmission survey at Harmony mine site II

				velocity of channel wave by transmission test											
	CH. #	2	3	4	5	12	7	8	9	10	11	13	14	15	
EVENT #		S1	S2	S3	S4	S5	S6	S7	S8	S9	S10	S12	S13	S14	
7	T12	5376.8	5620.3	5455.6	5542.6		5501.8	5714.3	5753.2		6018.3	5685.2	5681.7	5779.1	**5648.1**
17	T11		5500.1	5452.5	5517.2			5805.3					5766.5	5782.7	**5637.4**
22	T10	5169.3	5719.1	5704.1	5756.9	5651.2	5623.5	5746.0	5436.3	5575.3	5675.6	5797.3	5914.7	5826.6	**5661.2**
27	T9	5253.4	5422.0	5459.0		5460.9	5464.3	5555.9		5629.2	5411.3		5976.5	5955.3	**5558.8**
31	T8	4684.3	4815.8	4844.6	4884.6		4904.8				5210.6	5057.9	5162.7	5134.9	**4966.7**
37	T7	4316.8	4468.3		4557.1	4444.2		4836.1	4938.1	4902.0	4779.9		5004.0	4919.4	**4716.6**
43	T1		4378.1		4470.4	4461.2		4393.2	4455.0		4925.8		4823.2		**4558.1**
47	T2	4355.9	4610.8	4569.6	4523.1		4324.3	4395.9	4440.4	4459.5		4494.8		4539.0	**4471.3**

4.4 Reflection survey at Site II, Harmony Mine

The reflection survey at Site II included 10 individual surveys (blasting events). The seismic sources used for the surveys were 125 g explosives and caps. The explosives used and the associated event numbers for these surveys are listed in Table 4.9.

Table 4.9 A summary of the reflection surveys at Harmony Mine Site II

Hole #	Explosive (g)	Event #
R16	125	53
R13	125	58
R11	125	72
R9	125	85
R8	125	89
R7	125	97
R5	Cap	108
R4	Cap	114
R2	Cap	125
R1	Cap	129

The survey result shows that the reflected channel waves were evident for most events. However, because of the site geometry, there were several groups of channel waves, which often formed a "train" of channel waves. A challenge for the data analysis was to identify the arrivals which were reflected from the "void" (the other side of the pillar). The event discussed in the next section is such an example.

4.4.1 Case Study Event 72

Event 72 refers the reflection survey related to seismic source R11. The locations of R11 and the sensors are shown in Figure 4.9. The waveform for the event is given in Figure 4.10. The reflected signals for this event are strong. Their frequencies are also well defined, about 500 Hz. There are two distinct channel wave arrivals. One arrival is attributed to the wave path that is reflected off of the boundary at location 'A' and is contained in the signal signatures from sensors S1 through S10 in Figure 4.10. The other arrival is attributed to the wave path that reflects off of the boundary at location 'B' as contained in the signal signatures from sensors S12 through S14 in Figure 4.10. The corresponding ray paths for these two trends are also shown in Figure 4.9. The arrival readings (from top reflector) are given in the following table.

Triggering time (ms)	Sensor #	S1	S2	S3	S4	S5	S6	S7	S8	S9	S10
50	Arrival time (ms)	115.1	113.25	112.9	113.1	118.4	116	117.1	117.6	118.9	119.5

Table 4.10: Parameters of ellipses associated with event 72

Source*	Sensor**	Travel time (ms)	Travel distance (ft)	Half of foci distance (ft)	Half of major axis (ft)	Half of minor axis (ft)
R11	S1	65.1	335.9	66.9	168.0	154.0
R11	S2	63.3	326.4	73.2	163.2	145.8
R11	S3	62.9	324.6	74.5	162.3	144.2
R11	S4	63.5	327.6	76.5	163.8	144.8
R11	S5	68.4	352.9	78.2	176.5	158.2
R11	S6	66.0	340.6	80.3	170.3	150.2
R11	S7	67.2	346.6	86.2	173.3	150.3
R11	S8	67.6	348.6	87.5	174.3	150.8
R11	S9	68.9	355.5	90.0	177.8	153.3
R11	S10	69.4	358.3	89.9	179.2	155.0

* See Table 4.1 for source coordinates
** See Table 4.3 for sensor coordinates
*** Velocity: Channel wave 5160 ft/s

The ellipses calculated based on the travel times given in the above table are plotted in Figure 4.11. It is evident from the figure that these ellipses delineated the void with a good accuracy.

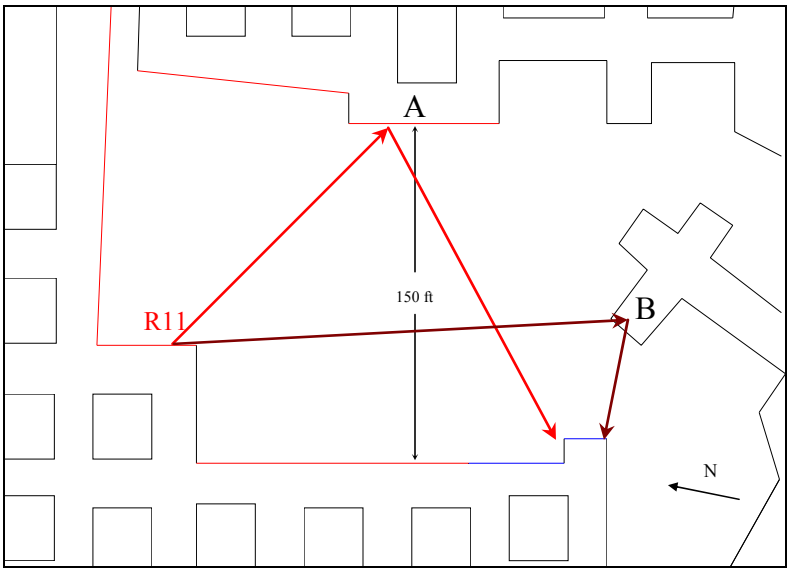

Figure 4.9 Testing setup for event 72.

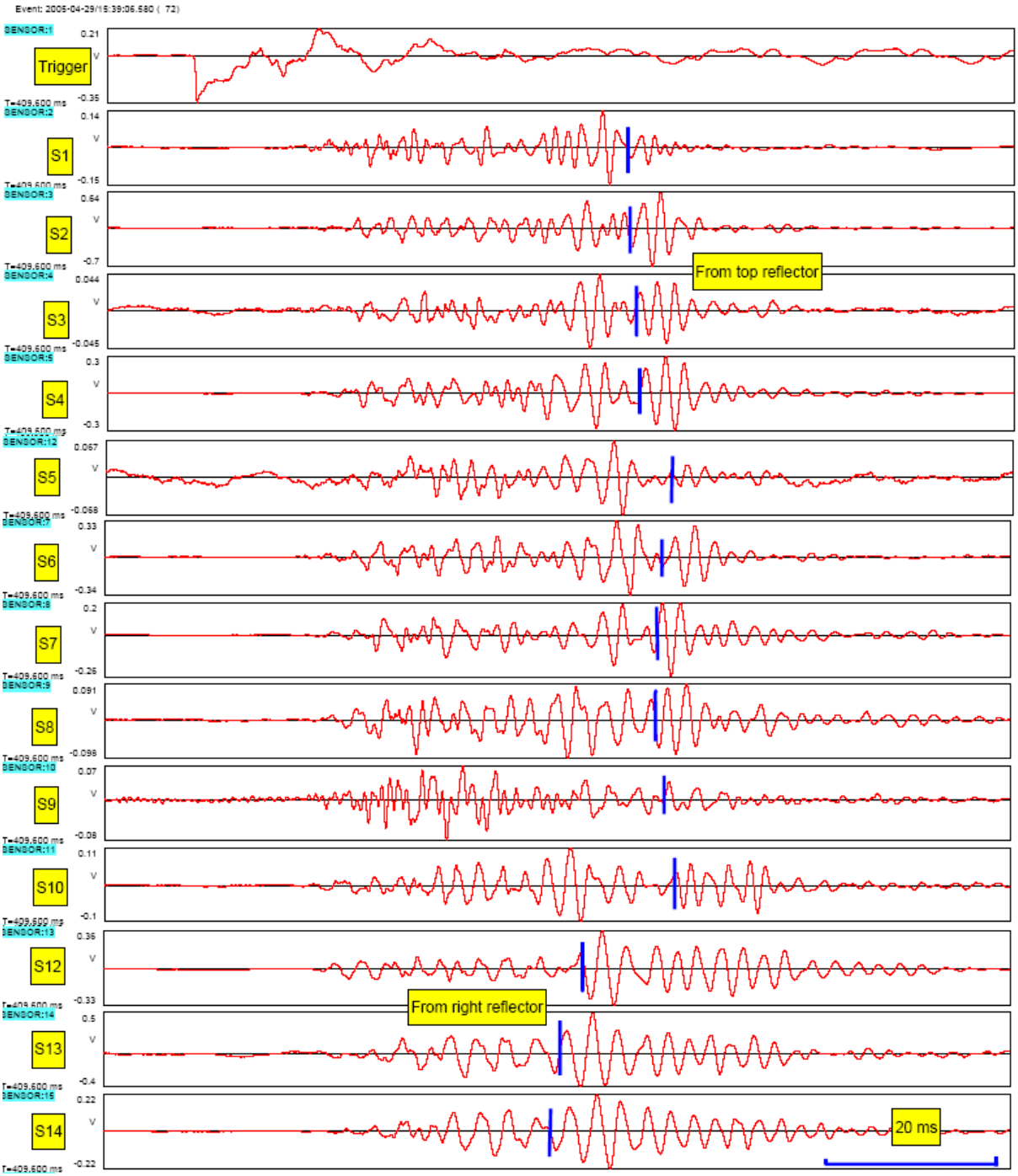

Figure 4.10 Signal waveform for a reflection survey carried out at Site II, Harmony Mine (display window: 35 - 140 ms for event 72).

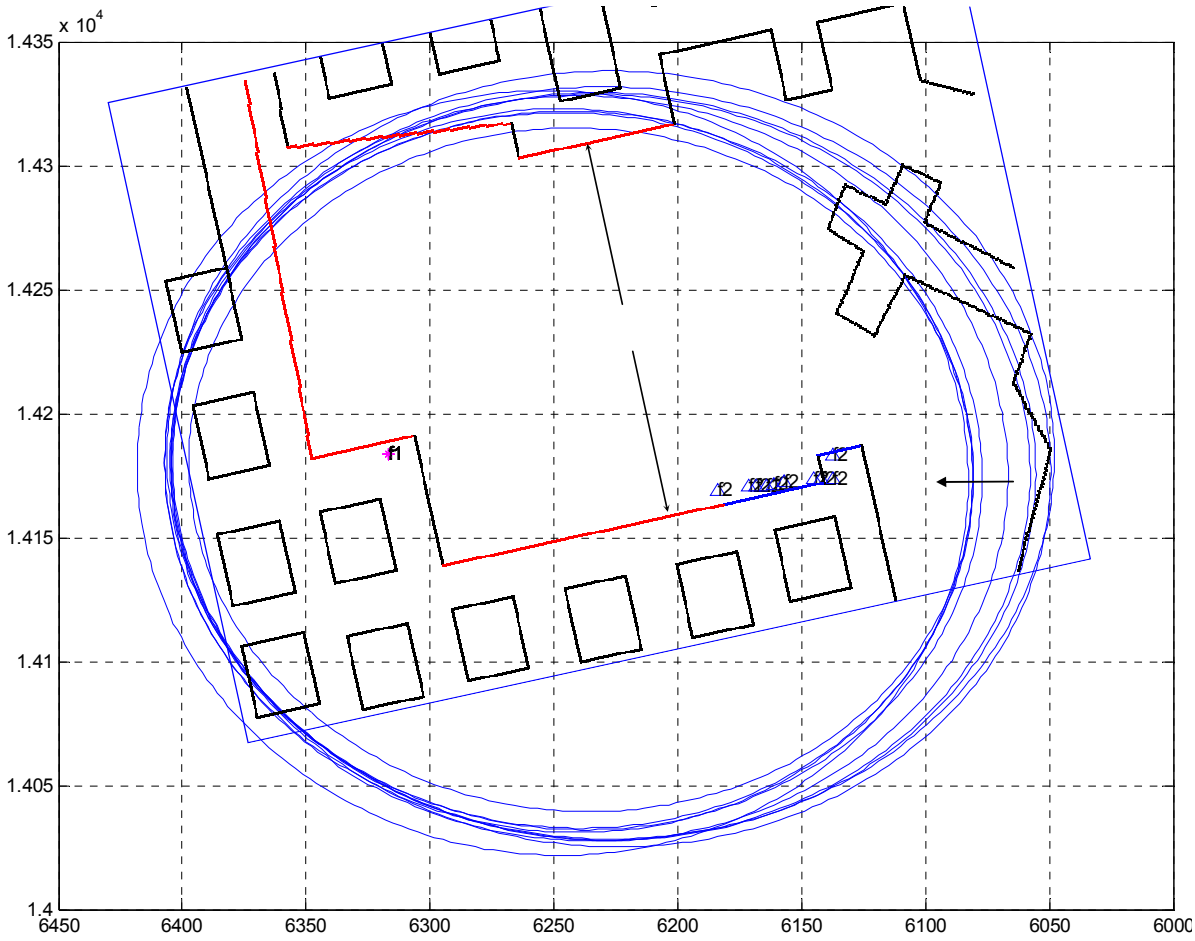

Figure 4.11 Void mapping with the ellipses associated with event 72 at Harmony Mine testing site. The void boundary is represented by a short red line. The locations of the sensors and the source as well as the associated ray paths are illustrated in Figure 4.9.

4.5 Void mapping

The elliptical method was used to map the void location and the result is shown in Figure 4.12. The channel wave velocity used for void mapping is 5160 ft/s. The pillar boundary is this case is well fitted by two red lines, the common tangent lines of the ellipses.

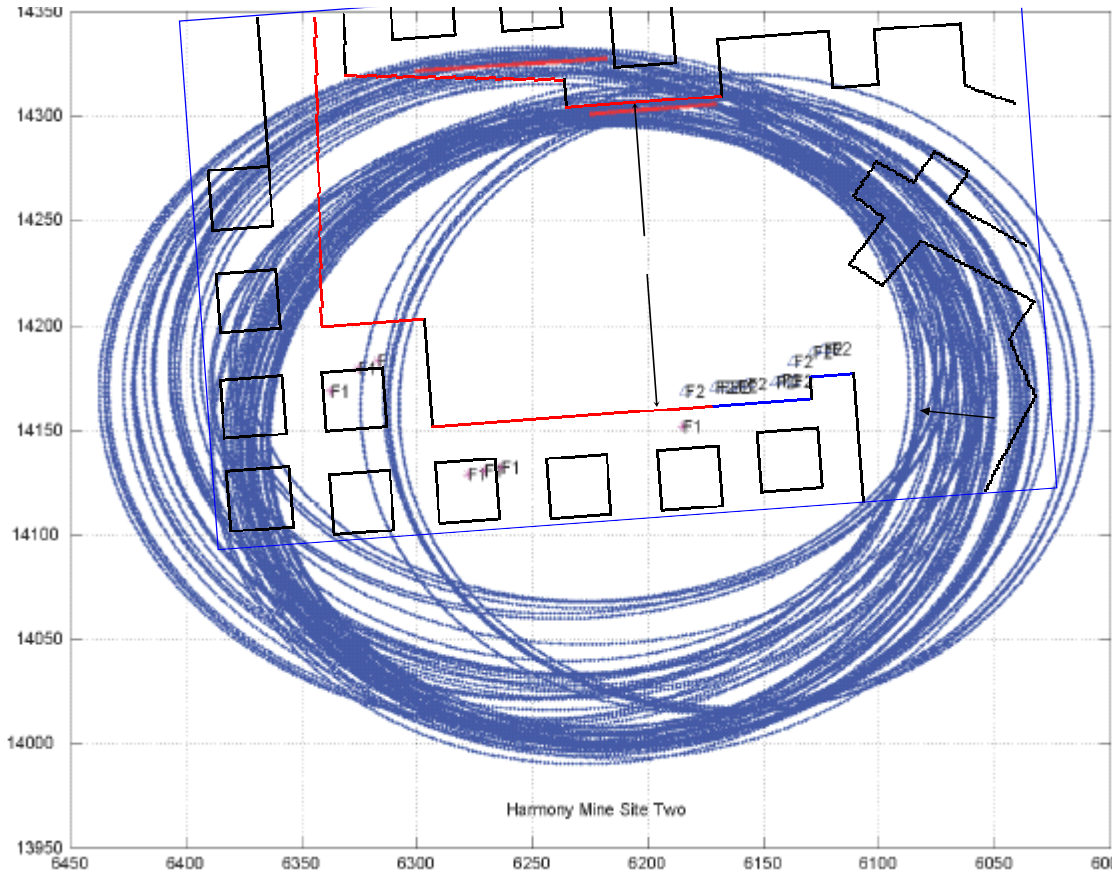

Figure 4.12 "Void" location (red lines) determined by the elliptical location method at Site II, Harmony Mine (red lines are the actual pillar boundary , which coincide with the common tangent lines of the ellipses).

4.6 Summary of the second test at the Harmony Mine

The main objective of the second test at the Harmony Mine was to investigate the effectiveness of the ISS based void detection technique over longer distances. The pillar width for the first test was 60 ft and it was increased to 150 ft for the second test. The testing result was quite positive for this mapping distance. The average mapping error in this case (Figure 4.12) is estimated at ±10 ft.

5. Demonstration at Harmony Mine

5.1 Introduction

On November 15, 2005, the Penn State project team demonstrated the ISS based void detection technique for the anthracite mine condition to MSHA and the mining industry at testing Site II, located in a room and pillar development area near the mine portal (Figure 5.1).

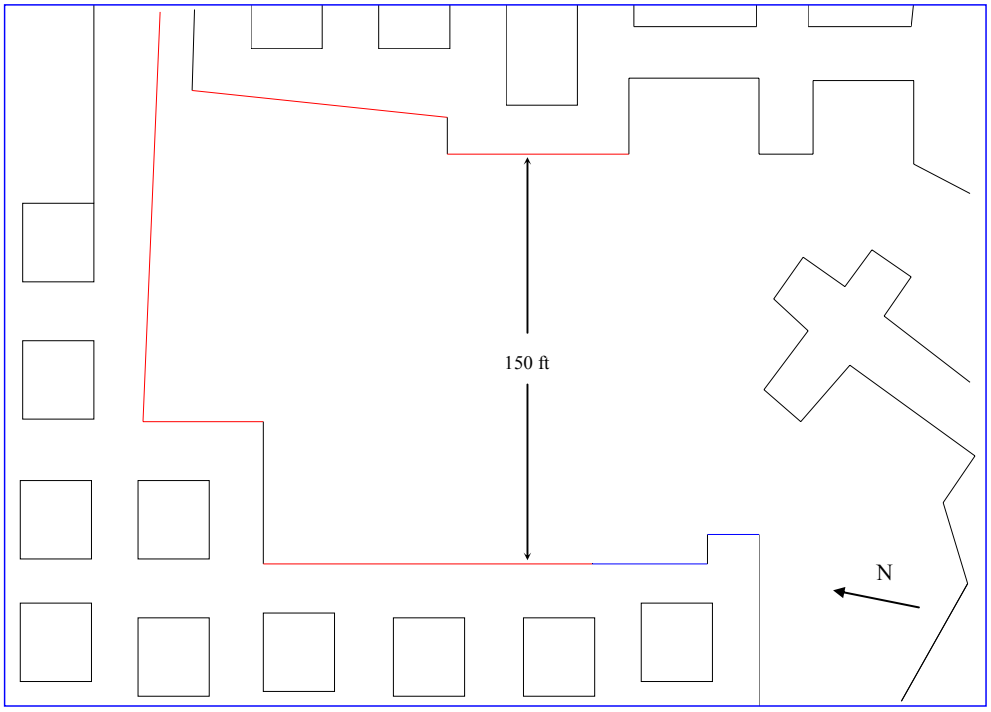

Figure 5.1 General layouts at Site II, Harmony Mine.

5.1.1 Demonstration objectives

There were two objectives for the demonstration. The first objective was to demonstrate the existence of channel waves and the reliability of using these channel waves for void detection in anthracite mine environments. The core issue for the ISS method was to assess the ability to generate and detect channel waves reliably. To demonstrate the feasibility of the ISS based void detection, this first issue needed to be addressed. Based on the results of two field tests at the Harmony Mine, Penn State believes that significant progress had been made in this regard. The second objective was to demonstrate that ISS based void detection could be used over distances of at least 150 ft in anthracite mine environments.

5.1.2 Testing site selection

The test site for the MSHA/industry demonstration was Site II (Figure 5.1) which was the same site used by Penn State for ISS void detection evaluations at the Harmony Mine on April 29, 2005. The primary reason this site was used for the demonstration was that the pillar width was of a thickness comparable to that deemed adequate for minimum barrier pillar size between active and abandoned workings. In order to demonstrate the practicability of the ISS based void detection technique, a minimum pillar size in the order of 150 – 200 ft was necessary. This pillar was specially developed by the mine for the second test conducted by Penn State.

In addition to its size, the site would allow Penn State to demonstrate the reliability of the technique in terms of the repeatability. If the performance of the technique is repeatable, the testing result from the demonstration should be, at least, as good as the earlier one. The other important advantage of using the same testing site was to evaluate the retrievable sensor installation technique under wet conditions. The test site was very wet with water seepage observed from many of the sensor holes.

5.2 An overview of the demonstration activity

The demonstration included two sessions, the technical meeting at the mine office and the field demonstration of the ISS based void detection technique at Site II.

5.2.1 Attendees of the demonstration

The attendees of the demonstration included MSHA and DEP officials, representatives from the mining industry and researchers from Penn State (Table 5.1). Figure 5.2 is the picture of the attendees taken at the mine portal.

Table 5.1 Attendees of the demonstration of ISS based void detection technique

Name	Affiliation	Title
George Gardner	MSHA	Senior Civil Engineer, (412) 386 – 6929 Program manager, MSHA void detection program
Gregory Mehalchick	MSHA, District 1	Senior Mining Engineer (570) 826 – 7749
Leonard P. Sargent	MSHA, District 1	(234) 648 – 1203
David Williams	DEP, Mine Safety	(570) 621 – 3141
Troy A. Wolfgang	DEP, Mine Safety	(570) 621 – 3140
Art Flick	Harmony Mine	Mine Superintendent
Ivan Swinehart	Harmony Mine	Mine Foreman
George Manhart	Harmony Mine	Assistant Mine Foreman
Maochen Ge	PSU	PI of the project (814) 865 – 5861
Andrew Schissler	PSU	Co-PI of the project (814) 863 – 7597
Hongliang Wang	PSU	Graduate research assistant (814) 865 – 3526
Jin Wang	PSU	Graduate research assistant (814) 865 – 3526

Figure 5.2 Demonstration participants at mine portal.

5.2.2 Technical meeting

Prior to the field demonstration, a technical meeting was held from 2:00 to 3:30 pm. During the meeting, Dr. Schissler first thanked Harmony Mine and the other industrial partners of Penn State for their support. He also thanked MSHA for its support and guidance. Dr. Ge then made a technical presentation.

Dr. Ge first briefly discussed the major theoretical and technical development work carried out by Penn State during the past year, which included 1)theory of experimental design – angled sensor holes, 2) theory of experimental design – sensitivity analysis, 3) theory of void mapping – elliptical void location, 4) theory of signal analysis – wavelet analysis of reflected signals, 5) retrievable sensor installation technique for 1-D sensors, 6) laboratory velocity measurement, 7) non-explosive seismic sources, and 8) retrievable sensor installation technique for 3-D sensors. The importance of this development work was that it provided the necessary foundation for the field portion of the project.

Following the general discussion, Dr. Ge briefly discussed the test results from two earlier tests carried out at the mine. There were three important achievements. The first one was the application of the retrievable sensor installation technique. The particular importance of this technique for the Harmony Mine was that it was essential for acquiring broadband signals at mine site, from 500 Hz channel waves to 3000 Hz P- and S-waves from the roof. Without this technique, it would be very difficult to apply the ISS based void detection technique at the mine site.

The second one was the demonstration of the presence of channel waves and the reliability of using these channel waves for void detection. The third one was the successful void mapping at both Site I and Site II.

In the meeting, Dr. Ge also discussed the experimental layout and the demonstration items.

After the presentation, the participants of the meeting had an enthusiastic discussion of the application of the ISS based void detection technique for coal mines. Dr. Ge also answered questions raised by the participants. .

To make the Demonstration productive, Penn State prepared six posters and a brochure. The posters were used to summarize the work in six general areas, which were 1) field test at Harmony Mine, 2) field test at FMC, 3) field test at General Chemical, 4) sensor installation technique, 5) laboratory testing techniques, and 6) theoretical developments (Figure 5.3). The brochure was distributed to the participants. It contained the basic information for the project, including the background information of MSHA's void detection project, an overall review of the project progress by Penn State, testing result from the Harmony Mine, and the Demonstration program.

Figure 5.3 Demonstration meeting at Harmony Mine where project posters were exhibited.

5.2.3 Field demonstration

The demonstrations began at 4:00 pm and ended at 7:00 pm. The process of the demonstration was very similar to the regular test. In fact, it was merely another regular test for Penn State from the data collection point of view. During the demonstration, four transmission surveys and six reflection surveys were carried out.

The demonstration items at the site included

- site inspection of the layout of sensor holes and blasting holes,
- site inspection of the setup of the data acquisition system,
- demonstration on installing sensors in the previously drilled holes,
- demonstration on installing sensor installation assemblies in newly drilled holes,
- demonstration on blasting preparation,
- demonstration on real-time data acquisition and brief discussion on received signals,
- inspecting blasting holes after blasting,
- demonstration on sensor retrieval operations, and
- demonstration on packaging the system.

Figure 5.4 MSHA and DEP officials observing real-time data acquisition at the demonstration site.

Figure 5.5 Sensor installation at the demonstration site.

5.3 Field demonstration at Site II, Harmony Mine

The field demonstration was carried out from 4:00 to 7:00 pm at Site II, which was located at the continuous miner section near the mine portal.

5.3.1 Site inspection prior to the field demonstration

The demonstration site was used by Penn State for its second test at the mine on April 29, 2005, about a half year prior to the demonstration. One of the reasons to use this site was to demonstrate the retrievable sensor installation technique; the technique allows the repeated use of previously prepared sensor holes.

On November 1, 2005, two Penn State researchers, Dr. Schissler and Mr. H. Wang, visited the mine. There were two purposes for this trip: 1) to inspect the sensor holes used for the second test and 2) to determine suitable locations for new sensor holes and blasting holes.

During the site visit, each drillhole was evaluated for water, dust, and shape. Most sensor holes were wet because of the site condition. Seepage was observed for sensor holes S5, S6, S11 and S12. Several drillholes had to be cleaned, which should be considered a normal operation and would not pose any problem for reusing these sensor holes.

5.4 Demonstration site and experimental design

The layout of the demonstration site is given in Figure 5.6. The pillar width is approximately 150 ft.

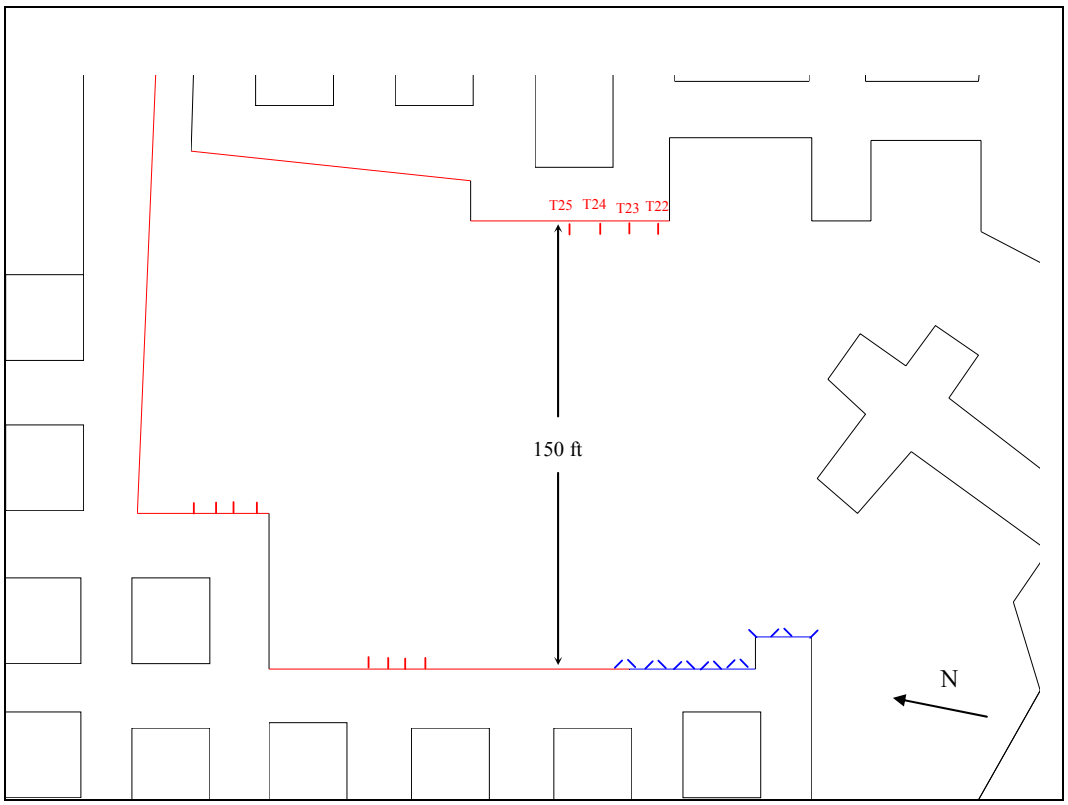

Figure 5.6 Demonstration site and the testing setup for the demonstration.

The site was utilized for both transmission and reflection surveys. The experimental setup included three general sections: sensor section, blasting sections for transmission survey, and blasting sections for reflection survey.

The specifications on the sensors, the data acquisition system, and the major operational parameters used for the test are given in Appendix I. The sampling rate and the recording window used for the test are 50,000 samples/second and 0.4 second, respectively.

5.4.1 Sensor section

The sensor section included 15 sensor holes, which were numbered from S1 to S15. The locations and orientation of these sensor holes are shown in Figure 5.7. The diameter of the sensor holes is 1.75". The length of the sensor holes vary. In general, the straight ones are 5 ft and the angled ones are 7 ft. The actual length of the sensor holes and the sensor coordinates are given in Table 5.2.

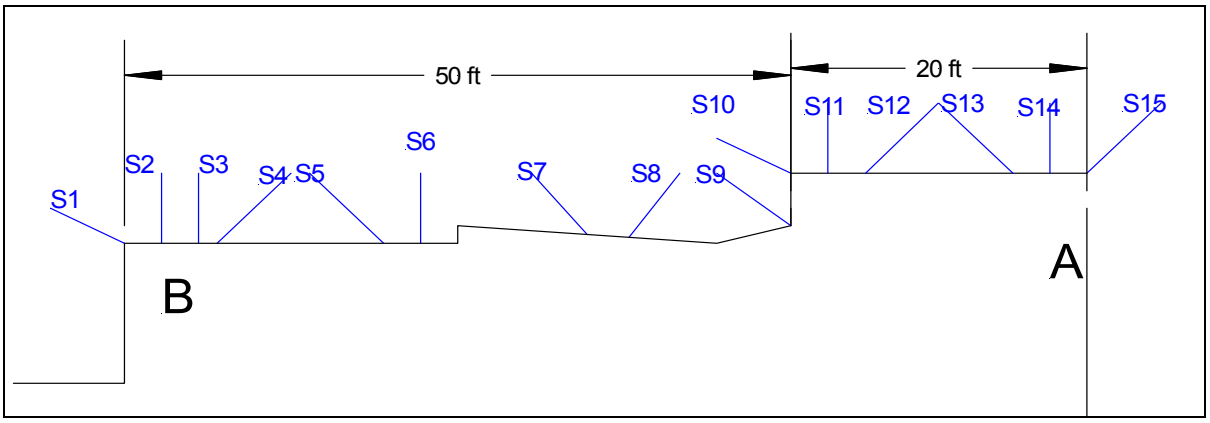

Figure 5.7 Sensor section at Site II, which was designed for both transmission and reflection surveys.

Table 5.2 Sensor hole information for Site II, Harmony Mine

Hole #	Channel #	Length (ft)	Sensor coordinate (ft)	
			East (x)	North (y)
S1	2	7	6184	14168.7
S2	3	5	6171.1	14170.6
S3	4	5	6168.6	14170.7
S4	5	7	6164.5	14170.7
S5	6	7	6161.1	14171.2
S6	7	5	6156.8	14172.2
S7	8	7	6144.9	14173.3
S8	9	7	6142.3	14173.8
S9	10	7	6137.2	14183.1
S10	11	5	6132.3	14186.4
S12	12	7	6128.7	14187.6
S13	14	7	6124.2	14188.5
S14	15	7	6120.6	14188.9
S15	16	7	6113	14190.1

5.4.2 Blasting section for transmission survey

There were 4 blasting holes prepared for the transmission survey, which were numbered from T21 to T25 (Figure 5.8). The coordinates for these drillholes are given in Table 5.3. All blasting holes were 4 ft long and 1.5” in diameter, drilled in the middle of the seam.

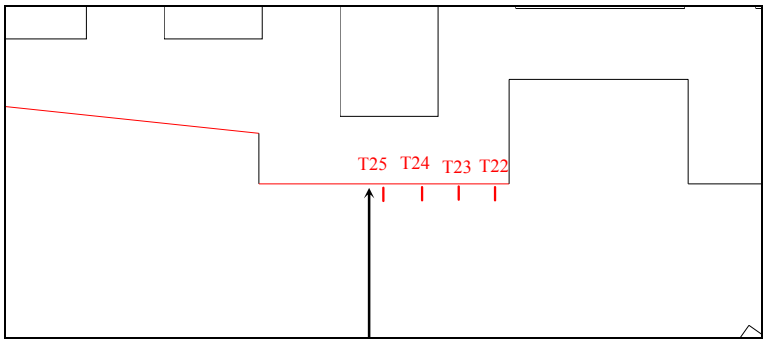

Figure 5.8 Blasting borehole locations for transmission survey.

Table 5.3 Coordinates of blasting holes for transmission survey at Site II, Harmony Mine

Hole #	Source coordinate (ft)	
	East (x)	North (y)
T24	**6217.3**	**14314.1**
T23	**6227.4**	**14310.7**
T25	**6206.5**	**14313.4**
T22	**6233.4**	**14308.8**

5.4.3 Blasting section for reflection survey

Six new blasting holes were prepared for the reflection survey. Because these blasting holes were very close to the ones used during the second test, they share the same hole ID numbers, which are S8, S9, S10, S11, S12, and S15. All blasting holes are 4 ft long and 1.5" in diameter. The coordinates of the drill holes which were used for the survey are given in Table 5.4.

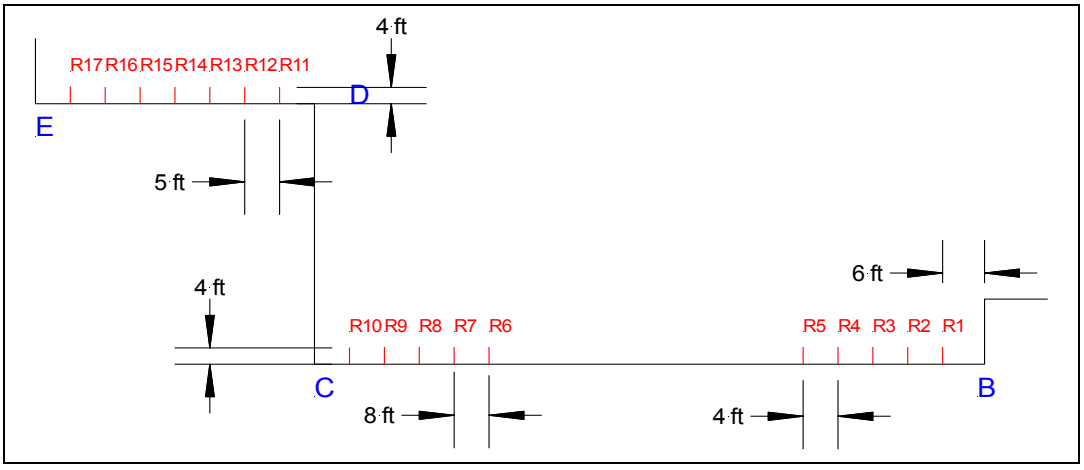

Figure 5.9 Blasting section for reflection survey at Site II, Harmony Mine.

Table 5.4 Coordinates of blasting holes for reflection survey at Site II, Harmony Mine

Hole #	Source coordinate (ft)	
	East (x)	North (y)
R11	6337.4	14168.8
R12	6325.5	14179.6
R15	6317.0	14183.4
R10	6278.0	14128.9
R9	6270.8	14130.6
R8	6263.6	14132.2

5.5 Transmission survey

Four transmission tests were carried out at the demonstration site. The corresponding blasting holes are T22, T23, T24 and T25. The general locations for these blasting holes and the associated transmission ray paths are illustrated in Figure 5.10. Caps and 250 gram (2") explosives were used as the seismic sources. The detailed information is summarized in Table 5.5.

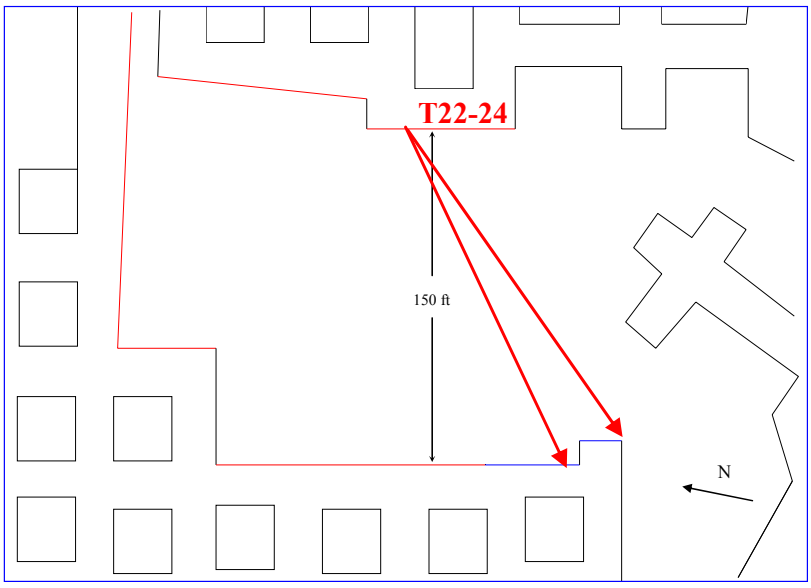

Figure 5.10 Illustration of ray paths associated with the transmission survey.

Table 5.5 A summary of the transmission survey at Harmony Mine Site II

Hole #	Explosive (g)	Event #
T24	Cap	28
T23	Cap	31
T25	250	36
T22	Cap	38

5.5.1 Characteristics of transmission signals

The transmission signals from these four surveys are similar and, as an example, the signals associated with event 38 are discussed here. Event 38 refers the transmission survey related to seismic source T22. The locations of T22 and the sensors as well as the corresponding ray paths for this event are illustrated in Figure 5.11. The signals for the event are given in Figure 5.12.

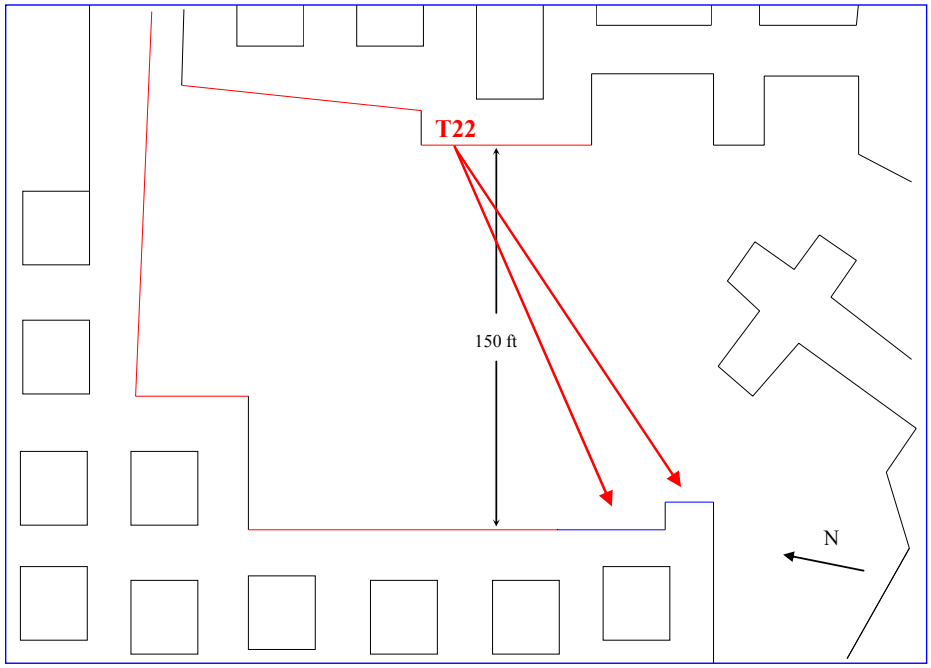

Figure 5.11 Illustration of ray paths associated with the transmission survey.

Figure 5.12 shows two clear channel wave arrivals. The first channel wave arrival is from the directly transmitted channel wave. The second channel wave, the result of a reflected wave path, arrives much later. The signals from two groups have very similar frequency for each channel. The arrival time readings for channel waves as well as reflected channel wave are listed in the following table.

Table 5.6 Arrival time reading for Event 38

PC CH. #	2	3	4	5	7	8	9	10	12	14	15	16
Sensor #	S1	S2	S3	S4	S6	S7	S8	S9	S12	S13	S14	S15
Direct Ch. Wave	65.1	65.05	65.1	64.8	66	66.1	65.6		68.8	69	67.2	
Reflected Ch. wave				89.5	89.8	90.25	90.7	86.6	88	87.9	88.35	

* Triggering time: 40.9 ms.

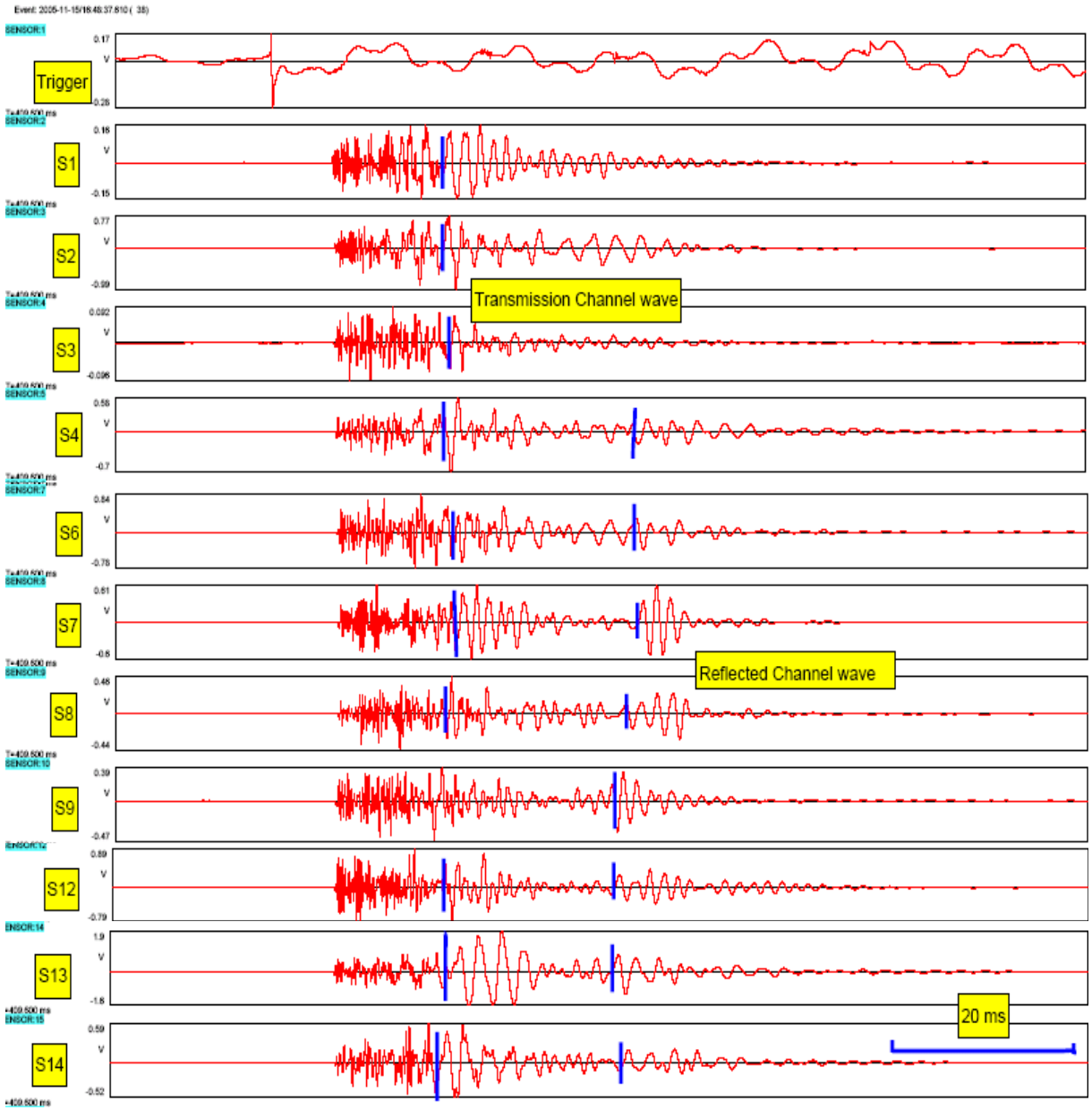

Figure 5.12 Signal waveform for a transmission survey carried out at Site II, Harmony Mine Demonstration test (display window: 20-150 ms for event 38).

The direct channel wave arrivals are often intermingled with other earlier wave arrivals as the signal signatures show in Figure 5.12. Therefore, one of the problems for the signal analysis is timing the arrivals of channel waves. A technique, that is new for this application, is wavelet transform. Figure 5.13 is an example.

The figure consists of three parts. The top one is the original signal, which is channel S8 in Figure 5.12. It is seen from the figure that the arrival of the direct channel wave is mixed with the S-wave arrivals transmitted through the roof. The example shows that this direct channel wave arrival as well as the arrival of the reflected channel wave can be accurately determined by the wavelet technique. The middle chart contains the wavelet transform coefficients (or amplitude) at the frequency (500 Hz). Gabor wavelet was used for the transform. The bottom one is the wavelet transform. The arrivals of two channel waves are indicated by two sharp onsets shown by part *(b)*.

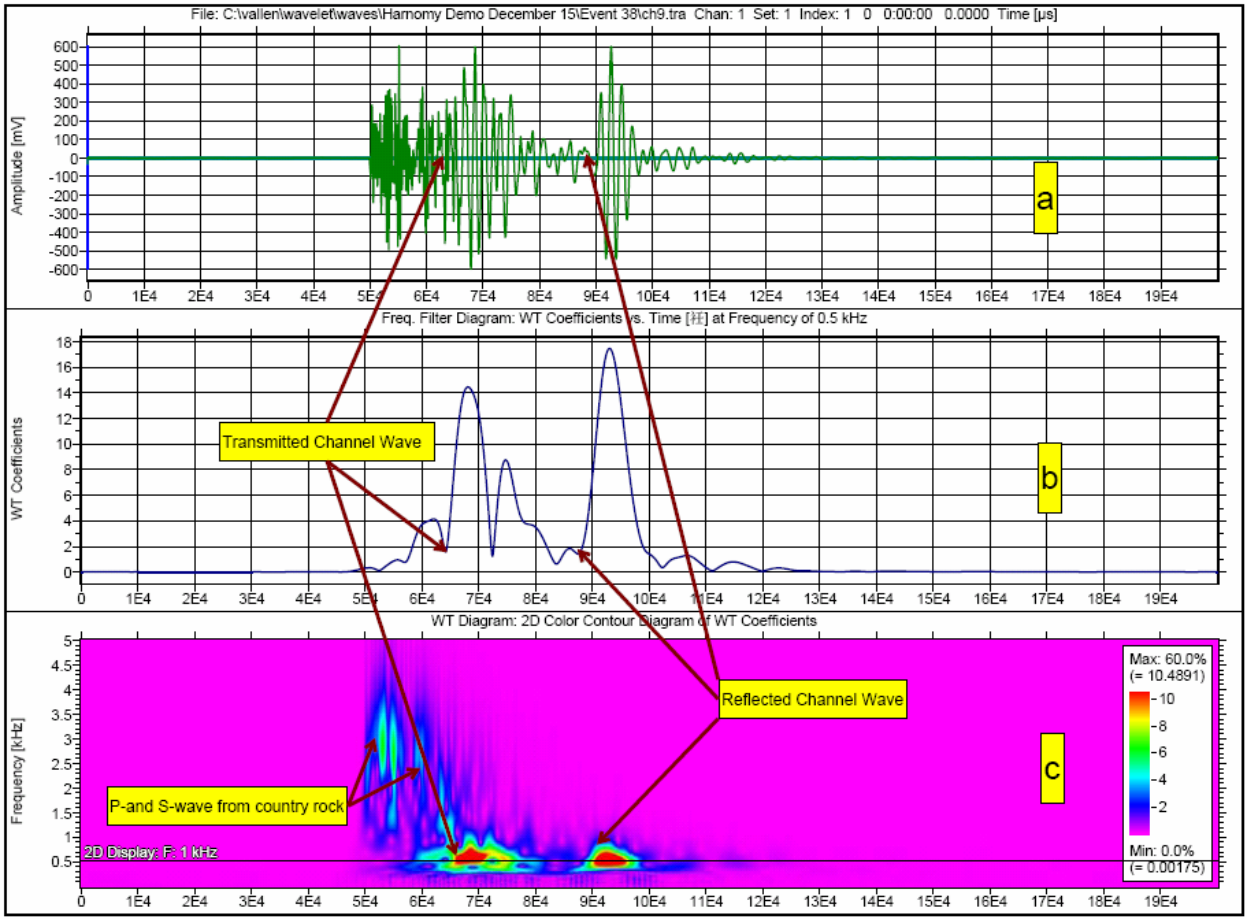

Figure 5.13 Application of wavelet transform for the ISS based void detection: timing the arrivals of direct and reflected channel waves (plot *(a)*: original waveform of channel S8 of event 38; plot *(b)*: filtered wavelet transform coefficient at frequency indicated in plot *(c);* plot *(c)*: 2D color contour of wavelet coefficient).

5.5.2 Velocity calculations for Site II

The channel wave velocity as well as the P- and S-wave velocities associated with coal and roof was calculated. The average velocity for the channel wave at Site II is 5152 ft/s. The raw data used for the calculation of the channel wave velocity are given in Tables 5.7 and 5.8.

Table 5.7 Source – receiver distances (ft) at Harmony Mine Site II

				Direct Travel Distance										
CH. #	2	3	4	5	6	7	8	9	10	11	12	14	15	16
	S1	S2	S3	S4	S5	S6	S7	S8	S10	S11	S12	S13	S14	S15
T24	149.3	150.8	151.5	152.8	153.6	154.3	158.3	159.1	153.6	153.4	154.5	156.3	158.2	162.0
T23	148.6	151.0	151.9	153.5	154.5	155.5	160.3	161.2	156.3	156.5	157.8	159.9	162.0	166.3
T25	146.6	147.2	147.7	148.8	149.3	149.7	153.1	153.7	147.6	147.1	147.9	149.6	151.3	154.7
T22	148.6	151.6	152.6	154.3	155.5	156.6	161.8	162.9	158.3	158.8	160.2	162.5	164.7	169.1
R15	150.3	163.4	165.9	170.0	173.3	177.8	189.8	192.4	198.0	202.9	206.4	211.2	215.1	222.6
R12	138.7	151.6	154.1	158.2	161.5	165.8	177.8	180.3	185.4	190.2	193.6	198.3	202.2	209.7
R11	134.6	147.5	150.0	154.0	157.3	161.7	173.6	176.1	181.1	185.9	189.3	194.0	197.9	205.4
R10	97.7	110.5	112.8	116.6	119.8	124.3	136.0	138.6	146.8	152.4	155.9	160.6	164.4	171.7
R9	103.2	116.2	118.6	122.4	125.6	130.2	141.9	144.5	152.5	158.1	161.6	166.4	170.2	177.6
R8	96.0	108.9	111.3	115.1	118.3	122.9	134.6	137.2	145.3	150.8	154.4	159.1	162.9	170.3

Table 5.8 Channel wave from coal seam velocities determined from transmission survey at Harmony mine site II

				velocity of channel wave by transmission test											
	CH. #	2	3	4	5	6	7	8	9	10	11	12	14	15	
EVENT		S1	S2	S3	S4	S5	S6	S7	S8	S9	S10	S12	S13	S14	Ave
28	**T24**	5266	5338	5420	5650		5338		5467	5223	6016		5429	4606	**5305**
31	**T23**	4755	4895	4947	5377	5107		5170	5587	5389			5682		**5212**
36*	**T25**														
38	**T22**	6142	6278	6304	6458		6240	6422	6595			5741	5782	6262	**6222**

*Event 36 by 2 inch explosive, signal waveform saturated.

5.6 Reflection survey at Site II, Harmony Mine

The reflection survey at Site II included 6 individual surveys (blasting events). The seismic sources used for the surveys were 250 grams explosives or caps. The explosives used and the associated event number for these surveys are listed in Table 5.9.

Table 5.9 A summary of the reflection surveys at Harmony Mine Site II

Hole #	Explosive (g)	Event #
R11	250	44
R12	250	50
R15	250	68
R10	250	71
R9	2 Caps	77
R8	1 Cap	81

The survey result shows that the reflected channel waves were evident for most events. However, because of the site geometry, there were several groups of channel waves, which often formed a "train" of channel waves. A challenge for data interpretation from this particular site was to identify the arrivals of the channel waves which were reflected from the "void" (the other side of the pillar). The event discussed in the next section is such an example.

5.6.1 Case Study Event 81

Event 81 refers the reflection survey related to seismic source R8. The locations of R8 and the sensors are shown in Figure 5.14. The waveform for the event is given in Figure 5.15. The signal frequency for the reflected channel waves is about 500 Hz. The arrivals of the reflected signals are clear for most channels and the corresponding readings are given in the table below.

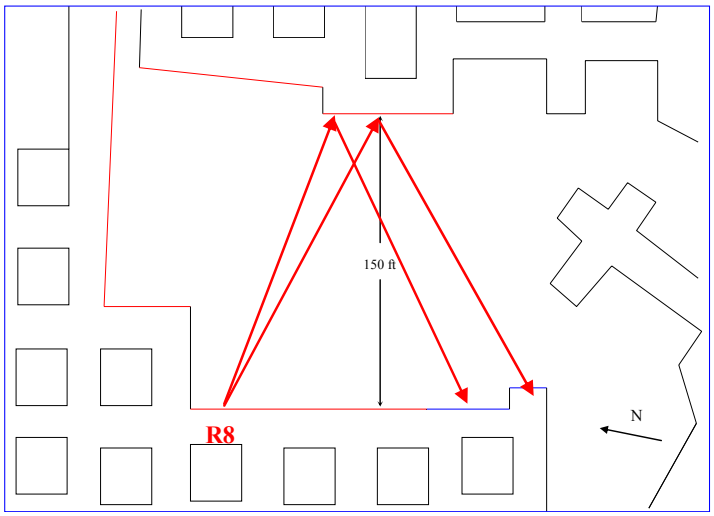

Figure 5.14 Testing setup for event 81.

Triggering Time (ms)	Sensor	S1	S2	S3	S4	S5	S6	S7	S8	S9	S10	S12	S13	S14
50	Arrival (ms)	107.2		107.4			107.8	108.25					108.45	108.35

The ellipses calculated based on the travel times given in the above table are plotted in Figure 5.17. It is evident from the figure that these ellipses delineated the void with a good accuracy.

Table 5.10 Parameters of ellipses associated with event 81

Source*	Sensor**	Travel time (ms)	Travel distance (ft)	Half of foci distance (ft)	Half of major axis (ft)	Half of minor axis (ft)
R8	S1	57.2	297.44	50.1	148.7	140.0
R8	S3	57.4	298.48	57.0	149.2	137.9
R8	S6	57.8	300.56	62.8	150.3	136.5
R8	S7	58.3	303.16	64.1	151.6	137.4
R8	S13	58.5	304.2	75.2	152.1	132.2
R8	S14	58.4	303.68	76.9	151.8	130.9

* See Table 5.4 for source coordinates
** See Table 5.2 for sensor coordinates
*** Velocity: Channel wave 5200 ft/s

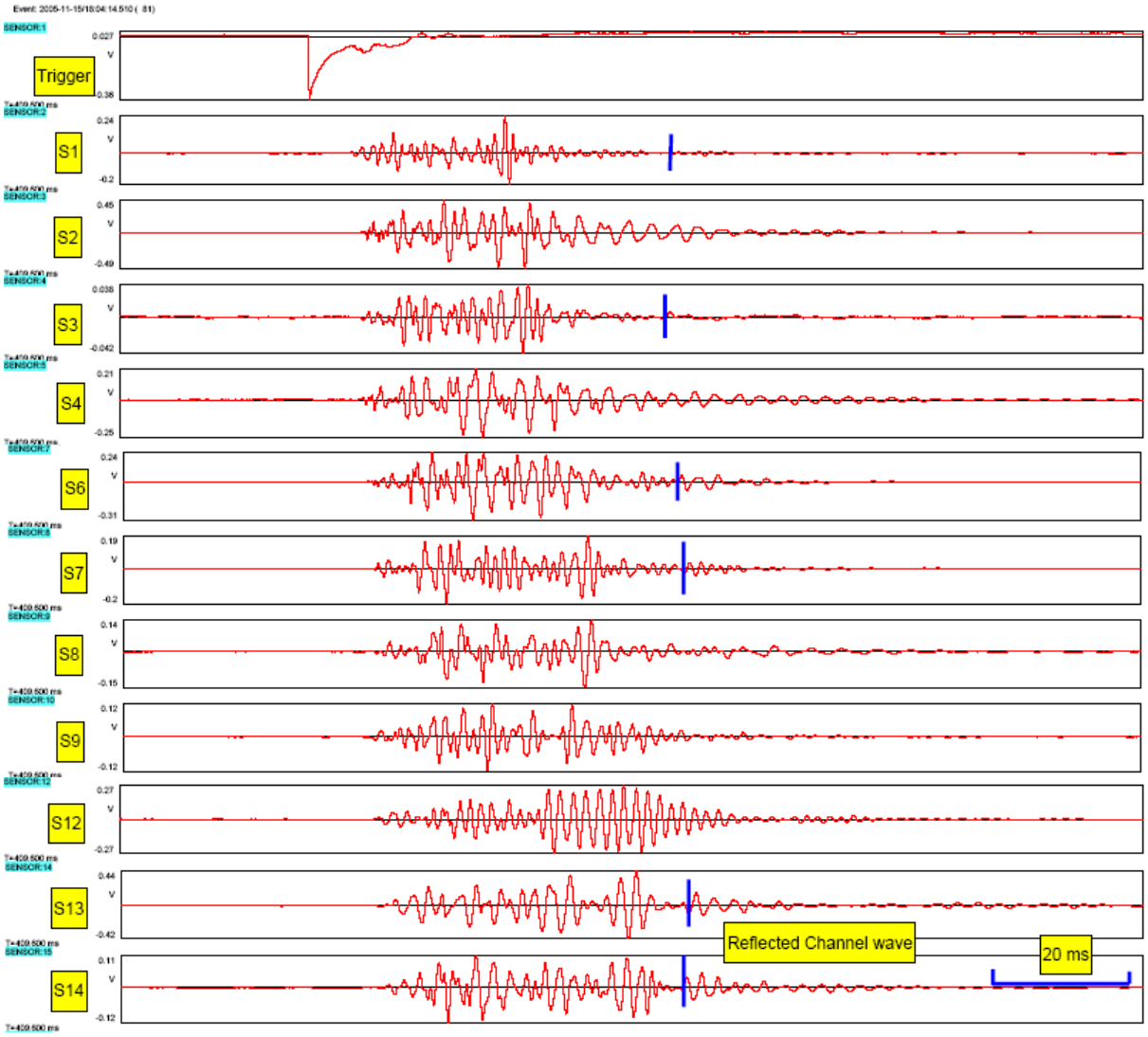

Figure 5.15 Signal waveform for a reflection survey carried out at Site II, Harmony Mine (display window: 20-180 ms for event 81).

The wavelet technique was used for improving timing the reflected arrivals. Figure 5.16 is a demonstration of this application. The figure consists of three parts. Part *(a)* one is the original signal, which is channel S14 in Figure 5.15. The middle one is the wavelet transform coefficient at 500 Hz and the bottom one is the wavelet transform. The arrival of the reflected channel wave in the figure is clearly defined by a sharp trough of the transformed curve (part *(b)*).

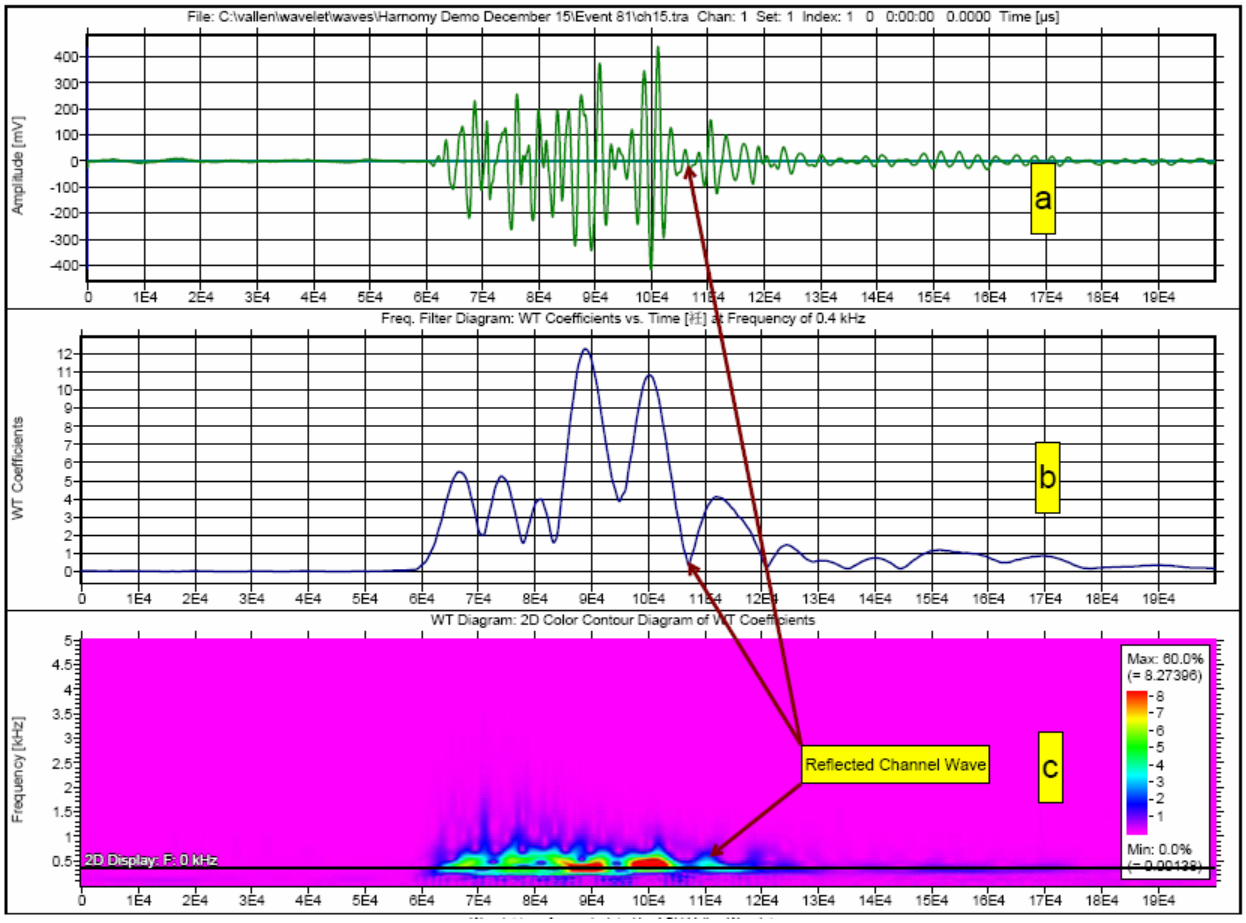

Figure 5.16 Using wavelet transform to timing the arrival of a reflected channel wave (plot *(a)*: original waveform of channel S14 of Event 81; plot *(b)*: filtered wavelet transform coefficient at frequency indicated in plot *(c)* (500 Hz); plot *(c)* shows 2D color contour of wavelet coefficient).

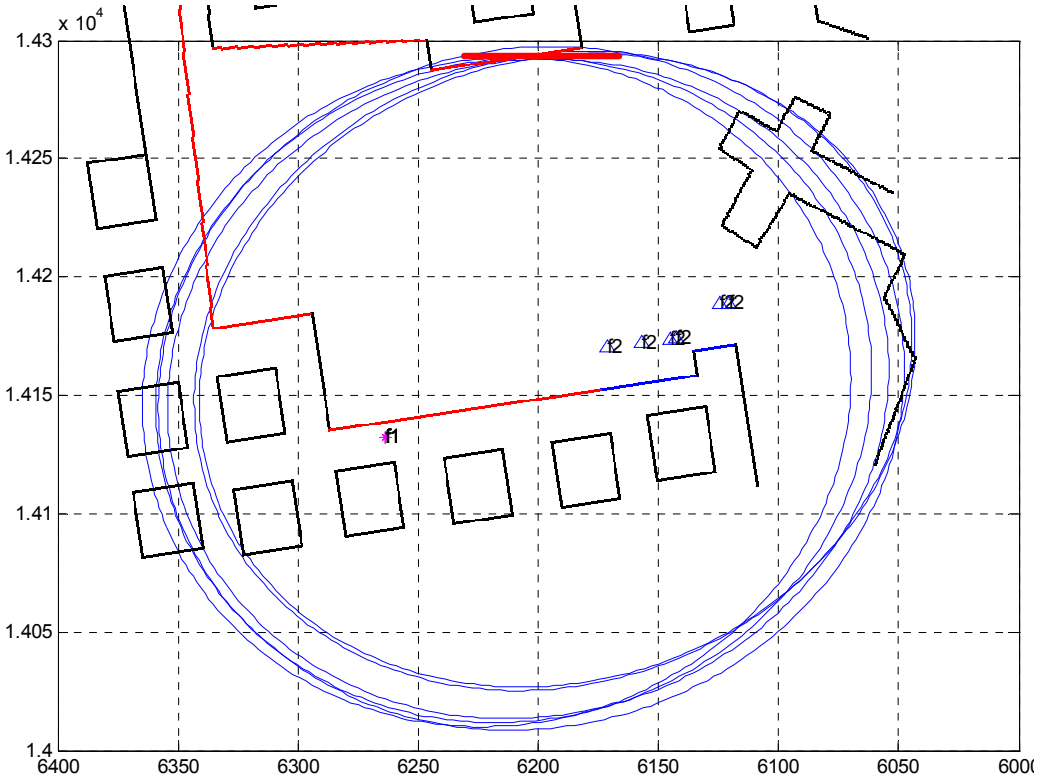

Figure 5.17 Void mapping with the ellipses associated with event 81 at Harmony Mine testing site. The void boundary is represented by a short red line. The locations of the sensors and the source as well as the associated ray paths are illustrated in Figure 5.14.

5.7 Void mapping

The elliptical method was used to map the void location and the initial result is shown in Figure 5.18. The channel wave velocity used for the calculation is 5200 ft/s. It is noted that the void boundary consists of two off-line sections. Corresponding to this feature, the ellipses can be divided into two groups. One group includes those which were associated with sources R7, R9 and R10 (Figure 5.19a). The signals corresponding to these sources were all reflected from the right section. The ellipses belonging to the second group were associated with three other sources, R11, R12 and R15 (Figure 5.19b). The signals originated with these sources could be reflected from either section, depending on the sensor locations.

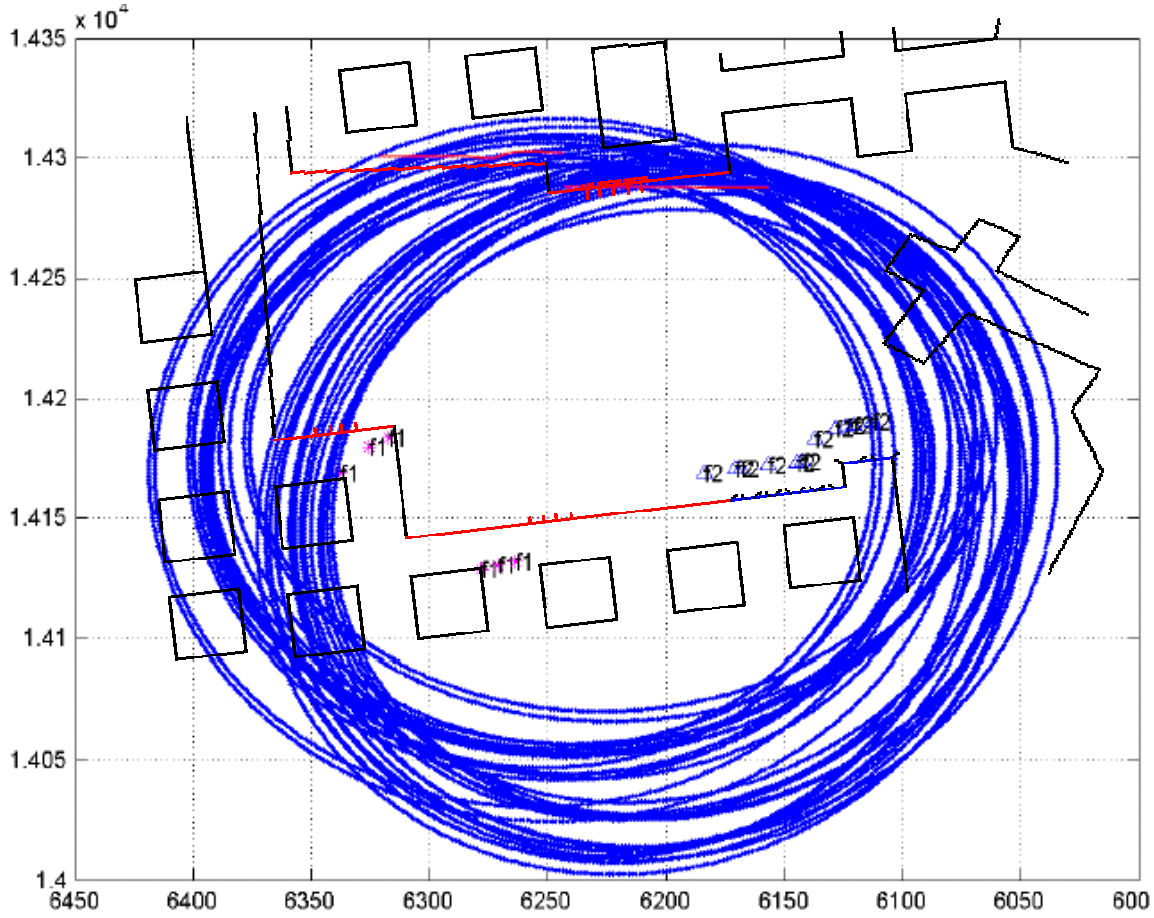

Figure 5.18 "Void" location (red lines) determined by the elliptical location method at Site II, Harmony Mine (red lines are the common tangent lines of the ellipses).

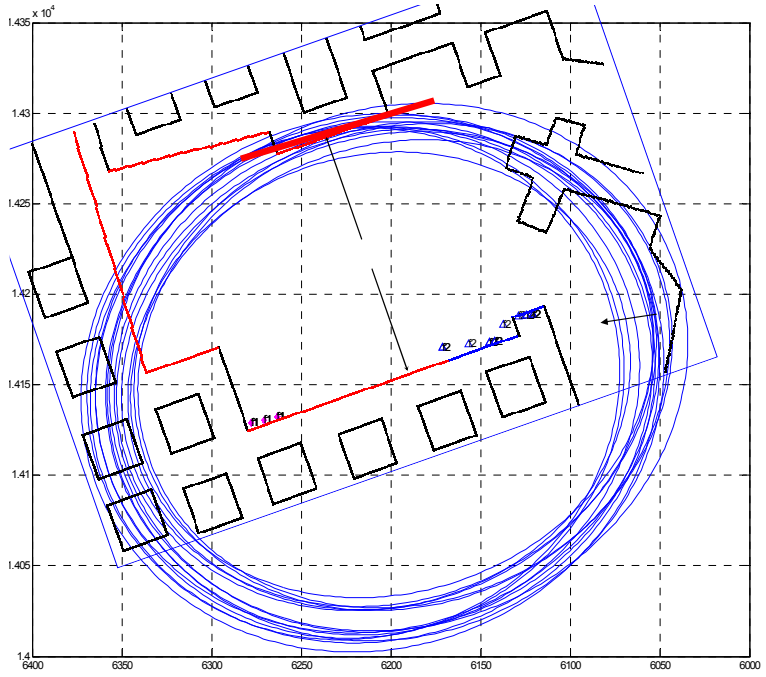

a. Ellipses associated with sources R7, R9 and R10. (Velocity: Channel wave: 5200).

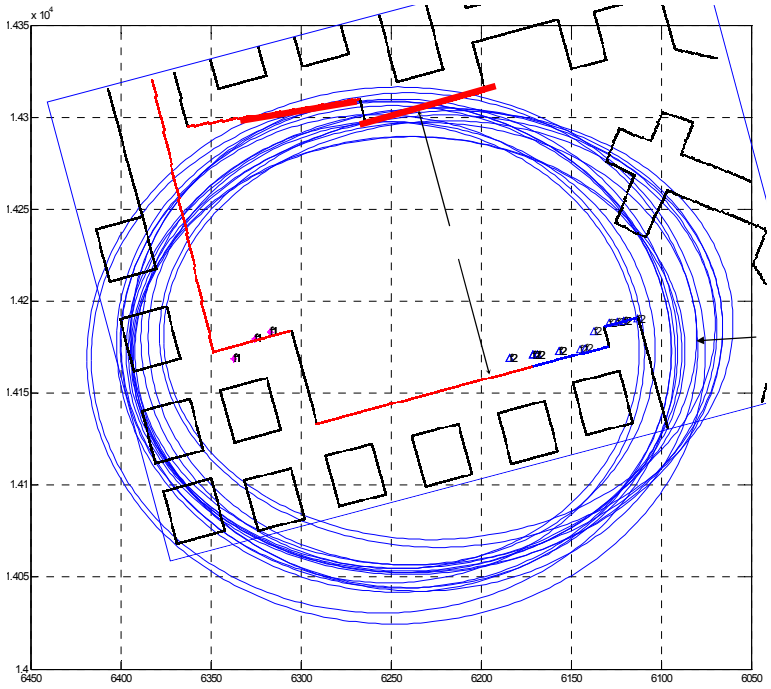

b. Ellipses associated with sources R11, R12 and R15. (Velocity: Channel wave: 5200).

Figure 5.19 Mapping the "void" section by section at Site II, Harmony Mine.

5.8 Summary of the Demonstration at the Harmony Mine

On November 15, 2005, Penn State held the official demonstration of the ISS based void detection technique for the anthracite mine environment to MSHA and the mining industry at Site II, Harmony Mine. It was one of the two official demonstrations requested by MSHA. The other one was carried out at FMC on August 23, 2005. FMC is a trona mine located at Green River, Wyoming.

The main objective of the demonstration was to show the feasibility of the ISS based void detection technique for the anthracite mine environment. Using Site II allowed Penn State to demonstrate both the range and the repeatability of the technique. It is noted that the same site was used for the second test at the Harmony Mine.

During the demonstration, MSHA and DEP officials witnessed the entire data acquisition process and observed real-time signals. The mapping result from the demonstration is very similar to the result from the second test at the mine.

6. Field Test at FMC Trona Mine

6.1 Introduction

On March 7 – 8, 2005, the Penn State project team conducted a field test at an FMC trona mine. It was the first of three tests carried out at trona mines. The purpose of this test and the following test at General Chemical, which will be discussed in the next chapter, was to investigate whether body waves in trona could be detected and utilized for void mapping.

6.1.1 Trona and void detection

Trona ($Na_3(HCO_3)(CO_3)\cdot 2(H_2O)$) is a water-bearing sodium carbonate (Figure 6.1). The processed trona is called soda ash, which can be in either a crystal or powder form.

Figure 6.1 Wyoming trona.

Trona is a commodity with a variety of uses and Wyoming is the source of about 90% of the nation's soda ash. Glassmaking consumes about half of soda ash output, followed by the chemical industry, which uses about a quarter of the output. Other uses include soap, paper manufacturing, and water treatment. All baking soda comes from soda ash.

One of the main problems of concern in the trona industry is how rapidly barrier pillars deteriorate in the presence of water. Barrier pillars are the pillars left in place to separate mined out areas and active mining areas. The long-hole drilling method, used to detect voids in advance of mining in coal mines, would induce water into pillars. Hence, this technique is not practical for trona mines and the use of some non-destructive testing method, such as geophysical techniques, is imperative.

When MSHA initiated its void detection program in 2003, General Chemical and FMC, two of the largest trona companies in Wyoming, immediately expressed to MSHA their enthusiastic support for the program and their eagerness to participate the program. Because of both the industrial need and MSHA's focus on void detection, MSHA requested Penn State to place a priority on the void detection project for the trona mine situations.

6.1.2 Challenges for void detection under the trona mine condition

Technically speaking, void detection in trona mine situations is fundamentally different from the in-seam seismic (ISS) method. The term *in-seam seismic* conventionally refers to the methods which utilize channel waves. A necessary condition for developing channel waves is that the wave propagation velocity in the seam under study must be much lower than that of the country rock. In general, this implies that the seam must be much weaker than the country rock which is typical of coal mine conditions.

Trona is much stronger than the surrounding country rock and, therefore, no channel waves will be developed. The void detection under these conditions has to rely on body waves (P- and S-waves), not channel waves. Several challenges are brought on by this difference. First, void detection in trona mine conditions will no longer possess the basic advantage of the ISS method, which uses the better defined channel wave signals. Contrarily, body waves propagate three-dimensionally and are much more difficult to detect. In addition, as different signals are used for void detection, the associated data analysis method used will be very different as well.

Although the void detection under the trona mine conditions is not ISS based, the term *ISS based void detection* is used in this report for all conditions. The term, therefore, should be broadly understood as the void detection method which may use either channel waves or the body waves (P- and S-waves) traveling within the seam, depending on the relative condition (velocity, density and strength) of the seam and surrounding country rock.

6.1.3 Trona mines in Wyoming

Wyoming has the world's largest deposits of trona with an estimated total reserve of 127 billion tons, of which 40 billion tons are currently considered recoverable. The location of this resource is shown in red on the map given in Figure 6.2.

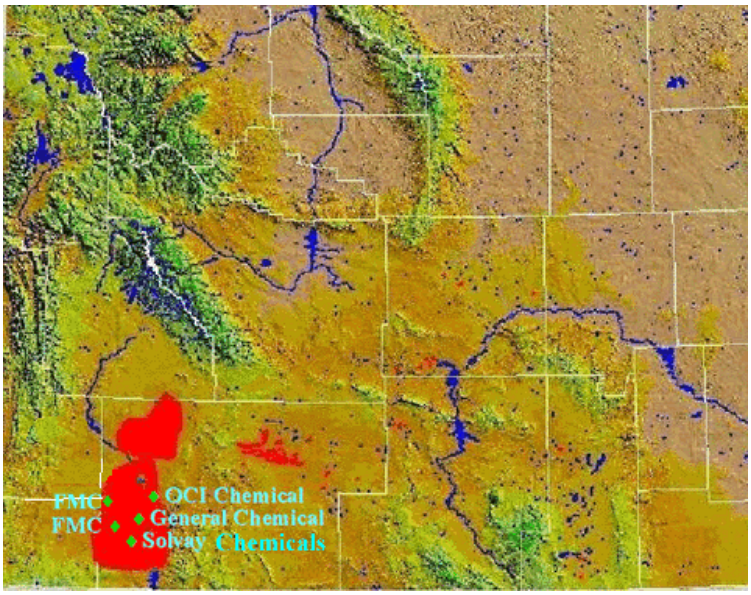

Figure 6.2 Map of Wyoming trona operations.

Trona mining in Wyoming began in 1947. The most common bed for Trona mining is bed 17 where mining is currently taking place. Bed 17 consists of a of very high quality trona, which is 12 feet thick and about 1,600 feet deep (Figure 6.3). The mining methods include room-and-pillar and longwall. All three field tests were carried out in this ore bed.

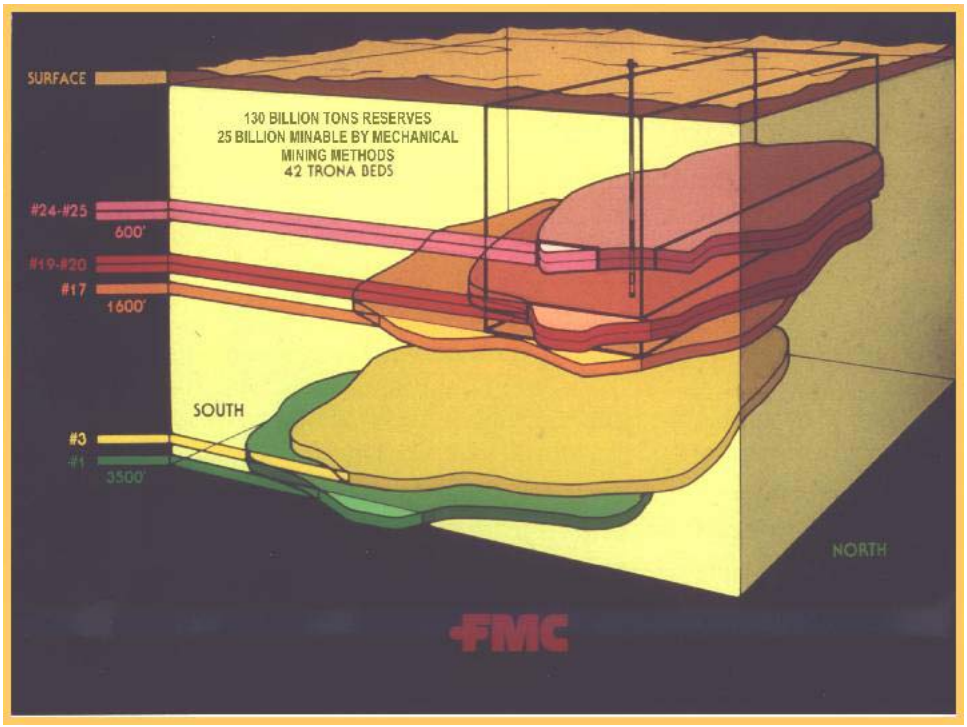

Figure 6.3 Wyoming trona deposition.

Currently, there are four major producers in the area, which are FMC, General Chemical, OCI, and Solvey Minerals. FMC is the largest with the annual production of 4.5 million tons in 2003.

6.1.4 Testing sites at FMC

Two testing sites were chosen for the field test at FMC, which are Site A and Site B (Figure 6.4).

Site A is a barrier pillar separating the active and mined out areas, located at the northern boundary of the active mining area. The mined out area is water filled. The pillar is 12 ft high and approximately 270 ft wide. The site was used for reflection testing.

Site B is a pillar of approximately 290 ft wide, located at the south-east corner of the active mining area. This site was used for a transmission test.

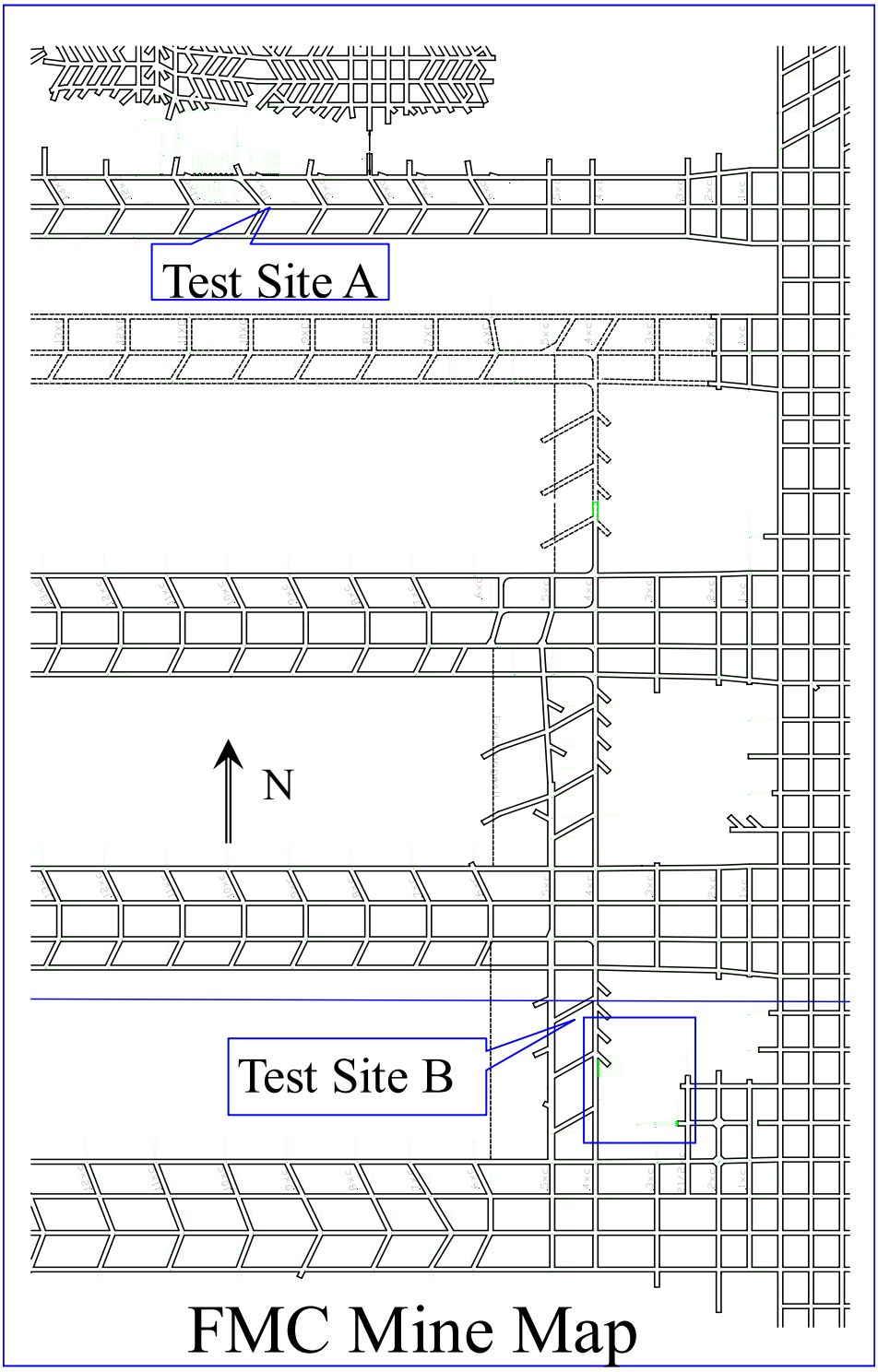

Figure 6.4 FMC mine map showing the locations of test sites A and B.

6.2 Transmission survey at site B

The transmission survey was carried out for two purposes: gaining familiarity with seismic signal signatures associated with trona and determining the P- and S-wave velocities in trona.

The specifications on the sensors, the data acquisition system, and the major operational parameters used for the test are given in Appendix I. The sampling rate and the recording window used at both site A and site B are 50,000 samples/second and 0.4 second, respectively.

6.2.1 Transmission survey design

In addition to a number of practical considerations, such as accessibility, power supply, the main consideration for choosing Site B was the pillar size. As the pillars used for the reflection survey were about 300 ft, it would be ideal if the transmission survey could be carried out on a pillar of comparable size. The pillar of this size was also ideal for testing the amount of the explosives needed for the seismic sources. It was also important for the velocity survey to be representative. Site B was chosen for these reasons.

Layout of site B

Figure 6.5 is a detailed view of site B, where the sensor section and the source (blasting) section are clearly marked. The pillar width measured between two sides of these sections is 290 ft. It is seen from the figure that these two sections are not directly opposed each other, but offset horizontally for about 150 ft. This source/receiver geometry was chosen for the purpose of producing oblique ray paths so that the effect of the angled sensor installation could be tested. The design also effectively increased the travel distance from the source section to the sensor section. The average signal travel distance was 325 ft.

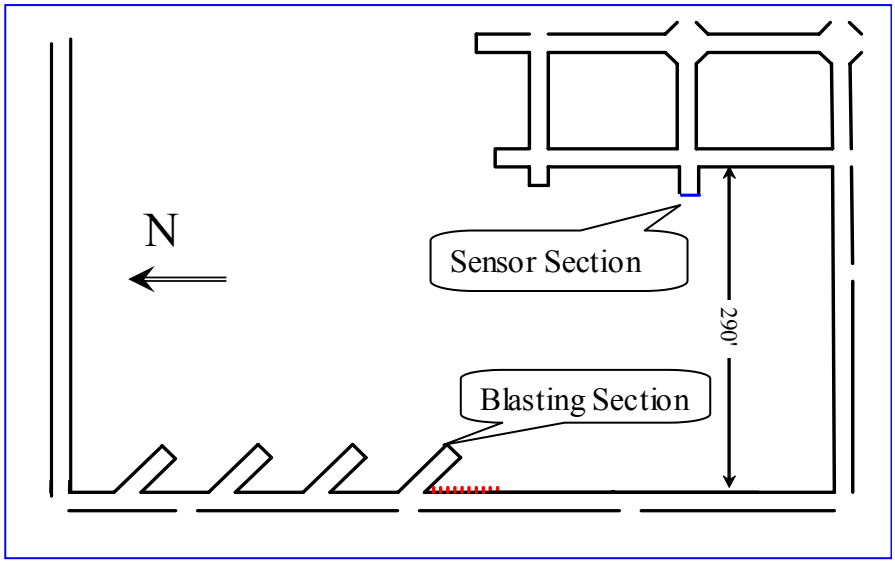

Figure 6.5 Testing site B: site utilized for transmission test at FMC.

Sensor section

Because of accessibility limitations, sensors had to be installed in the short entry shown in Figure 6.6, which was approximately 16.5 ft wide. This short entry also served as the field station for the transmission survey.

The arrangement of the sensor holes is shown in Figure 6.7. Seven sensor holes were drilled at the back of the entry, where the collar locations can be seen from Figure 6.6 as the vertical red lines marked at the back. Sensor holes were numbered from S1 to S7. Among them, S2, S4 and S6 were straight and the others were angled 45^{o} or 135^{o} horizontally from the rib. The length of sensor holes was 5 ft for straight holes and 7 ft for angled holes. The diameter for all sensor holes was 1.75". The sensor hole information is summarized in Table 6.1.

Figure 6.6 Field station for transmission survey, where the sensor holes were drilled at the face of the entry and the collar locations were marked by the vertical red lines.

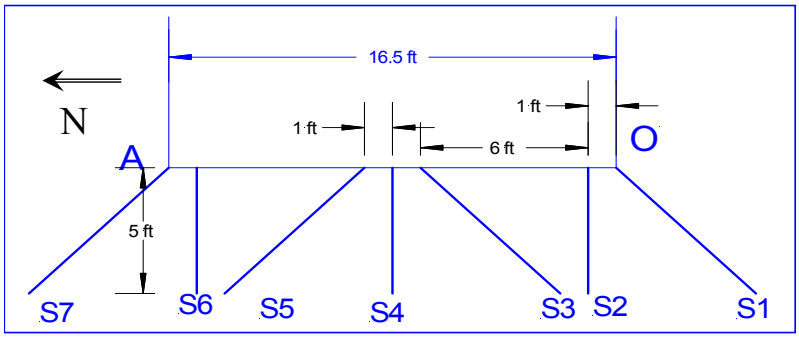

Figure 6.7 Sensor hole locations for transmission survey.

Table 6.1 Sensor hole information for site B, FMC

Hole #	Channel #	Length (ft)	Orientation	Sensor coordinate (ft)	
				East (x)	North (y)
S1	2	7	S45W	58567	31642
S2	3	5	E - W	58567	31648
S3	4	7	S45W	58567	31649
S4	5	5	E - W	58567	31655
S5	6	7	N45W	58567	31661
S6	8	5	E - W	58567	31662
S7	7	7	N45W	58567	31668

Seismic source (blasting) section

The seismic source section consisted of 10 blasting holes which were numbered from T1 to T10. Seven of these blasting holes were used during the survey (Figure 6.8) with T5, T7 and T9 not used. All blasting holes were 4 ft long and 1.5" in diameter, drilled from the middle of the seam.

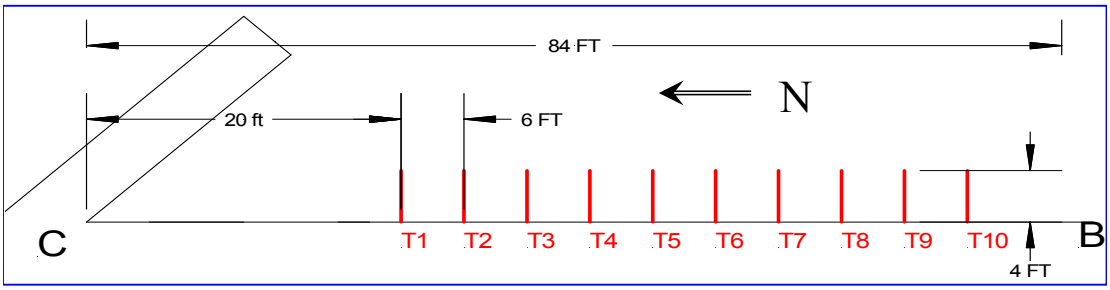

Figure 6.8 Blasting hole locations for transmission survey.

Table 6.3 Blasting hole information for site B, FMC

Hole #	Length (ft)	Source coordinate (ft)	
		East (x)	North (y)
T10	4	58304	31817
T8	4	58304	31829
T6	4	58304	31841
T4	4	58304	31853
T3	4	58304	31859
T2	4	58304	31865
T1	4	58304	31871

6.2.2 Characteristics of transmission signals

The transmission survey consisted of seven blasting events. The explosives used for the tests ranged from a single cap to 375 grams/hole. Table 6.3 is the summary of these testing events.

Table 6.3 A summary of the transmission tests at FMC

Hole #	Explosive (g)	Event #
T1	Cap	4
T2	Cap	60
T3	125	63
T4	375	65
T6	375	69
T8	375	73
T10	375	75

Transmission signals from three blasting events are shown in Figures 6.9 – 6.11. The signals shown in these figures correspond to three explosive usages: a cap (Figure 6.9), 125 grams (Figure 6.10), and 375 grams (Figure 6.11).

It can be seen from these figures that all of the signals are of very high quality. The first impression is that both P- and S-waves are very well defined, characterized by sharp arrivals and clear separations. The dominant frequencies for both P- and S-waves are relatively high, in the neighborhood of 3000 -5000 Hz.

Because of the arrangement of the angled sensor holes, the signal polarization is clearly seen. It is known from Figures 6.5 and 6.7 that sensor holes S7 and S5 are roughly parallel to the wave propagation direction and sensor holes S1 and S3 are almost perpendicular to the wave propagation direction. By theory, S7 and S5 should be much more sensitive to P-waves than S1 and S3, and S1 and S3 should be much more sensitive to S-waves than S7 and S5. A review of Figures 6.9 – 6.11 confirms this hypothesis.

Although the general characteristics of the transmission signals are very similar for three examples, the effect of the source strength on the signal strength is evident. First, the signal duration has a noticeable increase when the source changes from a cap to 375 g explosives. In addition, the signal amplitude also increased considerably. The average amplitude for the source with 375 gram explosives is about 200 times of the amplitude corresponding to the cap source. The relation of the amount of the explosives used and the average signal amplitude in terms of the recording voltage is given in Table 6.4.

Table 6.4 Source strength and signal amplitude

Hole #	Event #	Explosives	Average amplitude (voltage)
T1	4	Cap	0.023
T2	60	Cap	0.098
T3	63	125 (1”).	0.041
T4	65	375 (3”)	0.920
T6	69	375 (3”)	2.010
T8	73	375 (3”)	2.220
T10	75	375 (3”)	2.550

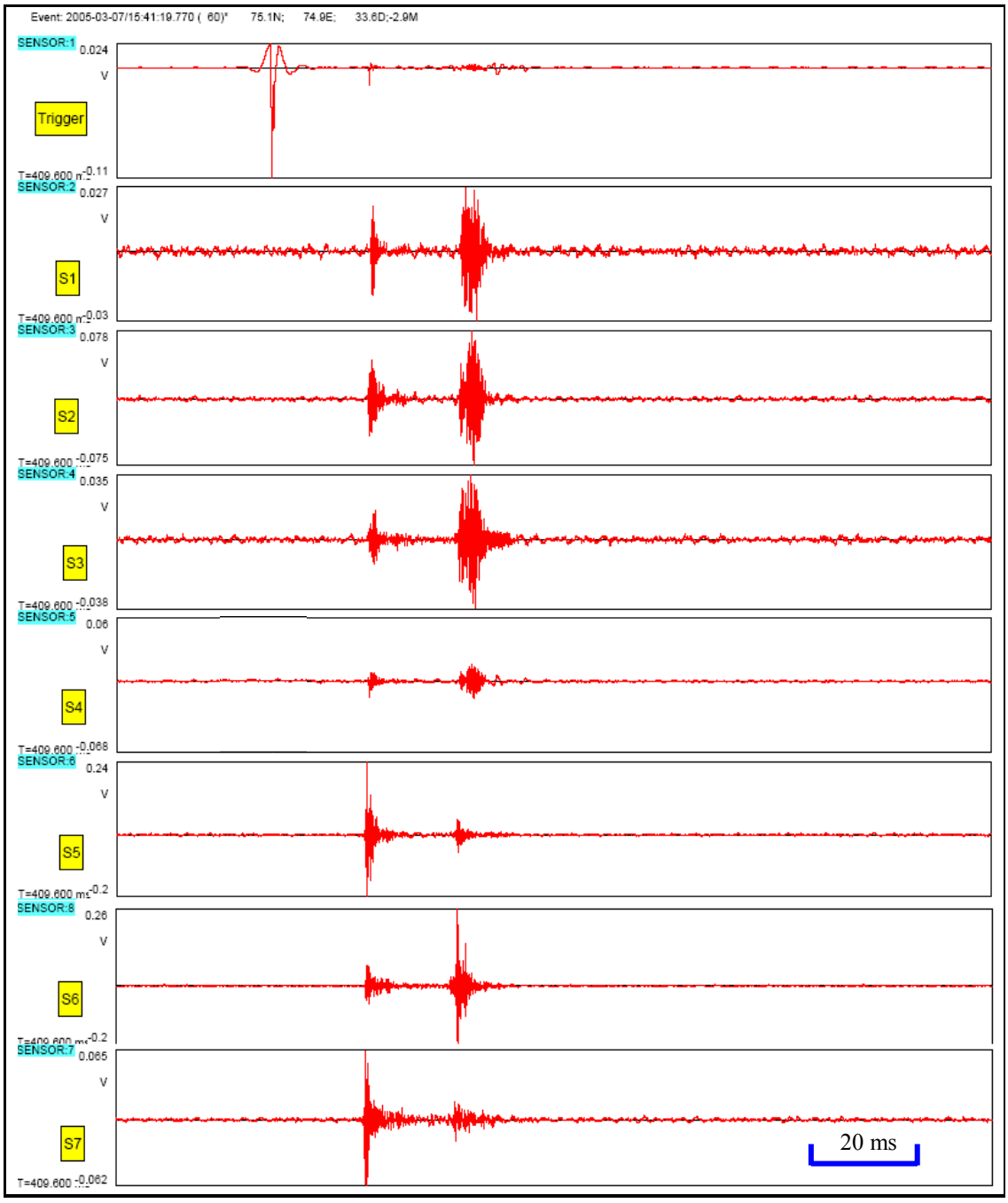

Figure 6.9 Transmission signals for event 60 (display window: 20 – 190 ms; seismic source: detonation cap; average travel distance: 337 ft).

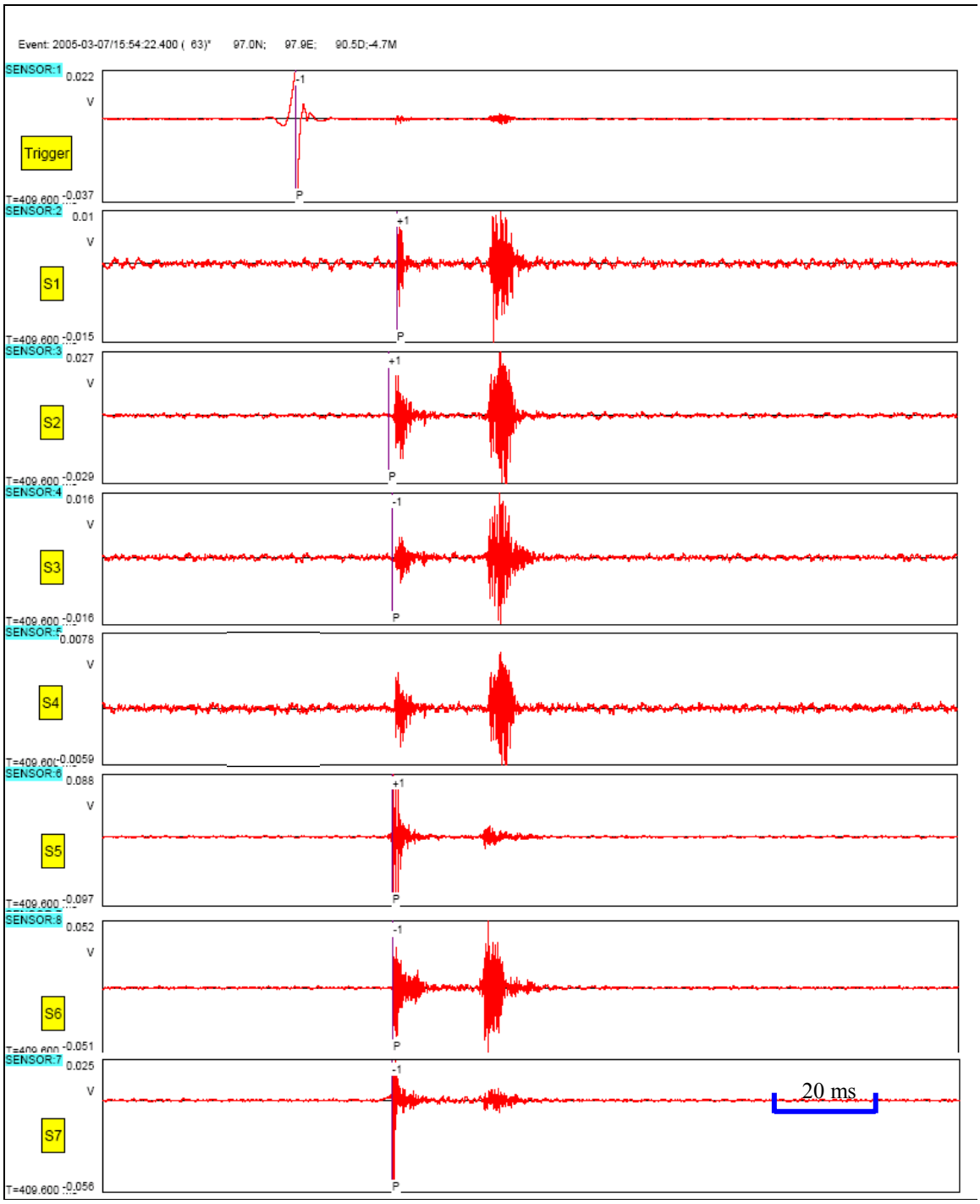

Figure 6.10 Transmission signals for event 63 (displaying window: 20 – 190 ms; seismic source: 125 gram explosive; average travel distance: 333 ft).

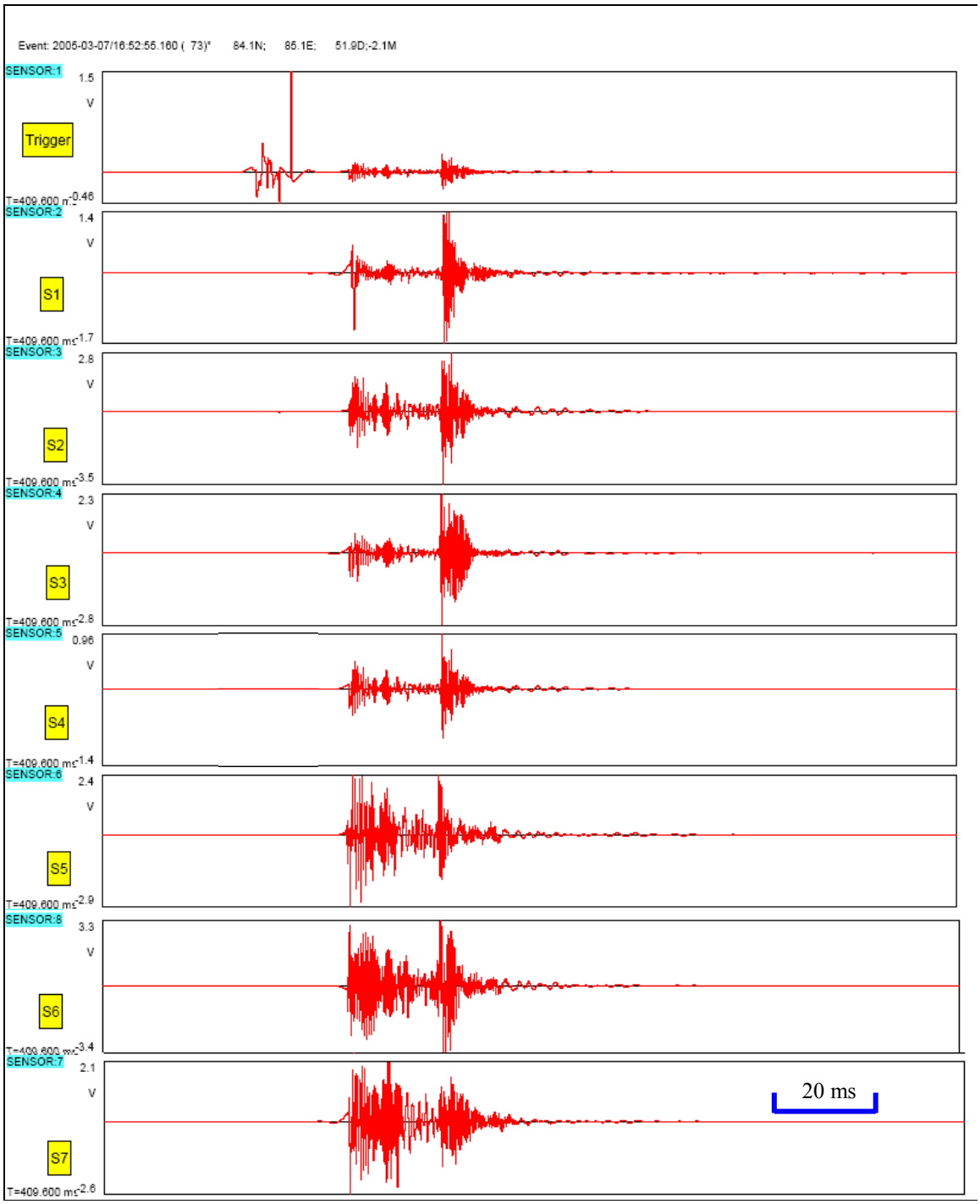

Figure 6.11 Transmission signals for event 73 (display window: 20 – 190 ms; seismic source: 375 gram explosive; average travel distance: 315 ft).

6.2.3 P- and S-wave velocities in trona

The transmission data from site B were utilized to determine P- and S-wave velocities in trona. The result is presented in Table 6.5.

Table 6.5 P- and S-wave velocities determined from transmission survey at site B, FMC

Wave type	Average Distance (ft)	Survey lines	Velocity (ft/s)	Standard deviation (ft/s)	Mean Standard deviation
P (compression)	325	49	16,777	205	1.20%
S (shear)	325	49	8,572	67	0.79%

Analysis of survey conditions

The velocity survey included 49 survey lines from 7 source locations to 7 sensors. The survey distance ranged from 302 ft to 349 ft with an average distance of 325 ft. Table 6.6 summarizes the distance data. Two conclusions may be drawn from these survey conditions. First, the size of database used for the velocity calculation is statistically significant. Second, the velocities determined with these survey distances can be considered representative of the rock mass values in that the effect of local anomalies (material properties, geological structures) on the average is taken into account.

Table 6.6 Source – receiver distances (ft)

Hole #	Source type	S7	S6	S5	S4	S3	S2	S1
T10	3" exp	302.3	305.3	305.9	309.0	312.2	312.7	316.0
T8	3" exp.	308.4	311.6	312.2	315.4	318.8	319.3	322.8
T6	3" exp.	314.9	318.2	318.8	322.2	325.7	326.3	329.9
T4	3" exp.	321.6	325.1	325.7	329.3	332.9	333.5	337.3
T3	1" exp.	325.1	328.7	329.3	332.9	336.6	337.3	341.1
T2	Cap	328.7	332.3	332.9	336.6	340.4	341.1	344.9
T1	Cap	332.3	336.0	336.6	340.4	344.3	344.9	348.8

* T# and S# represent blasting hole and sensor numbers, respectively.

Analysis of reading error

In this survey, both triggering time and signal arrival times were accurately recorded. The reading errors for P- and S-wave arrivals are in general less than 0.1 ms and 0.2 ms, respectively. If these errors are considered in terms of the travel distance, they are only 1.7 ft. Considering the magnitude of P- and S-wave velocities at the site, it can be concluded that they are not impacted significantly by reading errors. The P- and S-wave travel times determined from the recorded waveforms are tabulated in Table 6.7 and Table 6.8.

Table 6.7 P-wave travel time for individual ray paths (ms)*

Event No.	Hole #	Source type	S7	S6	S5	S4	S3	S2	S1
75	T10	3" exp	17.70	17.90	18.15	18.55	18.60	18.70	18.85
73	T8	3" exp	18.10	17.90	18.10	18.70	18.90	19.10	19.10
69	T6	3" exp	18.75	18.80	19.10	19.25	19.35	19.45	19.45
65	T4	3" exp	19.00	19.10	19.10	19.50	19.80	20.05	20.10
63	T3	1" exp	19.30	19.50	19.60	20.15	20.25	20.30	20.65
60	T2	Cap	19.65	19.70	20.05	20.50	20.50	20.60	20.85
4	T1	Cap	19.90	19.95	20.30	20.60	20.80	20.85	21.25

* Reading error < 0.1 ms

Table 6.8 S-wave travel time for individual ray paths (ms)*

Event No.	Hole #	Source type	S7	S6	S5	S4	S3	S2	S1
75	T10	3" exp.	34.75	35.25	35.80	36.25	36.35	36.60	36.95
73	T8	3" exp.	35.50	36.20	36.80	37.05	37.20	37.30	37.35
69	T6	3" exp.	36.20	37.25	37.55	37.95	38.00	38.20	38.50
65	T4	3" exp.	37.55	38.05	38.30	39.00	38.90	39.10	39.50
63	T3	1" exp.	37.60	38.00	38.20	39.40	39.50	39.65	39.80
60	T2	Cap	38.00	38.65	39.20	39.30	39.45	39.70	40.05
4	T1	Cap	38.25	38.55	39.55	40.00	39.95	40.40	40.75

* Reading error < 0.2 ms

Reliability analysis

The P- and S-wave velocities calculated from the survey data are presented in Tables 6.9 and 6.10. It is noted that the average P- and S-wave velocities are very consistent as indicated by very small standard deviations. The mean standard deviations (standard deviation/mean) for P- and S-wave velocities are only 1.2% and 0.79%, respectively. It is also noted from these tables there is no trend in either mean or standard deviation due to the amount of explosives used (the mean and standard deviation associated with each source).

Conclusions on velocity survey

The result of the above analysis can be briefly summarized: 1) the size of the database used for the velocity calculation is statistically reliable, 2) the calculated velocities are representative in terms of the distance range used which is compatible with the ones for the reflection surveys, 3) the effect of reading errors is negligible and the calculated velocities can be considered free of reading errors, 4) no trend exists due to the amount of explosives used, and 5) the accuracy and consistency are indicated by very small mean standard deviation, 1.2% and 0.79% for P- and S-waves, respectively. Because of these reasons, the P-wave velocity (16,777 ft/s) and the S-wave velocity (8,572 ft/s) determined from the survey can be considered very accurate.

Table 6.9 P-wave velocity along individual ray paths (ft/s)

Hole #	Source type	S7	S6	S5	S4	S3	S2	S1	mean	standard deviation
T10	3" exp.	17081.5	17058.6	16851.6	16655.7	16782.5	16721.6	16762.8	16844.9	165.0
T8	3" exp.	17040.9	17408.7	17246.1	16867.7	16866.6	16719.6	16899.8	17007.0	242.5
T6	3" exp.	16793.4	16926.3	16689.9	16738.0	16832.5	16776.4	16960.8	16816.8	97.9
T4	3" exp.	16927.9	17022.0	17052.9	16886.4	16814.6	16635.6	16779.5	16874.1	145.1
T3	1" exp.	16845.6	16855.6	16800.2	16522.6	16624.3	16614.1	16516.0	16682.6	148.2
T2	Cap	16726.9	16868.9	16604.9	16421.6	16605.8	16556.1	16542.3	16618.1	143.4
T1	Cap	16699.4	16843.0	16583.4	16525.2	16550.9	16542.3	16414.9	16594.2	138.2
Total average									**16777.0**	**205.3**

Table 6.10 S-wave velocity along individual ray paths (ft/s).

Hole #	Source type	S7	S6	S5	S4	S3	S2	S1	mean	Standard deviation
T10	3" exp.	8700.5	8662.4	8543.5	8523.1	8587.5	8543.5	8551.5	8587.4	67.9
T8	3" exp.	8688.4	8608.2	8482.4	8513.5	8569.3	8561.5	8642.2	8580.8	71.7
T6	3" exp.	8698.2	8542.7	8489.4	8490.3	8571.3	8541.9	8568.5	8557.4	70.4
T4	3" exp.	8565.4	8544.6	8504.2	8443.2	8558.6	8530.5	8538.4	8526.4	41.8
T3	1" exp.	8646.8	8649.6	8620.0	8450.0	8522.5	8506.1	8569.2	8566.3	76.8
T2	Cap	8649.6	8598.1	8493.1	8566.0	8629.1	8590.8	8611.9	8591.2	51.0
T1	Cap	8688.0	8716.4	8511.8	8510.5	8617.3	8537.3	8560.0	8591.6	84.1
Total average									**8572.0**	**67.0**

6.3 Reflection survey at site A

Site A is a barrier pillar separating the mined out and active mining areas, located on the northern side of the mine (Figure 6.4). The primary reason for using this site is that the mined out area is water filled, a condition that is critical for void detection techniques. From a mine safety point of view, the value of a void detection technique will be significantly diminished if it is not suitable for the water filled condition.

6.3.1Reflection survey design

The local condition of site A is shown in Figure 6.12. It is seen from the map that the void boundary is quite irregular. The only section which has a relatively flat surface and is suitable for a test is a short segment in the middle of the figure where "*water filled*" is marked. Adjacent to this section on the right is a V-shape pillar, which would exhibit seismic behavior like a "sink" absorbing the signals entering into the area. On the left are several short entries oriented in the same direction. The effect of these entries was unknown before the test. Because of these reasons, the section where "*water filled*" is marked was chosen as the target segment for the reflection survey.

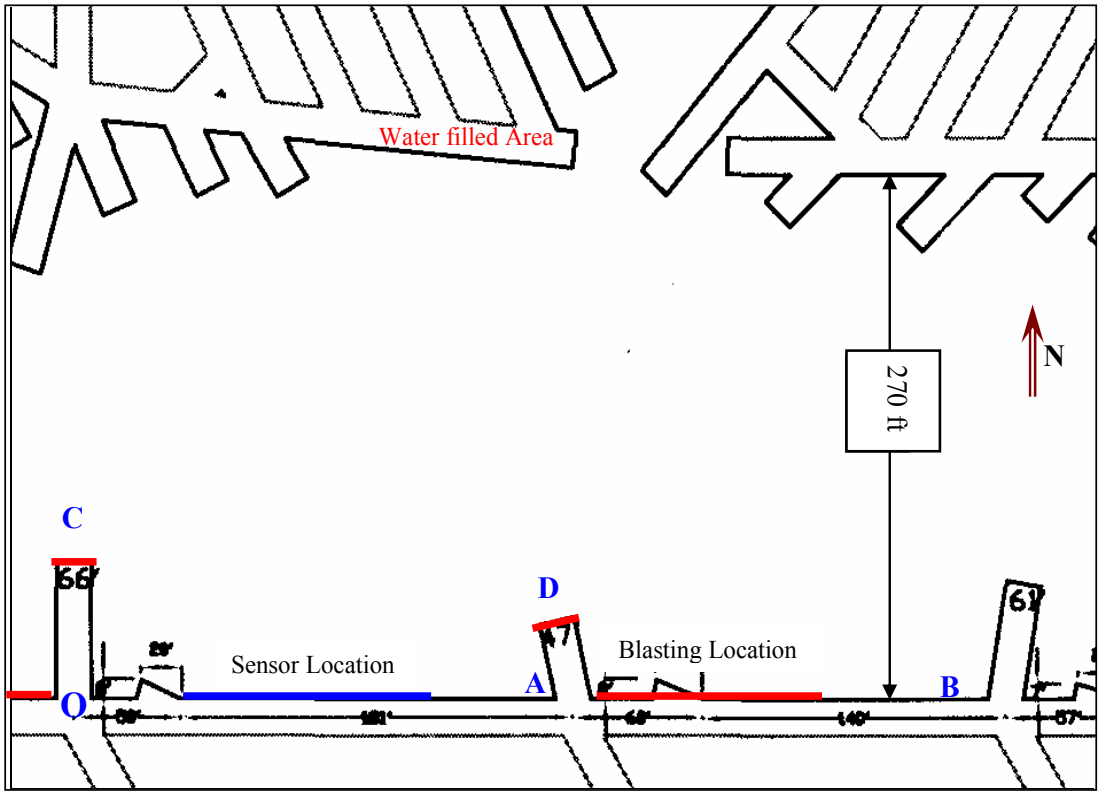

Figure 6.12 Map of site A, FMC

Sensor section

After the target segment was decided, the next task was to design the survey line. The survey line consisted of a sensor section and four general blasting locations. The sensor section included seven pairs of angled sensor holes, which were numbered from S1 to S14 (Figure 6.13). All these angled sensor holes were 7 feet deep and 1.75 inches in diameter. The information related to these sensor holes are given in Table 6.11.

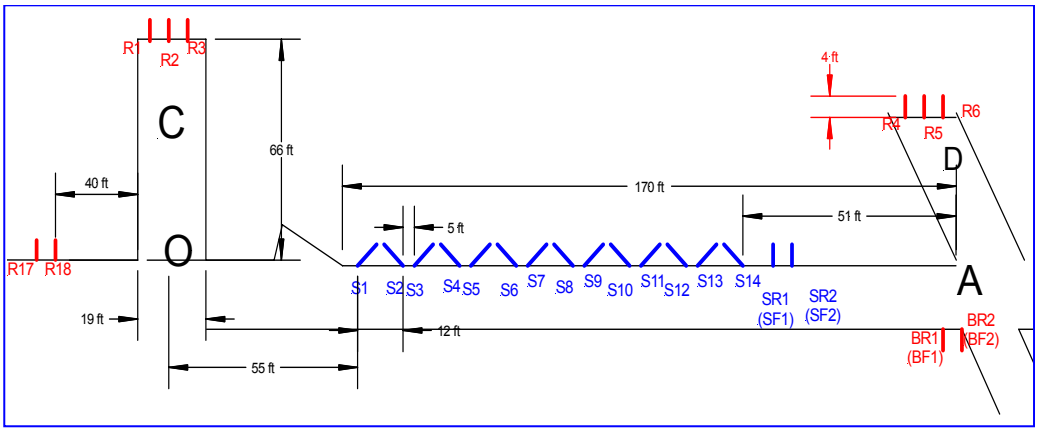

Figure 6.13 Sensor section designed for the reflection survey at site A, FMC.

Table 6.11 Sensor hole information for site A, FMC

Hole #	Channel #	Sensor coordinate (ft)	
		East (x)	North (y)
S1	2	56998.26	34894.65
S2	3	57000.26	34894.65
S3	4	57015.26	34894.65
S4	6	57017.57	34894.65
S5	7	57032.06	34894.65
S6	8	57034.26	34894.65
S7	9	57049.26	34894.65
S8	10	57052.32	34894.65
S10	12	57068.64	34894.65
S11	14	57084.01	34894.65
S12	15	57086.32	34894.65
S14	16	57102.42	34894.65
SF1	2	57114.42	34894.65

Blasting locations

A total of 18 blasting holes were prepared for the reflection survey, which were number from R1 to R18. These 18 holes were distributed over four general locations. The main location is shown in Figure 6.14, where 10 blasting holes, R7 – R16, were located. R16 is considered a limiting location; for any sources further to the right would result in the "sinker" becoming the expected reflector.

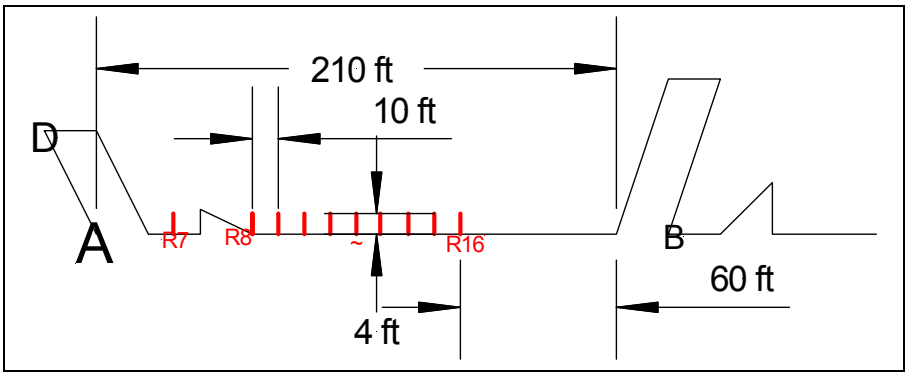

Figure 6.14 The main blasting section for the reflection survey at site A, FMC.

The other three locations are shown in Figure 6.13. One is located at the back of a small entry on the right side of the sensor section. The drill holes associated with this location are R4, R5 and R6. There are several advantages for this location. First, it is very close to the sensor section, and therefore, the associated ray paths will be nearly vertical. Second, it significantly reduces the signal travel distance. Third, the location is relatively flat and smooth and the effect of irregularities on wave propagation is minimal. Finally, it significantly reduces the interference of the (air) shock wave caused by blasting.

The other general location is the back of a small entry on the left side of the sensor section. In addition to taking advantage of having blasting holes in an adjacent entry just discussed the main reason for this location is to test the effect of the entries on the opposite side. Three blasting holes, R1, R2 and R3, were prepared for this location. The third general location is the left side of this entry, where R17 and R18 were located. These two blasting holes were designed to test the shading effect of the entry.

All blasting holes are 4 ft long and 1.5" in diameter, drilled in the middle of the seam. The coordinates of the blasting holes which were used for the reflection survey are listed in Table 6.12.

Table 6.12 Blasting hole information for site A, FMC

Hole #	Source coordinate (ft)	
	East (x)	North (y)
R1	56936.26	34959.65
R2	56943.19	34959.65
R4	57128.83	34940.65
R8	57220.87	34893.65
R10	57232.87	34893.65
R11	57238.87	34893.65
R12	57244.87	34893.65
R14	57256.87	34893.65
R16	57268.87	34893.65
R17	56888.26	34893.65
R18	56894.25	34893.65
BF1	57132.29	34865.23
BF2	57137.28	34865.23

6.3.2 Reflection surveys

The reflection survey included 11 individual surveys (blasting events). The explosives used for the surveys ranged from a single cap to 375 gram/hole. Table 6.13 is a summary of these surveys.

Table 6.13 A summary of the reflection tests at FMC

Hole #	Explosive (g)	Event #
R12	375	**7**
R11	125	**34**
R10	375	**39**
R14	375	**86**
R16	375	**95**
R8	375	**101**
R4	125	**108**
R1	125	**118**
R2	125	**123**
R17	125	**127**
R18	Cap	**132**
BF2	Cap	**150**
BF1	Cap	**153**

6.3.3 Types of reflected signals

Three types of reflected signals were identified, which are reflected P-waves, reflected S-waves, and reflected S-waves due to mode conversion (P-waves converted to S-waves at the boundary).

All reflected signals from the "void" boundary are associated with very high frequencies with a typical range of 4,000 – 5,000 Hz. Signals with 5,000 Hz are most typical. The corresponding

wave length for this typical frequency range is 3.3 - 4.4 ft for reflected P-waves and 1.7 - 2.1 ft for reflected S-waves.

The significance of these high frequency signals is that their wave lengths are much smaller than the seam height (10 – 12 ft), which leads to the high resolution of reflection surveys. The detection resolution of an object depends on the wave length. The smaller the wave length, the higher the resolution. The object will not be detectable if the wave length is larger than the object.

6.3.4 Case study: event 86

Event 86 refers the reflection survey related to seismic source R14, which is located at the main blasting section. The relative location of R14 and the sensors as well as the corresponding ray paths for this event is shown by Figure 6.15.

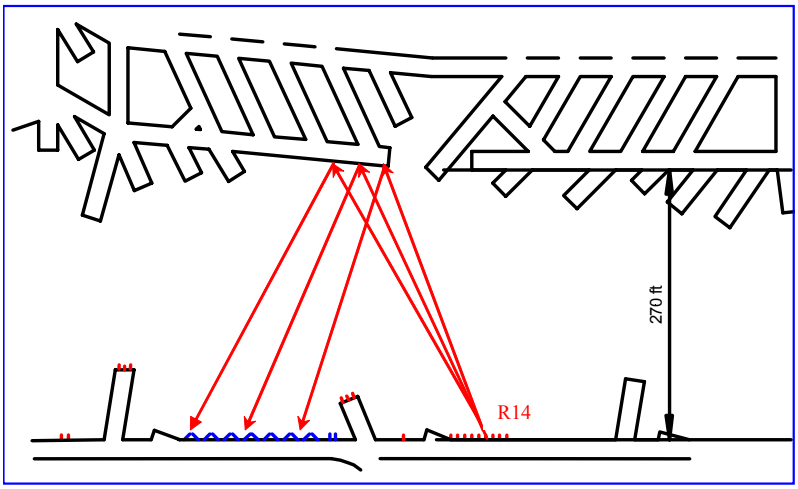

Figure 6.15 Test setup for event 86.

Figure 6.16 shows the arrivals of the reflected P-waves. It is seen from the figure that the pattern of the arrival is evident and the arrivals for most channels are clear. The readings of the P-wave arrival times are given in the following table. The triggering time for this event is 99.8 ms. The channels for sensors 9 and 13 were not working at the time. No readings are given for sensors 10, 11, 12 and 14 as the reflected P-waves could not be determined.

Table 6.14. P wave arrival times

Triggering time (ms)	Sensor #	S1	S2	S3	S4	S5	S6	S7	S8
99.8	Arrival time (ms)	132.2	132.2	131.1	131.1	129.1	129.84	126.8	126.8

Table 6.15 Parameters of ellipses associated with event 86

Source*	Sensor**	Travel time (ms)	Travel distance (ft)	Half of foci distance (ft)	Half of major axis (ft)	Half of minor axis (ft)
R14	S1	32.4	543.6	129.3	271.8	239.1
R14	S2	32.4	543.6	128.3	271.8	239.6
R14	S3	31.3	525.1	120.8	262.6	233.1
R14	S4	31.3	525.1	119.7	262.6	233.7
R14	S5	29.3	491.6	112.4	245.8	218.6
R14	S6	30.04	504.0	111.3	252.0	226.1
R14	S7	27	453.0	103.8	226.5	201.3
R14	S8	27	453.0	102.3	226.5	202.1

* See Table 6.12 for source coordinates

** See Table 6.11 for sensor coordinates

*** P-wave velocity: 16777 ft/s

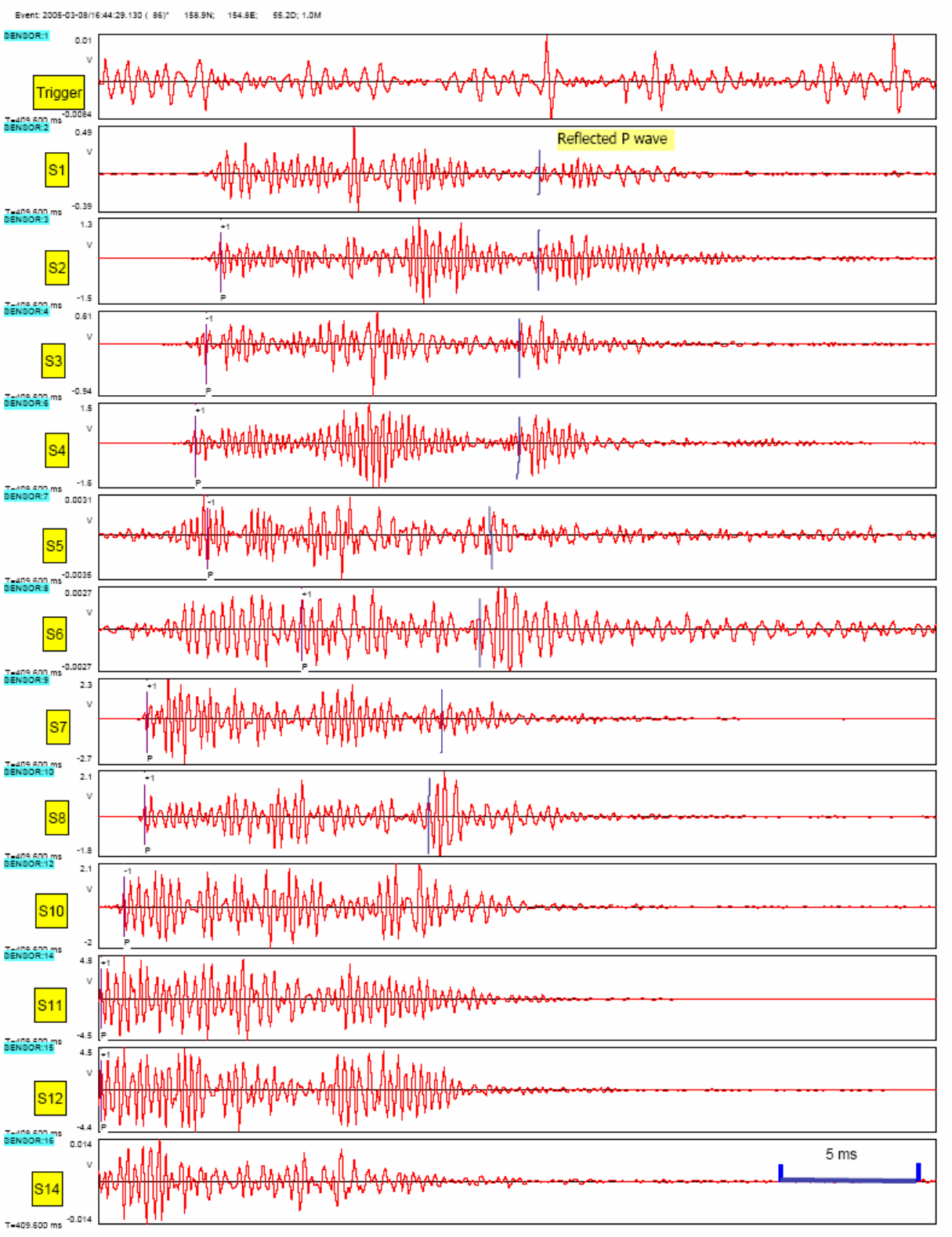

Figure 6.16 Event 86 showing the arrivals of the reflected P-waves (display window: 56 - 76 ms).

6.3.5 Case study: event 108

Event 108 refers to the reflection survey related to seismic source R4, which is located at the small entry on the right side of the sensor section. The relative position of R4 and the sensors as well as the corresponding ray paths for this event is shown in Figure 6.17.

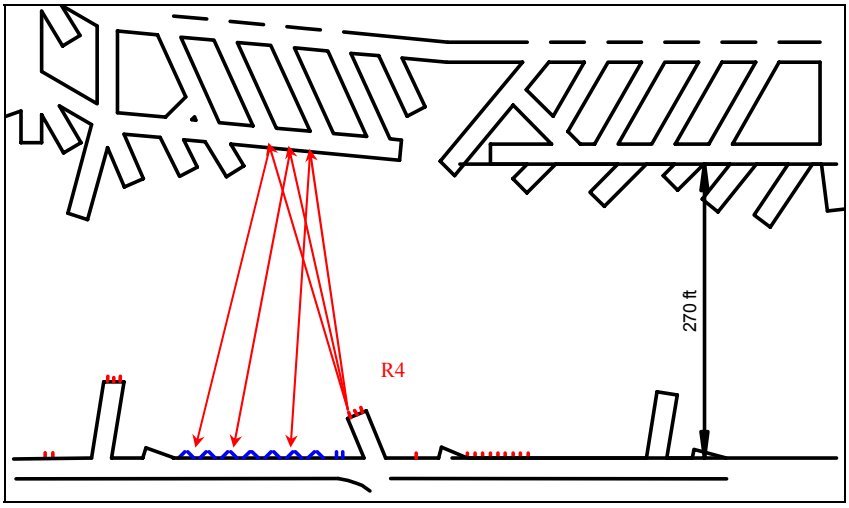

Figure 6.17 Test setup for event 108.

The complete waveforms recorded for this survey event are given in Figure 6.18. The trend of the reflected P-wave arrivals is clear as marked. The details of these reflected P-wave arrivals are shown in Figure 6.19. The readings of P-wave arrival times are given in the following table. The triggering time for this event is 49.00 ms. The channels for sensors 9 and 13 were not working at the time. No readings are given for S4, S5 and S6 as the reflected P-waves are not clearly shown.

Table 6.16. Reflected P wave arrival times

Triggering time (ms)	Sensor #	S1	S2	S3	S4	S5	S6	S7	S8	S10	S11	S12	S14
98	Arrival time (ms)	127.6	127.2	126.6				123.2	124.4	122.6	121.8	122.2	122.2

A very interesting observation about this event and the previous one (event 86) is the arrivals at the last four sensors. For event 86, it was difficult to identify the reflected P-waves at these channels, which is also the case for the adjacent blasting holes, such as R10. If we consider that fact that the P-wave arrivals for the current event are clearly seen, a likely cause of the missing data for event 86 is that this missing data was absorbed by the “sinker”, a V-shape pillar on the void side. The importance of this observation is that the test setup and the associated data analysis method have to be highly flexible for void detection in mines. If a stacking method had been used for data analysis and void mapping, which requires a straight survey line, this blasting location would have not been considered and utilized.

Table 6.17 Parameters of ellipses associated with event 108

Source*	Sensor**	Travel time (ms)	Travel distance (ft)	Half of foci distance (ft)	Half of major axis (ft)	Half of minor axis (ft)
R4	S1	29.6	496.6	69.2	248.3	238.5
R4	S2	29.2	489.9	68.3	244.9	235.2
R4	S3	28.6	479.8	61.3	239.9	232.0
R4	S7	25.2	422.8	46.0	211.4	206.3
R4	S8	24.4	409.4	44.6	204.7	199.8
R4	S10	24.6	412.7	37.9	206.4	202.9
R4	S11	23.8	399.3	32.1	199.6	197.0
R4	S12	24.2	406.0	31.3	203.0	200.6
R4	S14	24.2	406.0	26.5	203.0	201.3

* See Table 6.12 for source coordinates
** See Table 6.11 for sensor coordinates
*** P-wave velocity: 16,777 ft/s

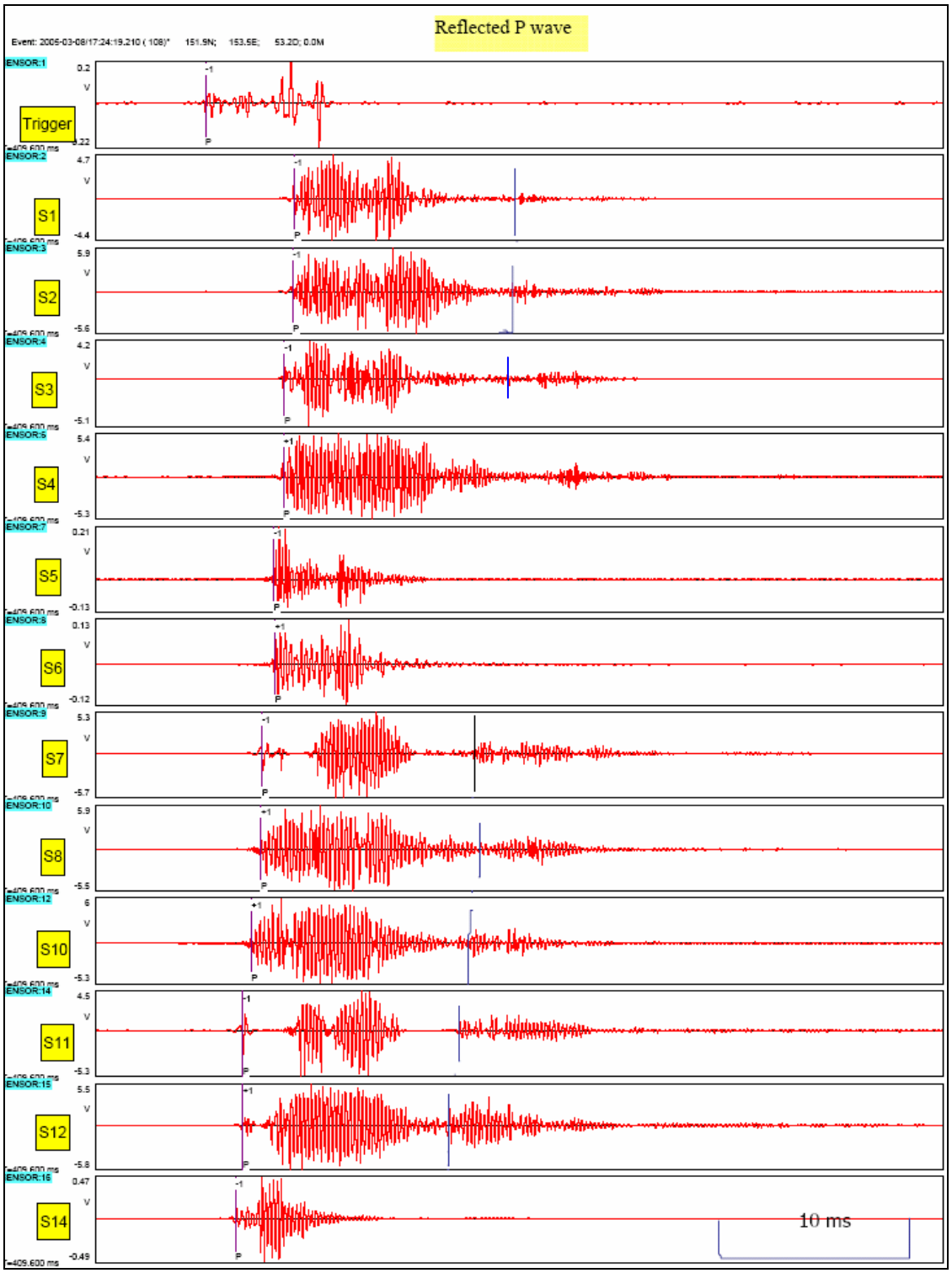

Figure 6.18 The complete waveforms recorded for event 108, where the trend of the reflected P-wave arrivals is clear seen as marked.

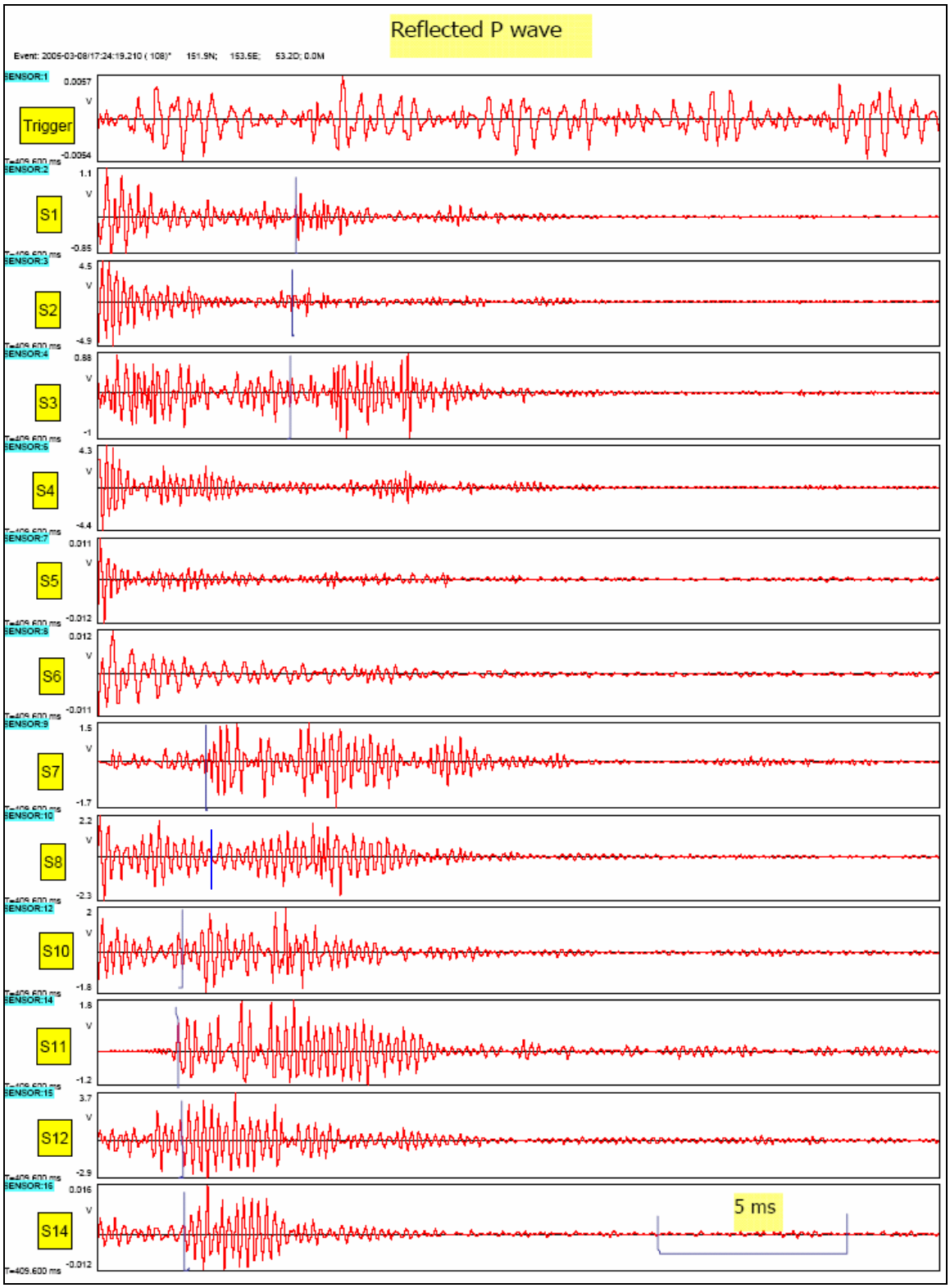

Figure 6.19 Details of the arrivals of the reflected P-waves for event 108 (display window: 59 – 79 ms).

6.3.6 Case study: Event 118

Event 123 refers the reflection survey related to seismic source R2, which is located at the small entry on the left side of the sensor section. The relative position of R2 and the sensors as well as the corresponding ray paths for this event is shown by Figure 6.20.

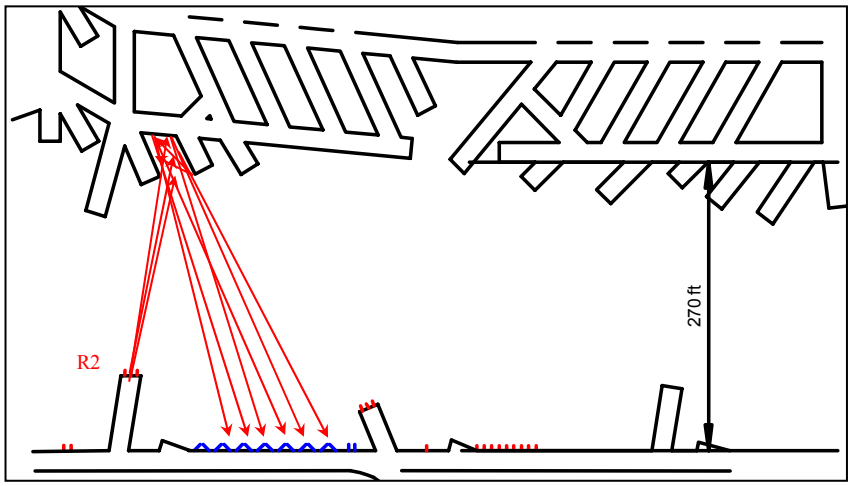

Figure 6.20 Test setup for event 118.

As it has been discussed earlier, one of the main reasons to arrange the seismic sources at this particular location is to test the effect of several parallel entries on the void side. The complete waveforms recorded for the survey are given in Figure 6.21. The trend of the reflected S-wave arrivals is clear. The details of these reflected S-wave arrivals are shown in Figure 6.22. The readings of S-wave arrival times are given in the following table. The triggering time for this event is 99.8 ms. The channels for sensors 9 and 13 were not working at the time.

Table 6.18. S wave arrival times.

Triggering time (ms)	Sensor #	S1	S2	S3	S4	S5	S7	S8	S10	S11	S12
99.8	Arrival time (ms)	144.6	144.6	145.2	146.1	147.1	147.8	147.9	148.5	149.3	149.3

Table 6.19 Parameters of ellipses associated with event 118

Source*	Sensor**	Travel time (ms)	Travel distance (ft)	Half of foci distance (ft)	Half of major axis (ft)	Half of minor axis (ft)
R2	S1	44.8	384.0	42.6	192.0	187.2
R2	S2	44.8	384.0	43.2	192.0	187.1
R2	S3	45.4	389.2	48.5	194.6	188.4
R2	S4	46.3	396.9	49.4	198.4	192.2
R2	S5	47.3	405.5	55.1	202.7	195.1
R2	S7	48.0	411.5	62.2	205.7	196.1
R2	S8	48.1	412.3	63.5	206.2	196.1
R2	S10	50.3	431.0	70.6	215.5	203.6
R2	S11	49.5	424.3	77.5	212.2	197.5
R2	S12	49.5	424.3	78.6	212.2	197.1

* See Table 6.12 for source coordinates
** See Table 6.11 for sensor coordinates
*** S-wave velocity: 8572 ft/s

An interesting phenomenon shown by both Figures 6.21 and 6.22 is the very long duration for the reflected S-waves. This is also the case for the other surveys conducted in the same area. We believe that this phenomenon was caused by the parallel entries on the reflection side. These parallel entries act as a special reflector to deliver the received energy to the direction they are oriented, which points to the sensor line.

The ellipses calculated based on the travel times given in the above table are plotted in Figure 6.23. It is evident from the figure that these ellipses delineated the void with a good accuracy.

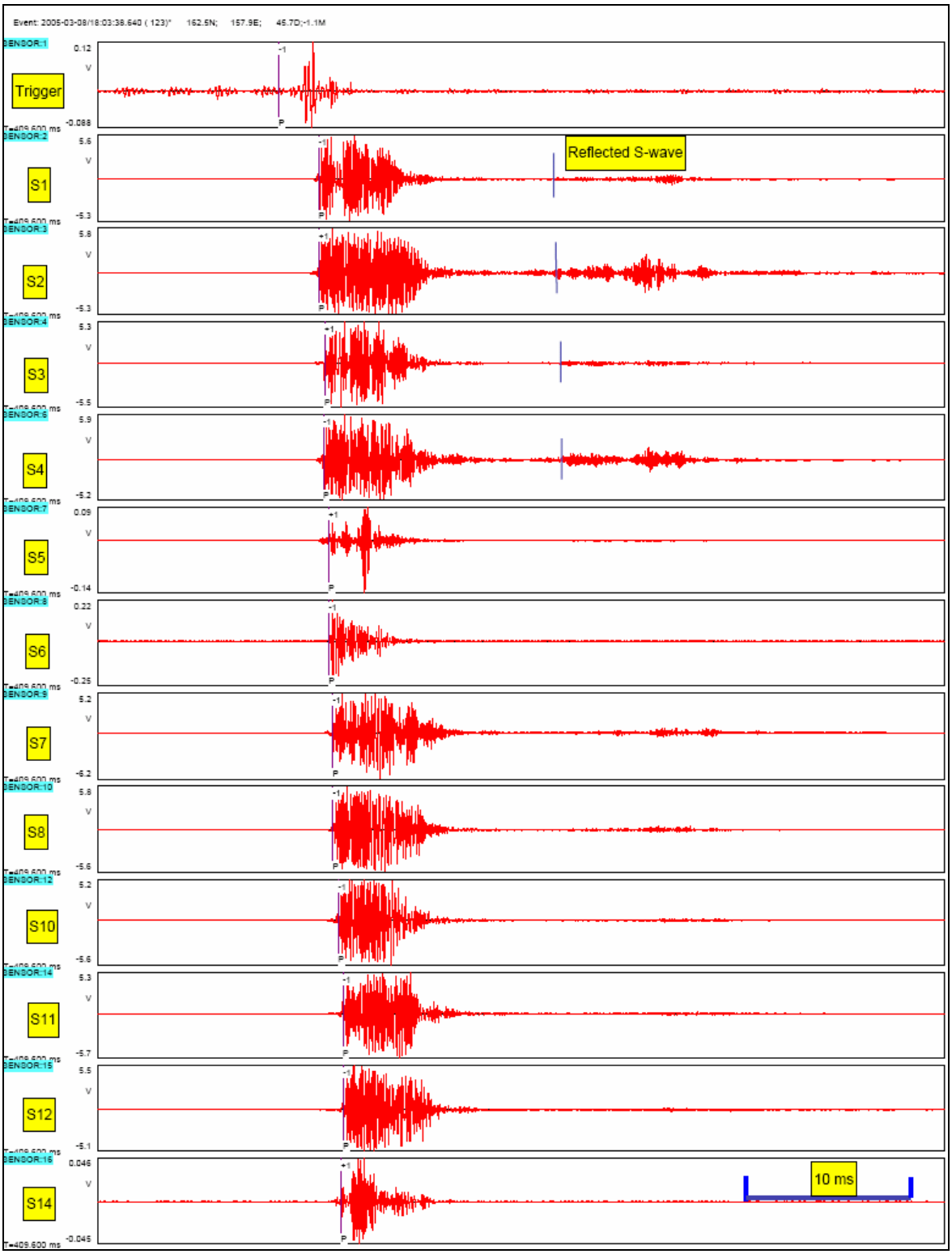

Figure 6.21 The complete waveforms recorded for event 118, where the trend of the reflected S-wave arrivals is clear seen as marked.

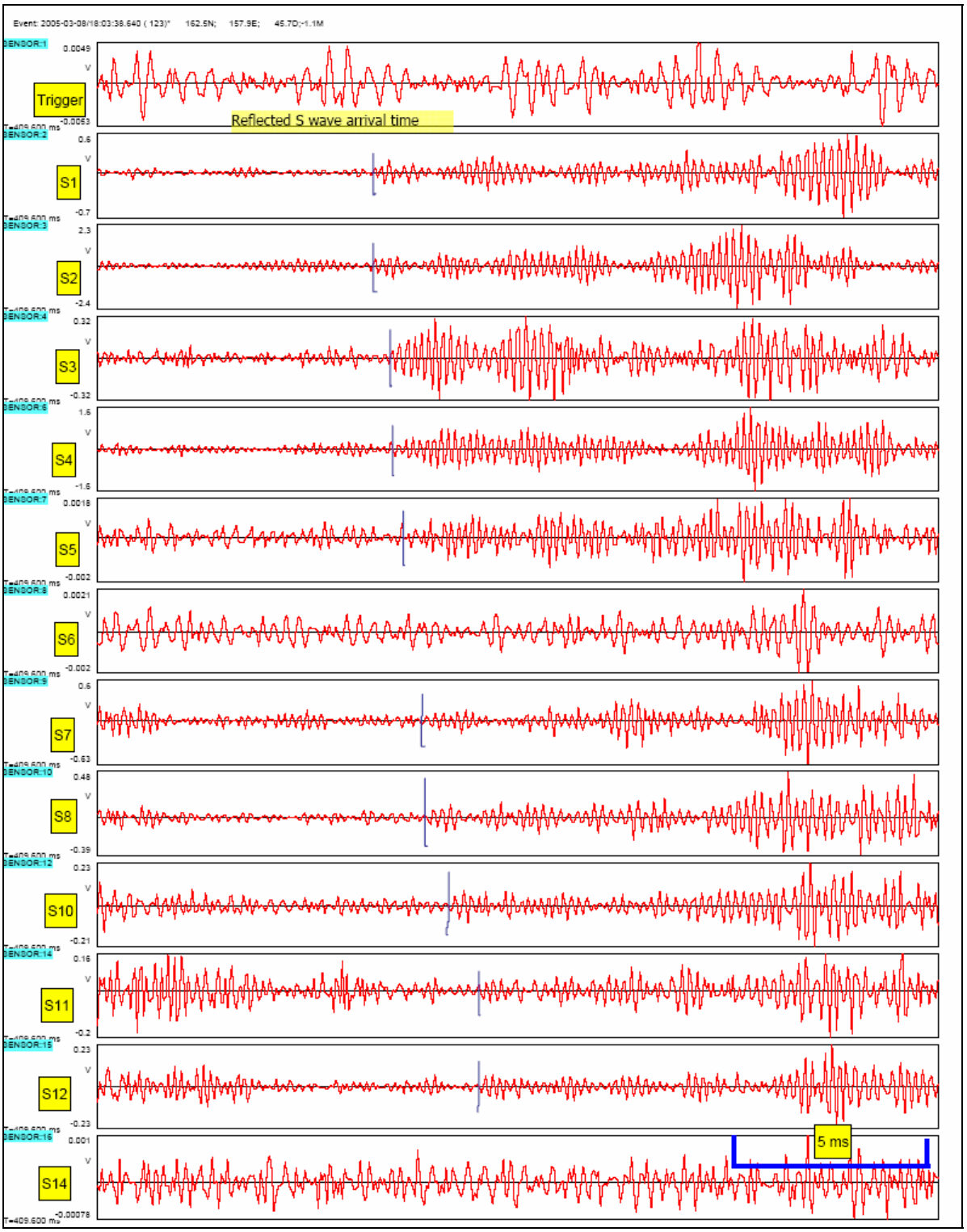

Figure 6.22 Details of the arrivals of the reflected S-waves for event 118 (display window: 65 - 86 ms).

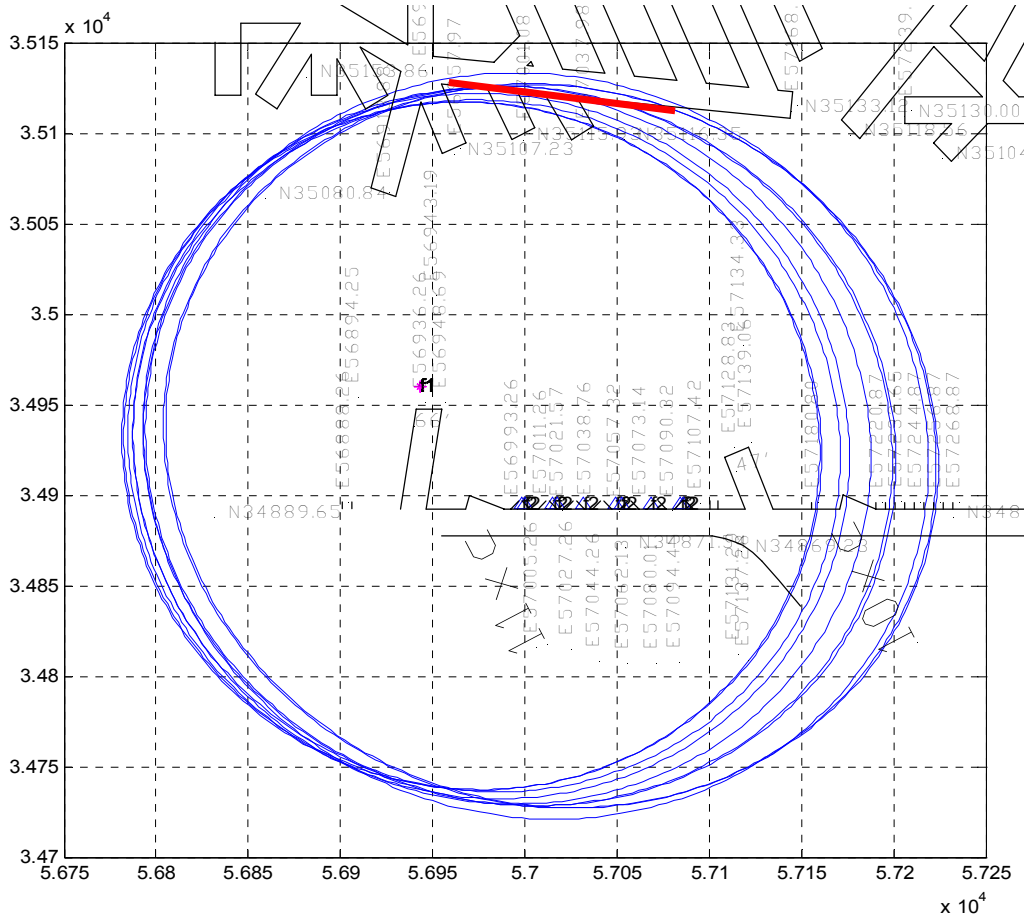

Figure 6.23 Void mapping with the ellipses associated with event 118 at FMC testing site. The void boundary is represented by a short red line. The locations of the sensors and the source as well as the associated ray paths are illustrated in Figure 6.20.

6.3.7 Void mapping

After the arrivals of reflected signals are determined, the next step is to map the void. In this project, the elliptical mapping method was used to delineate the void location. The result of the void detection at site A is given in Figure 6.24. The P- and S-wave velocities used for plotting are 16777 ft/s and 8572 ft/s, respectively.

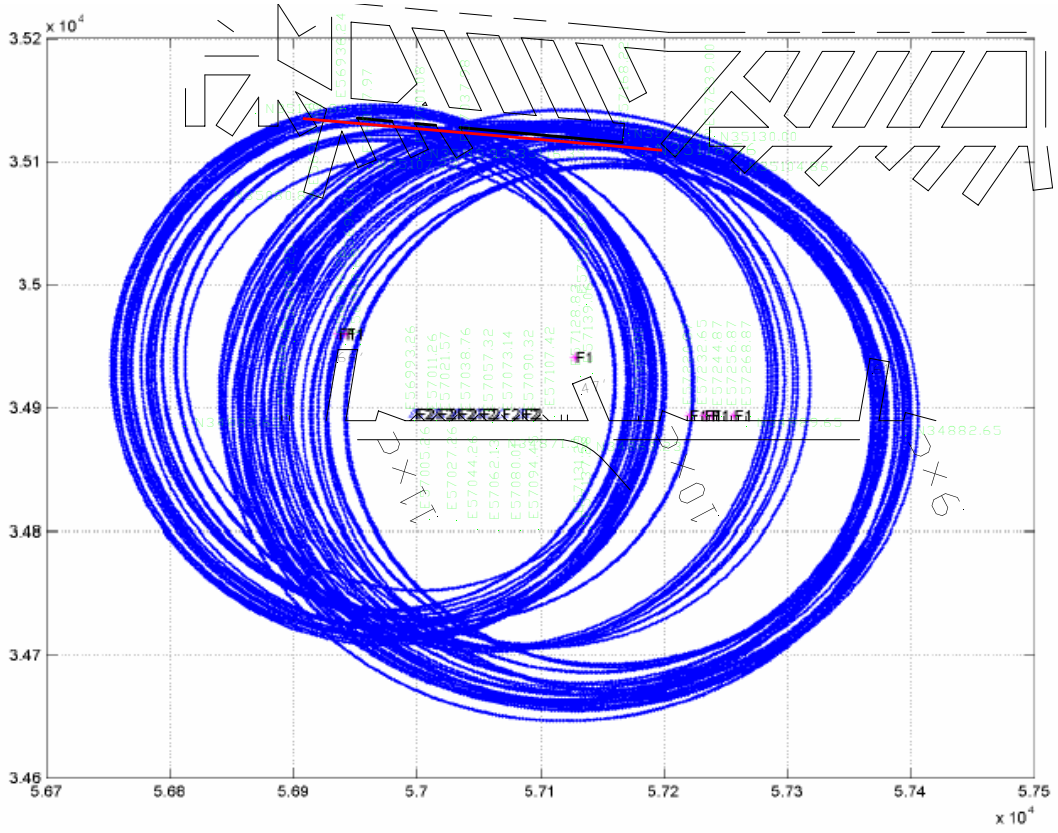

Figure 6.24 Void detection with the elliptical mapping method at site A, FMC.

With the elliptical mapping method, the void is delineated by the common tangent line, which is represented by a red line in figure 6.24. As it has been discussed, the target area for the reflection survey is a smooth inclined section in the middle. The red line coincides well with this void segment.

The arrivals of the signals used for plotting are accurate. The travel time errors for most data points are in the range of 0.25 – 0.5 ms. If this range is converted to location error, it is only a few feet, no more than 10 ft.

The accuracy is also shown by the fact that we can clearly see from the survey data the characteristics of the void boundary. For instance, if the reflection points are within the target area, a smooth segment in the middle, we could see many clear reflected signals. However, if they are within the V-shape area, we could hardly see any. The reason is that signals were trapped in the area. This phenomenon was discussed in section 6.3.5. If we plot the data point by point, there would be a "hole" in this region. If the reflection points are on the right hand area,

the data is less stable, which reflects the fact of irregular boundary in the area. The related discussion was given in section 6.3.6.

There are three distinctive groups of ellipses, which are associated with three blasting locations. To be able to process the data from these three different locations simultaneously is critical for a reliable mapping result. If a stacking method had been used for data analysis and void mapping, two groups of the ellipses would have not been available as the associated survey locations, two small entries would not have been considered because they are not on the same line as the sensor section.

6.4 Summary of the Field test at FMC

One of the main concerns with the trona mines in Wyoming is how rapidly barrier pillars deteriorate in the presence of water. Since void detection by the long-hole drilling method would induce water into pillars, the means left for measuring pillar width is restricted to non-destructive testing methods. Both the trona industry and MSHA considered the ISS based void detection technique a potential solution for the problem. It was for this reason that Penn State was requested to demonstrate the ISS based void detection technique at a trona mine. The field test at FMC was the first trona mine test.

Although the term "ISS based void detection technique" is used to develop the technique for determining the pillar width at the trona mines, it is important to note that the actual demonstration is based on a different scientific principle. For the ISS based technique, the in-seam waves, or channel waves are used. The required physical condition for the conventional ISS based technique is that the seam is softer than the country rocks. For the trona mines in Wyoming, the trona is much harder than the roof and floor strata. Therefore under these conditions, the body waves have to be used as the conventional reflection survey for the exploration purposes. The challenge in using the body wave for void detection is that the wave length has to be sufficiently short, much smaller than the seam thickness. In other words, the success of void detection in trona mines has to rely on the high frequency signals in the order of thousands.

The test at FMC was carried out at two sites: *Site A* and *Site B*. *Site A* was a barrier pillar, which was 12 ft high and approximately 270 ft wide. The void was water filled The site was used for reflection testing. *Site B* was a pillar of approximately 290 ft wide, which was utilized for a transmission test.

The testing result shows that both transmission signals and reflection signals are associated with very high frequencies, typically in the range of 3000 – 5000 Hz. The system used by Penn State was able to pick up these signals reliably. The high frequency signal is essential for identifying voids. It is also important for general data analysis. The testing result also shows that the body waves in trona are very stable and can be accurately determined. P- and S-wave velocities at the mine are 16,777 ft/s and 8,572 ft/s, respectively.

Three types of reflected signals were observed, which are P-wave, S-wave and S-wave due to mode conversion. The void was mapped by simultaneously processing these data. The mapping error was estimated ± 10 ft.

7. Field Test at General Chemical Trona Mine

7.1 Introduction

On March 9 – 10, 2005, the Penn State project team conducted a field test at General Chemical (GC) trona mine located in Wyoming. It was the second of three tests carried out at trona mines. The purpose of this test and the one carried out at FMC was to investigate whether body waves in trona could be detected and utilized for void mapping. The main difference between these two tests is the void condition as the site at FMC is water filled, while the site at General Chemical is air filled, or in a "dry" condition.

General Chemical is one of three initial industrial participants, which provided the enthusiastic support for the void detection project. The other two are FMC and the Harmony Mine.

7.1.1 General Chemical trona mine

General Chemical (Figure 7.1) is the second largest trona producer in Wyoming with an annual production of 4.2 million tons in 2003. Three other major producers in the area are FMC, OCI, and Solvey Minerals.

Figure 7.1 General Chemical trona mine in Wyoming.

General Chemicals, FMC, and Solvey Minerals are currently mining the same trona bed, known as bed 17 while OCI produces trona from beds 24 and 25 at a depth of 800 feet. Bed 17 consists of very high quality trona, which is 12 feet thick and about 1,600 feet deep (Figure 7.2). All three field tests were carried out with this ore bed. The location of the trona resource as well as the trona operations in Wyoming is given in Figure 7.3.

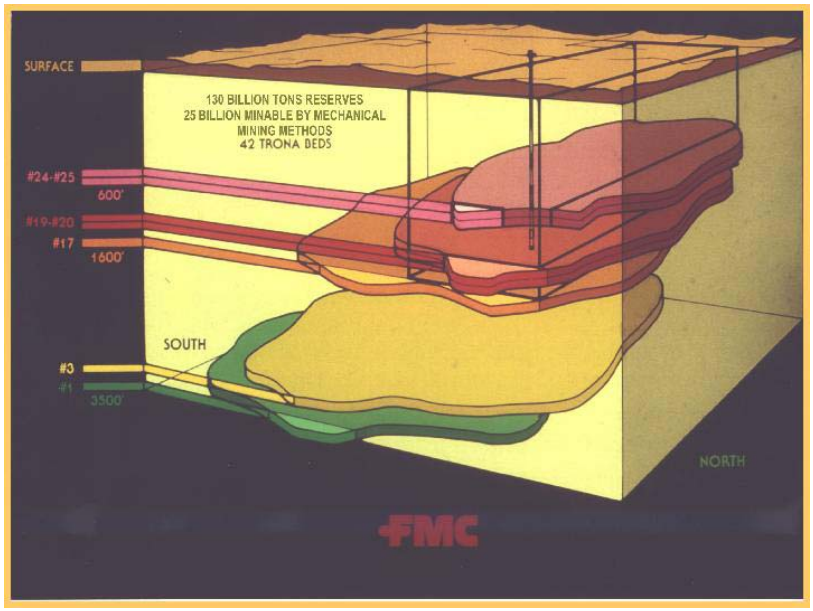

Figure 7.2 Wyoming trona deposition.

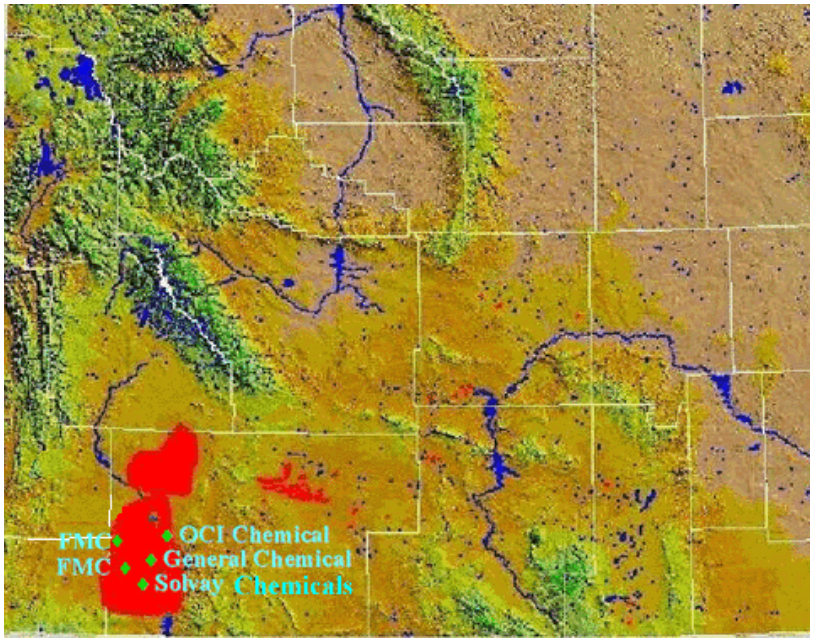

Figure 7.3 Map of Wyoming trona operations.

7.1.2 Test site at General Chemical

The test site is located at one end of a long pillar, which is approximately 340 ft wide (Figure 7.4). The site was utilized for both transmission and reflection surveys. The mine location of this long pillar is shown in Figure 7.5).

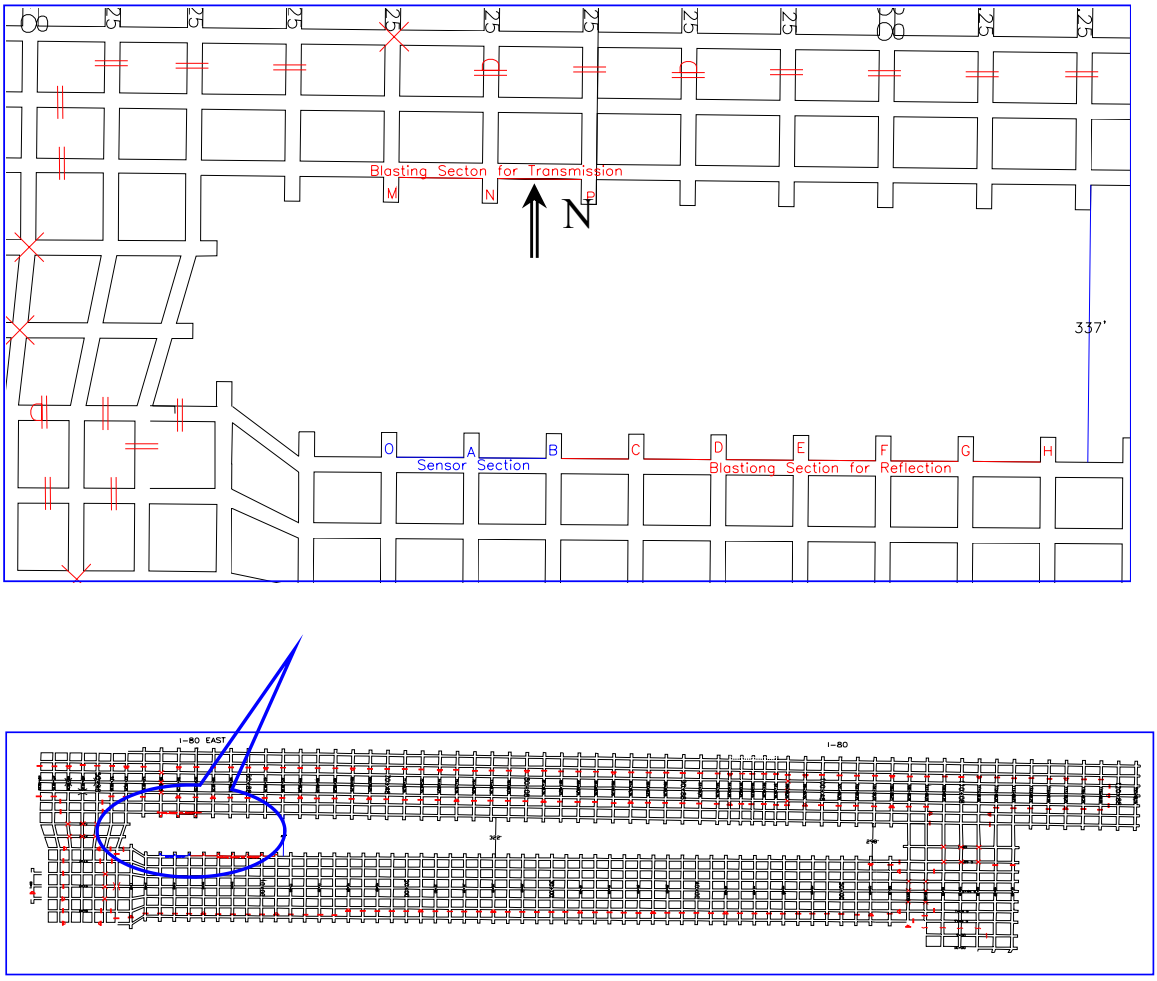

Figure 7.4 Testing site at General Chemical.

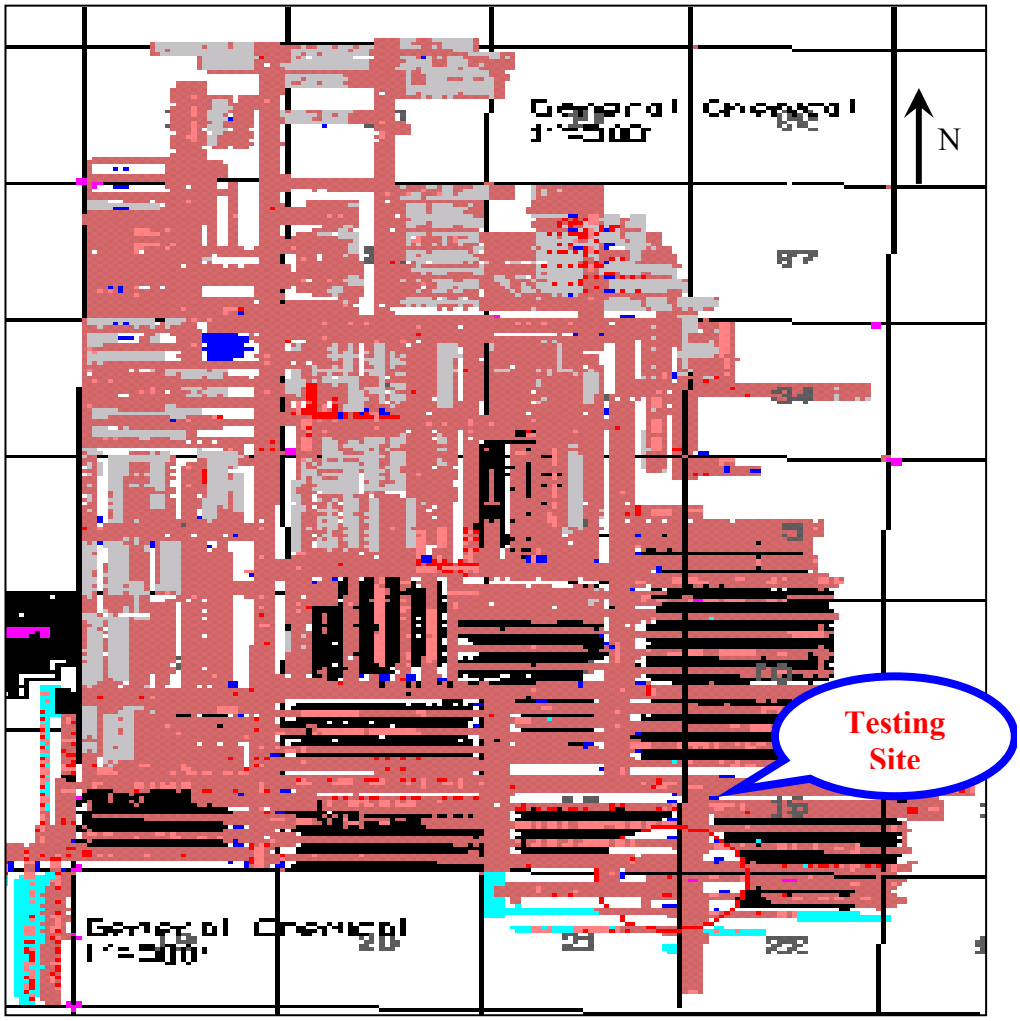

Figure 7.5 General Chemical mine map showing the locations of the test site.

7.2 Experimental design

The general layout of the testing setup is shown in Figure 7.6. There are three components to the design; sensor section, blasting section for transmission survey and blasting section for reflection survey.

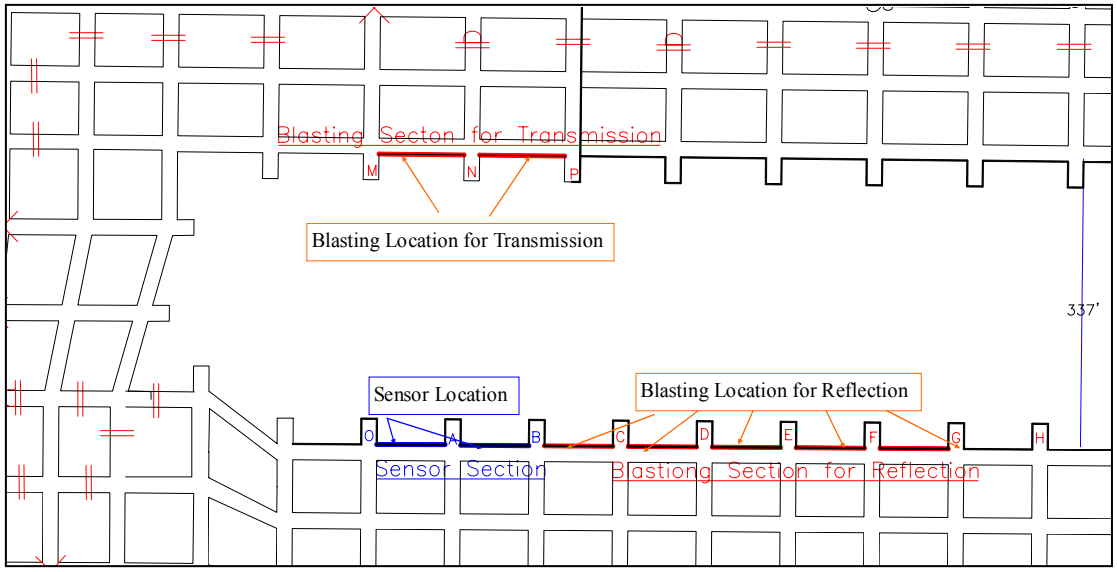

Figure 7.6 General layout of the testing setup at General Chemical.

The specifications on the sensors, the data acquisition system, and the major operational parameters used for the test are given in Appendix I. The sampling rate and the recording window used for the test are 25,000 samples/second and 0.8 second, respectively.

7.2.1 Sensor section

The sensor section consists of seven pairs of angled sensor holes, numbered from S1 to S14 (Figure 7.7). All of these angled sensor holes are 7 ft long and 1.75" in diameter. The location information related to these sensor holes is given in Table 7.1.

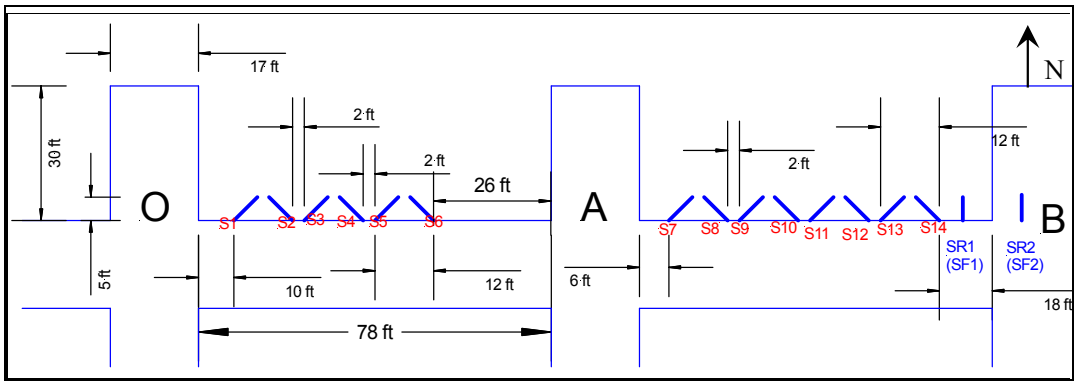

Figure 7.7 Sensor section designed for both transmission and reflection surveys at General Chemical.

Table 7.1 Sensor hole information for General Chemical

Hole #	Channel #	Sensor coordinate (ft)	
		East (x)	North (y)
S1	2	320030	237857
S2	3	320030	237859
S3	4	320030	237871
S5	6	320030	237885
S6	7	320030	237887
S7	8	320030	237951
S8	9	320029	237953
S9	10	320029	237965
S10	11	320029	237967
S11	12	320029	237979
S12	14	320029	237981
S14	16	320029	237995

7.2.2 Blasting section for transmission survey

The blasting section for the transmission survey consisted of 10 blasting holes which were numbered from T1 to T10 (Figure 7.8). All blasting holes are 4 ft long and 1.5" in diameter, drilled in the middle of the seam. Among these 10 holes, 4 were used for transmission survey. The coordinate data for these four holes are given in Table 7.2.

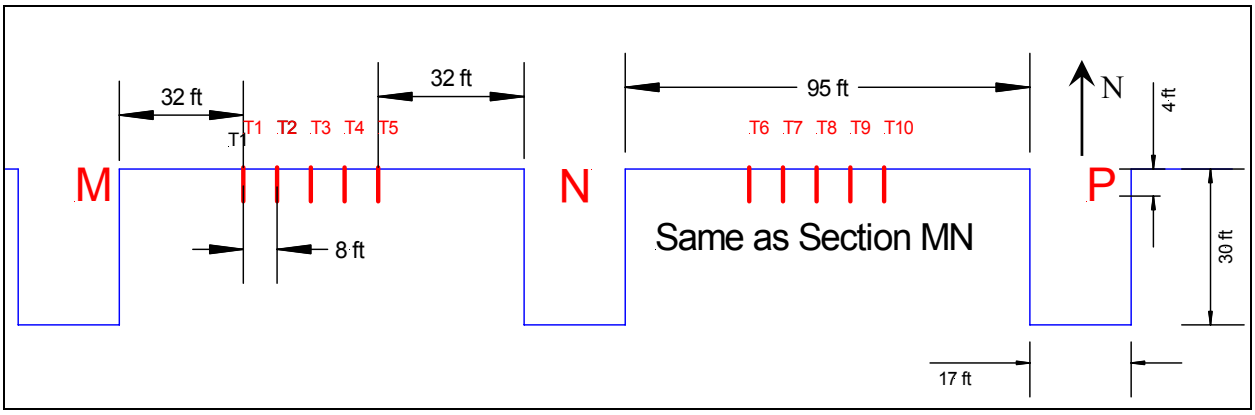

Figure 7.8 Blasting hole locations for transmission survey.

Table 7.2 Coordinates of blasting holes used for transmission survey at General Chemical

Hole #	Source coordinate (ft)	
	East (x)	North (y)
T1	320352	237869
T3	320352	237885
T8	320350	238016
T10	320350	238032

7.2.3 Blasting section for reflection survey

A total of 24 blasting holes were prepared for the reflection survey, which were number from R1 to R24. The locations of these 24 blasting holes are shown in Figure 7.9. These 24 blasting holes were on a straight line. The two sections given in the figure is for the convenience of the presentation. The joint of the two sections is the entry marked by E. All blasting holes are 4 ft long and 1.5" in diameter, drilled from the middle of the seam. The coordinates of the drill holes which were used for the survey are given in Table 7.3.

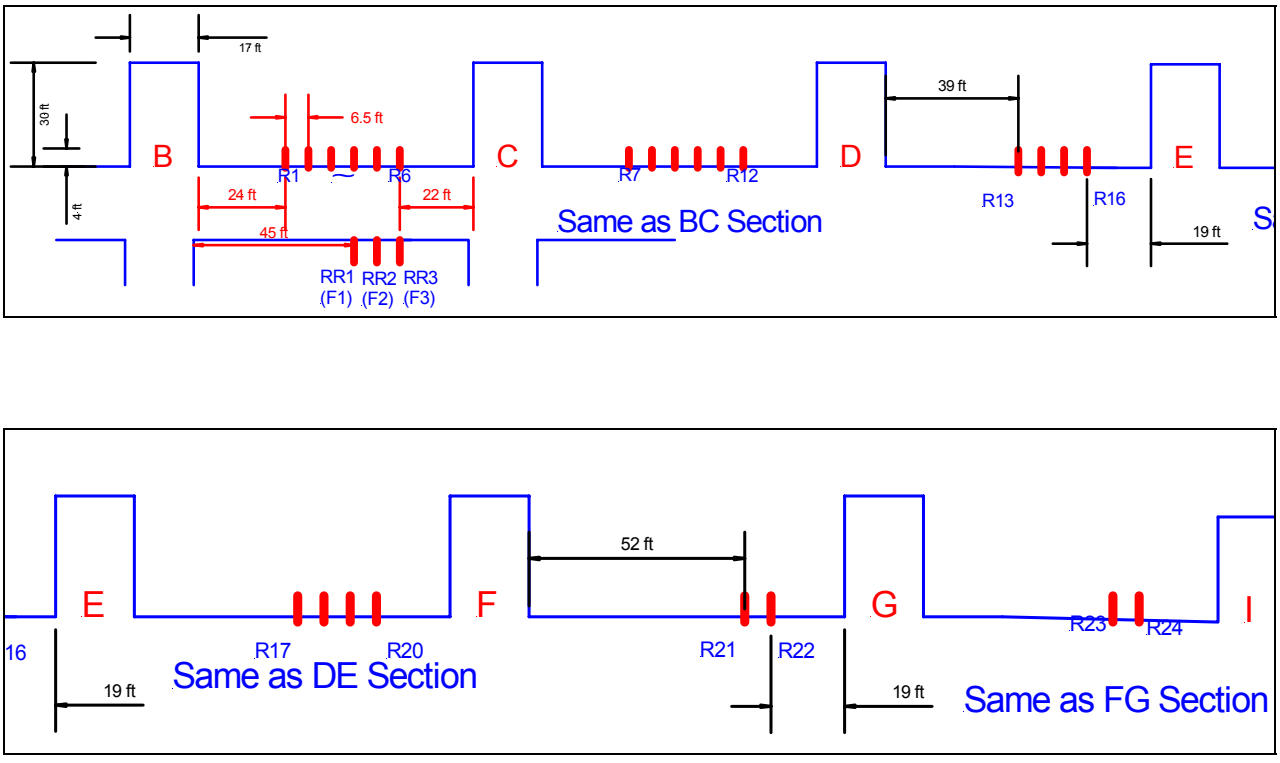

Figure 7.9 Blasting section for reflection survey at General Chemical.

Table 7.3 Coordinates of blasting holes for reflection survey at General Chemical

Hole #	Source coordinate (ft)	
	East (x)	North (y)
R6	320027.1	238091.1
R8	320026.5	238166.6
R10	320026.4	238179.6
R12	320026.3	238192.6
R14	320025.7	238275.1
R15	320025.6	238281.6
R18	320024.8	238385.9
R20	320024.7	238398.9
R22	320023.9	238498.9
R24	320023.1	238598.9
RR1	320000.8	238078.0
RF2	320000.6	238084.5
RR3	320000.6	238091.0
RF3	320000.7	238091.0

7.3 Transmission survey

The transmission survey at General Chemical consisted of four individual surveys (Figure 7.10). The explosives used for all four tests consisted of 375 grams of explosive. The testing information is summarized in Table 7.4.

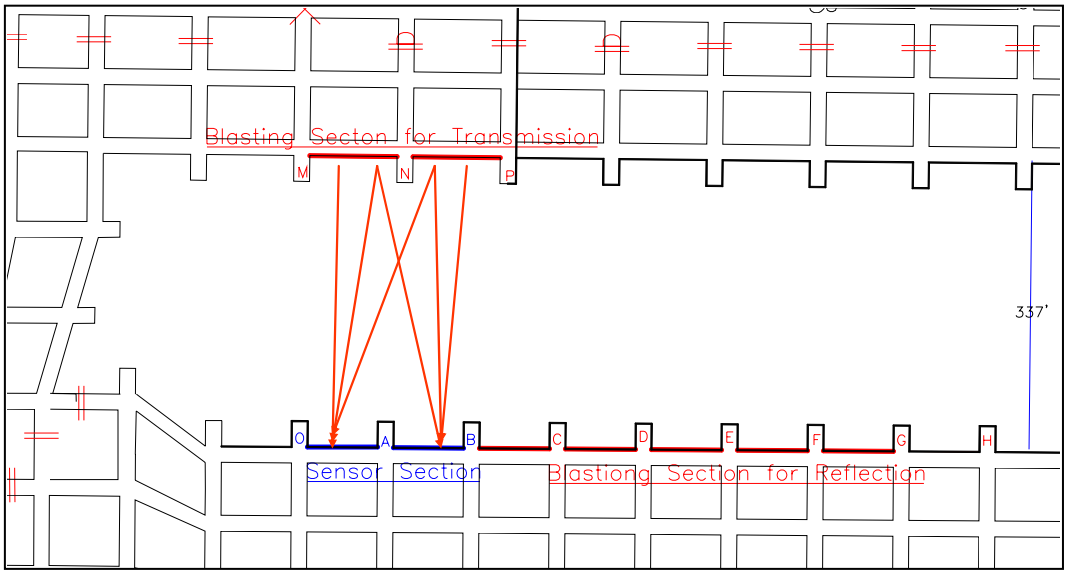

Figure 7.10 An illustration of ray paths associated with the transmission survey.

Table 7.4 A summary of the transmission survey at General Chemical

Hole #	Explosive (g)	Event #
T1	375	105
T3	375	107
T8	375	110
T10	375	112

7.3.1 Characteristics of transmission signals

Transmission signals from four surveys are similar and, as an example, the signals associated with event 110 are given in Figure 7.11. Both P- and S-waves are very well defined. The dominant frequencies for both P- and S-waves are very high, all in the neighborhood of 2500 - 5000 Hz . The average amplitudes for four surveys are listed in Table 7.5. They are roughly in the same order.

Table 7.5 Source strength and signal amplitude

Hole #	Event #	Explosives (gram)	Average peak amplitude (voltage)
T1	105	375	1.098
T3	107	375	1.262
T8	110	375	0.428
T10	112	375	0.641

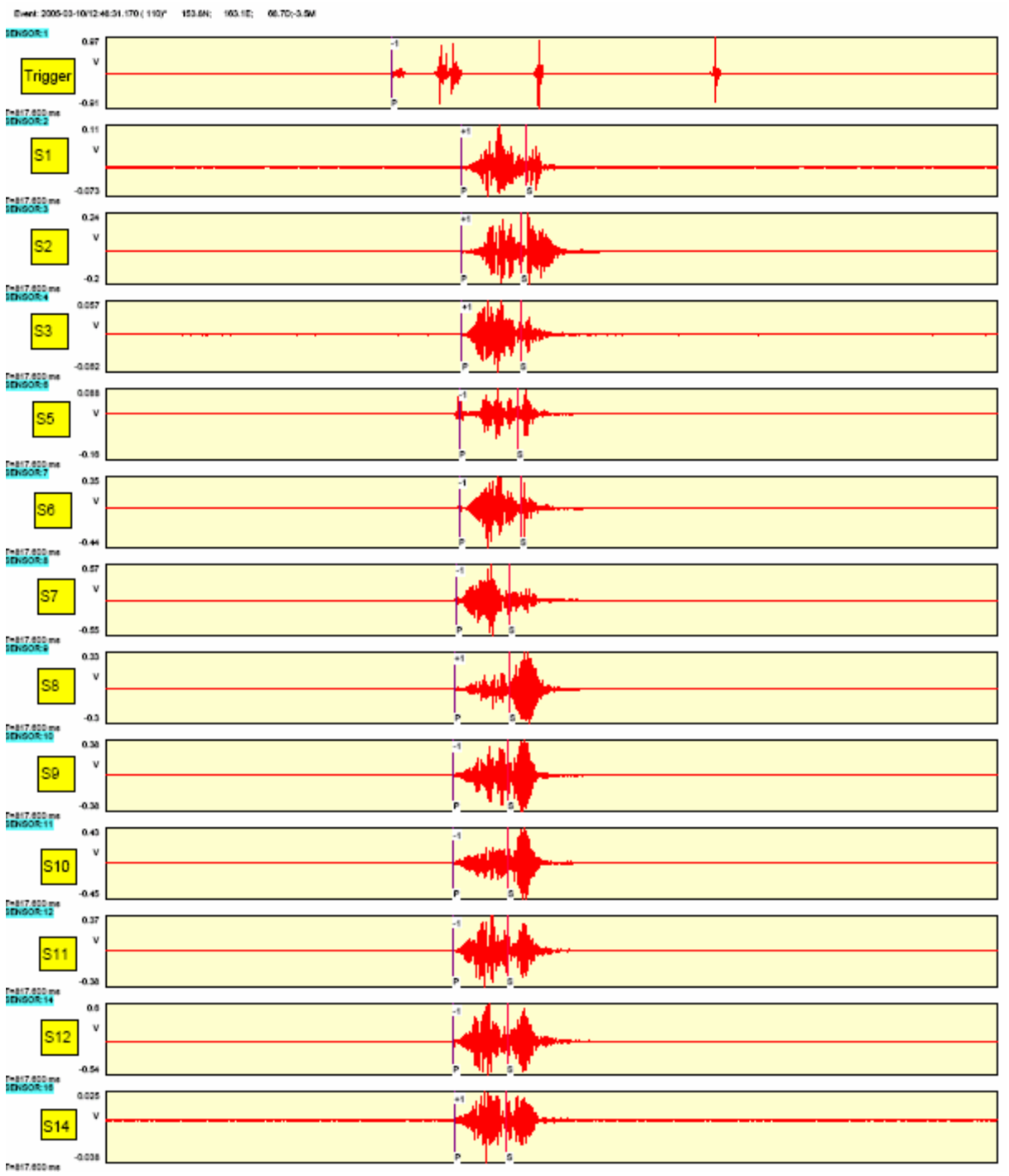

Figure 7.11 Transmission signals for event 110 (display window: 8 – 290 ms; seismic source: 375 gram explosive; average travel distance: 335 ft).

7.3.2 P- and S-wave velocities determined at General Chemical

The P- and S-wave velocities determined from four transmission surveys are listed in Table 7.6. The velocity survey included 48 survey lines from 4 source locations to 12 sensors. The survey distance ranged from 322 ft to 363 ft with an average of 334 ft. Table 7.7 summarizes the distance data. The velocities determined from these four surveys can be considered representative based on both the survey distance and the length of the survey lines.

Table 7.6 P- and S-wave velocities determined from transmission survey at General Chemical

Wave type	Average Distance (ft)	Survey lines	Velocity (ft/s)	Standard deviation (ft/s)	Mean Standard deviation
P (compression)	334	48	16,740	270	1.61%
S (shear)	334	48	8,754	170	1.94%

Table 7.7 Source – receiver distances (ft)

Hole #	S1	S2	S3	S5	S6	S7	S8	S9	S10	S11	S12	S14
T1	322.1	322.1	322.0	322.5	322.8	333.2	333.8	337.0	337.7	341.4	342.2	347.2
T3	322.8	322.7	322.0	321.8	322.0	329.3	329.8	332.5	333.1	336.3	337.0	341.4
T8	356.7	355.9	350.8	345.3	344.7	326.8	326.5	324.4	324.2	322.6	322.6	321.5
T10	363.8	363.0	357.4	351.4	350.8	330.1	329.7	327.0	326.7	324.5	324.4	322.6

* T# and S# denote blasting hole and sensor numbers, respectively.

Both triggering time and signal arrival times were recorded accurately. The reading errors for P- and S-wave arrivals are in general less than 0.1 ms and 0.2 ms, respectively. The P- and S-wave travel times determined from the recorded waveforms are tabulated in Tables 7.8 and 7.9.

Table 7.8 P-wave travel time for individual ray paths (ms)*

Event No.	Hole #	S1	S2	S3	S5	S6	S7	S8	S9	S10	S11	S12	S14
105	T1	19.2	19.2	19.0	19.2	19.1	19.6	19.3	19.4	19.5	19.5	19.7	21.2
107	T3	20.0	19.8	19.8	19.7	19.7	20.0	19.7	19.9	19.9	20.0	20.0	20.5
110	T8	22.1	22.1	22.5	21.6	21.5	20.7	20.1	19.8	19.8	19.7	19.7	20.1
112	T10	20.9	21.4	21.1	20.7	20.6	19.0	19.0	18.6	18.6	18.6	18.6	18.7

* Reading error < 0.1 ms

Table 7.9 S-wave travel time for individual ray paths (ms)*

Event No.	Hole #	S1	S2	S3	S5	S6	S7	S8	S9	S10	S11	S12	S14
105	T1	37.4	37.4	37.0	37.0	36.6	38.4	37.3	37.1	37.2	38.0	38.1	40.3
107	T3	37.7	37.8	38.2	38.6	37.4	37.0	37.4	37.7	37.3	37.7	37.9	38.7
110	T8	43.0	41.2	41.0	40.0	41.0	37.3	37.5	37.0	37.0	36.8	36.8	36.6
112	T10	42.3	41.5	40.5	39.7	40.1	36.8	36.8	36.9	36.2	36.5	36.9	37.2

* Reading error < 0.2 ms

The P- and S-wave velocities calculated from the transmission survey at General Chemical are presented in Tables 7.10 and 7.11. The average P- and S-wave velocities are 16,740 ft/s and 8,754 ft/s, respectively. The mean standard deviations (standard deviation/mean) for P- and S-wave velocities are only 1.6% and 1.9%, respectively.

7.3.3 A comparison study of the velocities determined from GC, FMC and Penn State Laboratory

Both in-situ and laboratory methods were utilized for determining the P- and S- wave velocities in trona and the surrounding roof and floor. There are two important conclusions: 1) the velocities in trona are much higher than those in roof and floor (Figure 7.12), and 2) P-and S-wave velocities in trona measured at FMC, General Chemical and the Rock Mechanics Laboratory of Penn State are consistent (Figure 7.13). For instance, the difference of the P- wave velocities measured from two field sites and the Penn State laboratory is only 67 ft/s, or 0.3%.

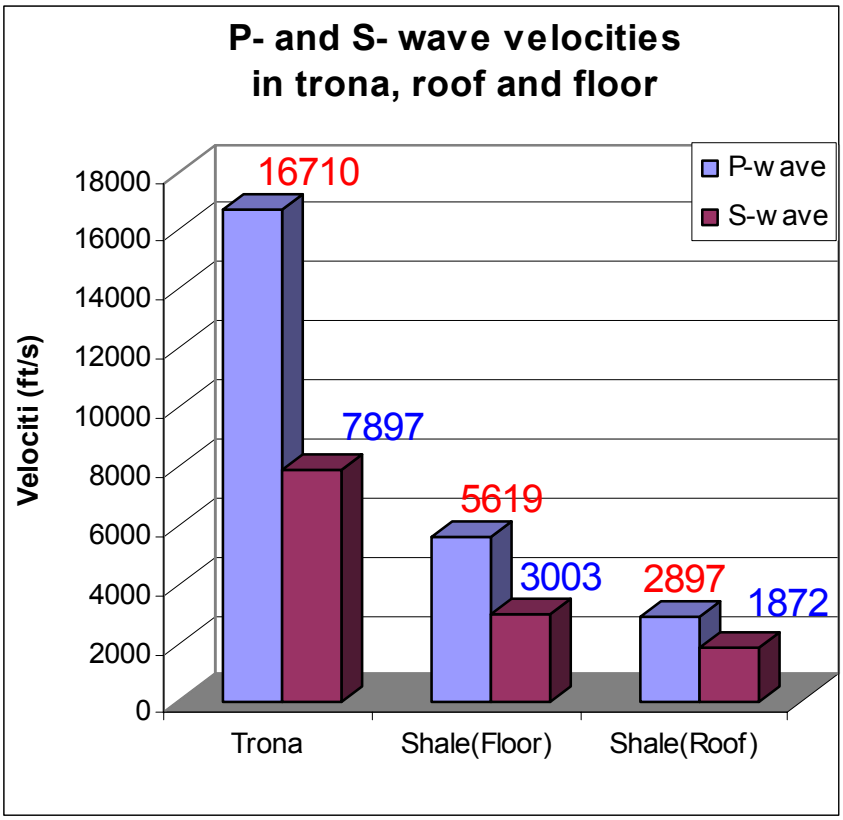

Figure 7.12 P- and S-wave velocities in trona, roof and floor.

Table 7.10 P-wave velocity along individual ray paths for General Chemical (ft/s)

Hole #	S1	S2	S3	S5	S6	S7	S8	S9	S10	S11	S12	S14	mean	Standard deviation
T1	16776.5	16778.4	16948.1	16798.3	16902.4	16999.1	17294.3	17372.1	17317.5	17507.0	17371.9	16376.2	17036.8	336.6
T3	16140.3	16300.1	16263.4	16336.7	16347.3	16466.0	16742.5	16709.9	16739.4	16814.4	16852.3	16654.3	16530.5	247.2
T8	16138.8	16102.8	15589.0	15986.3	16034.3	15786.4	16243.1	16383.6	16373.1	16375.7	16374.6	15993.7	16115.1	254.7
T10	17408.2	16960.9	16938.8	16977.1	17028.1	17371.4	17351.0	17581.3	17565.0	17448.6	17442.1	17253.0	17277.1	239.4
Total average													16740	269.5

Table 7.11 S-wave velocity along individual ray paths for General Chemical (ft/s)

Hole #	S1	S2	S3	S5	S6	S7	S8	S9	S10	S11	S12	S14	mean	Standard deviation
T1	8612.6	8613.5	8703.1	8717.0	8820.6	8676.6	8948.5	9084.1	9077.7	8983.8	8982.3	8614.8	8819.6	185.5
T3	8562.5	8538.1	8429.7	8337.7	8610.8	8900.5	8818.9	8820.3	8930.7	8920.1	8893.0	8822.1	8715.4	208.3
T8	8294.6	8637.7	8554.9	8632.6	8408.2	8760.8	8706.3	8767.4	8761.8	8766.4	8765.7	8783.4	8653.3	159.7
T10	8601.2	8746.1	8824.9	8852.0	8747.6	8968.9	8958.4	8862.1	9025.1	8891.6	8792.0	8672.9	8828.6	124.9
Total average													8754.2	170

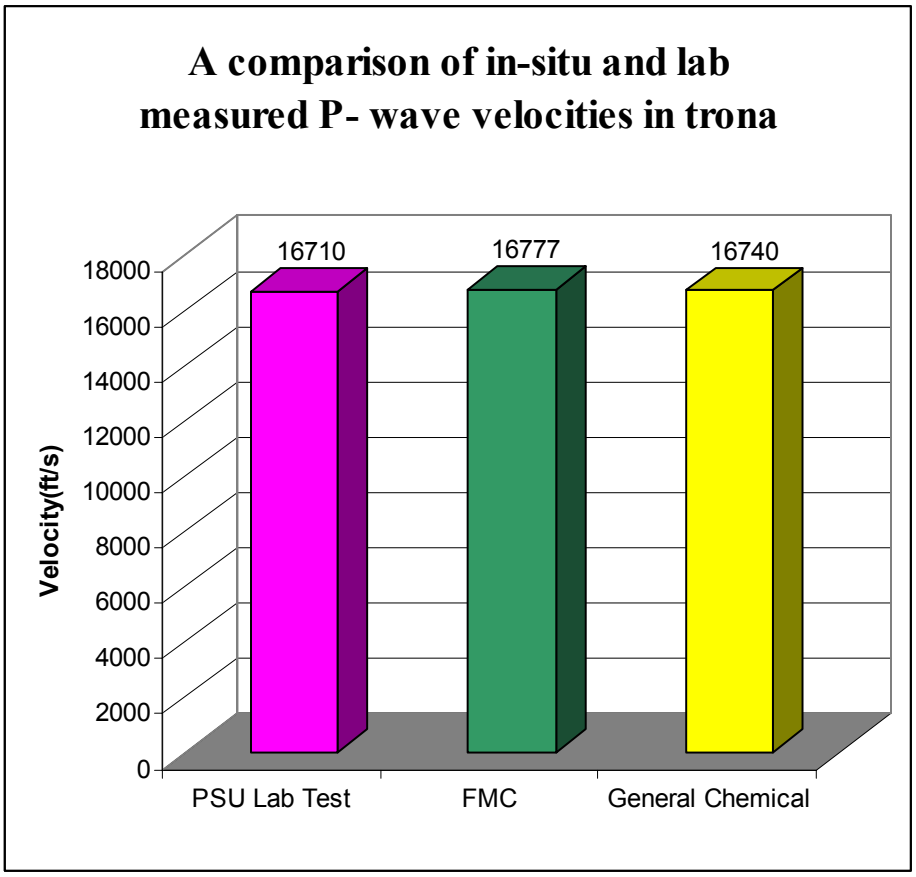

Figure 7.13 A comparison of in-situ and laboratory measured P-wave velocities in trona

7.4 Reflection survey at General Chemical

The reflection survey included eight individual surveys (blasting events). The explosives used for the surveys ranged from 125 gram to 375 gram. The amount of the explosives used and the associated event number for these surveys are listed in Table 7.12.

Table 7.12 A summary of the reflection surveys at General Chemical

Hole #	Explosive (g)	Event #
R6	125	173
R10	125	168
R12	250	165
R15	250	155
R18	250	148
R20	375	145
R22	375	124
R24	375	120
RR1	125	201
RR3	125	198
RF3	125	180

Three types of reflected signals were identified, which are reflected P-waves, reflected S-waves, and reflected S-waves due to mode conversion (P-waves converted to S-waves at the boundary). All reflected signals from the "void" boundary exhibit very high frequencies with a typical range of 2500 – 3000 Hz. Signals with 2500 Hz are most typical.

7.4.1 Case study: event 168

Event 168 refers the reflection survey related to seismic source R10. The relative location of R10 and the sensors as well as the corresponding ray paths for this event is shown by Figure 7.14.

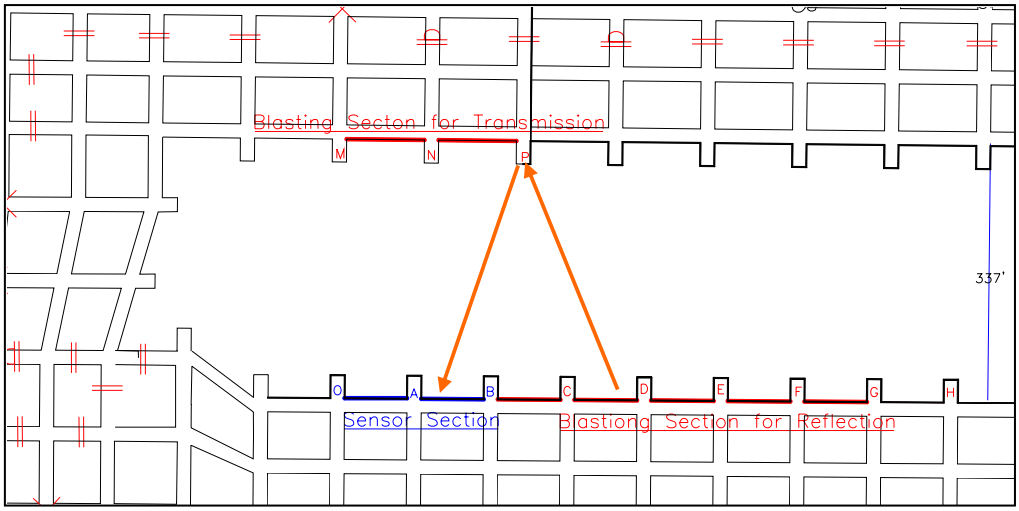

Figure 7.14 Test setup for event 168.

The waveforms of the event 168 are shown in Figure 7.15, where the arrivals of the reflected waves form a clear trend. Figure 7.16 is a close-up of the reflected arrivals. All these reflected signals exhibit very similar characters, which are converted S-waves (converted from P- to S-waves at the boundary). The dominant frequency is almost identical for all the reflected signals, which is 2500 Hz. The arrival readings are given in the following table.

Table 7.13 Reflected S wave arrival times (ms)

Sensor #	S1	S2	S3	S5	S6	S7	S8	S9	S10	S11	S12	S14
Arrival time (ms)						159.4		157.7	157.6	156.7	156.4	155.6

* Triggering time: 100.1ms

The ellipses calculated based on the travel times given in the above table are plotted in Figure 7.17. It is evident from the figure that these ellipses delineated the void with a good accuracy.

Parameters of ellipses associated with event 168 are given in Table 7.14

Table 3. 10 Parameters of ellipses associated with event 168

Source*	Sensor**	Travel time (ms)	Travel distance (ft)	Half of foci distance (ft)	Half of major axis (ft)	Half of minor axis (ft)
R10	S7	59.3	755.9	114.2	378.0	360.3
	S9	57.6	734.2	107.2	367.1	351.1
	S10	57.5	732.9	106.2	366.5	350.7
	S11	56.6	721.5	100.2	360.8	346.6
	S12	56.3	717.6	99.2	358.8	344.8
	S14	55.5	707.4	92.2	353.7	341.5

* See Table 7.3 for source coordinates

** See Table 7.1 for sensor coordinates

*** Velocity: for P- and S-wave velocities are 16740 ft/s and 8754 ft/s

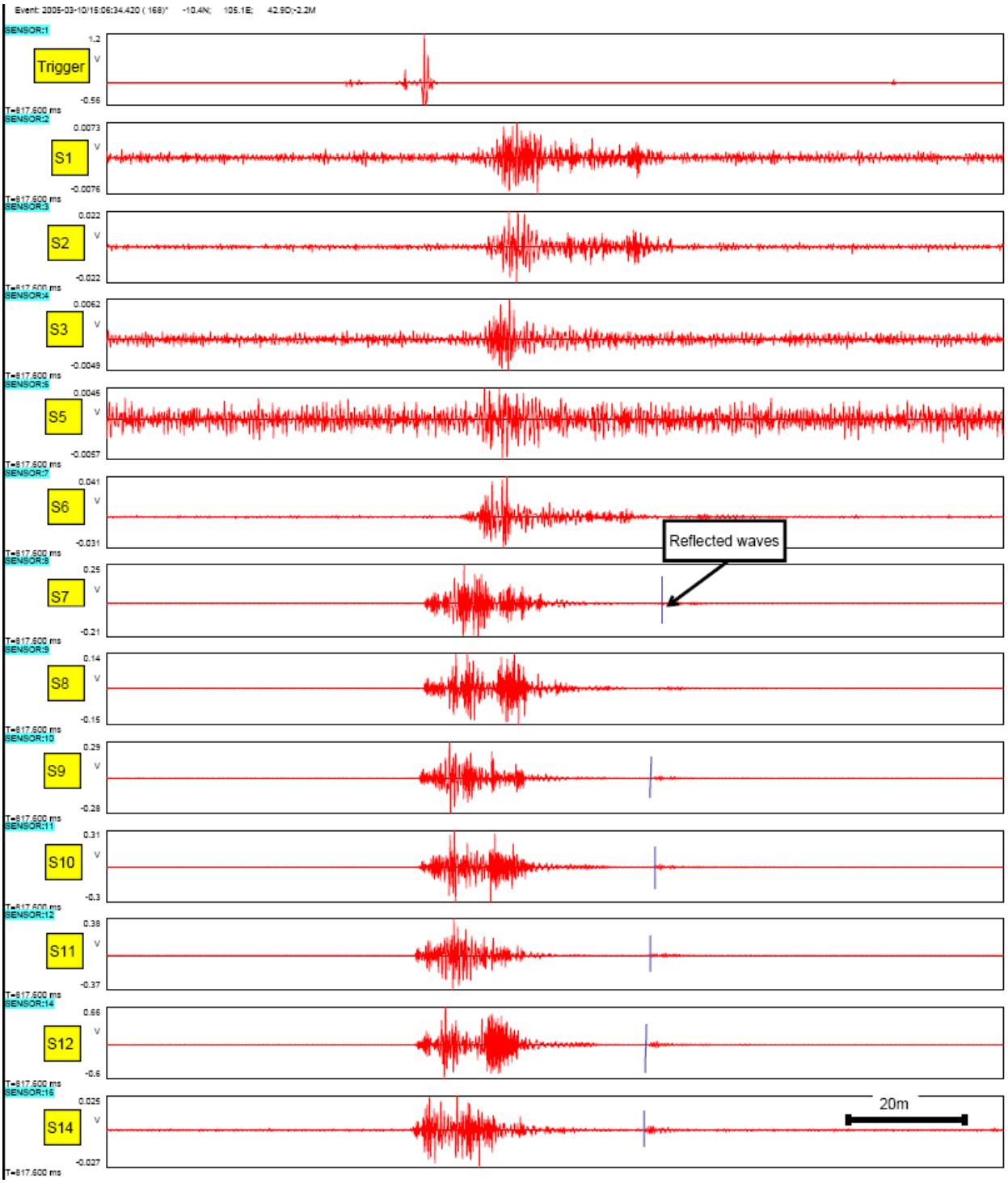

Figure 7.15 Waveforms of the event 168 where the arrivals of the reflected waves form a clear trend (display window: 56 - 220 ms).

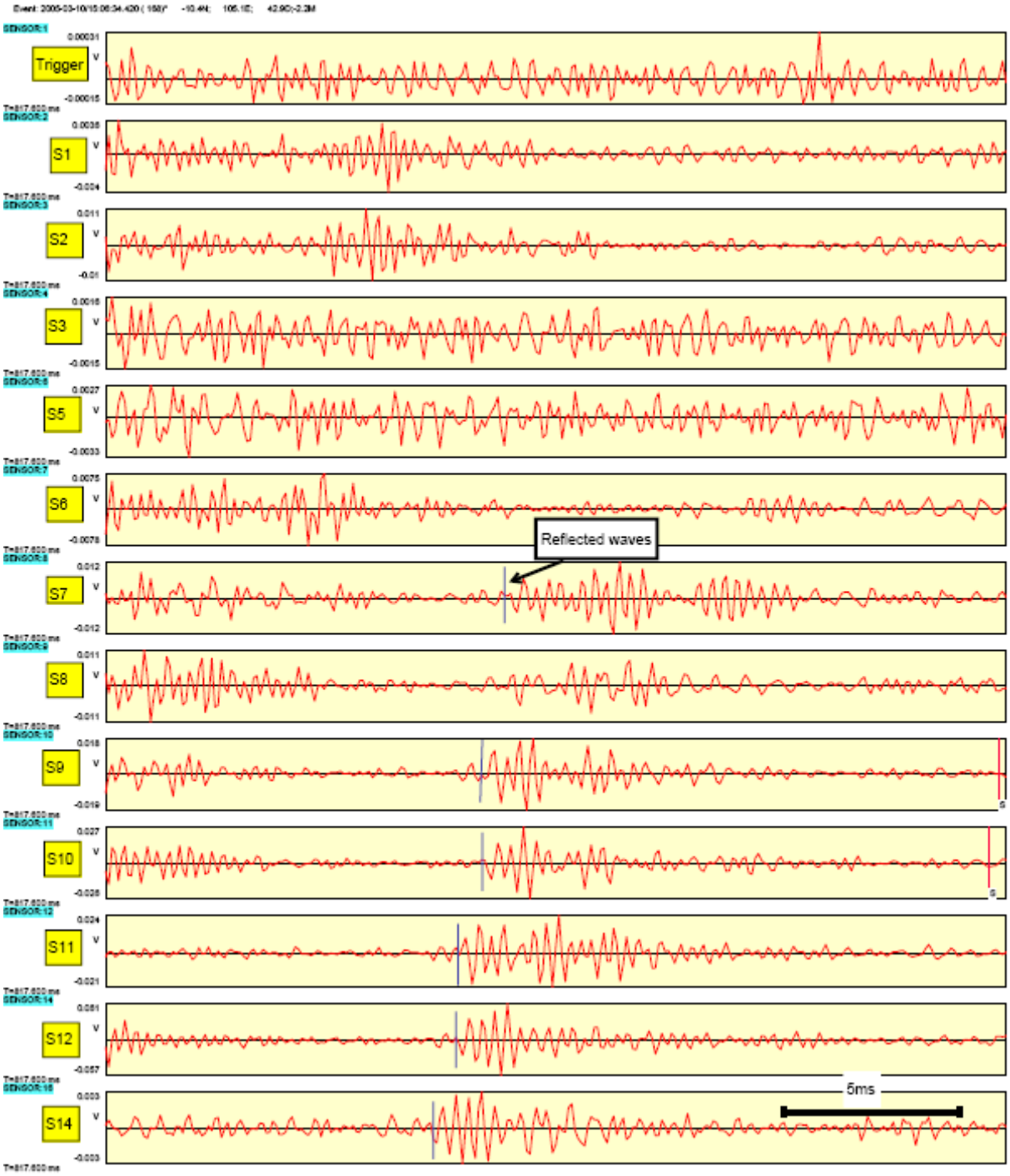

Figure 7.16 close-up of the reflected arrivals in event 168 (display window: 145 - 172 ms).

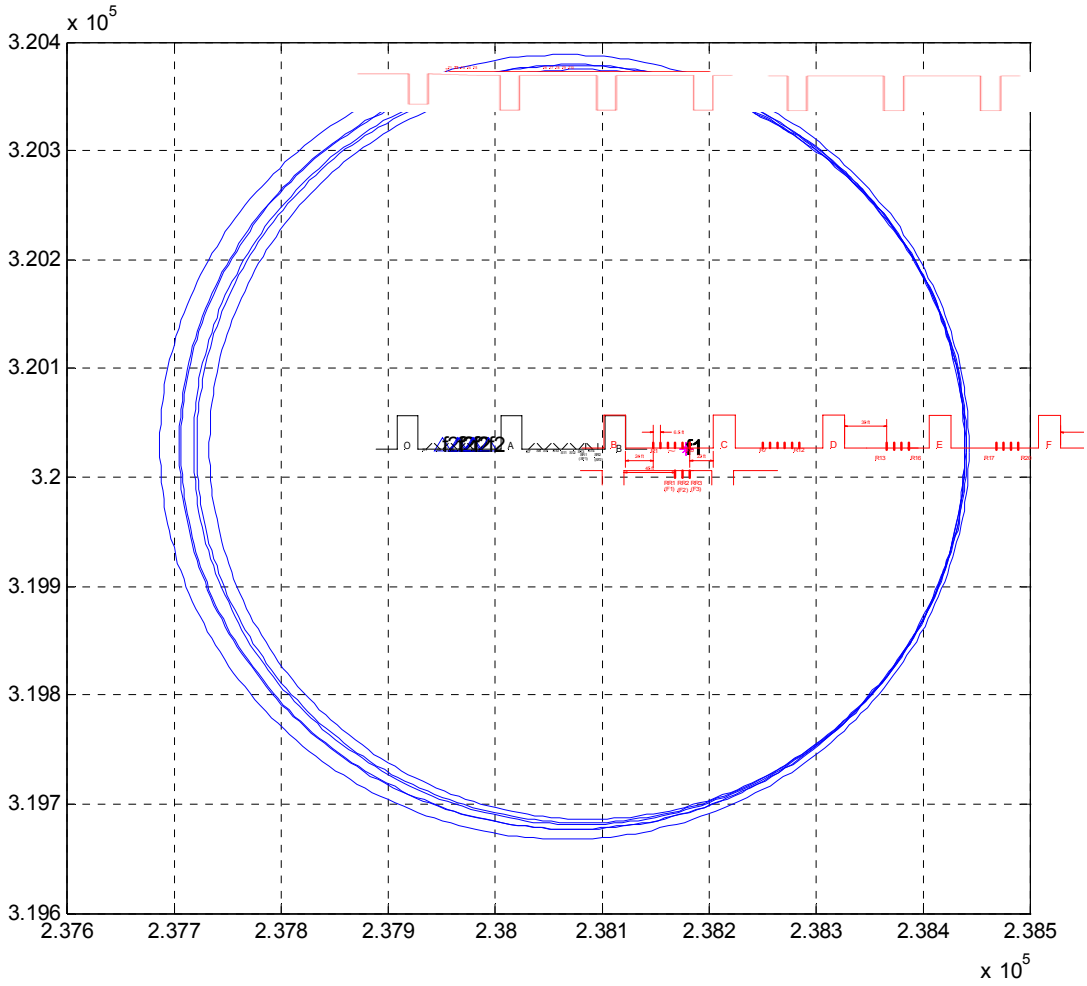

Figure 7.17 Void mapping with the ellipses associated with event 168 at General Chemical testing site. The void boundary is represented by a short red line. The locations of the sensors and the source as well as the associated ray paths are illustrated in Figure 7.14.

7.4.2 Void mapping

The result of void mapping is given in Figure 7.18. The P- and S-wave velocities used for plotting are 16740 ft/s and 8754 ft/s, respectively. It is known that, for the elliptical method, the void is delineated by the common tangent line of the ellipses. In this case, it coincides with the natural pillar line.

The ellipses plotted here represent the travel time information of three types of reflected signals: P-wave, S-wave, and S-wave due to mode conversion. The mapping error is estimated ±10 ft

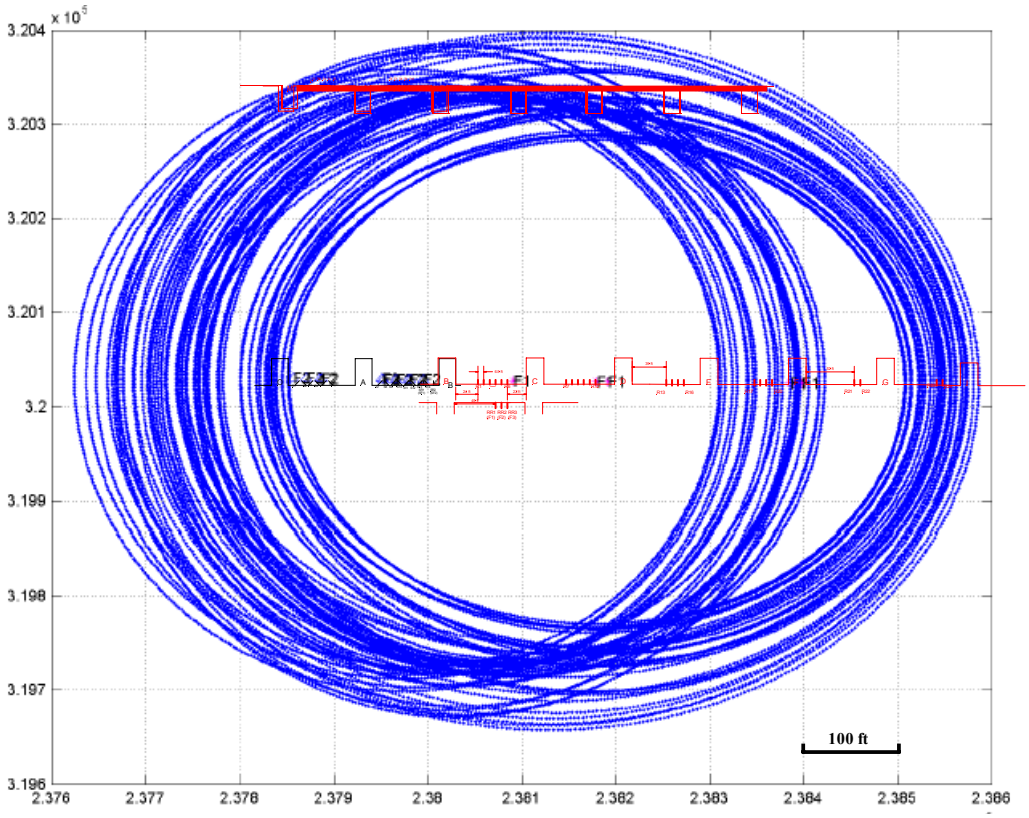

Figure 7.18 Void detection with the elliptical mapping method at General Chemical.

7.5 Summary of the Field test at General Chemical

The test at General Chemical was the second one associated with the trona mines in Wyoming. General Chemical and FMC mine the same trona seam side by side and, therefore, their general conditions are very similar. The testing site at General Chemical was a 340 ft wide pillar, which was utilized for both transmission and reflection surveys. The main difference between this site and Site I at FMC is the void condition. The void at Site I, FMC is water filled, while the site at General Chemical is air filled, or in a “dry” condition.

The testing result from General Chemical is very similar to that from FMC in terms of the velocity properties of trona, the characteristics of transmitted and reflected signals, and the mapping accuracy. We could not detect any differences for the signals reflected from water filled and air filled voids.

8. Demonstration at FMC Trona Mine

8.1 Introduction

On August 23 the Penn State project team demonstrated the ISS based void detection technique in trona mine conditions to MSHA and the trona industry in 349 West Development section of FMC's mine (Figure 8.1).

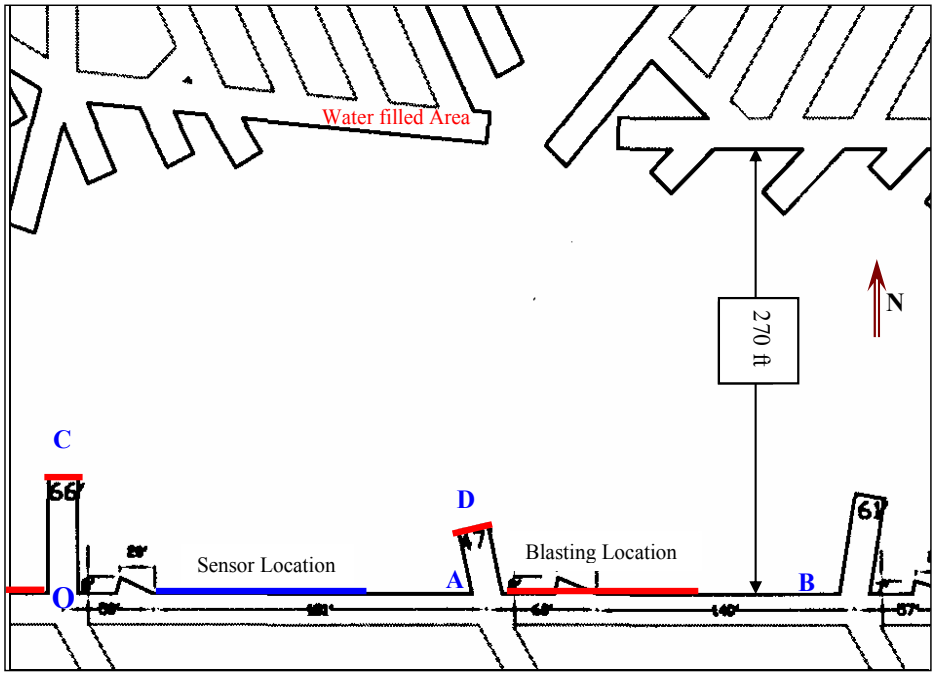

Figure 8.1 Demonstration site: 349 West Development, FMC.

8.1.1 Demonstration objectives

There were two basic objectives for the demonstration: 1) to show that the ISS based void detection technique utilizing high frequency body waves is able to detect a water-filled void up to 300 ft from the active mining area, which is the actual condition at the demonstration site, and 2) to show the potential of the technique as a reliable and practical tool for detecting the degradation barrier pillars due to water-induced dissolution, a major concern of the trona industry.

8.1.2 Testing site selection

The site used for the demonstration was 349 West Development, FMC. This same site was used by Penn State for the reflection survey in March, 2005. This site was selected for a number of reasons. First, the site was water filled. Void detection under water-filled conditions was a primary stipulation of both MSHA and the trona industry for any void detection studies and, as such, was one of the required demonstration conditions by MSHA.

The second consideration was the size of the pillar. The size of 300 ft used in the demonstration, was representative as it is typical of pillar sizes being used by the industry. This size, from the general mine safety point of view, is also large enough for the early detection of mine voids.

Third, Penn State would like to use this opportunity to demonstrate the reliability of the technique in terms of the repeatability. If the performance of the technique is repeatable, the test result from the demonstration should be, at least, as good as the one from the test carried out in March at the same site.

The other important advantage of using the same testing site was to allow Penn State to examine the retrievable sensor installation technique. The importance of the retrievable sensor installation technique is not just an economical consideration, but also a technical one for the trona mining industry. In order to determine the dissolution rate of barrier pillars, it is necessary to survey the pillar width periodically over an extended period of time. In order to have compatible data from these periodic surveys over a long time period, it is important to minimize the survey bias due to operational reasons. Hence, retrievable sensor installation is an important aspect of any testing protocol. With the retrievable sensor installation technique, one can place the same sensor at the same location and have the same coupling effect.

8.2 An overview of the demonstration activity

The demonstration included two parts, a technical meeting at Shaft No. 8 of FMC and a field demonstration of the ISS based void detection technique at the testing site of 349 West Development.

This section gives an overview of these two activities. The details of the field test and the associated data analysis are presented in section 8.3. The last part of this chapter, section 8.4, is a photo-essay presentation of the Demonstration, which shows a number of main field operations of the ISS based void detection technique.

8.2.1 Attendees of the demonstration

The attendees of the demonstration included MSHA officials, representatives from the trona industry and researchers from Penn State (Table 8.1).

Table 8.1 Attendees of the demonstration of ISS based void detection technique

Name	Affiliation	Title
Dai Choi	MSHA	Contracting Officer's Technical Representative (COTR)
Steve Pilling	MSHA	Field Office Supervisor, Rocky Mountain District
John Norgord	FMC	Sr. Engineering Associate
Christopher Pritchard	FMC	Sr. Mine Engineer
Rick Stablo	FMC	Mine Engineer
Ralph Mair	FMC	Certified Shot Firer
Mac Richardson	GC	Supervisor Mine Engineering
Keith Mullins	GC	Mine Safety Supervisor
Maochen Ge	PSU	PI of the project
Andrew Schissler	PSU	Co-PI of the project
Hongliang Wang	PSU	Graduate research assistant
Jin Wang	PSU	Graduate research assistant

8.2.2 Technical meeting

Prior to the field demonstration, a technical meeting was held. During the meeting, Dr. Schissler first thanked FMC and the other industrial partners of Penn State for their support. He also thanked MSHA for its support and guidance. Dr. Ge then made a technical presentation of the status of the project.

Dr. Ge first briefly discussed the major theoretical and technical development work carried out by Penn State during the past year, which include 1)theory of experimental design – angled sensor holes, 2) theory of experimental design – sensitivity analysis, 3) theory of void mapping – elliptical void location, 4) theory of signal analysis – wavelet analysis of reflected signals, 5) retrievable sensor installation technique for 1-D sensors, 6) laboratory velocity measurement, 7) non-explosive seismic sources, and 8) retrievable sensor installation technique for 3-D sensors. The importance of this development work is that it provided the basic foundation for the field portion of the project.

Dr. Ge emphasized that the most important achievement was the development of the retrievable sensor installation technique which allowed for acquiring the high frequency signals. Without this technique, the ISS based void detection would be impossible for trona mine condition.

Following the general discussion, Dr. Ge specifically discussed the tests carried out at FMC and General Chemical in March, 2005. His main conclusions are: 1) consistent and accurate P- and S-wave velocities in trona constitute a very favorable condition for reliable void detection, 2) all reflected signals captured are associated with very high frequencies in the range of 3000 – 5000 Hz, a precondition for high resolution surveys, 3) three types of reflected signals were observed under both water filled and dry conditions, which are P-wave, S-wave and S-wave due to mode conversion, and the use of three types of reflected signals significantly increases the physical data which can be used for void detection, 4) the elliptical mapping method provides an efficient means to use all available data simultaneously, 5) the mapping error for void detection in trona is about ± 10 ft for pillars up to 340 ft wide based on the actual survey results from FMC and

General Chemical, and 6) using high frequency body waves to detect voids, a specialized ISS technique for the trona mine condition, appears to be a reliable and cost-efficient method for long-term monitoring of barrier pillars in trona mines.

In the meeting, Dr. Ge also discussed the experimental layout and the demonstration items.

After the presentation, the participants at the meeting had an enthusiastic discussion of the application of the ISS based void detection technique for trona mines. Dr. Ge also answered various questions raised by the participants. .

To make the demonstration most productive, Penn State prepared two posters and a brochure. The two posters were used to present the major testing results carried out at FMC and General Chemical in March of 2005. A brochure was distributed to the participants, which includes the background information of MSHA's void detection project, an overall review of the project progress by Penn State, testing result from the trona mines, and the demonstration program.

8.2.3 Field demonstration

The field demonstration was held at 349 West Development from 10:00 am to 2:00 pm.

The process of the demonstration was very similar to the regular test. In fact, it was merely another regular test for Penn State from the data collection point of view. During the demonstration, a total of ten reflection surveys (ten blasts) were carried out.

The demonstration items at the site included

- site inspection of the layout of sensor holes and blasting holes,
- site inspection of the setup of the data acquisition system,
- sensor installation in the previously drilled holes (sensor anchors already at the drill hole bottoms, installed in March of 2005),
- sensor installation in newly drilled holes,
- blasting preparation,
- real-time data acquisition,
- inspecting blasting holes after blasting,
- sensor retrieval operations, and
- closing the field station.

8.3 Field demonstration at Site A, FMC

The field demonstration was held at Site A, 349 West Development, from 10:00 am to 2:00 pm. Figure 8.2 is a scene of the testing site, where the retrievable sensors were installed and the data acquisition system was set.

Figure 8.2 Underground working station for field demonstration at Site A, FMC.

8.3.1 Site inspection prior to the field demonstration

Site A, which was utilized for the demonstration, was the reflection site used by Penn State five months ago. One of the reasons to use this site was to demonstrate the retrievable sensor installation technique, which allows for the repeated use of the same sensor holes. This technique is a key element for using the permanent station model to monitor the rate of dissolution of trona pillars.

Because of this consideration, it was decided to use the sensor holes prepared in March if at all possible. A reconnaissance trip was arranged for the site inspection prior to the field demonstration. On August 5, 2005, Mr. Wang, a research assistant for the project, visited the site, accompanied by a mine engineer. His specific task was to assess the conditions of 14 sensors holes used in the first field test and 7 blasting holes left after the first test and whether these holes could be reused.

Each drillhole was evaluated in terms of water, dust, and shape. In general all the drillholes were in excellent condition and dry. Only sensor hole S5 contained a trace of moisture, possibly caused by a nearby wet joint (Figure 8.3). Most of the drillholes were clean. Several drillholes had to be cleaned, which should be considered a normal operation and does not pose any problem for reusing these sensor holes.

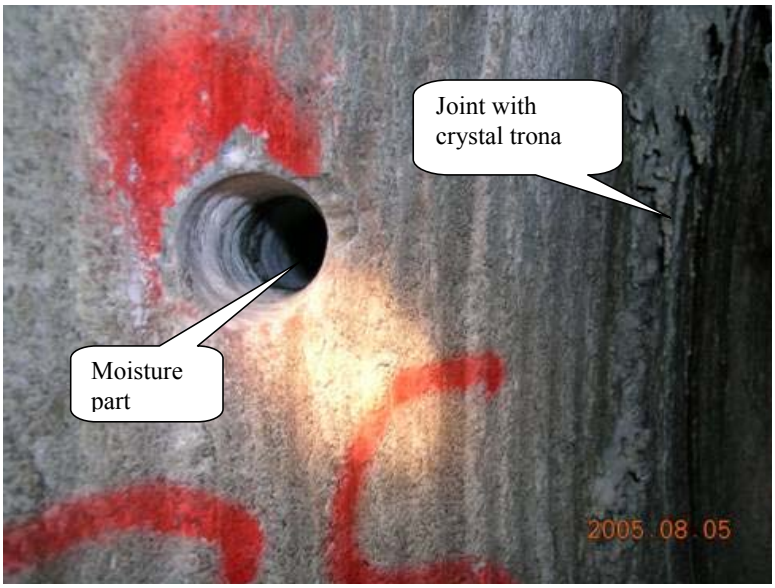

Figure.8.3 A trace of moisture showed in Sensor hole S5.

In addition to the visual inspection, each sensor hole was tested physically. Mr. Wang brought with him a sensor and the sensor installation tool kit. Each sensor hole was tested by installing and then retrieving the sensor (Figure 8.4). The anchorage strength was tested by pulling the sensor with about 50 lbs force. The testing result showed that all sensor anchors were firmly in place and both the sensor installation and retrieving operations were performed with ease. Table 8,2 and Table 8.3 are the recording data sheets used for sensor hole and blasting hole inspection.

Figure 8.4 Retrievable sensor was installed in the sensor hole used five months earlier.

Table 8.2. Data sheet for sensor hole inspection*

Sensor Holes	Water	Dust	Hole Shape	Anchor strength	**Manipulation** (Easy or hard?)	**Remark**
S1	No	Severe	good	good	Not easy	
S2	No	Clean	good	good	Very easy	
S3	No	Clean	good	good	Easy	
S4	No	Severe	ok			Screw buried by dust.
S5	Trace of moisture	Severe	ok	good	Easy	**See Picture.2**
S6	No	Severe	good			Can not see screw
S7	No	Clean	good	good	Very easy	
S8	No	Clean	good	good	OK.	
S9	No	Clean	good	good	Easy	Not used by first test
S10	No	Clean	good	good	Easy	
S11	No	Some	good	good	Very easy	
S12	No	Clean	good	good	Easy	**See picture .1**
S13	No	Severe	good			Anchor not installed before
S14	No	Severe	good			Anchor not installed before

*S1, S4, S5, S6, S13 and S14 need to be cleaned for the demonstration. Using air to clean out the holes should be done with care so that the sensor anchor installed at the borehole bottom is not damaged.

Table 8.3. Data sheet for sensor hole inspection

Blasting Holes	water	dust	shape	remark
R3	No	OK	Good	
R5	No	OK	Good	
R6	No	OK	Good	
R7	No	OK	Good	
R9	No	OK	Good	
R13	No	OK	Good	
R15	No	OK	Good	

8.3.2 Reflection survey design

The experimental setup for the demonstration was similar to the one used by Penn State at the site in March. For the demonstration, three new pairs of sensor holes and 5 new blasting holes were added. The additional sensor holes were prepared for demonstrating how to install retrievable sensors in newly drilled sensor holes. Otherwise, they were not necessary.

The specifications on the sensors, the data acquisition system, and the major operational parameters used for the test are given in Appendix I. The sampling rate and the recording window used for the test are 50,000 samples/second and 0.4 second, respectively.

Sensor section

The sensor section included seven old pairs of angled sensor holes, which were numbered from S1 to S14, and three new pairs of angled sensor holes, which were numbered from S21 to S26. (Figure 8.5). All these angled sensor holes were 7 ft long and 1.75" in diameter. The information related to these sensor holes are given in Table 8.4.

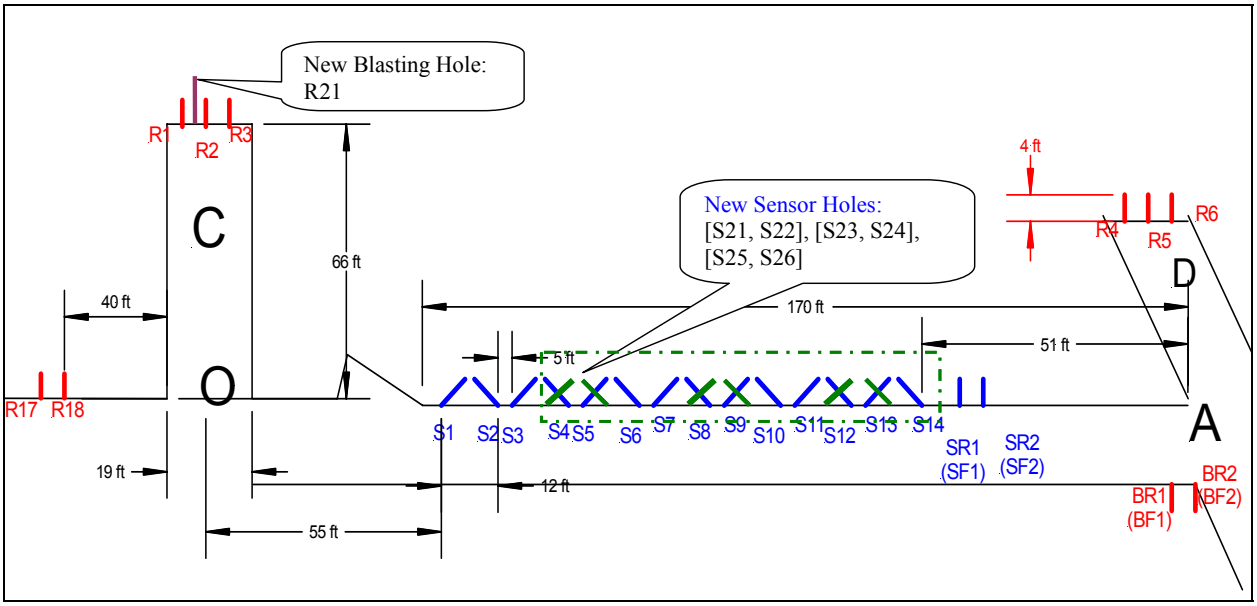

Figure 8.5 Sensor section designed for the reflection survey at site A, FMC.

Table 8.4 Sensor hole information for site A, FMC

Hole #	Channel #	Senor coordinate (ft)	
		East (x)	North (y)
S1	2	56998.26	34894.65
S2	3	57000.26	34894.65
S21	4	57024.4	34894.65
S22	6	57025.23	34894.65
S7	7	57049.26	34894.65
S8	8	57052.32	34894.65
S23	9	57059.15	34894.65
S24	10	57062.24	34894.65
S9	11	57066.62	34894.65
S10	16	57068.64	34894.65
S11	13	57084.01	34894.65
S12	14	57086.32	34894.65
S13	15	57100.44	34894.65
S14	The sensor hole was not used.		

Blasting locations

The blasting hole used for the demonstration included 4 unused blasting holes left from the previous test and 5 newly drilled holes. The four old ones are R3, R5, R13 and R15. The locations or R3 and R5 are shown in Figure 8.5 and R13 and R15 are shown in the figure below. The five newly drilled ones were number from R21 to R25. The location of R21 is shown in Figure 8.5 and the locations for others are shown in the following figure. All blasting holes are 4 ft long and 1.5" in diameter, drilled in the middle of the seam. The coordinate information related to these sensor holes are given in Table 8.5.

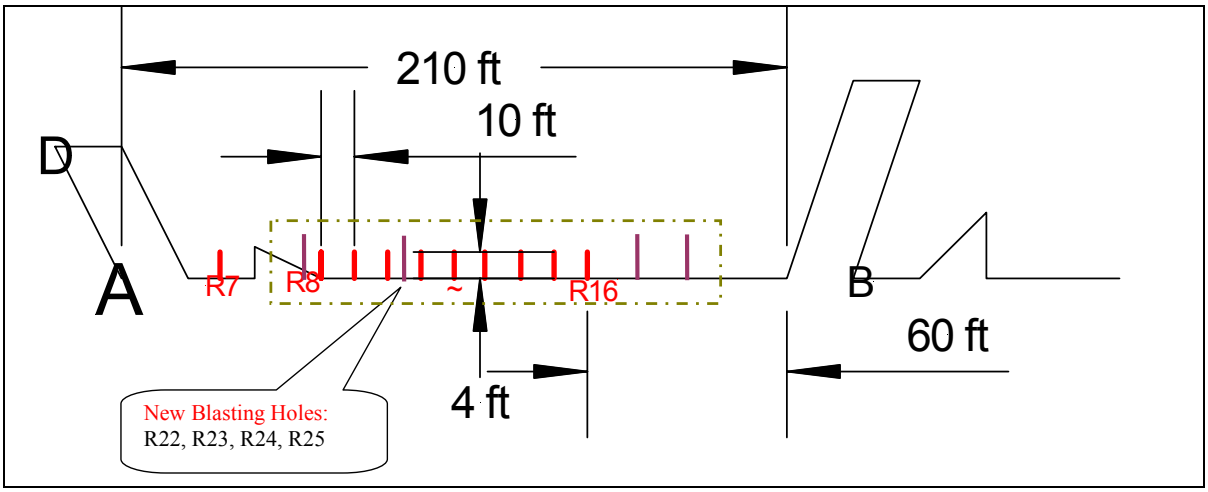

Figure 8.6 The main blasting section for the reflection survey at site A, FMC.

Table 8.5 Blasting hole information for site A, FMC

Hole #	Source coordinate (ft)	
	East (x)	North (y)
R3	56950.12	34959.65
R21	56939.56	34962.65
R25	57280.84	34896.65
R24	57274.87	34896.65
R15	57262.87	34893.65
R13	57250.87	34893.65
R23	57235.87	34896.65
R22	57214.82	34896.65
R5	57134.83	34940.65

8. 3.3 Reflection surveys

The reflection survey included 9 individual surveys (blasting events). The explosives used for the surveys ranged from a single cap to 375 gram/hole. Table 8.6 is a summary of these surveys.

Table 8.6 A summary of the reflection tests at FMC

Hole #	Explosive (g)	Event #
R3	Cap	**4**
R21	125	**10**
R25	375	**12**
R24	250	**16**
R15	250	**19**
R13	250	**30**
R23	250	**35**
R22	250	**37**
R5	250	**43**

In general, the signal quality for the demonstration was further improved. This was due to a number of the technical improvements, such as better ground connection, sound insulation of the sensor holes, and modification of the Sensor Interface Box (SIB).

The reflected signals observed included reflected P-waves, reflected S-waves, and reflected S-waves due to mode conversion (P-waves converted to S-waves at the boundary). All reflected signals from the "void" boundary contain very high frequencies with a typical range of 4,000 – 5,000 Hz. Signals with 5,000 Hz are most typical..

8.3.4 Case study: event 16

Event 16 refers the reflection survey related to seismic source R24, which was located at the right side of the main blasting section. The relative location of R24 and the sensors as well as the corresponding ray paths for this event is shown by Figure 8.7.

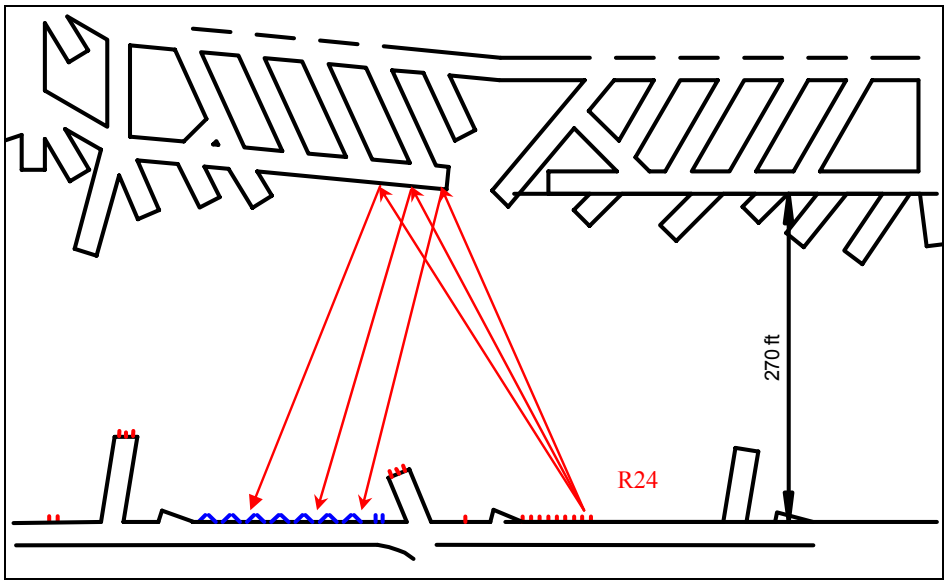

Figure 8.7 Test setup for event 16.

Figure 8.8 and 8.9 shows the arrivals of the reflected P-waves. The readings of the P-wave arrival times are given in the following table. The triggering time for this event is 49.9 ms.

Table 8.7 P wave arrival times (ms)

triggering time (ms)	PC Ch#	ch2	3	4	5	7	8	9	10	11	12	13	14	15	16
	Sensor #	S1	S2	S21	S22	S7	S8	S23	S24	S9	S10	S11	S12	S13	S14
49.9	P-wave					80.05	78.95	78.8	78.2	77.6					

Table 8.8 Parameters of ellipses associated with event 16

Source*	Sensor**	Travel time (ms)	Travel distance (ft)	Half of foci distance (ft)	Half of major axis (ft)	Half of minor axis (ft)
R24	S7	30.15	505.8	112.8	252.9	226.4
R24	S8	29.05	487.4	111.3	243.7	216.8
R24	S23	28.90	484.9	107.9	242.4	217.1
R24	S24	28.30	474.8	106.3	237.4	212.3
R24	S9	27.70	464.7	104.1	232.4	207.7

* See Table 8.5 for source coordinates

** See Table 8.4 for sensor coordinates

*** P-wave velocity: 16777 ft/s

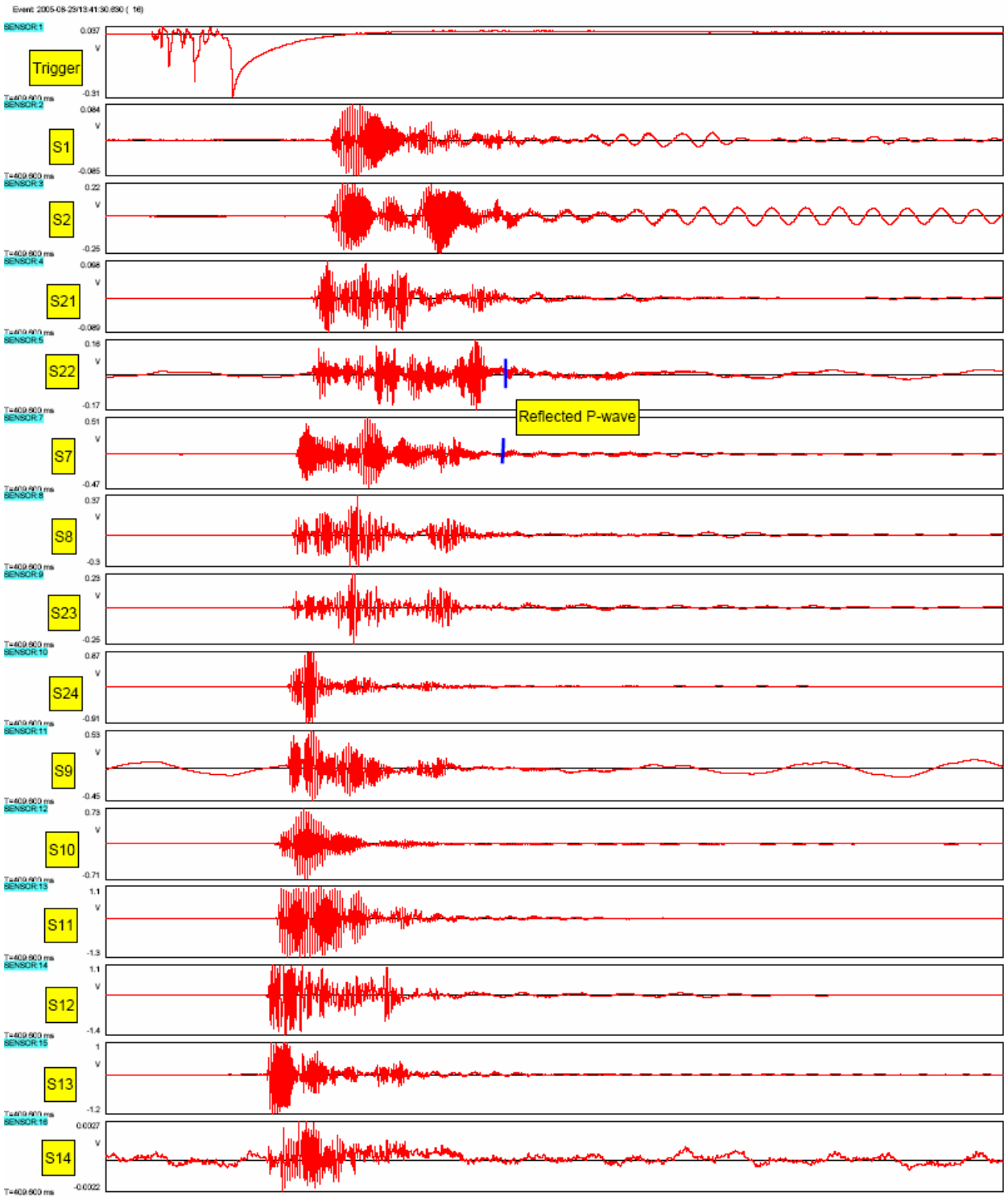

Figure 8.8 The complete waveforms recorded for event 16 showing the arrivals of P-waves (display window: 40-170 ms).

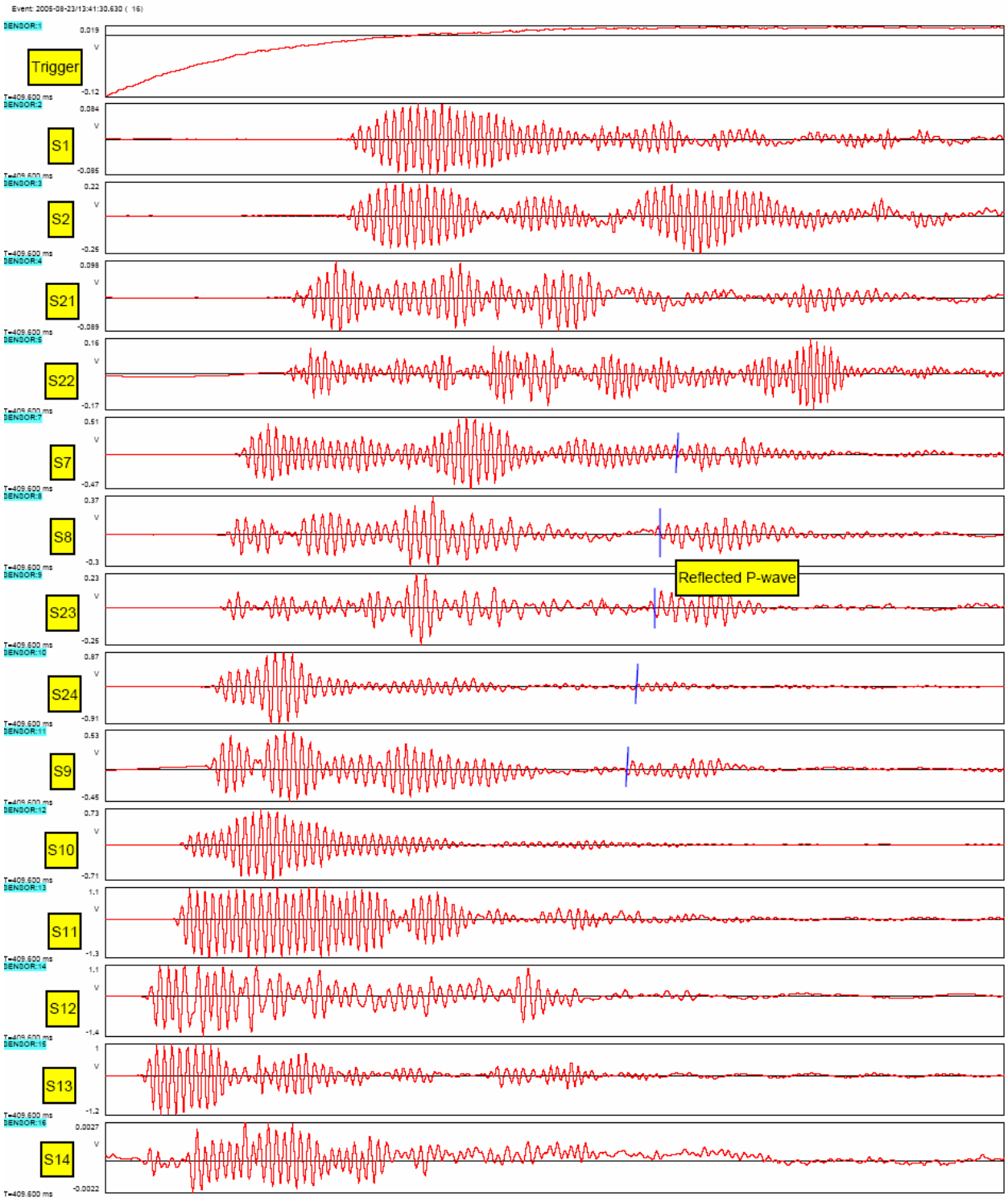

Figure 8.9 Event 16 showing the arrivals of the reflected P-waves (display window: 60-95 ms).

8.3.5 Case study: event 30

Event 30 refers the reflection survey related to seismic source R13, which is located at the middle of the main blasting location. The relative position of R13 and the sensors as well as the reflection ray paths which would be expected for this event is shown by Figure 8.10.

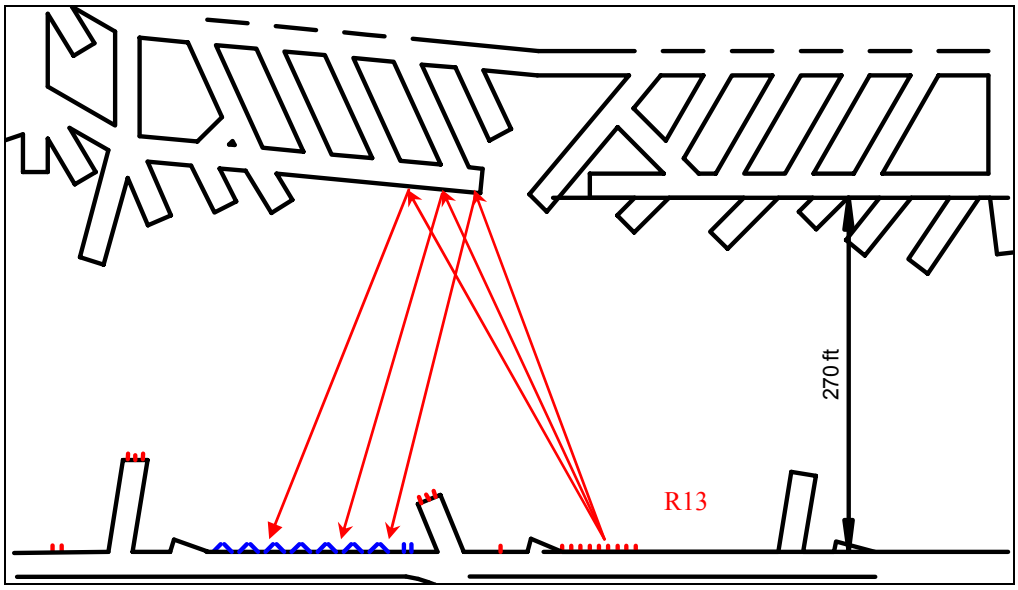

Figure 8.10 Test setup for event 30 and the ray paths from top reflection.

The waveforms recorded for this survey event are given in Figures 8.11 and 8.12. Figure 8.12 is a more detailed display of the event. The purpose of Figure 8.12 is to show two trends, reflected P-waves and reflected S-waves. The trend of the reflected P-waves is not difficult to understand. These reflected P-waves have the ray paths shown in Figure 8. 10. The one that makes this event interesting is the reflected S-waves, the second trend shown in Figure 8.12. Figure 8.13 is a close-up of these reflected S-waves. From the revised arrival sequence, it is known that these waves were reflected from a very different location. Based on the arrival time sequence between signal traces for known receiver locations and the arrival time readings, it was determined that these waves were reflected from the left top reflector as shown by Figure 8.14. The actual readings of these arrivals are tabulated in the following table. The triggering time for this event is 50.00 ms.

Table 8.9 Reflected S wave arrival times (ms)

PC CH#	ch2	3	4	5	7	8	9	10	11	12	13
Sensor #	S1	S2	S21	S22	S7	S8	S23	S24	S9	S10	S11
S-wave			**114.8**	**114.9**	**115.1**	**115.2**	**115.4**	**115.5**	**115.8**	**115.9**	**116.4**

* trigger time: 50 ms.

The ellipses calculated based on the travel times given in the above table are plotted in Figure 8.15. It is evident from the figure that these ellipses delineated the void with a good accuracy.

Table 8.10 Parameters of ellipses associated with event 30

Source*	Sensor**	Travel time (ms)	Travel distance (ft)	Half of foci distance (ft)	Half of major axis (ft)	Half of minor axis (ft)
R13	S21	64.8	555.5	113.2	277.7	253.6
R13	S22	64.9	556.3	112.8	278.2	254.3
R13	S7	65.1	558.0	100.8	279.0	260.2
R13	S8	65.2	558.9	99.3	279.4	261.2
R13	S23	65.4	560.6	95.9	280.3	263.4
R13	S24	65.5	561.5	94.3	280.7	264.4
R13	S9	65.8	564.0	92.1	282.0	266.5
R13	S10	65.9	564.9	91.1	282.4	267.3
R13	S11	66.4	569.2	83.4	284.6	272.1

* See Table8.5 for source coordinates

** See Table 8.4 for sensor coordinates

*** S-wave velocity: 8572 ft/s

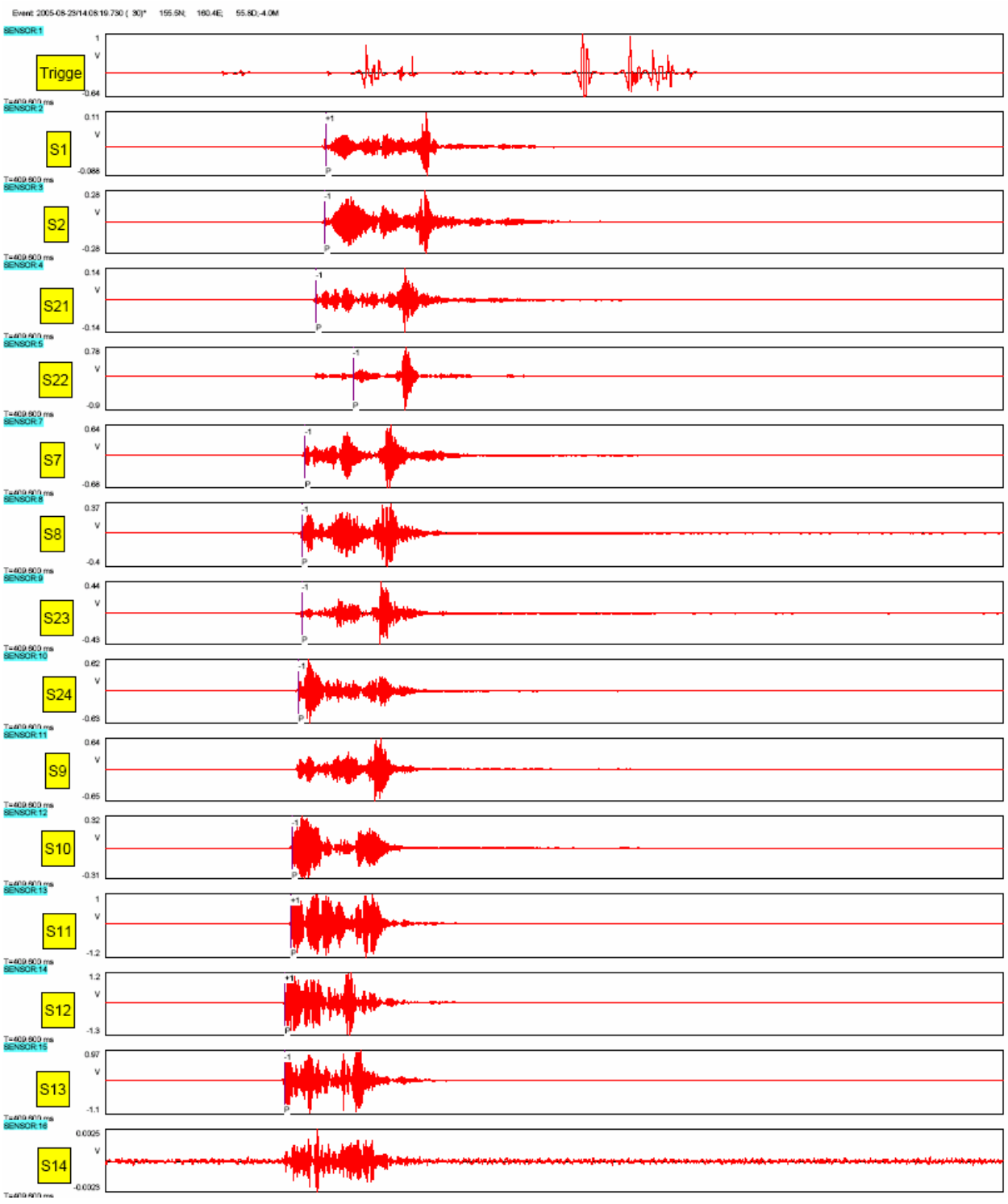

Figure 8.11 The complete waveforms recorded for event 30 (displaying window: 30-180 ms).

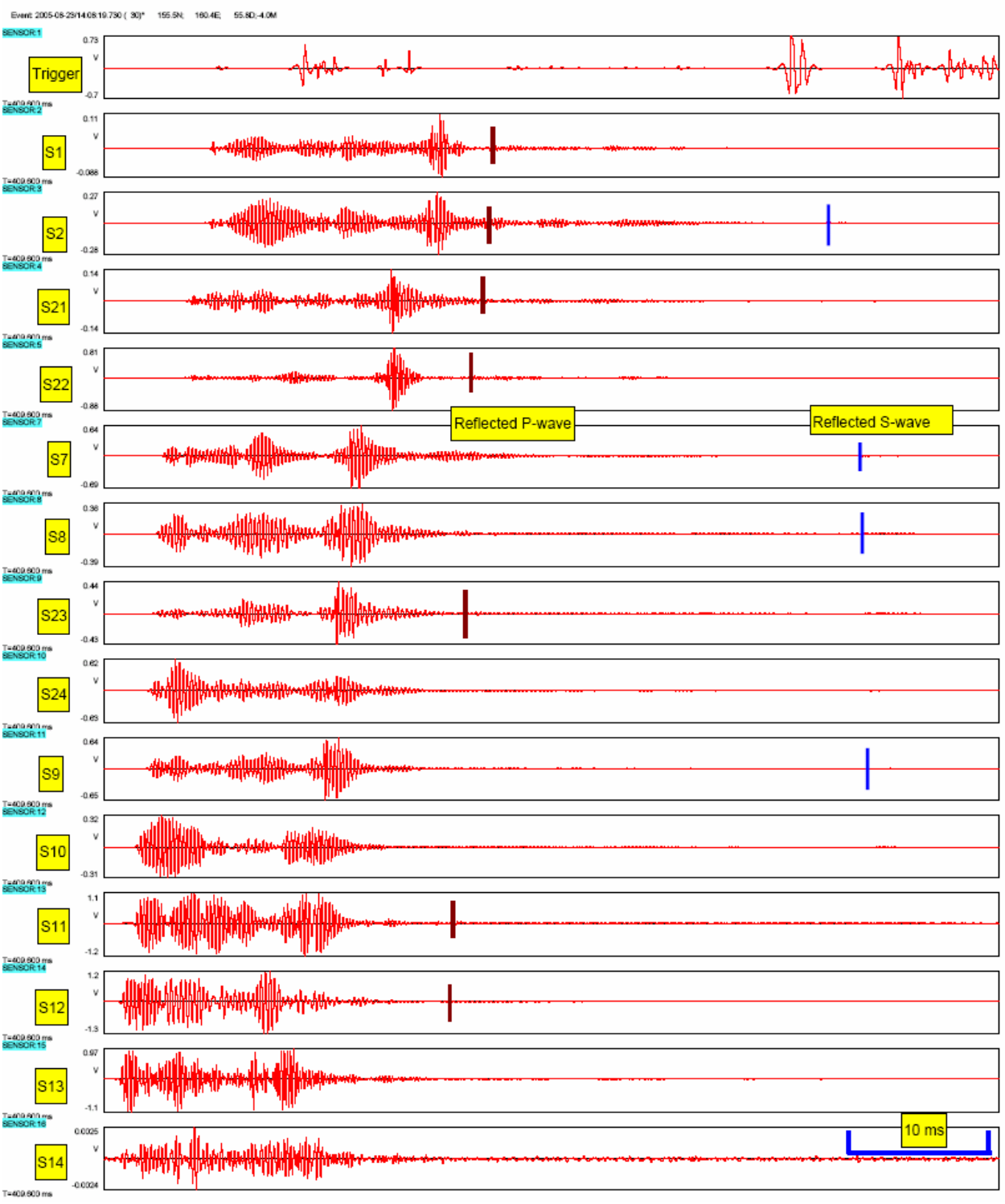

Figure 8.12 The waveforms of event 30 showing two reflected wave trends (display window: 60 -125 ms).

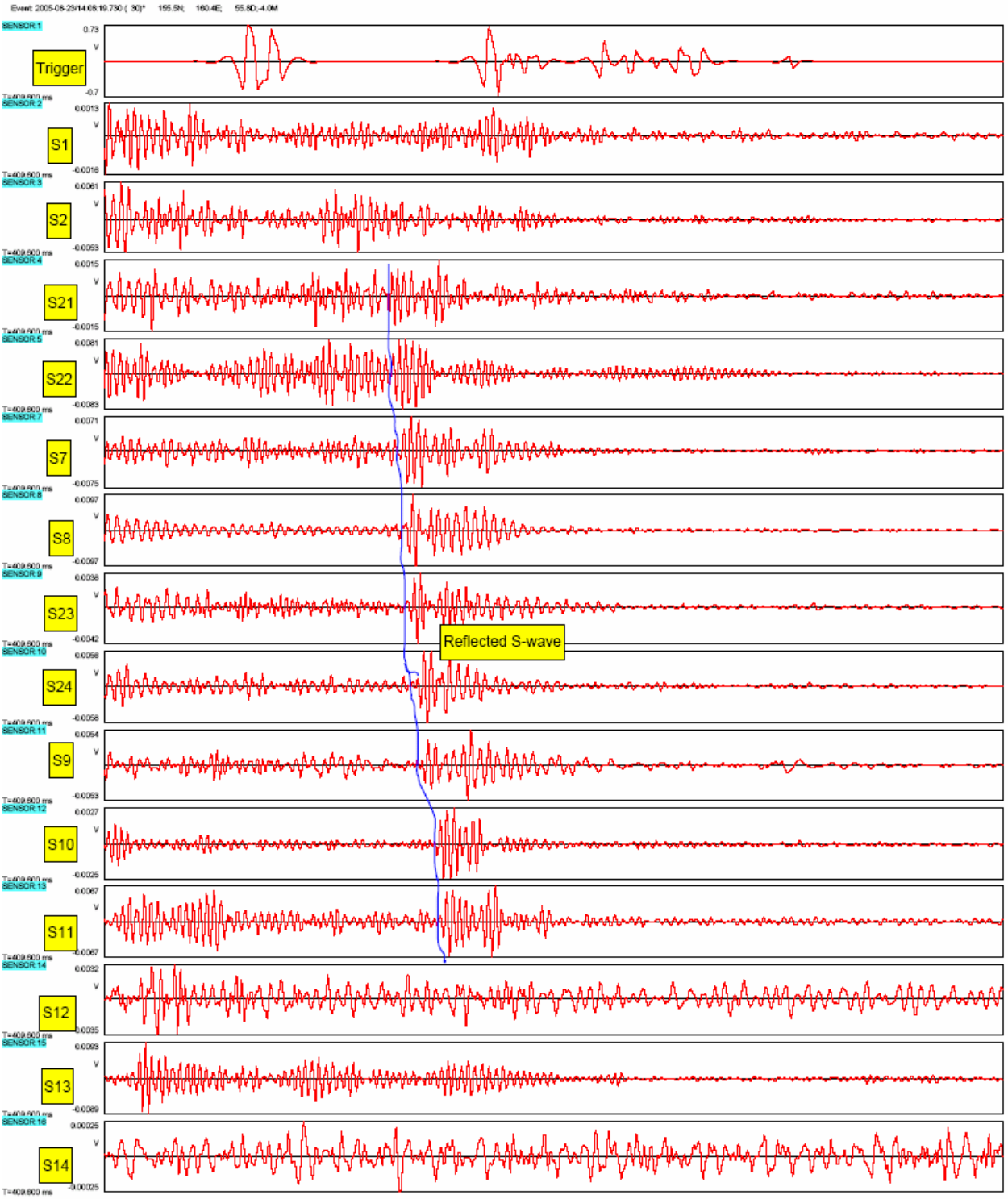

Figure 8.13 Details of the arrivals of the reflected S-waves for event 30 (display window: 100 - 140 ms).

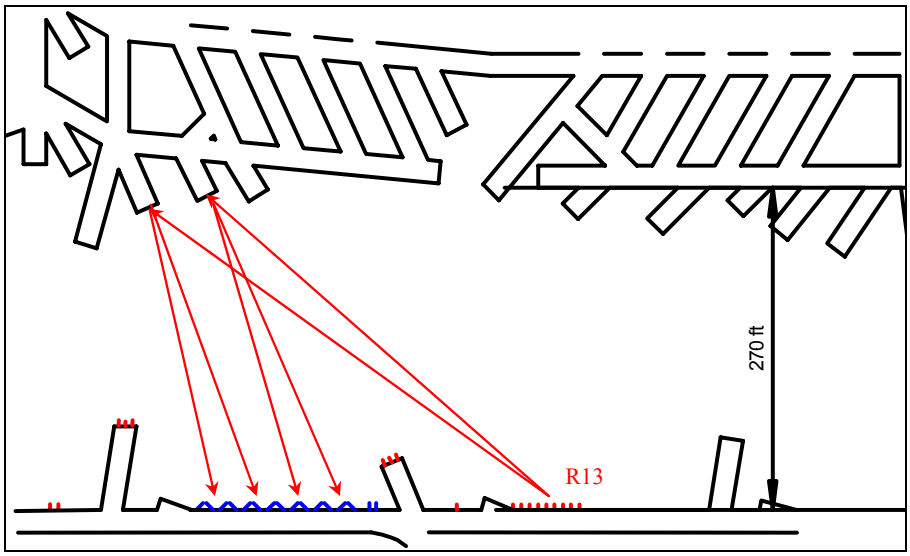

Figure 8.14 Ray paths of the reflected S-waves observed from event 30.

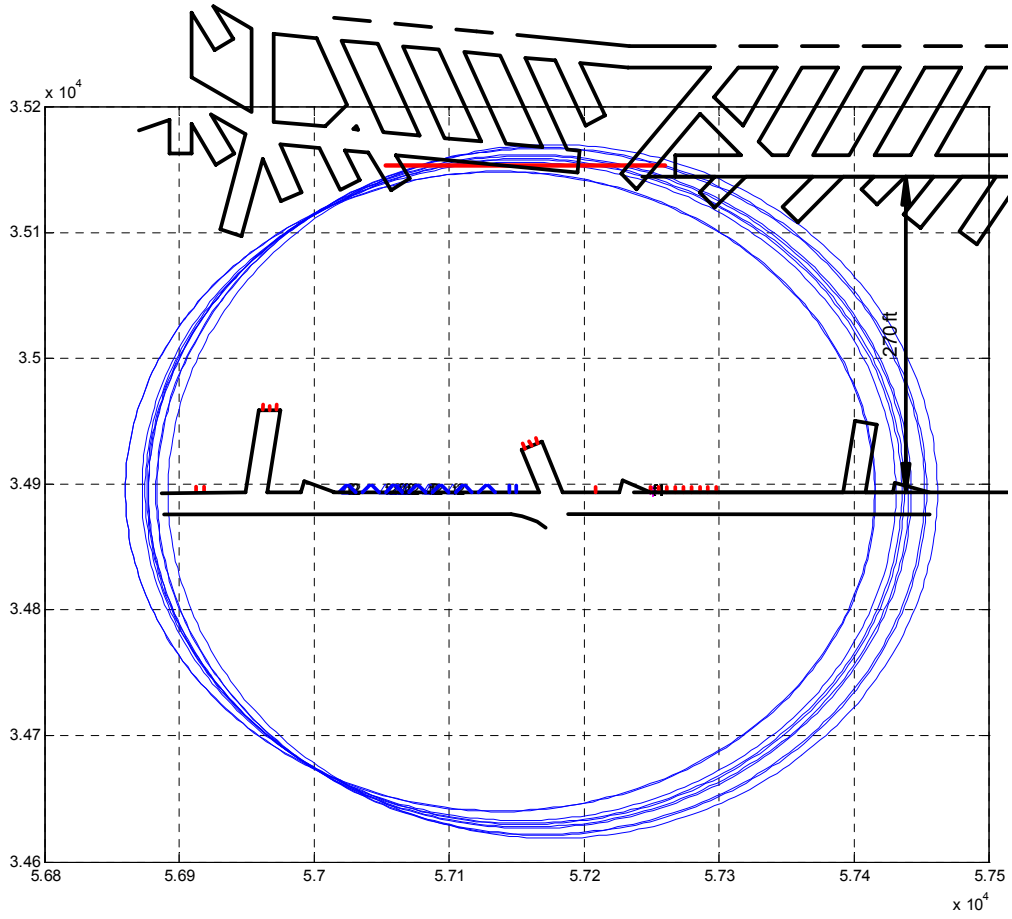

Figure 8.15 Void mapping with the ellipses associated with event 30 at FMC testing site. The void boundary is represented by a short red line segment. The locations of the sensors and the source as well as the associated ray paths are illustrated in Figure 8.10.

8.3.6 Case study: event 43

Event 43 refers the reflection survey related to seismic source R5, which is located at the small entry on the right side of the sensor section (Figure 8.16).

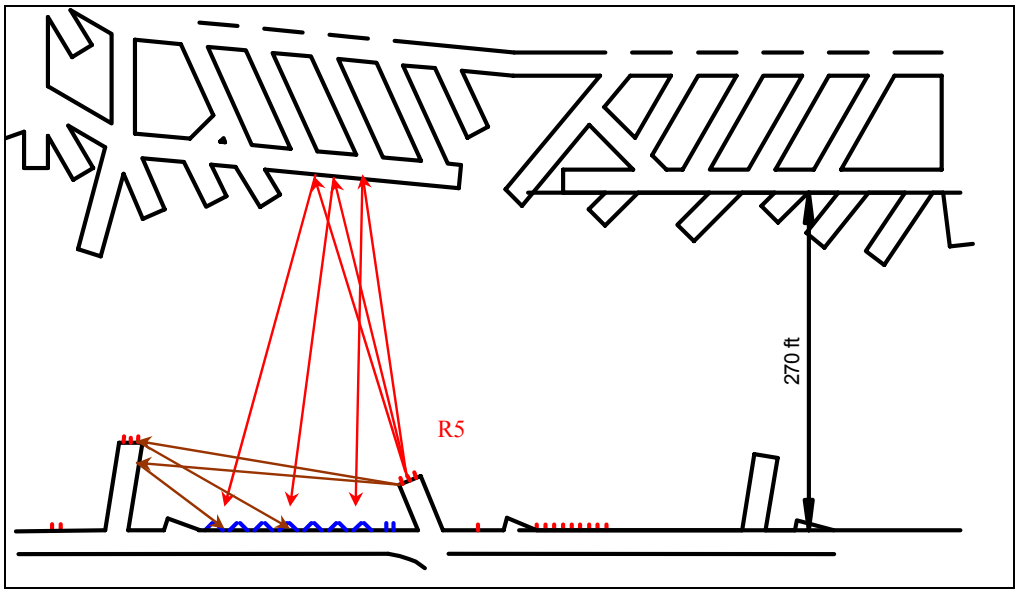

Figure 8.16 Test setup for event 118 and ray paths from top and left reflectors.

The waveforms recorded for this survey event are given in Figures 8.17 and 8.18. Figure 8.18 is a more detailed display of the event. The purpose of Figure 8.18 is to show the trends associated with two groups of the reflected waves. From Figure 8.18, the convergence of these two groups of reflected waves can be seen. This convergence of arrivals can be explained by reviewing the ray paths of these waves. For instance, the sensor installed in S1 was the first to receive the reflected wave from the adjacent entry and the last one to receive the reflected wave from the void. This is shown in Figure 8.18 by a large arrival time difference. The readings of S-wave and P- to S-wave arrival times are given in Tables 8.11 and 8.12. The mapping results based on these readings are presented in Figures 8.19 and 8.20. The related parameters of the ellipses are given in Tables 8.13 and 8.14. The triggering time for this event is 49.45 ms.

Table 8.11 Arrival times of reflected S-waves from the entry nearby sensor section (ms)

PC CH#	ch2	3	4	5	7	8	9	10	11	12	13
Sensor #	S1	S2	S21	S22	S7	S8	S23	S24	S9	S10	S11
S-wave	**80.85**	**81.25**	**81.85**	**82.85**	**83.45**	**84.35**	**84.9**				

Table 8.12 Arrival times of reflected P-to S- waves from the void (ms)

PC CH#	ch2	3	4	5	7	8	9	10	11	12	13
Sensor #	S1	S2	S21	S22	S7	S8	S23	S24	S9	S10	S11
P-wave (top)	**94.15**	**93.9**	**91.1**	**90.9**	**87.78**	**87.05**	**86.8**	**86.15**	**86.05**	**87.6**	**87.45**

Table 8.13 Parameters of ellipses associated with event 43 (left entry)

Source*	Sensor**	Travel time (ms)	Travel distance (ft)	Half of foci distance (ft)	Half of major axis (ft)	Half of minor axis (ft)
R5	S1	31.4	269.2	72.1	134.6	113.7
R5	S2	31.8	272.6	71.1	136.3	116.3
R5	S21	32.4	277.7	59.8	138.9	125.3
R5	S22	33.4	286.3	59.4	143.2	130.2
R5	S7	34	291.4	48.6	145.7	137.4
R5	S8	34.9	299.2	47.2	149.6	141.9
R5	S23	35.45	303.9	44.3	151.9	145.3

* See Table 8.4 for source coordinates
** See Table 8.5 for sensor coordinates
*** S-wave velocity: 8572 ft/s

Table 8.14 Parameters of ellipses associated with event 43 (top reflector)

Source*	Sensor**	Travel time (ms)	Travel distance (ft)	Half of foci distance (ft)	Half of major axis (ft)	Half of minor axis (ft)
R5	S1	44.7	566.6	72.1	283.3	274.0
R5	S2	44.45	563.4	71.1	281.7	272.6
R5	S21	41.65	527.9	59.8	263.9	257.1
R5	S22	41.45	525.4	59.4	262.7	255.9
R5	S7	38.33	485.8	48.6	242.9	238.0
R5	S8	37.6	476.6	47.2	238.3	233.6
R5	S23	37.35	473.4	44.3	236.7	232.5
R5	S24	36.7	465.2	43.0	232.6	228.6
R5	S9	36.6	463.9	41.1	231.9	228.3
R5	S10	38.15	483.5	40.3	241.8	238.4
R5	S11	38	481.6	34.3	240.8	238.4

* See Table 8.4 for source coordinates
** See Table 8.5 for sensor coordinates
*** Velocity: an average of P- and S-wave velocities, (16777 +8572)/2 = 12675 ft/s was used.

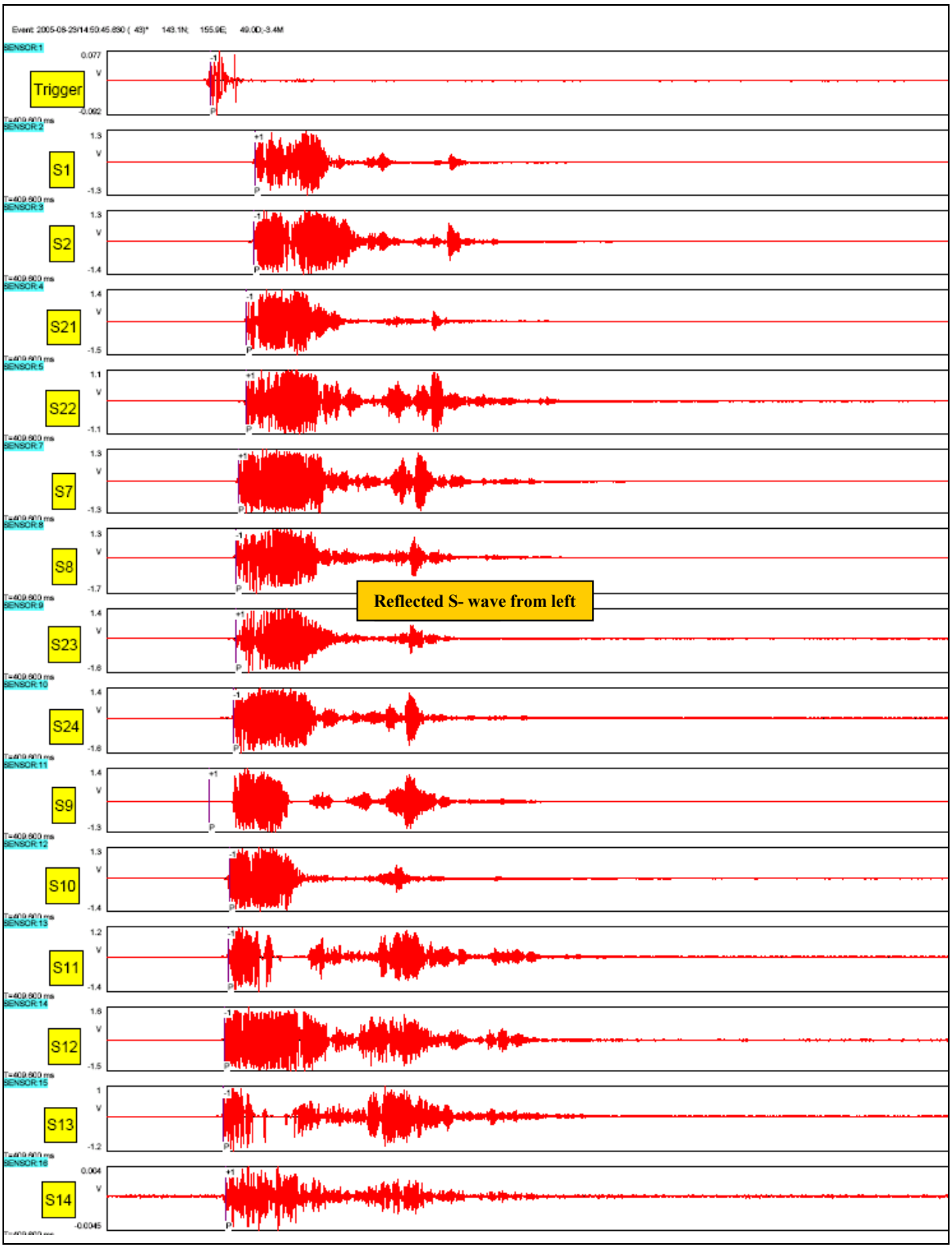

Figure 8.17 The complete waveforms recorded for event 118.

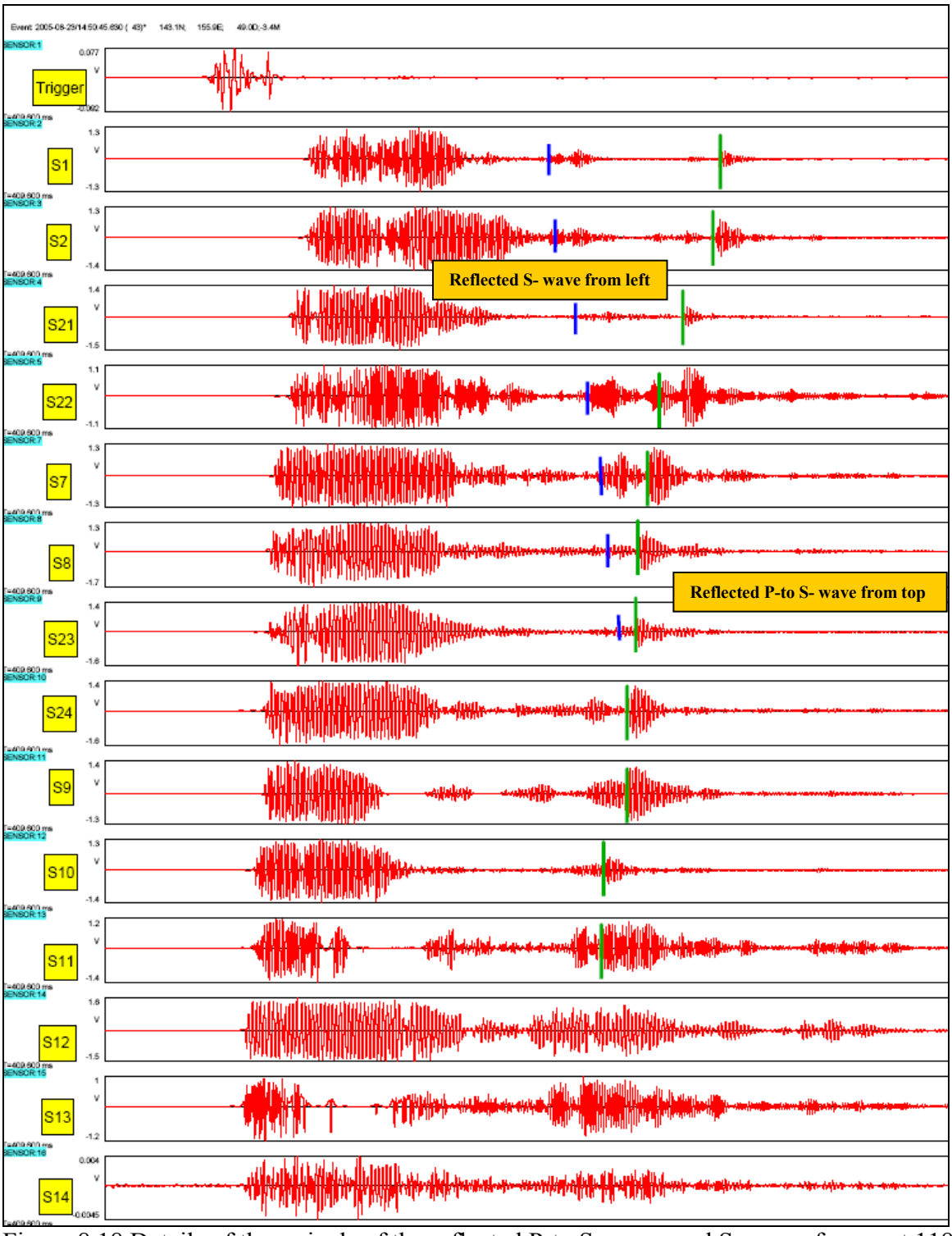

Figure 8.18 Details of the arrivals of the reflected P-to S-waves and S-waves for event 118 (display window: 65 - 86 ms).

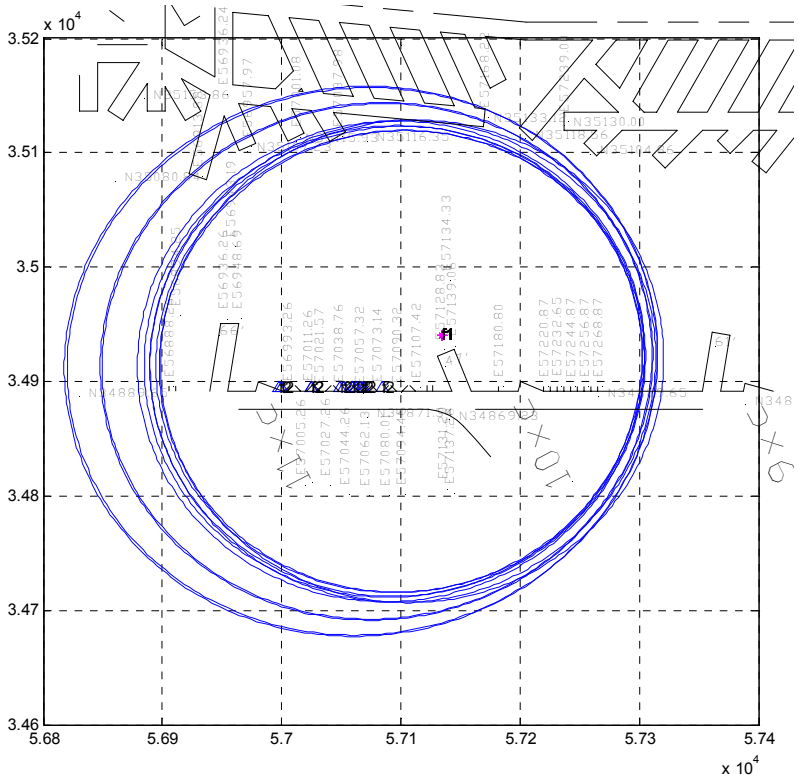

Figure 8.19 Void mapping with the ellipses associated with event 43 at FMC testing site (from top reflection)

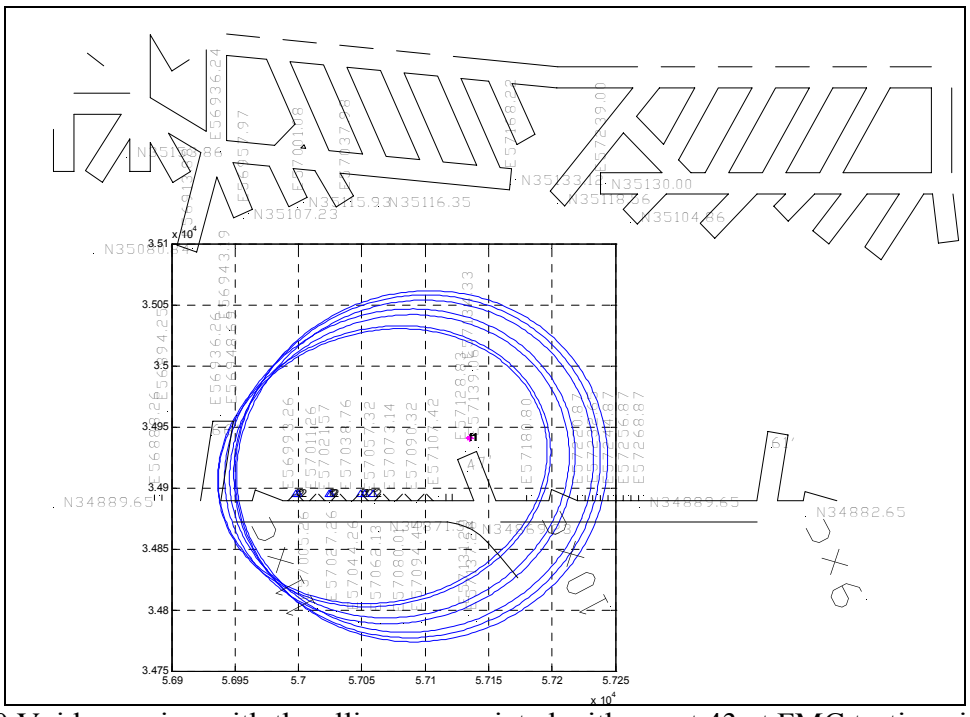

Figure 8.20 Void mapping with the ellipses associated with event 43 at FMC testing site (from left reflection)

8.3.7 Void mapping

The elliptical mapping method was used to delineate the void location. The P- and S-wave velocities used for plotting are 16777 ft/s and 8572 ft/s, respectively. The result of the void detection is given in figure 8.21. The result is very similar to the one obtained from the first test at FMC demonstrating the repeatability of the technique.

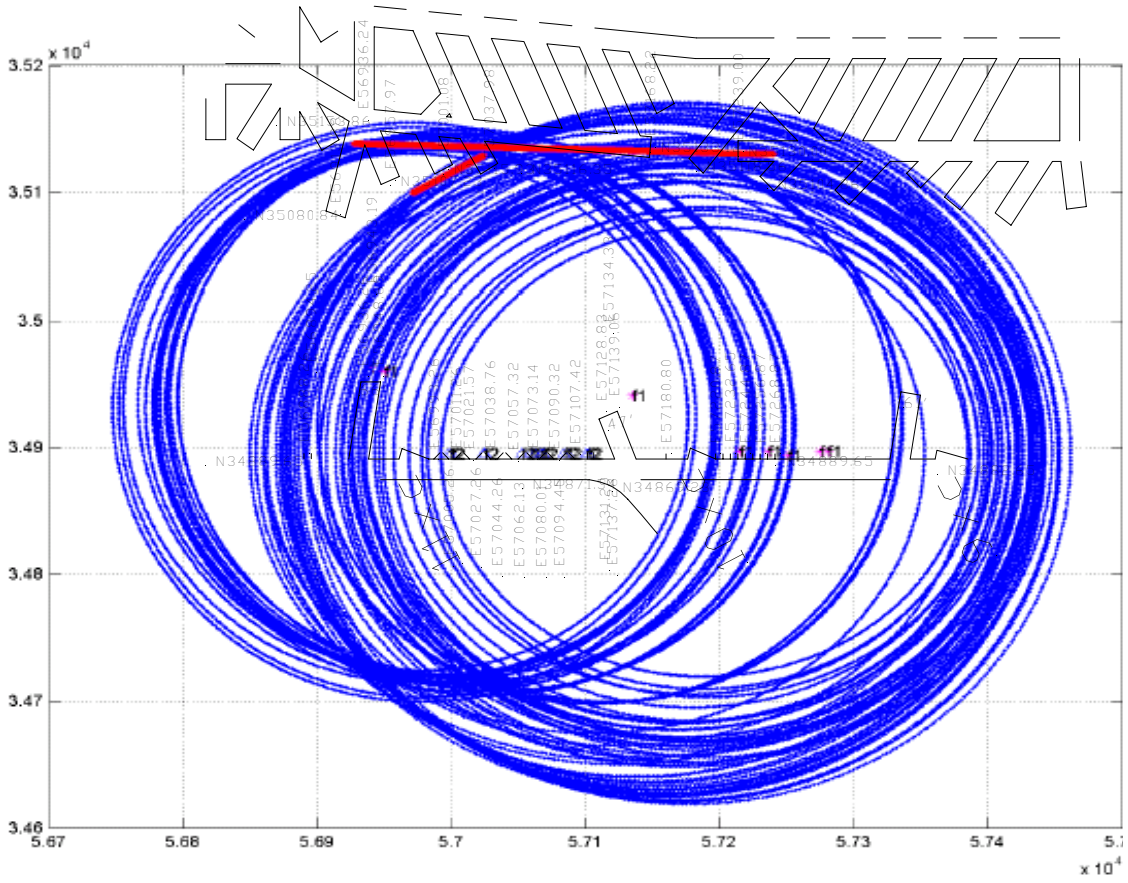

Figure 8.21 Void detection with the elliptical mapping method at site A, FMC.

8.4 Demonstration photo-essay

8.4.1 Demonstration photo-essay: Part I: Demonstration meeting

Demonstration meeting (Dr. Ge, PI of the project, reported to MSHA officials and industry representatives the status of the project).

Posters exhibited at the demonstration (The posters summarize the results of the tests carried out by Penn State team at FMC and General Chemical during the period of March 7 – 10, 2005).

8.4.2 Demonstration photo-essay: Part II: Preparing demonstration site by FMC

FMC carefully prepared the testing site for the demonstration, which included drilling new sensor and blasting holes and cleaning the existing and newly drilled sensor holes.

Alignment strings were used for guiding the drilling direction for both sensor and blasting holes.

Compressed air was used for creating “dust free” sensor holes.

Existing and newly drilled sensor holes (S21 was a newly drilled sensor hole for the demonstration. The parameters of the hole were marked clearly on the wall: 7' deep with a diameter of 1.75". S4 was drilled for the previous test and was reused for the demonstration. As marked by "blow out", it was further cleaned before the demonstration).

A thoroughly cleaned and dust-free sensor hole.

8.4.3 Demonstration photo-essay: Part III: Travel to the demonstration site

Testing equipment to be shipped to the site.

Leaving the shaft station for the demonstration site.

8.4.4 Demonstration photo-essay: Part IV: Testing site and system layout

Data acquisition system and sensor locations (The locations of the sensor holes are shown by the outlets of the blue cables as well as the blue insulation material plugged at the hole collar, the sound barrier).

8.4.5 Demonstration photo-essay: Part V: Sensor installation operation – resin mixing

Squeezing the resin out from a two-compartment tube.

Mixing resin with one-slot dowels.

Resin ready for using.

8.4.6 Demonstration photo-essay: Part VI: Sensor installation operations

Sensor holes were carefully cleaned and inspected prior to sensor installation.

Sensor installation.

8.4.7 Demonstration photo-essay: Part VII: Blasting operations

A scene at a blasting site.

Preparing the stemming material - FMC engineers helping in the demonstration.

Stemming a blasting hole.

Detonating.

8.4.8 Demonstration photo-essay: Part VIII: Real time data acquisition

Observing incoming signals at the demonstration site

Explaining to the MSHA official (left) the acquired signals.

8.4.9 Demonstration photo-essay: Part IX: Technical discussion at the site

MSHA officials and Penn State researchers discussing technical issues.

8.5 Summary of the Demonstration at FMC

On August 23, 2005, Penn State held the official demonstration of the ISS based void detection technique for the trona mine environment to MSHA and the mining industry at Site A, FMC. It was one of the two official demonstrations requested by MSHA. The other one was carried out at the Harmony Mine on November 15, 2005. The Harmony Mine is an anthracite mine located near Mt. Carmel, Pennsylvania.

The main objective of the demonstration was to show the feasibility of the ISS based void detection technique for the trona mine environment. Site A was chosen as the demonstration site for three reasons: a realistic detection range (270 ft), water filled void, and the repeatability of the technique. It is noted that the same site was used in the first test at the mine.

During the demonstration, MSHA officials witnessed the entire data acquisition process and observed real-time signals. The mapping result from the demonstration is very similar to the result from the second test at the mine.

Two conclusions can be drawn from the demonstration. First, by using high frequency body waves, the ISS based void detection technique is able to detect a water-filled void up to 270 ft. Second, the technique has a good potential to become a reliable and practical tool for detecting the degradation of barrier pillars due to water-induced dissolution, a major concern of the trona industry.

9. Field Test at Agustus Mine

9.1 Introduction

On December 8, 2005, the Penn State project team carried out a field test of the in-seam seismic (ISS) based void detection technique at the Agustus Mine. The test was mainly designed to map an abandoned mine adjacent to the mine property.

9.1.1 Agustus Mine

The Agustus Mine is a small bituminous mine located in Shade Township, Somerset County, PA (Figure 9.1). The Agustus mine recovers Upper Kittanning coal that is 36' to 48' thick at a depth of approximately 200' by the room-and-pillar mining method. The roof and floor are composed of shale of varying strength.

Figure 9.1 Geographic location of Agustus Mine.

9.1.2 Testing sites and the experimental design

The test at Agustus Mine was carried out at two sites, Site A and Site B. Site B is a 50' x 80' pillar which was utilized for the transmission test. Site A is a section of the entry located on the northern side of the mine for the reflection survey of the abandoned mine. Figure 9.2 shows the locations of the abandoned mine and the testing sites.

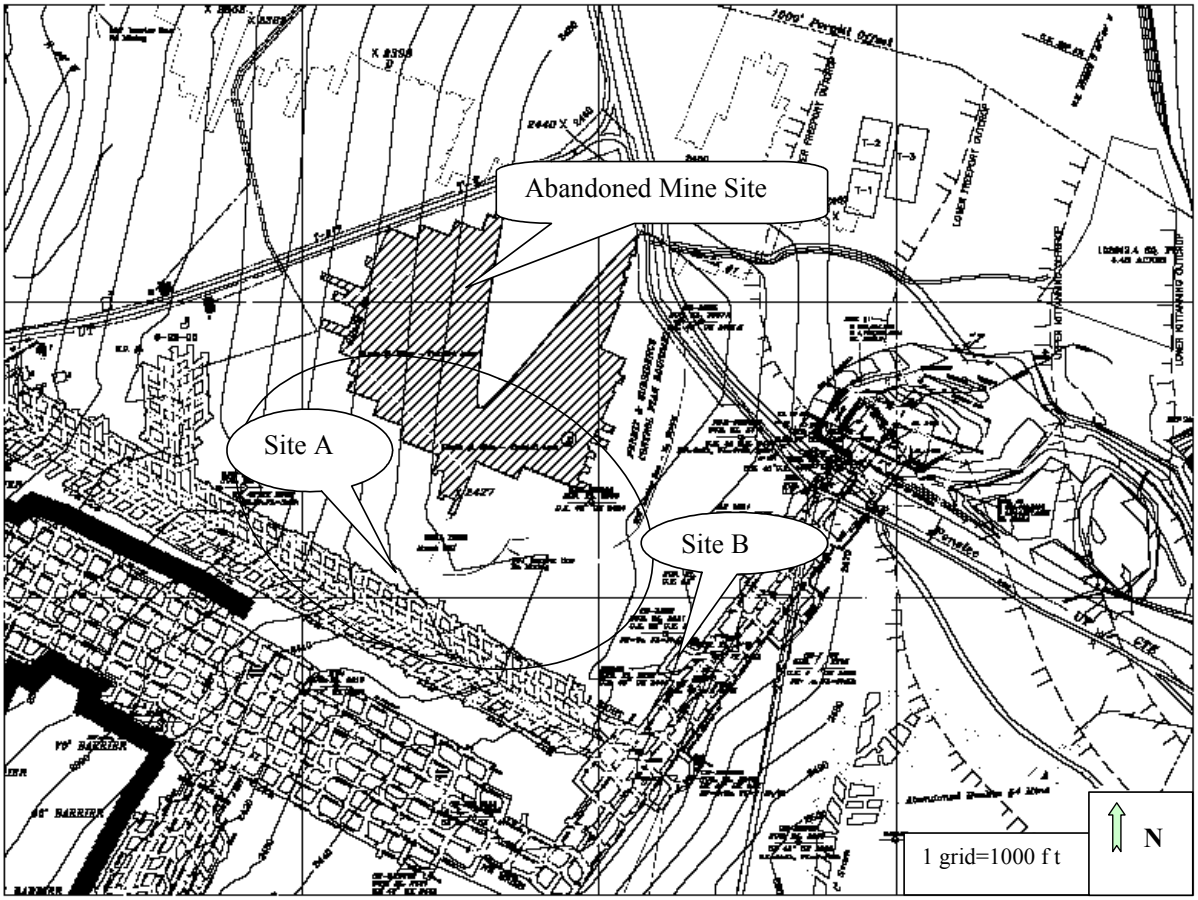

Figure 9.2 The abandoned mine and the testing sites (Site A and Site B were utilized for the reflection and transmission survey, respectively).

The specifications on the sensors, the data acquisition system, and the major operational parameters used for the test are given in Appendix I. The sampling rate and the recording window used for reflection surveys at site A are 25,000 samples/second and 0.8 second, respectively, and for transmission surveys at site B are 50,000 samples/second and 0.4 second, respectively.

9.2 Transmission survey at site B

The transmission survey was carried out for two purposes: obtain an understanding of seismic signals associated with coal and determining the velocities associated with the coal seam and country rocks.

9.2.1 Transmission survey design

The pillar which was used for the transmission survey is shown in Figure 9.3. The blasting holes were drilled along a rounded corner and the sensor section was located the side near the main entry.

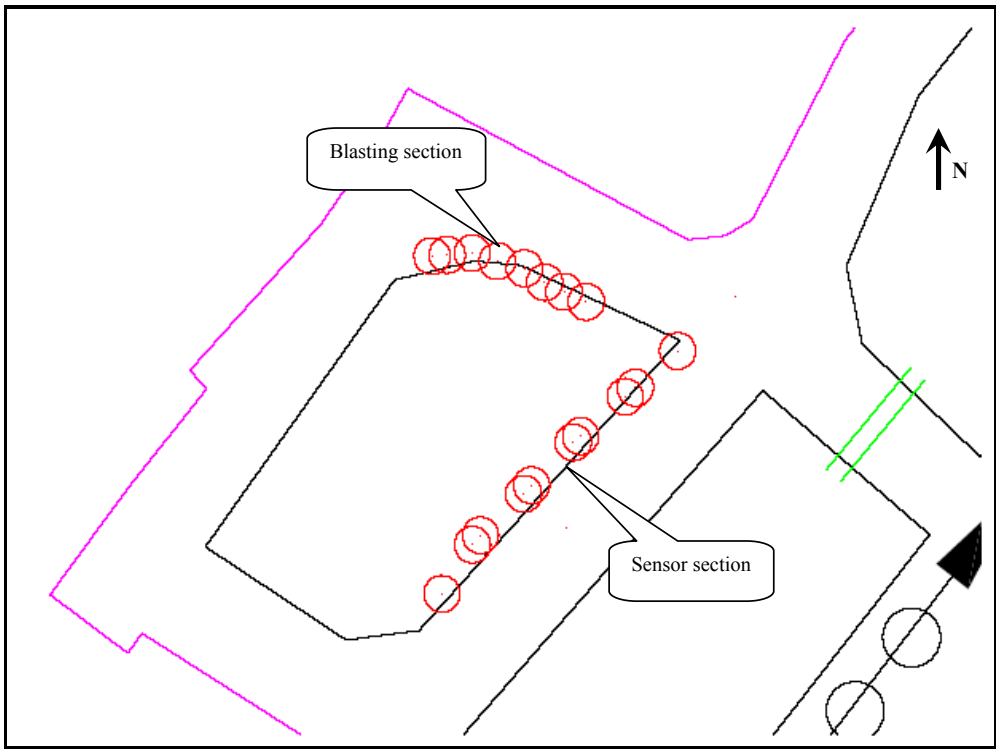

Figure 9.3 The pillar utilized for the transmission test at Site B, Agustus Mine.

Sensor section

Figure 9.4 shows the arrangement of the sensor holes. Sensor holes were prepared in pairs, inclined at 45º and 135º angles to the rib. They were 7 ft long with the tip distance of 2 ft and the collar distance of 12 ft. The sensor hole diameter was 1.75". Five pairs of sensor holes were drilled and they were numbered from S2 to S11. During the transmission test, three pairs of sensor holes were used, which involved sensors S4 – S9. The coordinates of these sensors are given in Table 9.1.

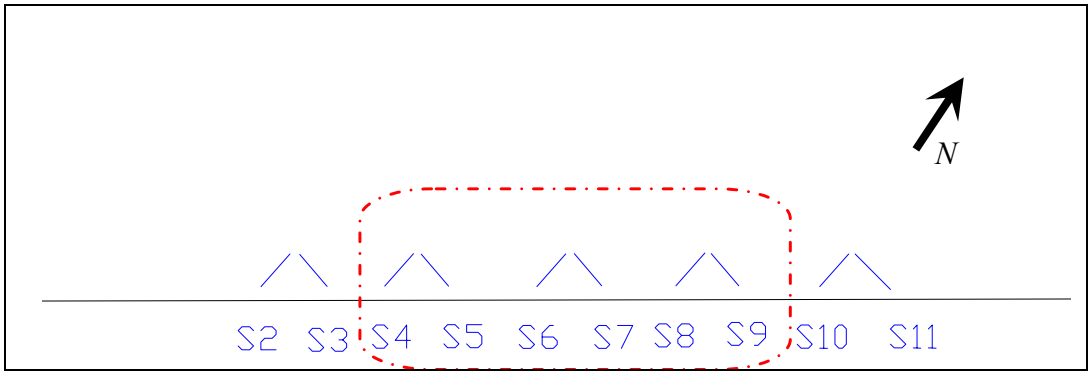

Figure 9.4 Sensor hole locations for transmission survey.

Table 9.1 Sensor hole information for site B, Agustus Mine

Hole #	Channel #	Length (ft)	Senor coordinate (ft)	
			East (x)	North (y)
S4	2	7	267762.3	1703279
S5	3	7	267764.2	1703281
S6	4	7	267772.6	1703290
S7	5	7	267774.4	1703292
S8	6	7	267783.1	1703300
S9	7	7	267784.4	1703302

Blasting hole section

A total of 8 blasting holes were drilled, which were numbered from T1 to T8, where T stands for transmission. All blasting holes were 4 ft deep with the diameter of 1.5". Four blasting holes were used for the survey, which were T4, T5, T6 and T7. The holes were roughly cleaned before loading and stemmed with 18" long clay dummies after loading. Caps were used for all four transmission surveys. The blasting hole information is summarized in Table 9.2.

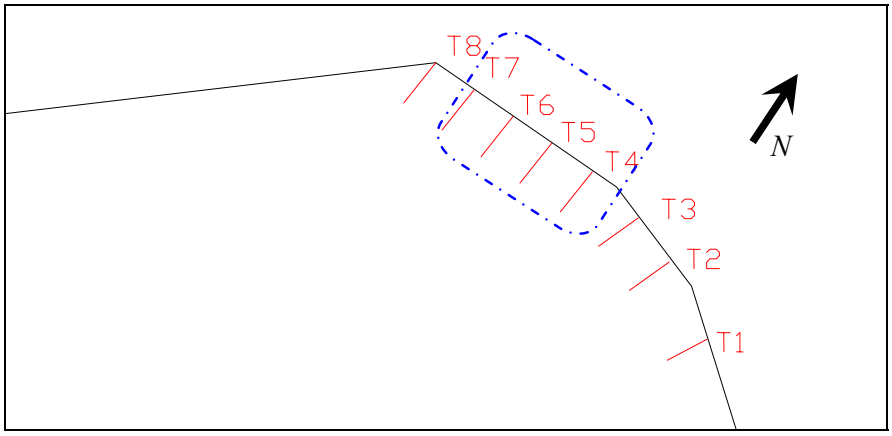

Figure 9.5 Blasting hole locations for transmission survey.

Table 9.2 Blasting hole information for site B, Agustus Mine

Hole #	Length (ft)	Source coordinate (ft)	
		East (x)	North (y)
T7	4	267821.4	1703274
T6	4	267821.8	1703279
T5	4	267820.1	1703285
T4	4	267818.6	1703290

9.2.2 Characteristics of transmission signals

Four transmission tests were carried out at Site B. The explosive type and event number for these transmission surveys are summarized in Table 9.3.

Table 9.3 A summary of the transmission tests at Agustus

Hole #	Explosive	Event #
T7	Cap	11
T6	Cap	17
T5	Cap	22
T4	Cap	28

The signals for these four transmission surveys are similar. To illustrate some general features, event 11 is utilized as an example and presented in Figures 9.6. There are two groups of waves. The first one features with the much high frequency in comparison with the second group. The dominant frequency for this group is about 1000 Hz. The waves for this group include P- and S-waves from the roof and floor. Although the separation of P- and S-waves is poor in general because of the short travel distance, it is still visible for few channels, such as S6 where a gap appears in the middle of the first group. The second group, which features a much lower frequency, about 200 Hz, is a result of channel waves. It is very interesting to note that these channels waves have very long durations, more than 200 ms, which are equivalent to a travel distance of 600 ft. A closer look of these channel waves indicate that they are composed by many smaller groups. These smaller groups are most likely due to the channel waves reflecting multiple times within the pillar.

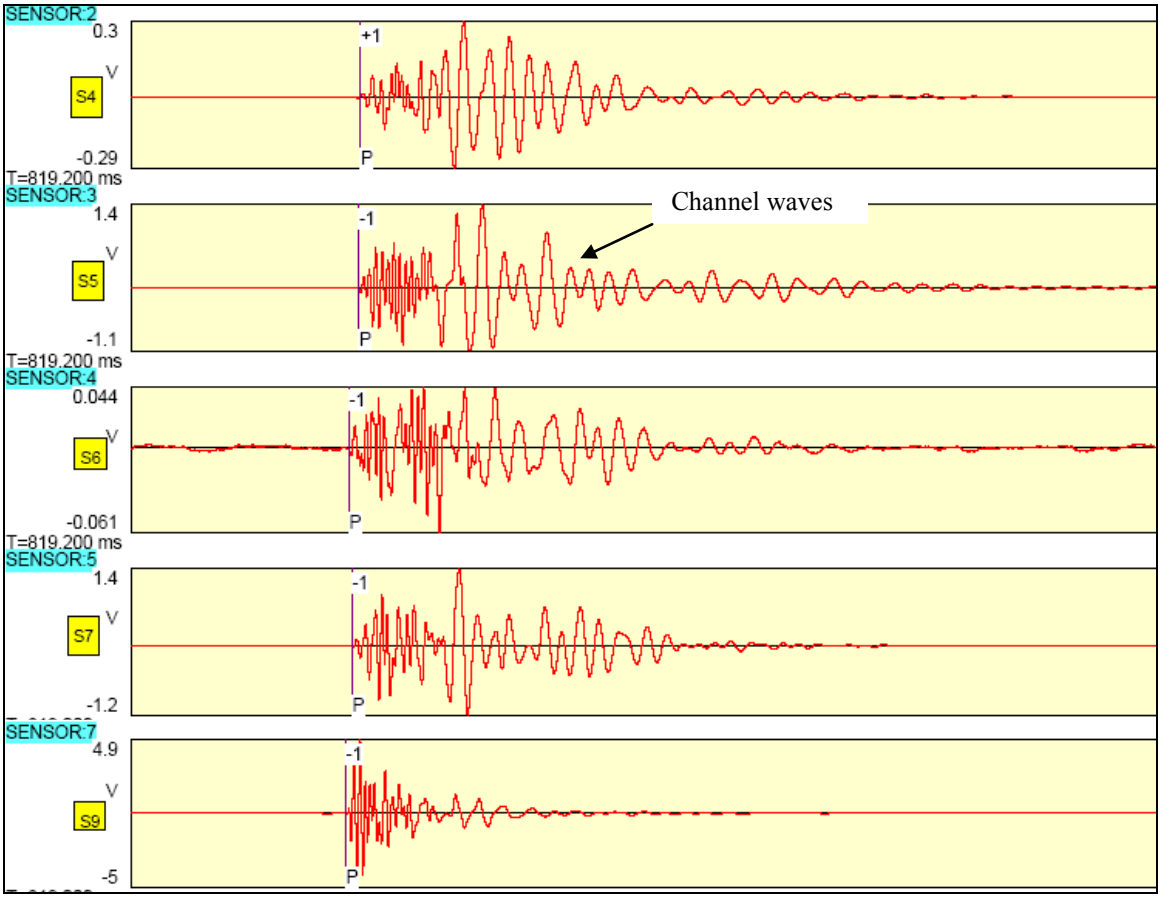

Figure 9.6 Transmission signals for event 11 (display window: 37 – 393 ms; seismic source: cap; average travel distance: 52 ft).

9.2.3 Channel wave velocities in Agustus Mine

The channel wave velocity was estimated with the data from the transmission survey. The data used for the calculation and the calculation result are summarized in the following tables.

The transmission survey included 20 survey lines from 4 source locations to 5 sensors. The survey distance ranged from 36 ft to 60 ft with an average of 52 ft (Table 9.4). The arrival times picked are listed in Table 9.5 and the corresponding channel wave velocities are given in Table 9.6. Table 9.7 is the summary of the channel wave velocity data.

Table 9.4 Source – receiver distances (ft)*

Hole #	Source type	S4	S5	S6	S7	S9
T7	Cap	59.2	57.5	51.6	50.3	46.2
T6	Cap	59.5	57.6	50.7	49.2	43.7
T5	Cap	58.1	56.0	48.2	46.5	39.7
T4	Cap	57.5	55.2	46.4	44.5	36.2

* T# and S# represent blasting hole and sensor numbers, respectively.

Table 9.5 Channel wave arrival times (ms)

Event No.	Hole #	Trig.	S4	S5	S6	S7	S9
11	T7	49.9		67.75		65	64
17	T6	45.4	63.6	64.5			
22	T5	49.9	67.05	66.55			
28	T4	49.9		66.3	64.65		

Table 9.6 Channel wave velocities for individual channels

Event No.	Hole #	Velocities(ft/s)				
		S4	S5	S6	S7	S9
11	T7		3223.3		3334.4	3273.5
17	T6	3267.1	3014.9			
22	T5	3385.2	3363.3			
28	T4		3367.7	3148.5		

Table 9.7 Summary of channel wave velocity data

Wave type	Average Distance (ft)	Survey lines	Velocity (ft/s)	Standard deviation (ft/s)	Mean Standard deviation
Channel wave	52	20	3,264	121	3.7%

9.3 Reflection survey at site A

Site A (Figure 9.7) was used for the reflection survey for delineating the abandoned mine. The survey line consists of three sections: the sensor section and two blasting sections.

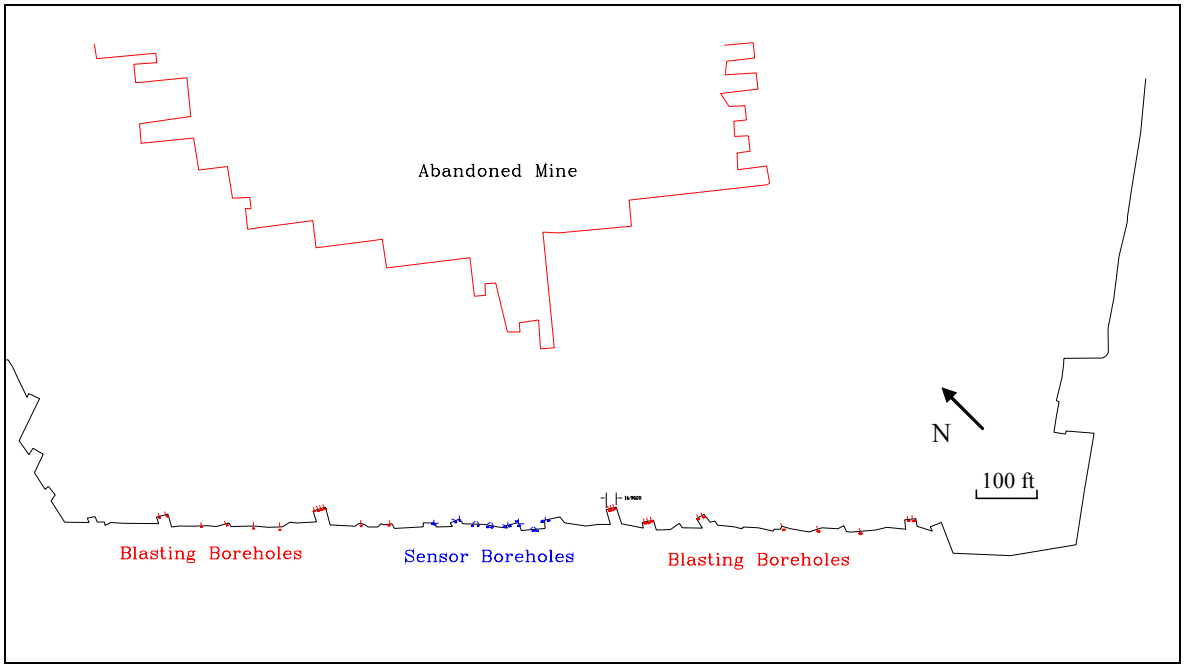

Figure 9.7 Map of site A, Agustus Mine.

9.3.1 Sensor section

The details of the sensor section are given in Figure 9.8. Sensor holes were arranged in pairs. The arrangement was made to facilitate the polarization analysis of signals. With the original design, 8 pairs or 16 individual sensor holes were drilled, which numbered from S2 to S17 as shown in Figure 9.8. Thirteen of these sensor holes were used for the sensor installation (S2, S4 and S5 were not used).

All sensor holes were drilled in the middle of the seam. To avoid the water accumulation problems in the drillholes, they were oriented slightly upwards. The diameter of the sensor holes was 1.75". The information related to these sensor holes are given in Table 9.8.

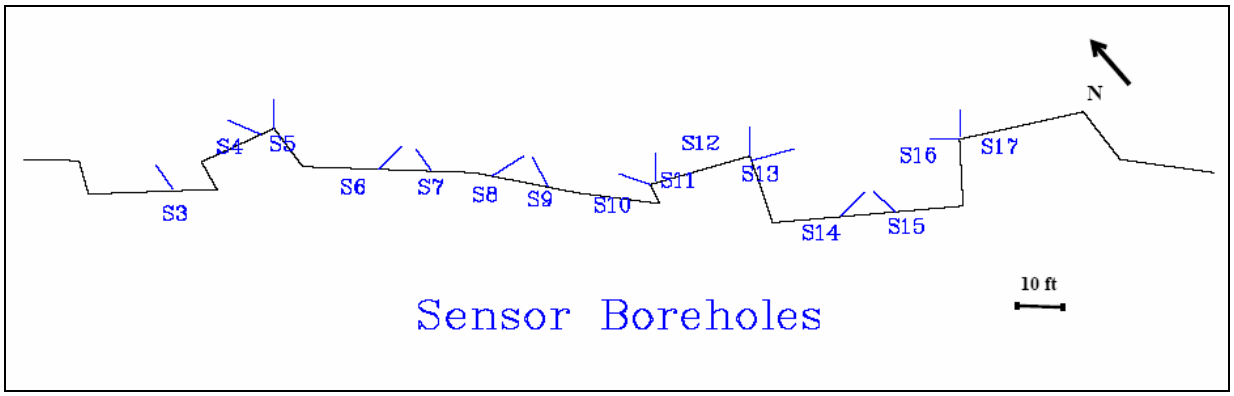

Figure 9.8 Sensor section designed for the reflection survey at site A, Agustus Mine

Table 9.8 Sensor hole information for site A, Agustus Mine

Hole #	Channel #	Length (ft)	Senor coordinate (ft)	
			East (x)	North (y)
S3	2	7	268092.0	1702209.4
S6	3	7	268081.7	1702244.5
S7	4	5	268074.9	1702253.1
S8	5	5	268061.3	1702272.1
S9	6	7	268054.6	1702281.5
S10	7	7	268045.3	1702301.0
S11	8	7	268045.2	1702302.5
S12	9	7	268044.7	1702316.7
S13	10	5	268043.7	1702318.0
S14	11	5	268022.9	1702331.6
S15	12	5	268017.6	1702343.5
S16	14	5	268026.5	1702355.6
S17	15	7	268027.7	1702357.0

The locations and orientation of the sensor holes were determined based on a number of general considerations during a prior site visit on October 28, 2005. The first consideration was the openness of the field in the vicinity of the sensor locations. The sensor hole locations must be open to the reflected waves and must not be shaded by any openings.

The second consideration was the coupling effect. In order to achieve the best coupling effect, the sensor hole sites should be as competent as possible. This was achieved by two measures. First, all sensor holes locations were determined by an onsite inspection of the rib condition. Highly fractured zones were avoided. Second, all sensors were installed 5 ft deep from the rib regardless of the local condition. Because of this, the actual length of the sensor holes varied

with their orientation and location. Under normal conditions, a distance of 5 ft for a 3 – 4 ft coal seam is considered well beyond the highly fractured zone of the pillar rib.

The third consideration was the orientation of the sensor holes. In order to facilitate the polarization analysis, the sensor holes were prepared in pairs with an orthogonal layout. Taking into consideration that the reflected signals would be likely to have near vertically incident angle with the rib line, efforts were made to have the sensor holes oriented parallel and perpendicular to the rib line, such as the orientation of the S16 and S17 in figure 9.8. It is noted from the figure that the inner corners of the cuts have to be used in order to have the sensor holes oriented in these directions. There are two added advantages to have the sensor holes drilled from these inner corners. First, they are considerably shorter because they were drilled vertically from the pillar surface. Second, it seems that sensors "hid" in the corner holes are less affected by the air pressure from blasting.

9.3.2 Blasting sections

There were two blasting sections, located on the left and right hand side of the sensor section, respectively (Figure 9.9). The two sections were designed for mapping the "nose" and both sides of the "nose" of the abandoned mine.

A total of 23 blasting hole were drilled. They were numbered from R2 to R24, where R stands for reflection. Blasting holes R2 – R12 were located on the left section (Figure 9.9A) and R13 – R24 on the right section (Figure 9.9B. All blasting holes were 4' long with a diameter of 1.5". The coordinates of the blasting holes which were used for the reflection survey are listed in Table 9.9.

Among 23 drilled blasting holes, 22 were used. The one that was not used is R17. All blasting holes were loaded with 375 grams of the explosive. The blasting holes were cleaned before loading and stemmed with 18" long clay dummies after loading. Several blasting related operations are shown in Figures 9.10 – 12.

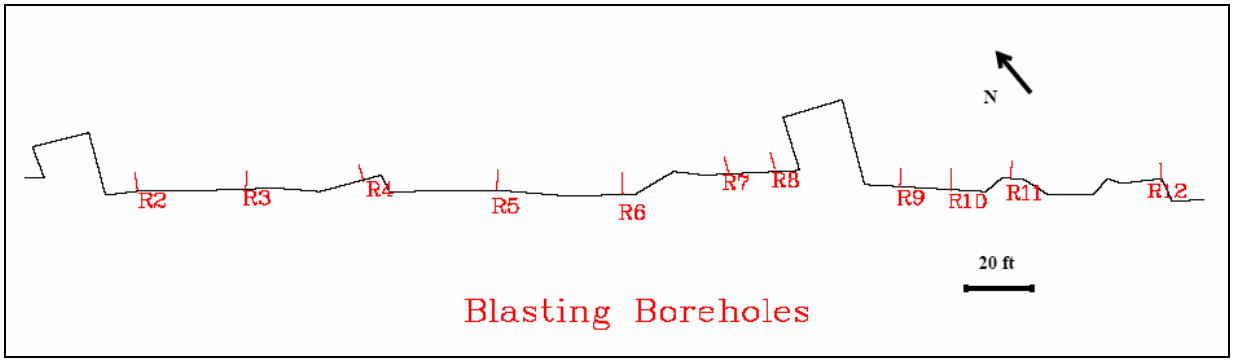

A. Blasting Holes R2 - R12 on the left section.

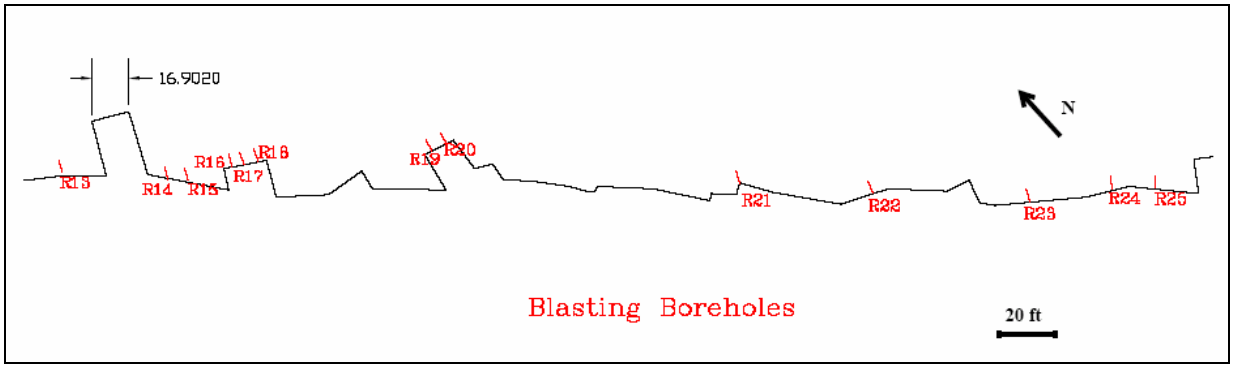

B. Blasting Holes R13 – R24 on the right section.

Figure 9.9. Blasting hole locations on two blasting sections.

Table 9.9 Coordinates of the blasting holes used at site A, Agustus Mine

Hole #	Source coordinate (ft)	
	East (x)	North (y)
R2	268307.6	1701804.3
R3	268290.2	1701837.6
R4	268274.9	1701869.2
R5	268249.4	1701915.7
R6	268224.4	1701957.8
R7	268216.4	1701993.7
R8	268204.9	1702011.9
R9	268181.0	1702049.1
R10	268174.1	1702061.0
R11	268167.0	1702082.4
R12	268141.6	1702129.4
R13	267973.3	1702444.9
R14	267952.2	1702481.8
R15	267944.7	1702490.2
R16	267942.1	1702506.8
R18	267940.2	1702518.8
R19	267900.0	1702603.0
R20	267899.5	1702609.8
R21	267823.2	1702715.4
R22	267794.2	1702761.0
R23	267756.4	1702828.3
R24	267745.7	1702856.7

Figure 9.10 Clean blasting hole R6 for reflection test.

Figure 9.11. Setup the explosive for hole R6.

Figure 9.12 Preparing the detonation.

9.3.3 Analysis of reflection survey result

The reflection survey included 22 individual surveys (blasting events). The explosives used for the surveys were 375 gram/hole. The associated event numbers are listed in Table 9.10.

Table 9.10 A summary of the reflection tests at Agustus mine

Hole #	Explosive (g)	Event #
R2	375	58
R3	375	92
R4	375	98
R5	375	111
R6	375	119
R7	375	126
R8	375	134
R9	375	167
R10	375	182
R11	375	186
R12	375	192
R13	375	13
R14	375	1
R15	375	292
R16	375	285
R18	375	276
R19	375	263
R20	375	244
R21	375	228
R22	375	227
R23	375	211
R24	375	209

Figure 9.13 shows the originally recorded waveforms for event 186. The relative position of the blasting location for this event, R11, and the sensor section is shown in Figure 9.14.

There are two apparent wave trains shown in Figure 9.13. The first one was associated with direct arrivals, including P- and S-waves from the roof and floor and the channel waves from the coal seam. Figure 9.15 provides a closer look at these waves. The timing for these arrivals can be can be determined very accurately.

The dominant frequency for the channel waves is about 200 Hz. The velocity of the channel wave is estimated at 3319.0 ft/s, which is consistent with the channel wave velocity determined from the transmission survey (3,264 ft/s).

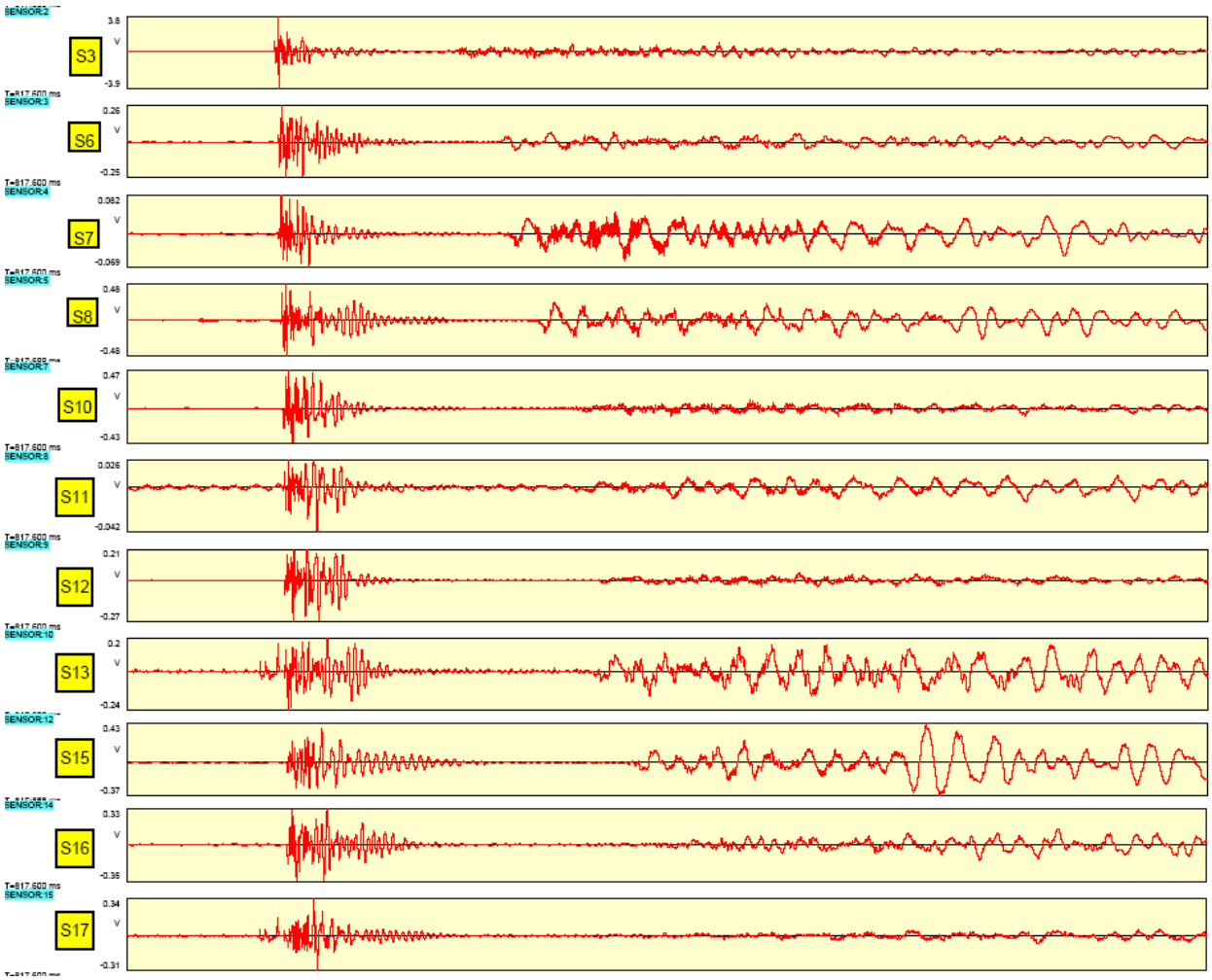

Figure 9.13 Originally recorded waveforms for event 186.

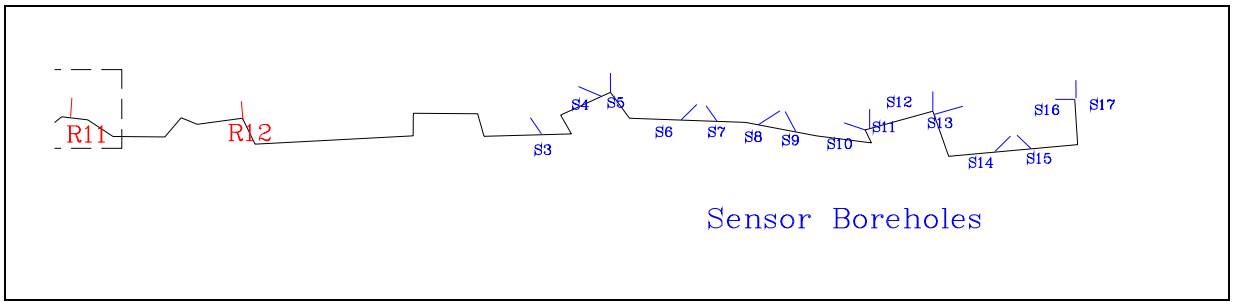

Figure 9.14 Locations of blasting hole R11 and sensor section.

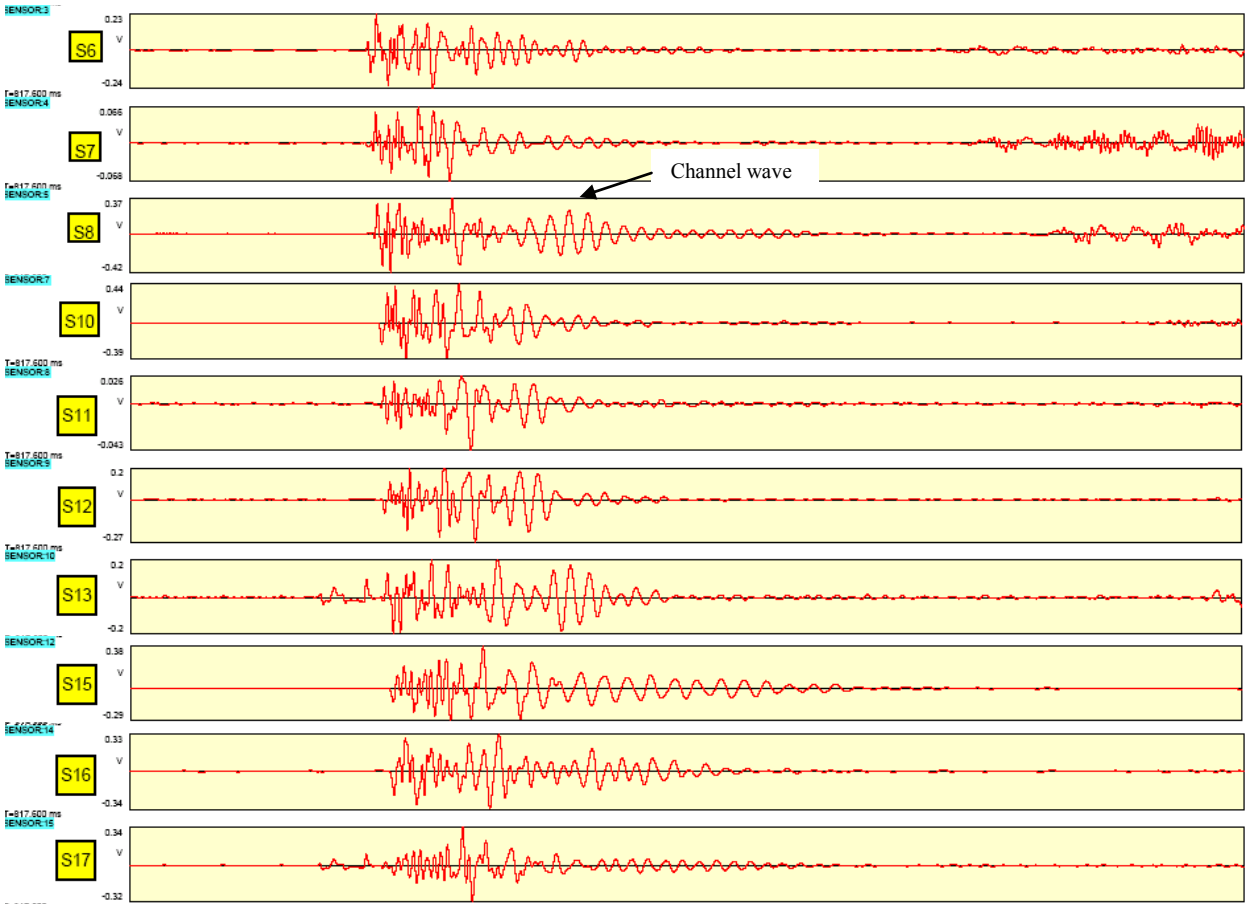

Figure 9.15 A closer look of recorded waveforms for event 186.

The second wave train was caused by (air) shock waves. They featured with large amplitudes and very long durations. This second wave train created a severe problem for the project as they overshadowed the reflected signals. Figure 9.16 shows the result after the low and high frequencies were filtered by a band pass filter of 70 – 300 Hz. The dotted blue line denotes the expected arrival times for the reflected signals. Some wave character changes can be seen around this time line, but the shock waves are so strong that a clear delineation is not possible.

The blast caused shock wave is a special problem associated with the ISS based void detection. This is because the ISS test is conducted in a confined environment. Penn State has paid a special attention to the problem since the beginning of the project and has taken several measures to deal with it. The first one is to seal sensor holes with the commercial insulation material. This has been a standard practice for Penn State for its field tests. All sensor holes used at the Agustus Mine were sealed with the blue foam shown in Figure 9.17 (the picture was taken from the testing site at the Harmony Mine).

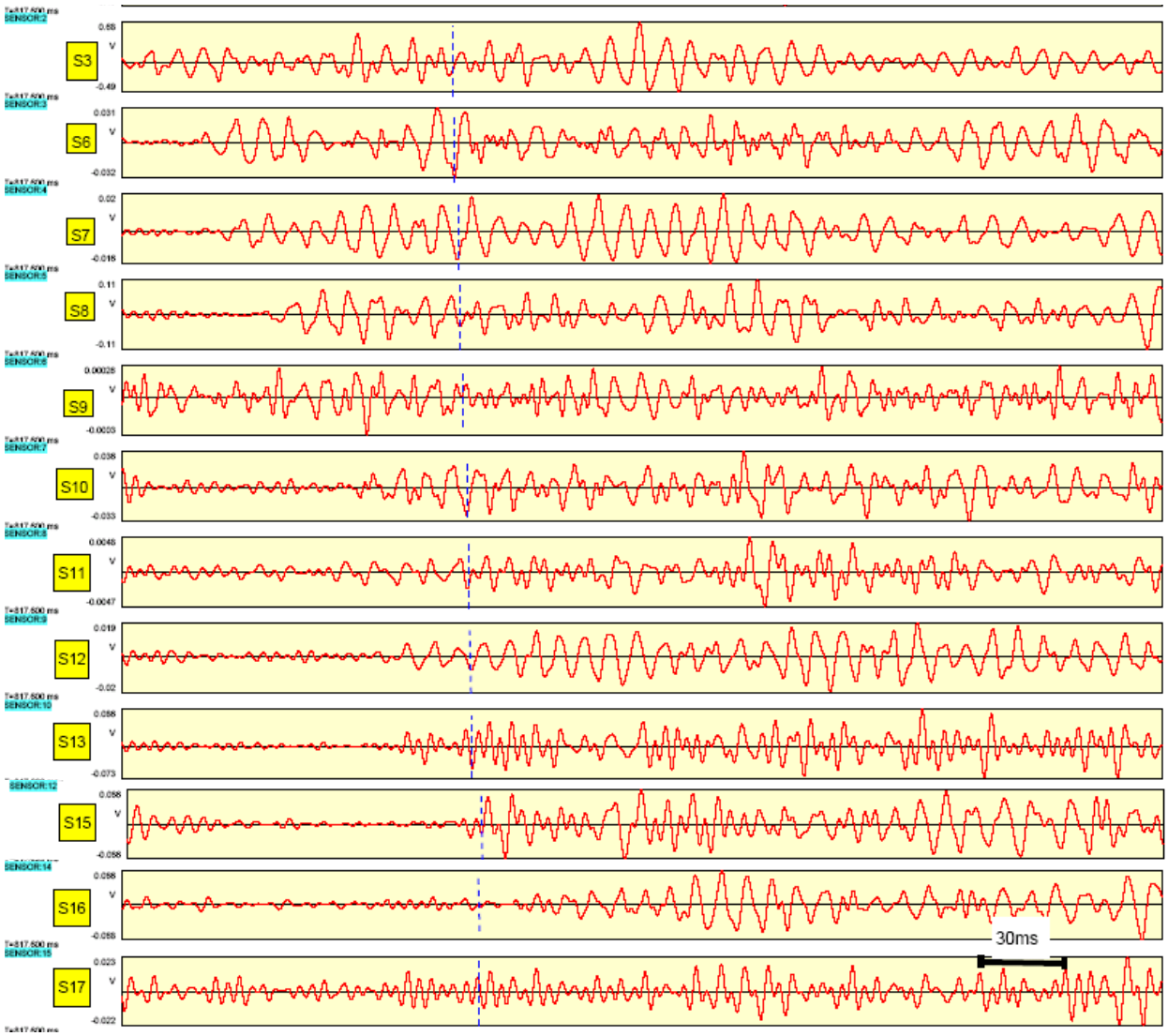

Figure 9.16 The result after a band pass filter of 70 – 300 Hz was applied to the event given in Figure 9.13 (the dotted blue line denotes the expected arrival times for the reflected signals).

Figure 9.17 Sensor holes were sealed with the blue foam to prevent the interference by shock waves (picture was take at testing site II, Harmony Mine).

The second measure is to put the blasting holes in other entries if possible. This arrangement reduces the shock wave energy at the sensor section. Penn State has found that this is a quite efficient means to deal with the shock wave problem. During the planning stage, we visited the testing site to see if there were suitable entries for this purpose. There were several short entries which might be used for the purpose. Unfortunately, none of them were accessible.

The third measure is to reduce the amount of explosives. There is a delicate balance surrounding the amount of explosives to be used. For the ISS based void detection, there is always a concern whether the seismic source is strong enough. With "common" sense, it seems that one would be safer by using more explosives. But on the other hand, a strong seismic source could induce excessive direct arrivals and excessive shock waves. In addition to their direct negative impact by interfering with reflected signals, they may significantly reduce the system sensitivity. In the case of the Agustus Mine, the main concern before and during the test was whether the seismic source strong enough because of very large distance.

The shock waves encountered at the Agustus Mine were much stronger than the ones from any previous tests when the equivalent explosives were used. Other than the layout of the mine at the site, it is unknown whether there were any other contributing factors. The incident, however, is a strong warning on the devastating effect of shock waves. Penn State will take two measures to prevent the similar incidents. First, Penn State will initiate a research for developing the air-tight sensor hole sealing technique, which should be simple and easy to operate while will not pose any potential problems for using the retrievable sensor installation technique. The second measure is the systematical testing on the amount of the explosives needed for each site.

9.4 Summary of the test at Agustus Mine

The Agustus Mine is a small bituminous mine. The main purpose of the test at the mine was to collect the basic information on the application of the ISS based void detection for the bituminous mine environment, which would be the focus of Phase II and Phase III.

The test at Agustus Mine was carried out at two sites, Site A and Site B, which were utilized for the reflection survey and transmission survey, respectively. The reflection test was designed to map an abandoned mine, which was 400 – 1000 ft away.

Both direct arrived and reflected channel waves were observed during the transmission test. The direct arrived channel waves were also observed from the reflection surveys. The dominant frequency for the channel waves is about 200 Hz. The velocity of the channel wave is about 3300 ft/s.

The main difficulty encountered in the reflection survey was strong (air) shock waves, which completely overshadowed reflected channel waves. The basic solution is to develop the air-tight sensor hole sealing technique, which should be simple and easy to do while not posing any potential problems for using the retrievable sensor installation technique. The second measure is the systematical testing on the amount of the explosives needed for each site.

10. Conclusions and Future Work

10.1 General summary and related conclusions

The goal of the project is to demonstrate an ISS based void detection technique which can be used reliably by the mining industry.

The ISS based void detection technique developed for this project is intended for two very different application conditions. One application, referred to as the conventional in-seam seismic (ISS) method, is utilized in situations where the seam is weaker than the country rocks and channel waves are used for the study. The second application is diametrically opposite from the first where the seam is stronger than the country rocks. In this latter case, instead of channels waves, body waves (e.g. P- and S-waves) are used for the study, and, therefore, the technique used under these conditions is no longer referred to strictly as the conventional ISS method. For this reason, "*the ISS based void detection technique*" as used for this project should be broadly understood as the void detection technique which utilizes the waves traveling in the seam. These waves may be either channel waves or body waves (P- and S-waves), depending on the relative condition of the seam and its country rocks.

The main challenge for the project is one of reducing the ambiguity that is conventionally associated with geophysical methods. Geophysical methods, including ISS, are convenient and relatively inexpensive, and can be very efficient if used properly. The methods, however, can also be very ambiguous with respect to data retrieval and interpretation. If a geophysical method is to be proved reliable for void detection, the problem of ambiguity must be addressed.

Our strategy to deal with the ambiguity problem was to emphasize fundamentals. Each basic aspect of the ISS based void detection technique was carefully evaluated in terms of its reliability, accuracy and efficiency. This evaluation consisted of necessary development work to refine and develop the techniques basic and essential to the project, including sensor installation, experimental design, data analysis and void mapping.

The field tests were the core part of the project. A total of seven tests, including two demonstrations, were carried out for three types of mining conditions: trona, anthracite and bituminous coal. Two demonstrations were given at FMC and the Harmony Mine on August 23 and November 15, 2004, respectively. These tests were not just for calibration and evaluation. They were the basic information source for improving the technique as well as for understanding the related science.

In terms of the final goal of the project, the progress of the project in Phase I may be viewed from two aspects. First, the prototype of the ISS based void detection technique projected by Penn State was developed through a logical progression of technical development work in the areas of sensor installation, experimental design, data analysis and void mapping. Although the technique is still in its early stage and many works remain to be done, we believe that our first year's work has established a solid framework for the ISS based void detection technique.

Second, the demonstrations at both the FMC trona mine and the Harmony anthracite mine were successful. The "voids" which were approximately 270 ft and 150 ft away, respectively, were detected with the accuracy of ± 20 ft. The void at the FMC site was water filled.

The demonstration at FMC trona mine is particularly significant at this stage. The test result has shown that the void detection under the strong seam conditions may have to rely on very high frequency signals. The reflected signals from three tests at the trona mines were all in the range of 3 – 5 kHz. This phenomenon, if can be further studied and confirmed, implies that the high frequency survey is essential for in-seam void detection under the strong seem condition, which may also partially explain why studies under the similar condition (strong seam) were rare prior to the current study.

10.1.1 Development of the basic techniques for the ISS based void detection

In order to have a functional ISS based void detection technique that could be tested and demonstrated in Phase I, the technical development work was carried out in four basic areas, which are retrievable sensor installation technique, experimental design, signal analysis, and void mapping.

Retrievable sensor installation technique

The retrievable sensor installation technique was developed for two specific reasons. First, it is essential for the technique to be economically feasible. The unit cost of the sensor is $600 and typically 15 sensors are installed for each test. If these sensors were not retrievable, the sensor costs alone for each test would be $9,000.

Second, it was developed for achieving the best possible coupling effect. If the ISS based void detection technique is to be a practical tool, it has to be able to detect voids some distance away, which will largely depend on the coupling effect. A good coupling effect is critical for acquiring the high frequency signals over long distances.

The retrievable sensor installation technique developed during this project has fulfilled our design expectations. All our field tests have demonstrated that the technique is extremely reliable for acquiring high frequency signals while simple and easy to operate. The development of this technique is pivotal for the project as it resolved one of the most important problems for the project: the ability to acquire the high quality data.

The author has engaged in microseismic and geotomography studies for some 25 years. He believes that this technique will have many unique and important applications.

Experimental design

One of the major problems to be addressed by this project is how to reduce the ambiguity associated with the proposed technique. A sound experimental design is a fundamental approach to address this problem as it determines the stability of the associated mathematical system, or more specifically with our case.

The experimental design involves many theoretical and practical issues. Our effort for Phase I was limited to a number of critical issues, which include sensitivity analysis, angled sensor pairs and site investigation.

Sensitivity analysis Errors in input data, such as signal arrival time and signal travel velocity, are inevitable. The effect of these errors on the void detection accuracy largely depends on the experimental setup. Because of its fundamental importance, a theoretical study was initiated at the beginning of the project on the effect of the testing setup influence on the accuracy and reliability of void detection.

Angled sensor holes The ISS technique relies on positive identification of incoming signals, including wave types/wave groups and their incident directions. With a single trace information (waves from one component sensor), this identification work is in general difficult, and often is impossible. Using angled sensor pairs provides a simple and efficient solution for the problem, and is the basic method used for this purpose.

Site investigation The testing sites for the ISS based void detection vary from location to location. In order to make a sound experimental design, a thorough investigation of the testing site (from survey line to void) is necessary. A summary of our experiences is given in the users' manual.

Data analysis

Similar to experimental design, data analysis is critical for the ISS base void detection. It is also a subject related to many theoretical and practical issues. Again, our effort was limited to a number of critical issues, such as identifying the reflected signals. There are many additional studies which could not be done at this stage, such as hodogram analysis and attenuation study. We plan to carry out these studies during Phase II and Phase III, given the opportunity.

The study on the identification of the reflected signals was proceeded with several different approaches, most notably, pattern analysis, analysis method associated with angled sensor pairs, and wavelet analysis. Wavelet analysis, a mathematical tool for studying non-stationary frequency characters, provides an ideal means for detecting newly merged signals. With the help of 3D display of wavelet transform, many reflected signals, which are difficult to be see in the original waveforms, can be identified.

Void mapping

In this project, the elliptical method was developed for mapping the mine voids. The method provides a simple and convenient means for void detection. It can utilize all signals reflected from the similar location to delineate the void boundary in the area regardless of the locations of sources and receivers, the type of signals, and the survey sequence. As the method represents the reflection data directly, it avoids many mathematical manipulations which would be necessary otherwise if the other methods are used. This characteristic makes the method much more stable than any other methods. The method also provides an intuitive means to analyze the cause of missing data so that using the missing data becomes part of the process of void location.

10.1.2 Field tests and demonstration of the ISS based void detection

A total of seven tests, including two demonstrations, were carried out for three types of mining conditions: trona, anthracite and bituminous coal. Two demonstrations were given at FMC and the Harmony Mine on August 23 and November 15, 2004, respectively.

Demonstration and field tests at the trona Mines

Penn State held its first demonstration at FMC on August 23, 2005. Prior to the demonstration, two field tests were carried out at FMC and General Chemical (GC) on March 7 - 10, 2005. The detecting distance is about 270 ft at FMC and 350 ft at General Chemical. The void was water-filled at FMC and dry at General Chemical. The main observations from these three tests are summarized as follows.

Consistent and accurate P- and S-wave velocities The P- and S-wave velocities at the mine sites appear extremely consistent. For instance, the P-wave velocity measured at FMC site, GC site and Penn State Laboratory are 16777 ft/s, 16740 ft/s, and 16710 ft, respectively. The maximum difference among those three measured values is only 67 ft/s, or 0.3% of the average P-wave velocity. This consistency constitutes a very favorable condition for reliable void detection.

High frequency reflected signals A very unique characteristic of the reflected signals observed at both FMC and General chemical is their high frequencies, typically in the range of 3000 – 5000 Hz. This character is a precondition for high resolution surveys. It also greatly facilitates the work to identify the reflected signals.

Using three types of reflected signals for void location Three types of reflected signals were observed under both water filled and dry conditions, which are P-wave, S-wave and S-wave due to mode conversion. Using three types of reflected signals significantly increases the physical data which can be used for void detection.

Reliable void mapping The elliptical mapping method provides an efficient means to use all available data simultaneously, including 1) data from different surveys, 2) data from different source locations, and 3) three different types of reflected signals. The method is also simple, convenient, and reliable.

Void mapping error The mapping error for void detection in trona is about ± 10 ft for pillars up to 340 ft wide based on the actual survey results from FMC and General Chemical.

Based on the testing result at the trona mines, the ISS based void detection technique developed by Penn State appears to be a promising tool for the trona industry to study the pillar dissolution problem.

The void detection experience at the trona mines should be useful for many other mines where the seam is stronger than the country rocks.

Demonstration and field tests at the Harmony Mine

Penn State carried out the demonstration of the ISS based void detection at the Harmony Mine, an anthracite mine, on November 15, 2005, and two field tests on February 7-8, and April 29, 2005, respectively. The tests at the Harmony Mine were conducted at two sites. The site for the first test was a pillar of 60 ft wide. The site for the second test and the demonstration was a 150 ft wide pillar.

The field tests and the demonstration at the Harmony Mine were one of the most important components of the project. The significance of these tests for the ISS based void detection can be viewed from three aspects. The first was the demonstration of the critical importance of the retrievable sensor installation technique for the ISS based void detection. At the Harmony site, the signal frequency ranges from 500 Hz for channel waves to over 3000 Hz for P- and S-waves from the roof and floor. In order to differentiate channel waves from the others as well as to obtain a complete signal profile for the site in terms of the signal frequency, velocity and attenuation, the ability of acquiring broadband signals is essential and the retrievable sensor installation provides a reliable means to fulfill this requirement. The test result at the mine site also demonstrated that one would not be able to record the signals with the required frequencies if the sensors were simply wedged in the ground.

The second one was the demonstration of the existence of channel waves and the reliability of using these channel waves for void detection under the anthracite mine condition. The core issue for the ISS method was the ability of catching the channel waves with the predictable quality. To demonstrate the feasibility of the ISS based void detection, this was the first issue to be addressed. The presence of the channel waves were demonstrated from three different types of the tests, which are transmission survey, reflection survey, and particularly designed "roof and floor" survey.

With the "roof and floor" surveys, sensors were installed in the roof, floor and coal seam on one side of the pillar and the seismic sources were placed 5 ft deep boreholes drilled in the roof and floor. The testing result shows that the signals received by the sensors installed in the coal and the sensors installed in the roof and floor have two distinctive patterns. The signals for the sensors installed in the roof and floor very similar. Both are featured with high frequencies which are tapered off rapidly. For those sensors installed in the coal, the signal duration is much longer. The channel waves were developed at some later stage with large amplitudes.

Finally, the ISS technique was demonstrated for the void detection distance up to 150 ft under the anthracite mine condition, the distance that was large enough to warrant the practicability of the technique. Since the same site was used for the second test and the demonstration and the very similar result was obtained, the reliability of the technique was also demonstrated in terms of its repeatable performance.

Field test at the Agustus Mine

On December 8, 2005, the Penn State project team carried out a field test of the in-seam seismic (ISS) based void detection technique at the Agustus Mine. The Agustus Mine is a small bituminous mine located in Shade Township, Somerset County, PA. The mine is approximately 200' below the surface. The coal is mined from Upper Kittanning by the room-and-pillar mining

method. The seam in the mine premise has a typical thickness of 36” - 48”. The roof and floor are composed of shale of varying strength.

The test at Agustus Mine was carried out at two sites, Site A and Site B. Site B is a 50’ x 80’ pillar which was utilized for the transmission test. Site A is a section of the entry located on the northern side of the mine for the reflection survey of the abandoned mine. The reflection test was designed to map an abandoned mine adjacent to the mine property.

Both direct arrived and reflected channel waves were observed during the transmission test. The direct arrived channel waves were also observed from the reflection surveys. The dominant frequency for the channel waves is about 200 Hz. The velocity of the channel wave is about 3300 ft/s.

We could not positively identify reflected channel waves because they were overshadowed by strong (air) shock waves. The shock waves encountered at the Agustus Mine were much stronger than the ones from any previous tests when the equivalent explosives were used. Other than the layout of the mine at the site, it is unknown whether there were any other contributing factors.

The blasting caused shock wave is a special problem associated with the ISS based void detection. This is because the ISS test is conducted in a confined environment. Penn State has paid a special attention to the problem since the beginning of the project and has taken several measures to deal with this problem. The first one is to seal sensor holes with the commercial insulation material. This is now standard practice for Penn State for its field test. All sensor holes used at the Agustus Mine was sealed with the blue foam.

The second measure is to put the blasting holes in other entries if possible. This arrangement reduces the shock wave energy at the sensor section. Penn State has found that this is a quite efficient means to deal with the shock wave problem. During the planning stage, we visited the testing site to see if there were suitable entries for this purpose. There were several short entries which might be used for the purpose. Unfortunately, none of them were accessible.

The third measure is to reduce the amount of explosives. There is a dedicated balance on the amount of explosives to be used. For the ISS based void detection, there is always a concern whether the seismic source is strong enough. With the “common” sense, it seems that one would be safer by using more explosives. But on the other hand, a strong seismic source could induce excessive direct arrivals and excessive shock waves. In addition to their direct negative impact by interfering with reflected signals, they may significantly reduce the system sensitivity. In the case of the Agustus Mine, the main concern before and during the test was whether the seismic source strong enough because of very large distance.

The Penn State researchers believe that the problem encountered at the Agustus Mine is solvable. The basic solution is to develop the air-tight sensor hole sealing technique, which should be simple and easy to do while not posing any potential problems for using the retrievable sensor installation technique. The second measure is the systematical testing on the amount of the explosives needed for each site.

10.1.3 Other related studies

During Phase I, Penn State also carried out several potentially important studies related to the ISS based void detection, which are non-explosive seismic sources, energy transmission device, and retrievable 3D sensor installation technique.

Non-explosive seismic sources

The study of non-explosive seismic sources was carried out for two purposes: 1)identifying suitable methods for laboratory and field calibration studies, and 2) assessing the possibility of using non-explosive sources for reflection survey. The non-explosive seismic sources which were evaluated include four types of hammers, Schmidt Hammer and pneumatic source ("paint gun").

Schmidt Hammer provides a constant impact energy. However, it appeared to generate a series of four or more separate seismic events for each activation, and, therefore, is not suitable as a seismic source.

An advantage of the paint gun is that the impact energy can be controlled by adjusting the shooting distance. The device, however, has some problems to be practically used. For the field application, its impact energy is not large enough. Schmidt Hammer also has the similar problem. In the laboratory, the noise associated with shooting is a concern.

Both the field and laboratory tests have shown that the combination of a heavy hammer and *Simple mechanical impact system* (SMIS) has a potential to become a viable solution for the non-explosive seismic sources.

Energy transmission device

To be practical for a non-explosive seismic source, there are two problems to be addressed: strength and repeatability. When a seismic source is generated by a mechanical impact at the pillar surface, such as the rib of a coal pillar, both the strength and repeatability will be difficult to achieve.

The simple mechanical impact system (SMIS) developed during the project provides an efficient solution to the problem. The system can sustain very large impacts and can be used repeatedly. The system is also retrievable, and, therefore, the use of the system is very convenient and involves almost no material cost.

3D sensor installation technique

A difficult problem for the ISS based void detection technique is signal identification, including detecting the reflected signals from all recorded ones and identifying the type of reflected signals. A reliable means of acquiring this information is to compare how signals are polarized and three-dimensional sensors are ideal for this purpose.

Conventionally, 3D sensors have to be installed in cement filled boreholes, which would make the technique economically unfeasible for the void detection purpose. It is for this reason that the possibility of developing a retrievable 3D sensor installation technique was explored, and as the result of this study, a prototype of the installation device was developed. The technique is based

on the "expandable mandrel" concept used in holding odd sized hollow cylindrical work pieces in a lathe. As it was discussed in Chapter 2, we believe that this is a very promising technique.

10.2 Future work

The future work discussed here is neither the request for additional work, nor the justification for Phase II and Phase III. The work for Phase II and Phase III was discussed in the revised plan submitted to MSHA on August 24, 2004 and approved by MSHA subsequently. The discussion here serves two purposes. The first one is to provide MSHA some more detailed information based on our work carried out in Phase I, such as testing site selection. The second one is some suggestions regarding the use of Phase I results for the industry.

10.2.1 Test in bituminous mines

As discussed in our revised proposal, the focus for Phase II and Phase III is the field test of the ISS based void detection for various bituminous mine conditions. According to the revised proposal, four field tests will be scheduled for each of Phase II and Phase III.

During Phase I, the Penn State team secured several testing sites from Amfire Mining and Black Wolf after visiting these companies/mines and discussing with them the ISS tests. As the results of these discussions, four mine sites were offered by the companies for the test, which are the Quecreek Mine, the Ondo Extension Mine, the Ridge Mine and the Madison Mine. The preliminary plan for Penn State is to have two tests at the Quecreek Mine and two tests at the Ridge Mine.

<u>The Quecreek Mine</u>

There are several reasons to use the Quecreek Mine as a primary testing site. First, due to the Quecreek incidence, the mine is a symbol of the coal mine industry, showing the urgent need for void detection techniques. Second, the mine condition is representative of many small coal mines in the region: shallow depth (about 300) and thin seam (Upper Kittanning (C') seam, ranging in thickness between 38" to 62"). Third, the mine management is very supportive for the test. Finally, the Penn State team considers the mine a suitable testing site. In fact, Penn State had done some planning work, including two mine site visits, a underground tour of the potential testing sites, and collection and testing of the coal and roof samples.

The first testing site, which will be used for the calibrations and for the initial reflection test, was identified during the second mine visit. The second site, a pillar of 200 – 300 ft wide, has to be determined after the permission of Phase II as it will be created during the mining process.

<u>The Ridge Mine</u>

The main reason to use the Ridge Mine is its coal seam, the Pittsburgh coal seam (8' to 10' in height), which is the best known coal seam in US. During the visit of Amfire in 2004, the company indicated to Penn State that the mine could facilitate the test by arranging the reflection surveys at two mining stages with two different pillar widths. Because of this, both testing sites will be determined after permission to conduct Phase II.

10.2.2 Further technical development

The first year work at Penn State was limited to those most critical issues involving field testing and data analysis. There are a number of problems that remain to be studied. If the ISS based void detection technique is to be a reliable industrial tool, these problems have to be adequately addressed. In this sense, the ISS based void detection technique is still at an early stage of evaluation and has to be further developed, refined and enhanced.

A number of studies are critical at this stage. The most important one is signal identification. Signal identification is a problem which is inherently difficult. This is because the identification of reflected signals is affected by many factors and there are no simple rules and procedures to follow. Penn State intends to address the problem through a systematic engineering approach. With this approach, a variety of the data analysis methods, such as pattern recognition, spectrum analysis, polarization, wavelet, and hodogram, will be utilized to form comprehensive solutions.

The second problem is to develop an analytical or numerical procedure for the optimized solution of the common tangent assessment in the elliptical modeling approach. Currently, this is done manually. The third issue is enhancing the user's manual. In addition to the necessary development work, the procedures for experimental design, data analysis and void mapping have to be documented with the use of more charts, figures and tables to allow ease of use to users of this technique.

10.2.3 Industrial testing and applications

The future studies discussed here are two potential applications of the ISS based void detection technique. They are not part of the proposed work for Phase II and Phase III, but, we believe, are significant for MHSA's void detection program.

<u>Pilot study on the pillar dissolution problem in trona mines</u>

One of the major concerns with the trona industry is whether barrier pillars, which are used to separate the mined out and active mining areas, will be gradually dissolved by water, and if so, the rate of this process. As the dissolution rate is a function of saturation, which in turn depends on the local conditions (mining, geology and hydrogeology), data from field monitoring would be essential for making a reliable assessment.

The horizontal drilling, the method which is considered the most reliable means for detecting abandoned mines in the coal industry, is not suitable for the trona condition, as the drill holes would induce water into the pillars. Some non-destructive methods would be essential in order to solve this problem.

Based on the result of three successful tests at FMC and General Chemical, the ISS based void detection technique seems a promising solution for the problem. The idea is that permanent monitoring stations (sensor holes with sensor attachment assembly) are established at locations of concern and reflection surveys are carried out at these stations periodically (say, every one or two years) to determine the pillar width. All reflection survey results will be preserved as "X-ray" records for the pillars under study.

With the ISS based void detection technique developed at Penn State, the cost for using this technique is minimal. As sensors can be installed at the time when a survey is needed, one set of the monitoring equipment would be enough for all existing trona mines in Wyoming.

Further study at another mine with a strong ore seam

A hypothesis based on the testing result from the trona mines is that the ISS based void detection technique is not only effective for trona mines, but also a viable means for the mines with the stronger ore seams in general. If this is the case, a large array of non-coal mines, such as limestone and various salt mines, would also benefit from the MSHA's void detection program. In order to test this hypothesis, two field tests may be carried out initially, one at a limestone mine and one at a salt mine. If the testing results are positive for both sites, this will provide additional confidence in the hypothesis.

References

Brentrup, F. K., 1970. Seismische vorfelderkundung zur ortung tektonischer storungen im steinkohlenbergbau. *Gluckauf* **106**, 933-938

Brentrup, F. K., 1971. Flozdurchschallung aus Tiefbohrlochern. *Gluckauf* **107**, 685-690.

Brentrup, F. K., 1979a. Die entwicklung einer schlagwettergeschutzten Digitalapparatur fur die Flozwellenmessung, *Gluckauf Forschungs Hefte* **40**, 11-15.

Brentrup, F. K., 1979b. Flozwellenseismische Vorfelderkundung. *Gluckauf* **115**, 820-823.

Darken, W. H., 1975. A finite-difference model of channel waves in coal seams. Golden, Colorado School of Mines, USA, Master's thesis No. 1729

Dresen and Ruter, 1994. Seismic Coal Exploration, Part B: In-seam Seismics. Pergamon, New York, NY.

Evinson, F. F., 1955. A coal seam as a guide for seismic energy. *Nature* **176**, 1224-1225.

Ge, M. and L. Laverdure, 1995. Critical review of tomographic studies at the Lockerby Mine, Falconbridge Ltd. Final report to the Mining Research Directorate, Ontario, 87p.

Gardner, H. G. and K. K. Wu, 2005. Use of available and emerging methods for location of air and water filled cavities in mines – Status report on MSHA demonstration projects. SME annual meeting, Salt Lake City.

Guu, J. Y., 1975. Study of seismic guided waves in the continuity of coal seams. Golden Colorado School of Mines, USA, Ph.D. thesis No. T 1770.

Krey, T., 1962. Boundary waves as a tool of applied geophysics in coal mining. Paper presented at the 32nd SEG Meeting, Calgary, Canada.

Krey, T., 1963. Channel waves as a tool of applied geophysics in coal mining. *Geophysics* **28**, 701-714.

Krey, T., 1976a. In-seam seismic exploration techniques, in coal exploration 1, Proc.1st International coal exploration symposium, London, U.K., (ed) W.L.G. Muir, Miller-Freeman Publishers, San Francisco, USA.

Krey, T., 1976b. Possibilities and limitation of in-seam seismic exploration. Coal seam discontinuity symposium, Pittsburgh, Pennsylvania, USA.

Leitinger, H., 1969. Investigations of displacements in a layered halfspace by the finite-difference method. Golden, Colorado School of Mines, USA, Ph.D. thesis No.T. 1770.

Rodriguez R., R. Brendlinger, H. Naumann, and L. Browning, 1994. Underground high resolution seismic method as a low cost alternative for mapping sandstone replacement channels in coal mines. Proc. 13th International Conference on Ground Control in Mining, pp. 233-238.

Rodriguez, R., E. and H. Naumann, 1995. Application of underground in-seam seismic methods (UISS) to map the coal seam structure across longwall panels. Proc. 14th International Conference on Ground Control in Mining, pp. 261-272.

Rodriguez, R., 1996. Theoretical aspects of in-seam 3-D channel waves. Geophysics Journal. This paper may not be published.

Su, F. C., 1976. Seismic effects of faulting in coal seams: numerical modeling. Golden, Colorado School of Mines, USA, Ph.D. thesis No. 1869.

Young, G. B. and L. W. Braile, 1976. A computer program for the application Zoeppritz's amplitude equations and Knott's energy equations. *Bull. Seism. Soc. Am.* **66**, 1881-1885.

Appendix I

Testing equipment, material and software used for the project

This appendix lists the major equipment, material and software used for field tests.

Table I – 1 Equipment and material used for field tests

Equipment/material	Description	Manufacturer
ESG Hypersion data acquisition system	16-channel, 16-bit resolution, MSHA certified	ESG
A1030 uniaxial accelerometer	Sensitivity: 30V/g, frequency response: 50 – 5000 Hz to within ±3 dB, 3 V/g, MSHA certified	ESG
Wire-breaking recording device	For system triggering	ESG
Sensor cable	20 AWG, 2 pair copper w/shielding	Belden Electronics
Sensor installation kit	For installing retrievable sensors	Penn State
Lokset Resin	For grouting sensor anchors	Minova USA
Stemming clay	For stemming blasting holes	Webb Manufacturing

Table I – 2 Software used for data analysis

Software	Description	Developer
ESG –IS-001L	This software was purchased along with the data acquisition system. It is a general software package used for seismic data processing and visualization.	ESG
AGU-Vallen Wavelet	Wavelet analysis package	Vallen
Matlab 7.0	Drawing ellipses	The MathWorks

Table I – 3 Parameters for data recording

Mode	Recording window (second)	Sampling Rate (samples/second)
Mode I	0.4	50k
Mode II	0.8	25k

Appendix II

Directories of the recorded data

This appendix lists the directories of the recorded data, which are contained in a CD included with the report.

File Name
In-Seam Seismic Void Detection Field Tests
The Penn State University

Directories
2005-2-8: Harmony Mine site one Test

2005-3-7 FMC site B tests

2005-3-8 FMC site A tests

2005-3-10 General Chemical tests

2005-4-29 Harmony mine site two test

2005-8-23 FMC (site A) demonstration test

2005-11-15 Harmony mine (site 2) demonstration test

2005-12-8 Agustus mine test